AD_____

Award Number: W81XWH-10-1-0536

TITLE: Protein Aggregation Inhibitors for ALS Therapy

PRINCIPAL INVESTIGATOR: Richard B. Silverman, Ph.D.

CONTRACTING ORGANIZATION: Northwestern University
Evanston, IL 60208-1108

REPORT DATE: July 2013

TYPE OF REPORT: Final

PREPARED FOR: U.S. Army Medical Research and Materiel Command
Fort Detrick, Maryland 21702-5012

DISTRIBUTION STATEMENT: Approved for Public Release;
Distribution Unlimited

REPORT DOCUMENTATION PAGE

Form Approved
OMB No. 0704-0188

1. REPORT DATE	**2. REPORT TYPE**	**3. DATES COVERED**
07/30/2013	Final	1 July 2010– 30 June 2013

4. TITLE AND SUBTITLE
Protein Aggregation Inhibitors for ALS Therapy

5a. CONTRACT NUMBER

5b. GRANT NUMBER
W81XWH-10-1-0536

5c. PROGRAM ELEMENT NUMBER

6. AUTHOR(S)
Richard B. Silverman, Richard I. Morimoto, Robert J. Ferrante, Donald R. Kirsch
Betty Diamond

E-Mail: r-silverman@northwestern.edu

5d. PROJECT NUMBER

5e. TASK NUMBER

5f. WORK UNIT NUMBER

7. PERFORMING ORGANIZATION NAME(S) AND ADDRESS(ES)

Northwestern University
Evanston, IL 60208-1108

8. PERFORMING ORGANIZATION REPORT NUMBER

9. SPONSORING / MONITORING AGENCY NAME(S) AND ADDRESS(ES)
U.S. Army Medical Research and Materiel Command
Fort Detrick, Maryland 21702-5012

10. SPONSOR/MONITOR'S ACRONYM(S)

11. SPONSOR/MONITOR'S REPORT NUMBER(S)

12. DISTRIBUTION / AVAILABILITY STATEMENT
Approved for Public Release; Distribution Unlimited

13. SUPPLEMENTARY NOTES

14. Amyotrophic lateral sclerosis (ALS) is a fatal neurodegenerative disease characterized by progressive loss of motor neurons, leading to death within 3-5 years. Gulf War veterans, and military personnel in general, exhibit a significant increased risk of developing ALS. There is no effective treatment for ALS; riluzole, the only FDA-approved drug for ALS, extends median survival by only 2-3 months. The genetic linkage of several mutations in the gene for Cu/Zn superoxide dismutase (SOD 1) in some cases of familial ALS provided the first indication of a potential causal factor in the disease. We identified three chemotypes (pyrazolones, cyclohexane-1,3-diones, and pyrimidine-2,4,6-triones) that provide protection from toxicity and block aberrant protein aggregation caused by mutant SOD1. Each of these chemotypes was modified to improve potency and pharmacological properties; our best compounds in each chemotype extended life of the ALS mouse model by 13%, 13%, and 31% (10 mg/kg bid), respectively. Maximum tolerated doses of all were high, indicating low toxicity. Four approaches were taken to identify protein target(s) of the pyrazole class. Affinity bait experiments identified proteins involved in proteasomal activation; photoaffinity experiments identified heat shock protein (HSP) 27 and related proteins. All of these results provide new potential treatments for ALS.

15. SUBJECT TERMS Amyotrophic lateral sclerosis; Superoxide dismutase 1; Arylsulfanyl pyrazolones; Cyclohexane 1,3-diones; Pyrimidine 2,4,6-triones; G93A

16. SECURITY CLASSIFICATION OF:			**17. LIMITATION OF ABSTRACT**	**18. NUMBER OF PAGES**	**19a. NAME OF RESPONSIBLE PERSON**
a. REPORT	**b. ABSTRACT**	**c. THIS PAGE**			USAMRMC
U	U	U	UU	87	**19b. TELEPHONE NUMBER** *(include area code)*

Table of Contents

Page

INTRODUCTION

Amyotrophic lateral sclerosis (ALS) is a fatal neurodegenerative disease characterized by the progressive loss of motor neurons, leading to muscle atrophy, paralysis, and death within 3-5 years. Sporadic (~90% of cases) and familial forms of the disease display similar clinical and pathological features. ALS typically affects people between 40-70 years of age (average 55 years) with an incidence of ~2 cases per 100,000 individuals, which corresponds to a 1 in 2000 lifetime risk to develop the disease. An increased prevalence of ALS has recently been observed, with the worldwide affected population estimated to reach ~108,000 patients by 2012 with one-third residing in the U.S. It has recently been reported that Gulf War veterans exhibit a significant increased risk of developing ALS, and extends more generally to the military service outside of the Gulf War. ALS patients are often affected in the prime of their lives, and retain full intellectual awareness of their inexorably declining motor faculties during the disease progression. There is no effective treatment for ALS; riluzole, a presumptive anti-glutamatergic agent, is the only FDA-approved therapeutic drug for ALS, which only extends median survival by 2-3 months. The genetic linkage of several mutations in the gene for Cu/Zn superoxide dismutase (SOD 1) in some cases of familial ALS (FALS) provided the first indication of a potential causal factor in the disease process. Recent studies have now linked FALS to sporadic ALS (SALS) through common SOD1 containing astrocytes, demonstrating that SOD1 is a viable target for both FALS and SALS, providing further impetus for the identification of compounds active in mutant SOD1 disease models.[1] These similarities in the clinical and pathological features of FALS and SALS has led investigators to use the FALS phenotype as a strategy for elucidating disease pathogenesis and defining novel treatments in both forms of the disease. Although the underlying biochemical alterations and the mechanisms of neuronal degeneration remain unknown in ALS, it has been postulated that protein misfolding and aggregation may be an early event that triggers both damaging and compensatory molecular processes and genetic programs that are toxic to neurons, altering transcription through the sequestration of proteins and leading to activation of signaling cascades associated with mitochondrial dysfunction, energy metabolism defects, inflammation, oxidative stress, apoptosis, excitotoxicity, and global deleterious effects on protein homeostasis, all of which may underlie the ALS pathology. Employing a high-throughput screen (HTS) of a library of >50,000 compounds, we have identified three chemotypes (Figure 1), arylsulfanylpyrazolones (AXP, X = S), pyrimidine-2,4,6-triones (PYT), and cyclohexane-1,3-diones (CHD), which provide protection from toxicity and block aberrant protein aggregation caused by mutant SOD1. The last year has been focused on enhancing potency and/or pharmacokinetic properties of the three chemotypes, testing our best compounds from last year at different doses in the ALS mouse model, and investigating possible mechanisms of action of the compounds.

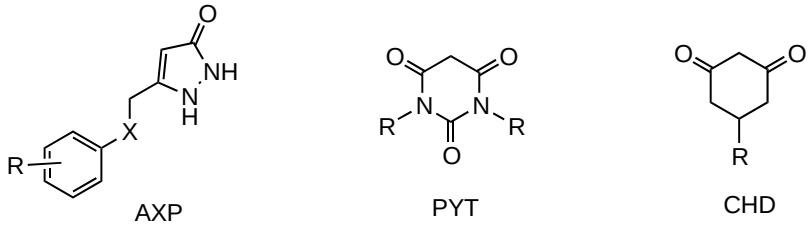

Figure 1. Three active chemotypes from the HTS

BODY

Biological Activity and New Analogue Synthesis

Primary cell-based assay for guiding analogue synthesis

To guide analogue synthesis, we utilize a cellular model in which cell death depends on the expression of G93A-SOD1. Cytotoxicity is determined in cultured PC12 cell lines expressing G93A-SOD1, using the cell viability reagent Calcein AM. To determine potency, analogues are tested for restoration of cell viability via a dose response experimental design format. Analogues of compounds that protect against mutant SOD1-induced cytotoxicity in the cell-based assay are then prioritized for in vivo studies in the G93A transgenic mouse.

Originally, Cambria Pharmaceuticals was responsible for assay design and implementation and had primary responsibility for all biological assays. As a consequence of the closure of Cambria in 2012, the assay technology was transferred to the Morimoto Laboratory at Northwestern University. To ensure accuracy in the transfer of technology, we began by testing the three original chemotypes (Figure 1), arylsulfanylpyrazolones (AXP, X = S), pyrimidine-2,4,6-triones (PYT), and cyclohexane-1,3-diones (CHD), identified in the high-throughput screen. Consistent with previous studies at Cambria, we found that these three scaffolds provided protection from toxicity caused by expression of mutant SOD1. After demonstrating the successful transfer of the cell-based assay, new compounds modified from the AXP, CHD, and PYT cores were tested to direct future structural modifications. This report covers the entire period of grant support.

SAR of aryloxanylpyrazolones

Once the ASP class of compounds was identified, numerous analogues were made. We also were interested in trying to determine the target(s) of action of this class of compounds (*vide infra*), and several biotinylated analogues were made for pull-down studies (**1a-d**). The in vitro EC_{50} of **1** (R_1 = R_2 = H) in our mutant SOD1-PC12 aggregation assay was 0.067 uM, so the long, bulky side chain attached to N^1 of the pyrazolone ring did not appear to have a significant effect on the activity of the parent molecule; it appears that steric hindrance is not a problem at that position. Methylation of N^1 of **1** (R_1 = Me, R_2 = H), not surprisingly, also had a similar EC_{50} (0.75 uM). However, the N^1,N^2-dimethyl analogue (**1**, R_1 = R_2 = Me) was inactive! This was telling us something very important about the N^2-H. Therefore, we carried

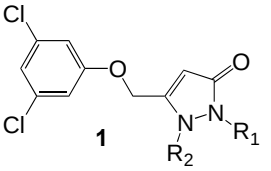

1

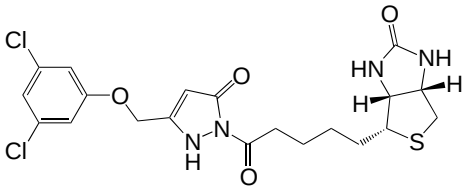

1a, EC_{50} = 0.56 uM

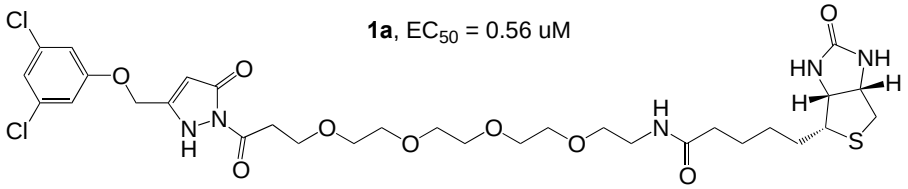

1b, EC_{50} = 0.67 uM

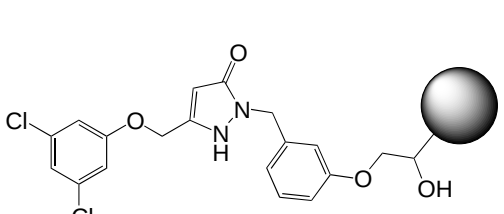

1c, EC_{50} = TBD

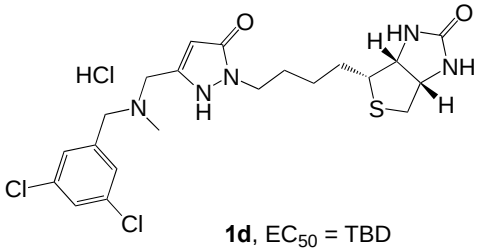

1d, EC_{50} = TBD

out a SAR study on analogues of **1** to determine the importance of this N-H, and the results are summarized in Table 1. All of the N^1-substituted compounds are active except for **1f, j, k,** and **o**. Compound **1f** is intriguing because it is small and not bulky. It was thought that the hydroxyl group of the hydroxyethyl group could form an intramolecular hydrogen bond, via a 6-membered ring, to the N^2-H, thereby destroying any activity. To test that hypothesis, the corresponding hydroxypropyl analogue (**1g**) was made, which would require a much less

stable 7-membered ring intramolecular hydrogen bond, and, indeed, activity returned. An increase in electron-withdrawing ability should also have an important effect on activity because of its decrease in pKa of N^2-H. In fact, **1h** and **1i** have increasingly lower activity, and **1j**, **1k**, and **1o** are inactive, as expected for an electron-withdrawing effect. To further confirm these results, other cycles were incorporated in place of the pyrazolone ring (**2**-**4**); none of these were active. These results support the importance of N^2-H in its activity, presumably some hydrogen-bonding interaction with a target that is essential for activity. It also has guided our thinking in terms of sites for attachment of groups for pull-down mechanism of action experiments.

Table 1. SAR studies of substituted pyrazolones.

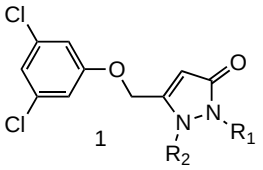

1

Entry	R_1	R_2	EC_{50} (μM)
a	H	H	0.067
b	Me	H	0.67
c	Me	Me	>32[a]
d	Biotin	H	0.56
e	Peg_4-Biotin	H	0.67
f	CH_2CH_2OH	H	>32
g	$CH_2CH_2CH_2OH$	H	0.34
h	Ph	H	1.03
i	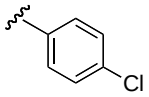	H	1.73
j	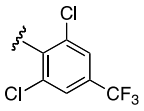	H	>32
k	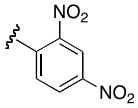	H	>32
l	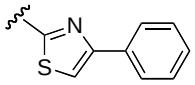	H	1.00
m	Bn	H	0.13
n	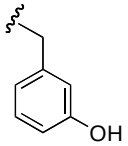	H	0.36
o	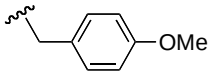	H	>32
p	CHO	H	0.49
q	Ac	H	0.27
r	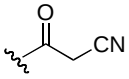	H	0.42
s	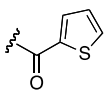	H	0.31

t	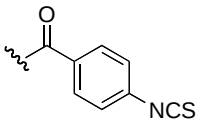	H	0.33
u	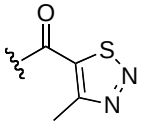	H	1.71
v	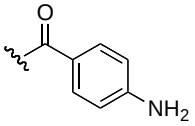	H	0.93
w	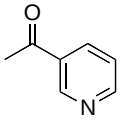	H	1.32

[a]>32 μM indicated EC_{50} not reached at highest concentration

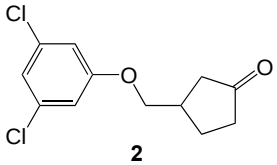

2

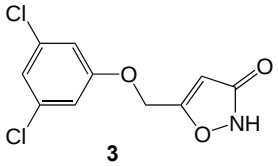

3

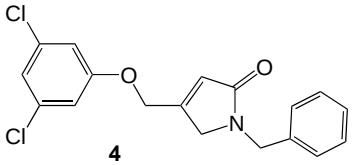

4

Amine analogs of arylsulfanylpyrazolone (ASP), the arylazanylpyrazolone (AAP) analogs

Different sulfur-containing linkers (X) in the ASP compounds (see Figure 1) were synthesized, and X = S was most potent. However, sulfide-containing compounds showed rapid metabolic degradation. When X = O, the metabolism diminished greatly, and when an analog with X = O and R = 3,5-dichloro was administered to the G93A ALS mouse at 20 mg/kg, an enhancement in life expectancy of 13% was observed (*vide infra*). This was not as large an increase as was hoped, so additional dosing studies were carried out (*vide infra*) and further modifications to the ASP structure (CMB-087229), varying X, were made. We believe that greater enhancement of life expectancy was not attained because of the poor bioavailability of the compound. As such, additional analogs were developed. When X = NH, moderate potency (1.1 uM), excellent solubility (≥500 uM) and plasma stability (>60 min), good microsomal stability ($T_{1/2}$ 95 min with human and 30 min with mouse microsomes) were observed, but Caco-2 values were low, predicting poor bioavailability: A->B, 1.3 x 10^{-6} cm s^{-1} and B->A, 24.2 x 10^{-6} cm s^{-1}, suggesting an efflux substrate (efflux ratio, ER 19.2). We suspected that the NH may be responsible, so a series of N-substituted analogs (ASP, X = NR) was synthesized, all of which were active (Figures 2-4). Microsome stability also improved ($T_{1/2}$ for human microsomes >180 min). Caco-2 permeability improved considerably for the N-Me analog (ER 3.5), but still remained out of the optimal range in addition to having low permeability. In addition, N-substituted analogs were used for our target identification studies (*vide infra*).

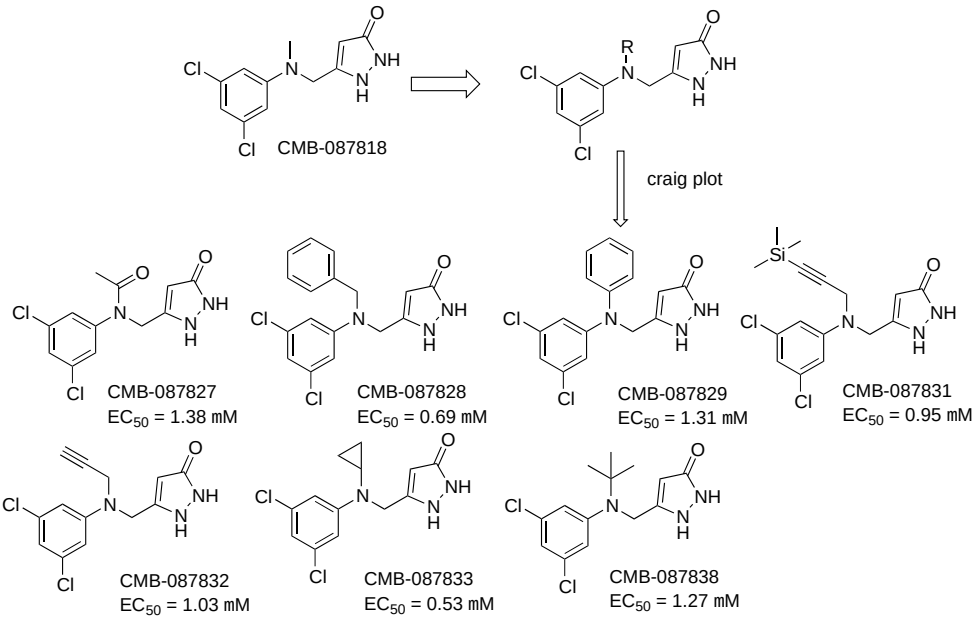

Figure 2. N-Substituted analogs based on the N-methyl derivative

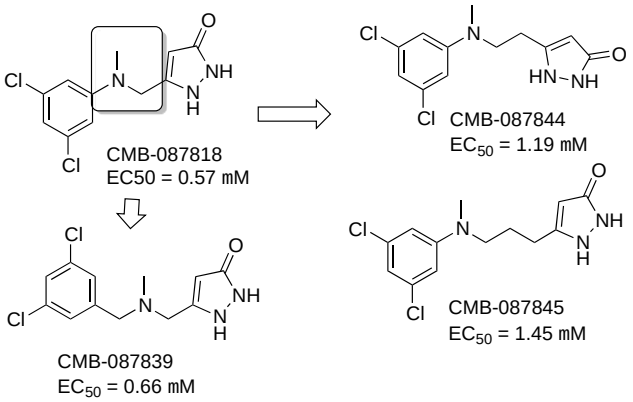

Figure 3. Effect of linker length

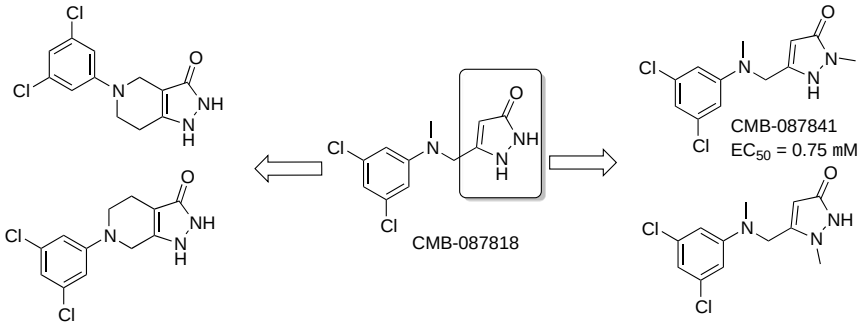

Figure 4. Cyclic analogs and pyrazolone modified analogs

Because alkylation (R^1 = alkyl or arylalkyl) gave active analogues that had much improved microsome stability, and Caco-2 permeation was better, we continued to pursue analogues of **5** (Figures 5-9). On the basis of these results, a SAR is depicted in Figure 10.

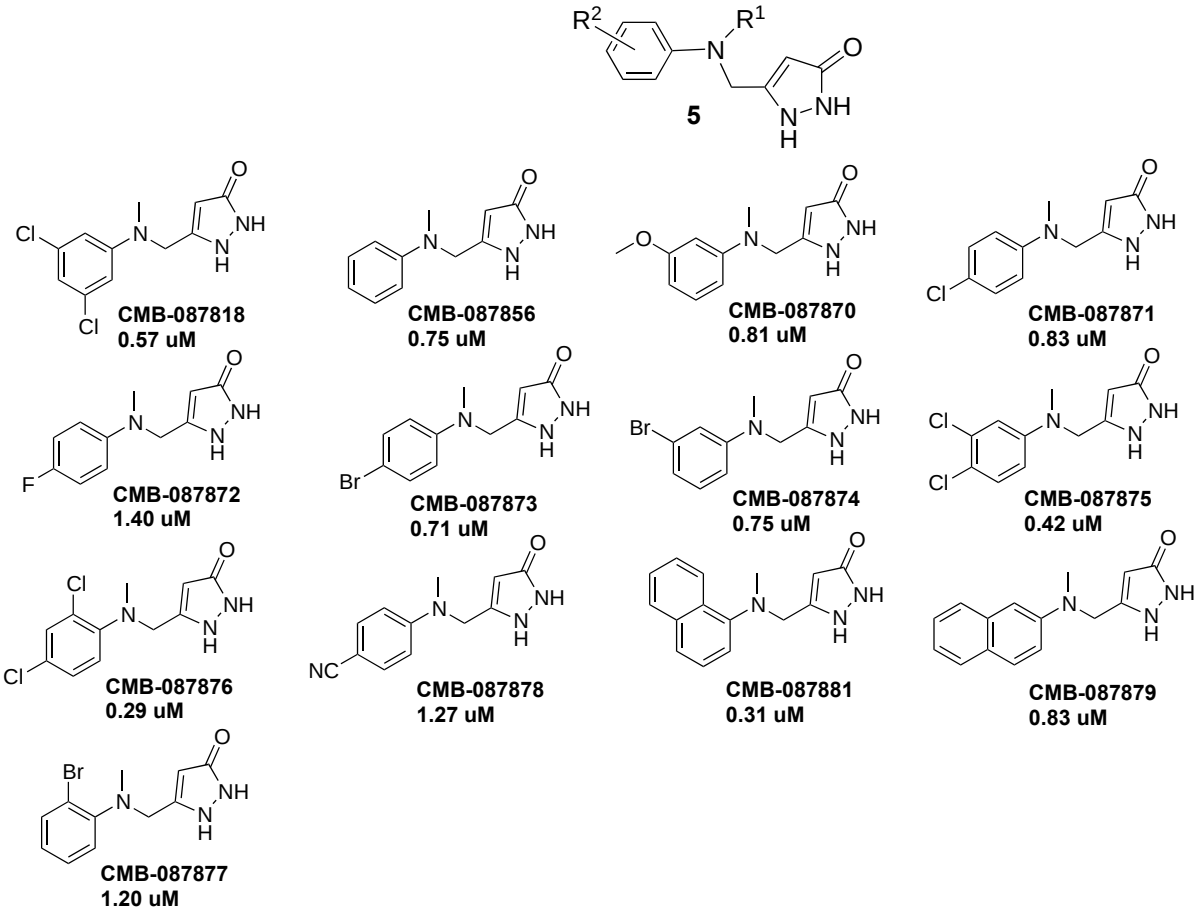

Figure 5. Modification of the aryl moiety

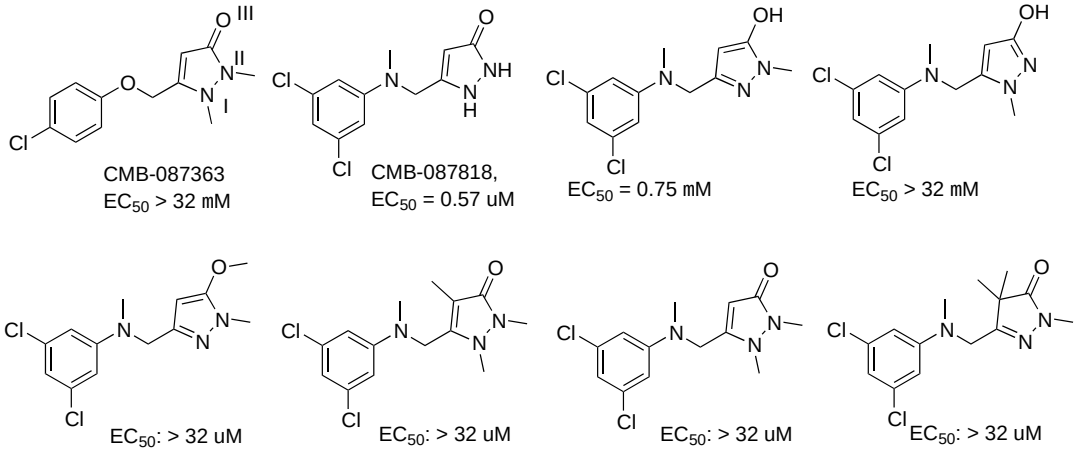

Figure 6. Modifications of the pyrazolone moiety

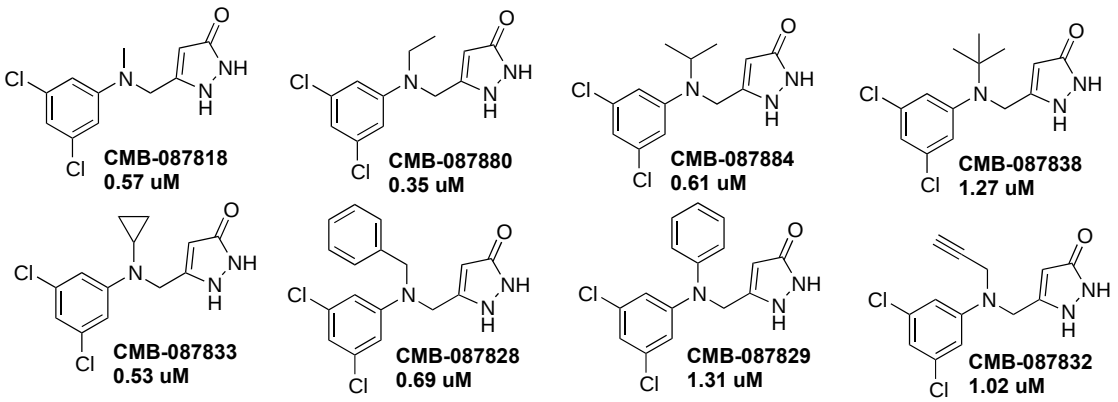

Figure 7. Modification of the N-substituent

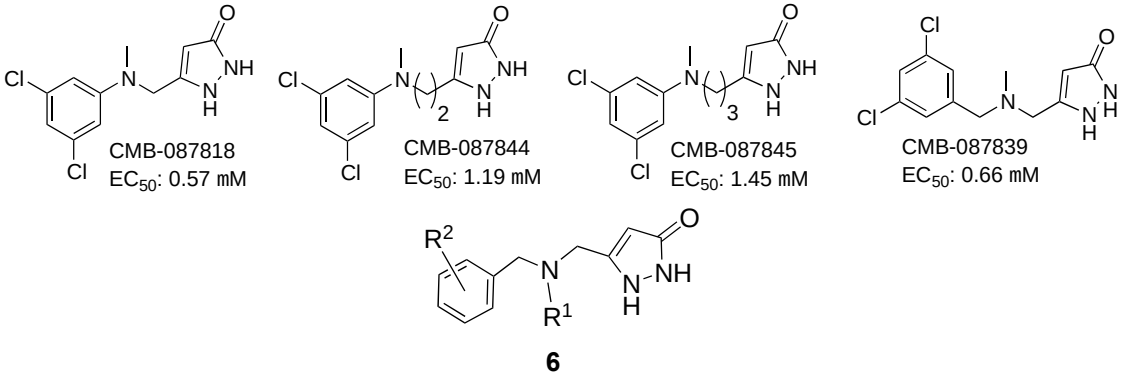

Figure 8. Modification of the linker length

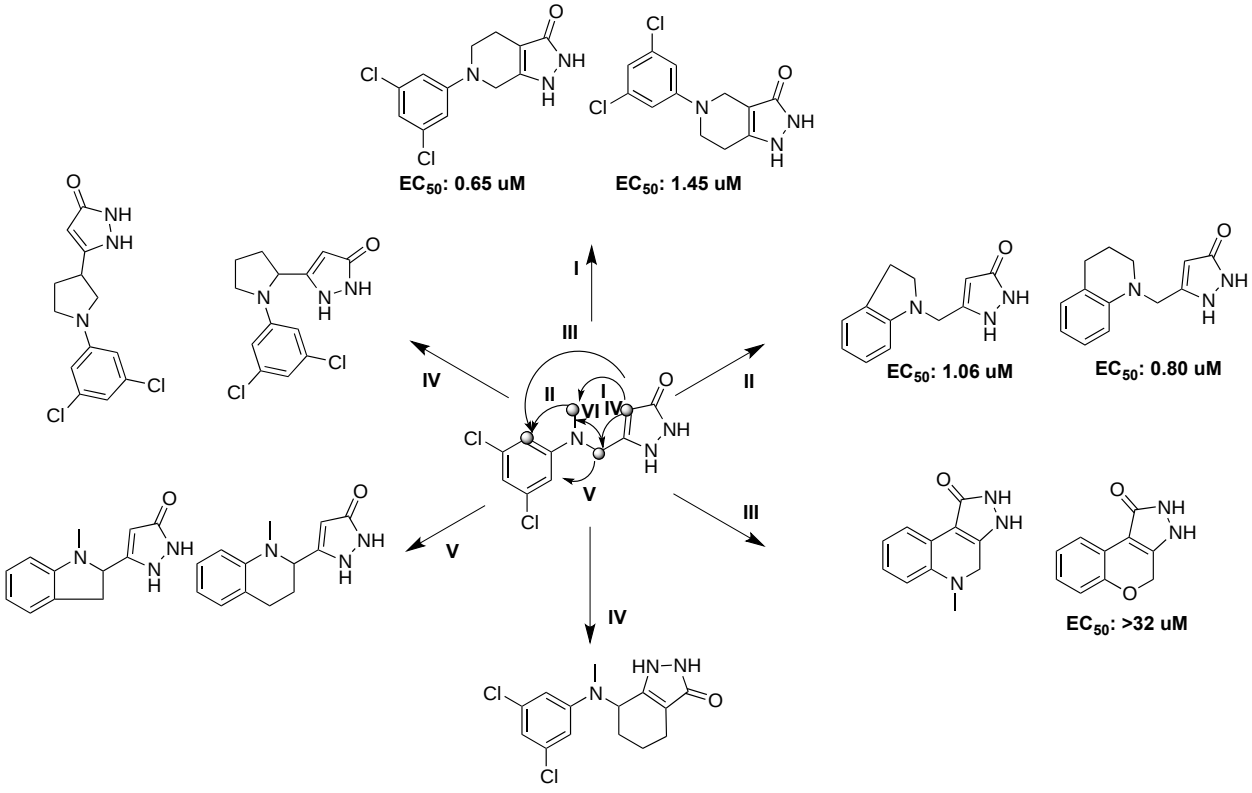

Figure 9. Modification by cyclization of the linker

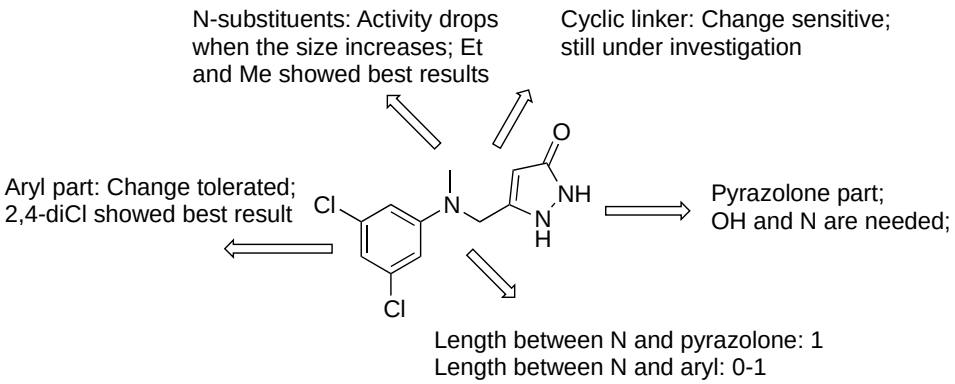

Figure 10. SAR summary

As shown in Figure 8, the placement of the nitrogen atom along the side chain is important. The most relevant site for our studies is the placement in the middle of the chain (Figure 8, **6**, R^1 = Me, R^2 = 3,5-dichloro), which was comparable in potency to **5** but much more stable in microsomes (>180 min, human), good Caco-2 permeability and low efflux ratio (0.8). The importance of this compound is that the nitrogen basicity of **6** (R^1 = Me, R^2 = 3,5-dichloro) (pKa ~8.5) is much greater than that in **5** (R^1 = Me, R^2 = 3,5-dichloro) (pKa ~5); consequently, salts can be made with **6**. Several salts were made: HCl, citrate, tartrate, sulfate, and phosphate salts. They were all much more soluble than the parent molecule, with the HCl salt being the most soluble. In animal testing with these compounds it was observed that the mice were severely irritated by the HCl salt, mildly irritated by the tartrate salt, but not irritated by the citrate salt. However, citric acid was not sufficiently acidic to allow the salt to be stable. Therefore, the phosphate and sulfate salts were made, which also did not irritate the animals.

SAR studies with cyclohexane-1,3-dione (CHD) analogues

We had found that one of our most potent CHD analogues (CMB-086874, **7**), which also had good ADME properties, exhibited no life extension of the ALS mouse, even at 20 mg/kg. However, we subsequently found that, unlike all other active compounds, **7** did not penetrate neurons, so we searched for CHD analogues that could penetrate neurons and identified two positive structures (**8** and **9**). The most potent (**8c**) was found to

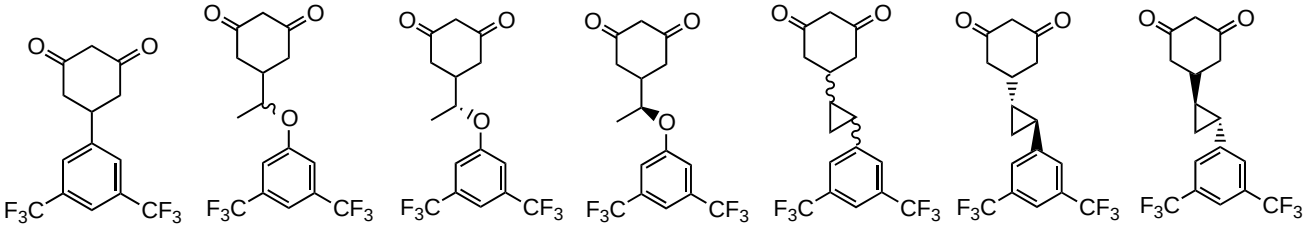

have excellent in vitro ADME properties in terms of plasma ($T_{1/2}$ >60 min) and microsomal stability ($T_{1/2}$ 74 min, human; 52 min, mouse microsomes), Caco-2 permeability (24.1 x 10^{-6} cm s^{-1}) with low efflux ratio (0.1), and no MTD reached, even at 5 g/kg after 5 days (no observable toxicity). ALS mouse studies are discussed below.

Animal PK and Efficacy Studies

Effect of CMB-021805 on SOD1 G93A ALS Mice

Genetic mouse models have played a critical role in the study of human neurological disorders by providing accurate and experimentally accessible systems to study mechanisms of pathogenesis, to characterize biomarkers of disease, and to test potential therapeutic strategies for translation in patients with neurodegenerative diseases. The G93A mutant SOD1 transgenic mouse model is one of the most widely

employed models of ALS as it replicates many of the symptoms observed in ALS patients. The similarities in the clinical and pathological features of familial and sporadic ALS has led investigators to use the familial ALS phenotype (G93A mice) as a strategy for elucidating disease pathogenesis and defining novel treatments for both forms of the disease. In our original submission we showed that compounds from PYT (CMB-021805), ASP (CMB-087229), and CHD (CMB-086874) scaffolds were efficacious in the protein aggregation assay. The

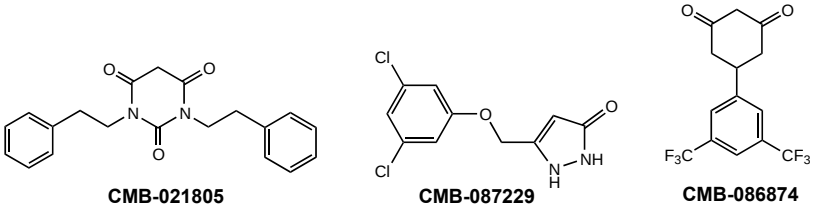

CMB-021805
PYT

CMB-087229
ASP

CMB-086874
CHD

PYT molecule, CMB-021805, was chosen as the first NCE compound for testing in the G93A ALS mouse model. Behavioral results of Open-Field analysis showed a marked significant protective effect in a dose dependent manner using CMB-021805 (Figure 11).

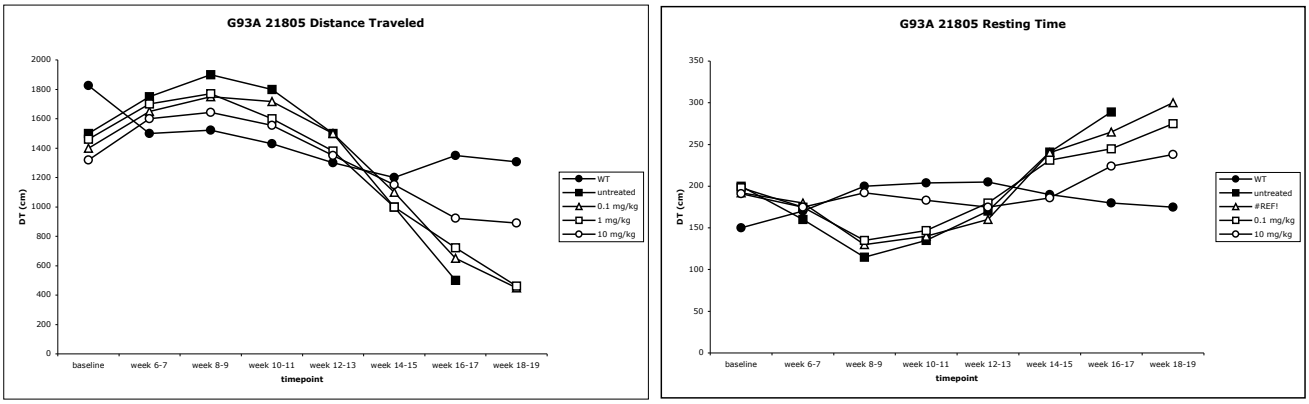

A B

Figure 11. Open field test results using CMB-021805 are dependent on motor performance and can be evaluated via multiple parameters. One easy way to conceptualize this parameter is 'resting time' (graph B). As disease develops in the animals, their muscles become weak and they need to spend more time resting. In graph B the resting time for the wild type (healthy) animals changes little over time. Untreated ALS animals begin to rest significantly more in week 14-15 as disease becomes more severe. Disease is so severe in week 18-19 that these untreated mice become untestable. CMB-021805 was effective in decreasing resting time during this period. There was a dose-dependent improvement, with the greatest improvement at the highest dose (10 mg/kg).

Also, CMB-012805 treatment significantly extended survival in the G93A ALS mice in a dose dependent manner in comparison to untreated G93A mice (Figure 12). We extended these studies by increasing the dose administration to 20 mg/kg (Figure 8B).

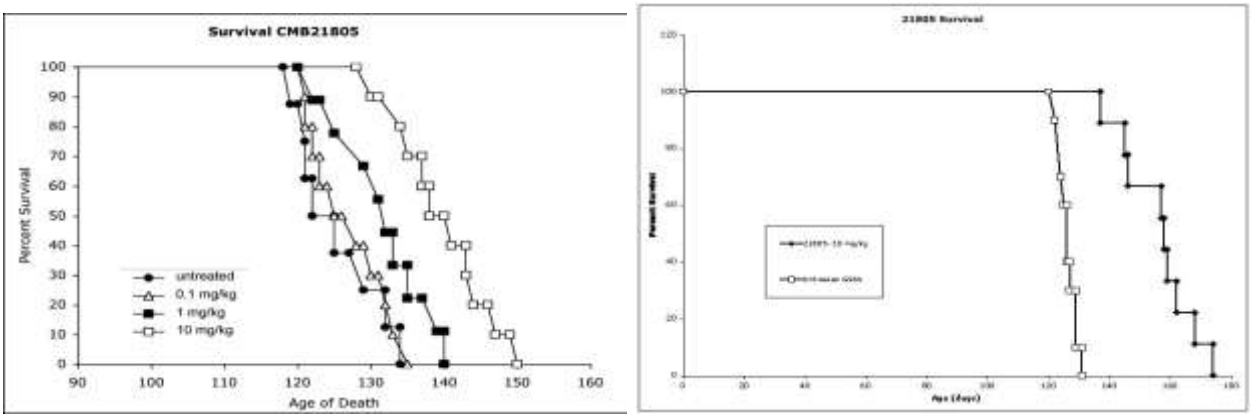

A B

Figure 12. Kaplan-Meier Survival Curve of Dose Response Using CMB-021805 in G93A mice. Figure A includes 0.1, 1, and 10 mg/kg dosing, while Figure B includes 20 mg/kg dosing.

These experiments resulted in a remarkable improvement in survival extension resulting in 11.9% and 26.4% extension in lifespan in the 10 mg/kg and 20 mg/kg highest doses, respectively (untreated G93A mice: 124.6 ± 3.7 days; 0.1 mg/kg CMB-021805-treated G93A mice: 126.5 ± 4.3 days; 1 mg/kg CMB21805-treated G93A mice: 131.2 ± 5.1 days; 10 mg/kg CMB-021805l-treated G93A mice: 139.4 ± 5.9 days, $p<0.01$; 20 mg/kg CMB-021805-treated G93A mice: 157.5 ± 11.7 days, $p<0.01$). Since our original submission, we have extended our efficacy studies administering CMB-021805 and CMB-087229 in G93A ALS mice. We performed maximum tolerated dose studies to ensure that each had similar outcomes. Since the half-life of CMB-021805 is relatively short, we carried out additional dosing trials in the G93A mice administering 30 mg/kg and 10 mg/kg BID, along with 20 mg/kg CMB-021805 for comparison to the previous trial. These additional studies provided critically vital information in the evaluation of CMB-021805 and demonstrated that the results are reproducible. The 30 mg/kg dose resulted in no significant increase in survival over 20 mg/kg, suggesting that this dosing level was near to the cumulative toxicity level. While the 20 mg/kg dose was the same as that previously observed (25.5% survival extension), the 10 mg/kg BID dose resulted in almost 31% life extension in the G93A mice! *This finding is second to none and higher than any result reported in this animal model* (Figure 13). These survival findings have now been replicated in the Ferrante laboratory.

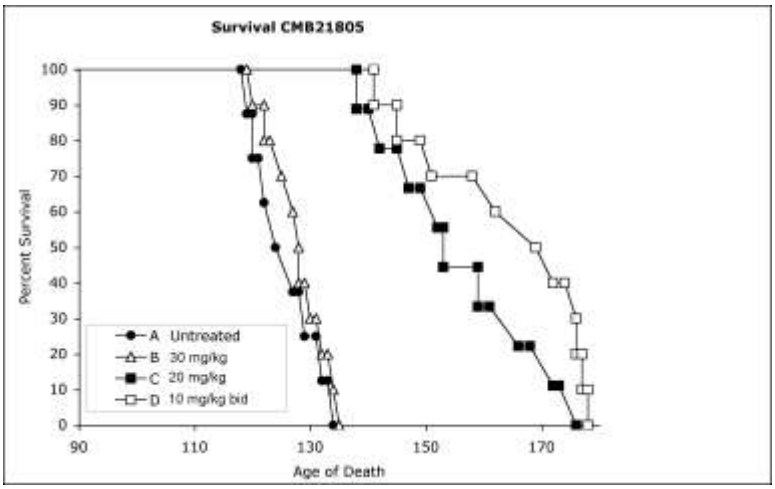

Figure 13. CMB-021805 treatment significantly extended onset of death and survival in the G93A ALS mice in a dose dependent manner, in comparison to untreated G93A mice. Survival extension was significant at the 20 mg/kg and 10 mg/kg bid doses. The 30 mg/kg dose of CMB-021805 did not significantly extend life span mice (untreated G93A mice: 125.25±4.3 days; 30 mg/kg CMB-021805-treated G93A mice: 127.6±4.7 days, $p<0.42$; 20 mg/kg CMB-021805-treated G93A mice: 157.2±10.1 days, $p<0.01$; 10 mg/kg bid CMB-021805-treated G93A mice: 163.8±12.2 days, $p<0.01$). Survival extension: 25.5% at 20 mg/kg; 30.8% at 10 mg/kg BID.

Neuropathological analysis in untreated G93A mice at 120 days revealed marked gross spinal cord atrophy, with neuronal loss in the ventral horns from the lumbar spinal cord in untreated G93A mice, in comparison to wild type littermate control mice (Figure 14). The pathology findings in the untreated G93A mice were significantly reduced by CMB-021805 (20 mg/kg) administration. There was significant gross atrophy of the lumbar spinal cord in untreated G93A mice, in comparison to WT littermate control mice (WT littermate control: $3.26 \pm 0.21 \times 10^6$ μm^3, untreated G93A mice: $2.15 \pm 0.42 \times 10^6$ μm^3, $P<0.001$) with significant amelioration of gross spinal cord atrophy in CMB-21805-treated mice at the 20 mg/kg dose (CMB-021805- treated G93A mice: $3.05 \pm 0.27 \times 10^6$ μm^3, $p<0.01$). The gross atrophy was largely associated with the ventral horn of the lumbar spinal cord (WT littermate control: $7.07 \pm 0.37 \times 10^5$ μm^3, untreated G93A mice: $4.97 \pm 0.53 \times 10^5$ μm^3 , $p<0.01$) and was significantly improved by CMB-021805 (20 mg/kg) treatment (CMB-021805-treated G93A mice: $6.68 \pm 0.41 \times 10^5$ μm^3, $p<0.05$). Consistent with the above findings, there was marked ventral horn neuronal loss in the untreated G93A mice, as compared to the WT littermate control mice (WT littermate control: 96.4 ± 11.2; untreated G93A mice: 23.7 ± 17.3, $p< 0.0001$) (Figure 14A and C), with

significant reduction in neuronal loss as a consequence of CMB-021805 administration, in comparison to the untreated G93A mice (CMB-021805-treated G93A mice: 69.7 ± 14.1, $p<0.05$) (Figure 14B).

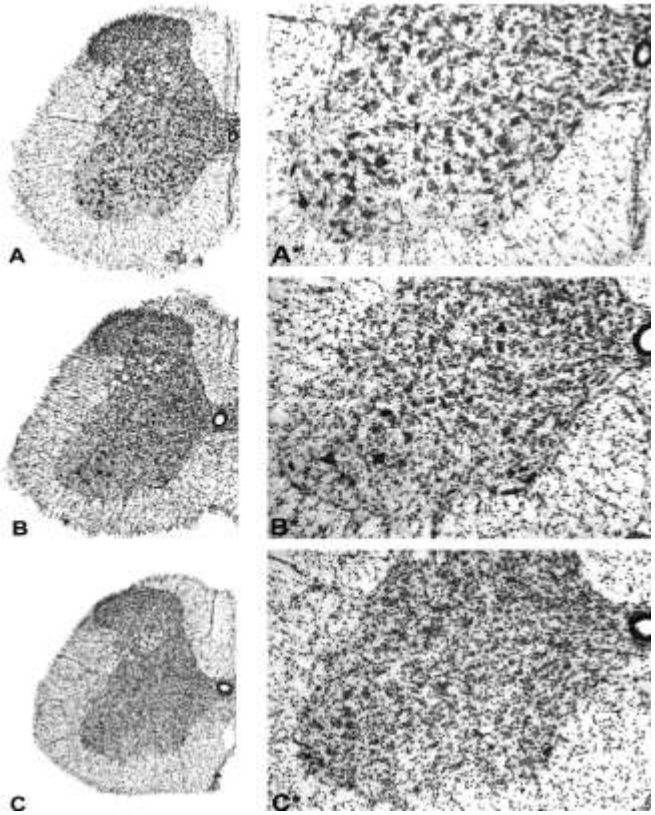

Figure 14. Neuroprotective effects of CMB-021805 (20 mg/kg) in the lumbar spinal cord in G93A transgenic ALS mice. Nissl staining of the lumbar spinal cord from (A) wild-type mice, (B) G93A mice treated with CMB-021805, and (C) untreated G93A mice shows a marked gross atrophy in untreated G93A mice. Treatment with 21805 significantly improved the gross neuropathological changes, as shown in Figure B and B*. High magnification photomicrographs of Nissl staining in the ventral horn from the same sections in A, B, and C of the lumbar spinal cord from (A*) wild-type mice, (B*) G93A mice treated with 21805, and (C*) untreated G93A mice demonstrates ventral neuron loss and atrophy in untreated G93A mice. The treatment with 21805 markedly improved these neuropathological changes.

Furthermore, the neuropathology results showed a significant neuroprotection from the gross loss of white and grey matter in CMB-021805 treated G93A mice at 126 days, by 26% and 28%, respectively (Figure 15). Stereological analysis demonstrated a 36% reduction in the loss of ventral horn neurons. These results confirm and extend the earlier studies using CMB-021805.

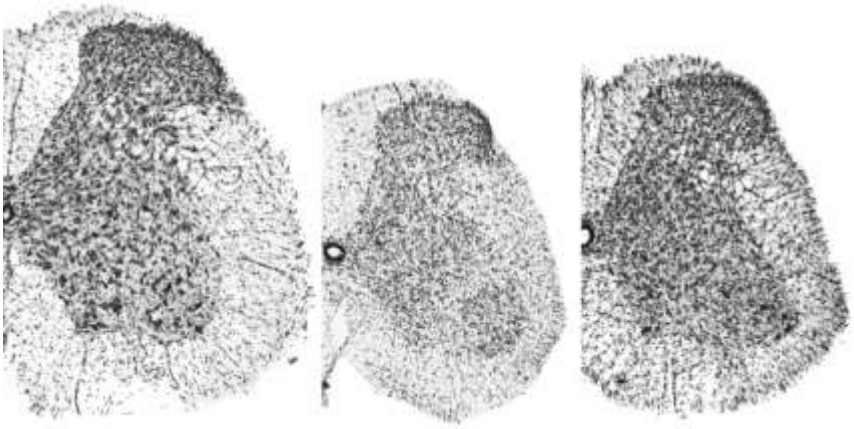

A B C

Figure 15. Neuropathology analysis of the 10 mg/kg BID dose of CMB-021805 at 126 days showed marked improvement in both gross tissue loss of white and grey matter in the spinal cord of treated G93A mice (C) in comparison to untreated G93A mice (B) at 26% and 28%, respectively. There was 36% reduction in ventral horn neuron loss in the CMB-021805-treated G93A mice.

Effect of CMB-087229 on SOD1 G93A ALS Mice

The ASP molecule, (CMB-087229, **1a**), also showed significant dose-dependent extension in survival. Control and transgenic mice of the same age (± 3 days) and from the same **"**f**"** generation were selected from multiple litters to form experimental cohorts. The tolerable dose range for **1a** was determined in wild-type mice by increasing the dose b.i.d. one-fold at each ip injection; the maximum tolerated dose was 75 mg/kg. On the basis of the studies performed to determine tolerance and blood brain levels, the dose levels of 1.0, 10, and 20 mg/kg

once a day were administered, starting at 6 weeks of age, throughout the lives of the G93A mice. Administration of **1a** resulted in a significant extension in survival in the G93A ALS mice in a dose dependent manner in comparison to untreated G93A mice (Figure 16A). The most efficacious dose (20 mg/kg) resulted in a life extension of 13.4%. In addition, motor performance, as measured by open field analysis in distance traveled at the 20 mg/kg dose was significantly improved over the untreated from 8-11 weeks (Figure 16B).

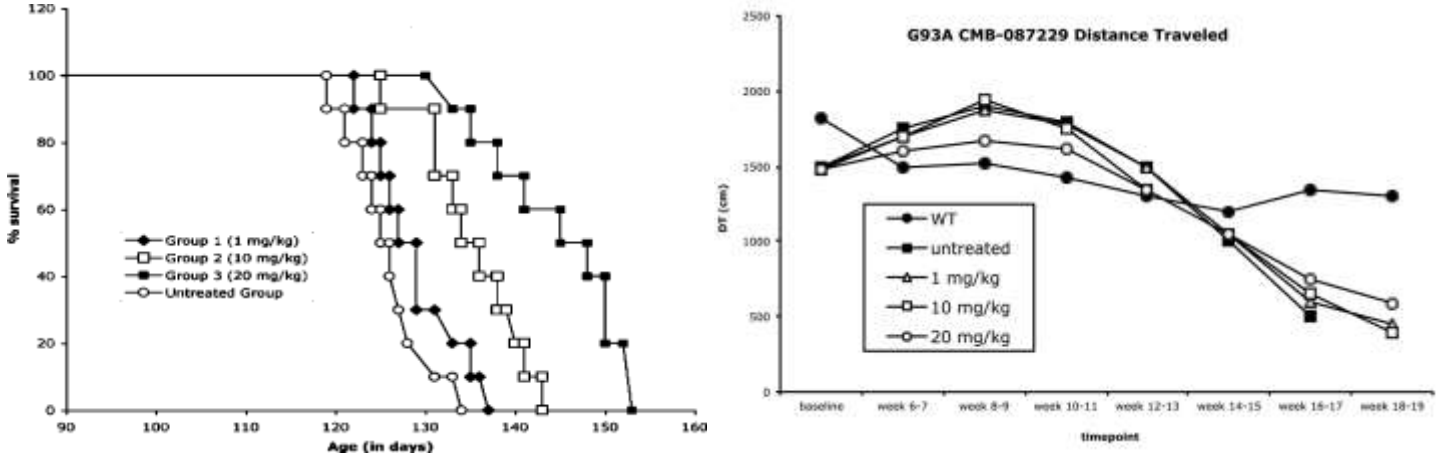

A. B.

Figure 16. A. Kaplan−Meier plot of **1a**-treated SOD1 G93A ALS mice: untreated group, 125.7 ± 4.9 days; group 1 (1 mg/kg), 129.2 ± 5.3 days; group 2 (10 mg/kg), 135 ± 5.5 days; group 3 (20 mg/kg), 142.5 ± 8.2 days; $p < 0.05$. **B.** Motor performance as measured by open field showed that the **1a** 20 mg/kg dose was significantly improved between 8 and 11-week time points.

We carried out an additional dosing trial in the G93A mice administering 30 mg/kg and 10 mg/kg BID, along with 20 mg/kg CMB-087229, as we had done with CMB-021805 (Figure 17). These results did not extend survival more than the 13% that we observed in the first trial. Body weight analysis showed no significant difference from the 20 mg/kg dosing. Survival studies also showed no significant difference with either 30 mg/kg or 10 mg/kg BID. The neuropathology findings were not significantly different, as well, at any dose. Therefore, we concluded that CMB-087229 might have reached its greatest efficacy at 20 mg/kg with an approximate 13% survival extension.

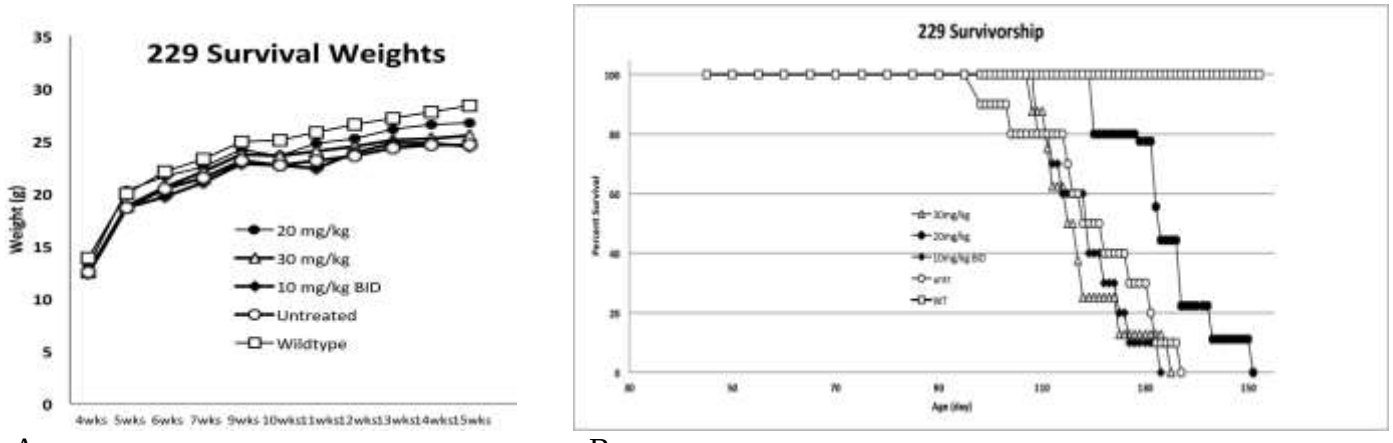

A B

Figure 17. Body weight change showed no significant differences using CMB-087229 at 30 mg/kg and 10 mg/kg BID (A). In addition, there were no significant differences in survival over that of the 20 mg/kg dose at 13% increase.

Neuropathology analysis, using the most efficacious dose in the survival and open field analyses of 20 mg/kg, showed that gross atrophy of the spinal cord was not significantly different in **1a**-treated versus untreated G93A mice, although greater than the untreated group. While there was a reduction in gross atrophy of the lumbar spinal cord in **1a**-treated G93A mice, in comparison to untreated G93A mice (untreated G93A

mice: 2.26 ± 0.44 x 10^6 µm^3; **1a**-treated G93A mice: 2.61 ± 0.27 x 10^6 µm^3, p<0.48) it was not significant. Consistent with the above findings, there was no significant reduction in ventral horn neuronal loss in the **1a**-treated G93A mice, as compared to the untreated G93A mice (untreated G93A mice: 26.3 ± 17.2; **1a**-treated G93A mice; 45.1 ± 15.3, p<0.42), although there was a greater number of neurons remaining in the **1a**-treated mice.

In vivo half-life of 8c and activity in the SOD1 G93A ALS mouse model

Maximum blood levels of **8c** (CMB-087820) by i.p. administration occurred at 12 h, but brain penetration was only 8.3 uM. Control and transgenic mice of the same age (± 3 days) and from the same "f" generation were selected from multiple litters to form experimental cohorts. The tolerable dose range for **8c** was determined in wild-type mice by increasing the dose b.i.d., and the maximum tolerated dose was over 5 g/kg with a cumulative dose of 10 g/kg. On the basis of the ADME and MTD studies, the dose levels of 10, 20, and 30 mg/kg were administered daily, starting from 6 weeks of age to the end of life of the G93A mice. Administration of **8c** resulted in a 13% extension in survival at 20 mg/kg compared to untreated G93A mice (Figure 18). This result is slightly better than that observed for the only FDA approved drug riluzole, which showed a lifespan extension of 10-11% at 22 mg/kg in the same animal model. Possibly the reason better life extension was not obtained with **8c** was because brain penetration was found to be only 8.3 uM, a few percent of the blood level, which may account for the relatively low activity observed.

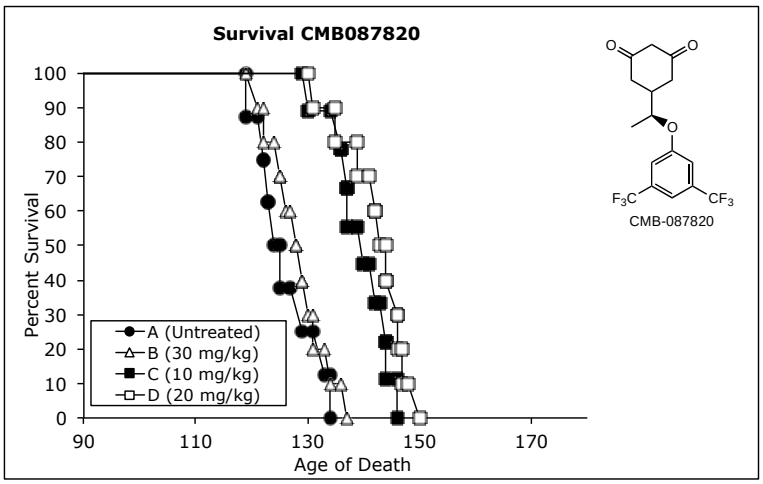

Figure 18. Kaplan-Meier plot of **8c**-treated SOD1 G93A ALS mice: untreated group, 125.7 ± 4.3 days; group 1 (10 mg/kg), 139.2 ± 8.3 days; group 2 (20 mg/kg), 142.0 ± 9.1 days (p < 0.03); group 3 (30 mg/kg), 127.9 ± 4.7 days; p < 0.05). CMB-087820 is **8c**.

Neuropathology analysis in untreated G93A mice at 120 days revealed marked gross spinal cord atrophy, with neuronal loss in the ventral horns from the lumbar spinal cord in untreated G93A mice, in comparison to wild type littermate control mice. The pathology findings in the untreated G93A mice were not significantly reduced by **8c** (20 mg/kg) administration, the best dose found in the behavioral and survival analyses. While there was a reduction in gross atrophy of the lumbar spinal cord in **8c**-treated G93A mice, in comparison to untreated G93A mice (untreated G93A mice: 2.15 ± 0.46 x 10^6 µm^3; **8c**-treated G93A mice: 2.45 ± 0.29 x 10^6 µm^3, p<0.57) it was not significant. Consistent with the above findings, there was no significant reduction in ventral horn neuronal loss in the **8c**-treated G93A mice, as compared to the untreated G93A mice (untreated G93A mice: 25.1 ± 16.8; **8c**-treated G93A mice; 39.2 ± 14.1, p<0.38).

In vivo half-life of the phosphate salt of 6 (R^1 = Me, R^2 = 3,5-dichloro) and activity in the SOD1 G93A ALS mouse model

Eight wild-type mice were given increasing doses of the phosphate salt of **6** (R^1 = Me, R^2 = 3,5-dichloro) injected IP twice per day, starting at 40 mg/kg and doubling with every dose thereafter. After 640 mg/kg was

injected, 50% of mice began to show mild symptoms of discomfort, including huddling, piloerection, trembling and an altered gait. After 1280 mg/kg, 50% of mice showed severe adverse affects, including a decrease in body temperature, altered breathing, and severely impaired movement. After 2560 mg/kg, 25% of the mice were dead. Thus, the MTD, defined as the maximum dose at which no adverse effects were seen, is 320 mg/kg. The phosphate salt of **6** (R^1 = Me, R^2 = 3,5-dichloro) has good blood-brain barrier penetration with a $T_{1/2}$ of 3 h; the brain:blood ratio is 0.9 (Figure 19).

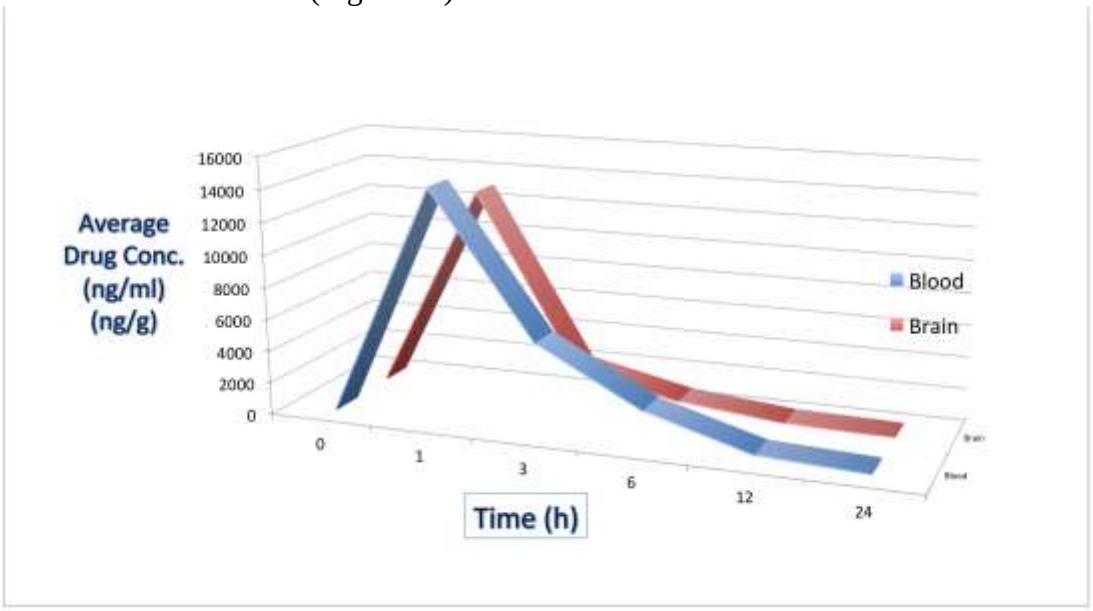

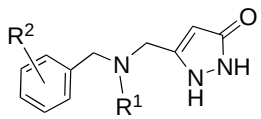

6

Figure 19. Blood and brain concentration of the phosphate salt of **6** (R^1 = Me, R^2 = 3,5-dichloro) after injection with 300 mg/kg.

Mice received daily injections of 20 mg/kg of the phosphate salt of **6** (R^1 = Me, R^2 = 3,5-dichloro). The cohorts were made of 12 male mice each and distributed based on parentage, weight and genotype. IP injections of drug began at 30 days of age and continued until death. There was a slight, but not significant, difference between the treated and untreated animals with regard to distance traveled, resting time, ambulatory time, ambulatory counts, body weight, and survival.

We continued to breed, characterize, and maintain selective stocks of transgenic mutant G93A ALS mice and littermate control mice for the drug discovery and translational studies. Fifteen breeding triads (1 male, 2 females) were organized every 2 months, and on average eight pups were born per litter. Seventy five to eighty percent of the dams became pregnant, which provided 100 littermate wild type and 100 mutant G93A mice. All mice were genotyped and ear tagged at 15 days to ensure proper placement into the studies. Mice were weaned at 21 days and placed into experimental cohorts for maximum tolerated dose, PK, or in vivo preclinical trials. Mutant SOD1 copy number was analyzed to ensure that the mice were genetically comparable and that there had not been a change in the mutant gene copy number. Male mice were used as breeders for the next generation. The MTD and PK studies required 10 and 18 mice, respectively. The preclinical trials required 50 mice, 40 mutant G93A, and 10 littermate control wild type mice.

Maximum Tolerated Dose (MTD) and Pharmacokinetic (PK) Studies of Other Analogues

We performed MTD and PK studies using nine novel compounds generated in the Silverman laboratory. Some studies were repeated because they were a new batch of compound or to resolve toxicity issues. The compounds included CMB-087229 (**1a**), CMB-087816 (**10**), CMB-086874 (**7**), CMB-021805 (**11**), CMB-087839 (**6**, R^1 = CH_3, R^2 = 3,5-dichloro), CMB-087885 (**12**, X^- = chloride), **12** (X^- = tartrate), **12** (X^- = citrate), **12** (X^- = phosphate), and CMB-087822 (**9c**). Repeat MTD and PK analyses were completed on new

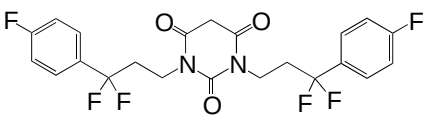

10

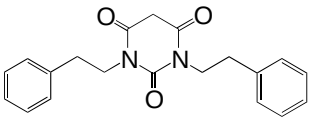

11

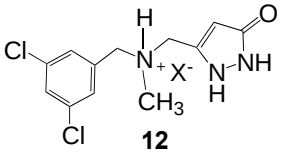

12

compound shipments of **1a** and **11** to ensure that their activity was comparable to the previously synthesized agents. These agents were used in a novel or repeat preclinical trial with G93A mice and for mechanistic studies. Compounds **10** and **7** failed to reach MTD with a dose of 5,000 mg/kg.

A summary of the animal efficacy studies is shown in Table 2.

Table 2. Summary of Advanced Compound Status

Compound	Scaffold	Structure	Key observations
CMB-021805 **11**	PYT	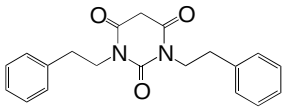	MTD = 100 mg/kg, excellent oral absorption, good BBB penetration (~33% blood level), short half life (~60 min in vitro, ~45 min.), maximum 31% lifespan extension in ALS mice
CMB-087816 **10**	PYT	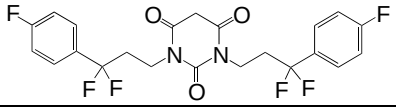	MTD >5000 mg/kg, short half life (~80 min in vitro)
CMB-087229 **1a**	AXP, X = O	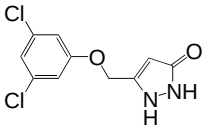	MTD = 75 mg/kg, good BBB penetration (~55% blood level), maximum 13% lifespan extension in ALS mice, poor bioavailability?
CMB-087839 **6**	AXP, X = NR	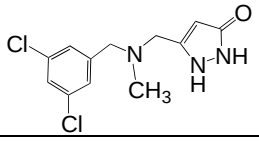	MTD LD_{50} = 1280 mg/kg
CMB-087889 **12**	AXP, X = NHR	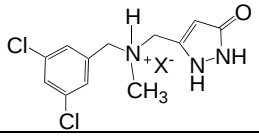	Chloride and tartrate salts are irritants in mice – phosphate salt was well tolerated with MTD 320 mg/kg
CMB-086874 **7**	CHD	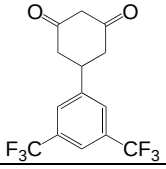	MTD = 75 mg/kg, excellent BBB penetration (100% blood level), in vitro half life >180 min., no effect on lifespan in ALS mice, inactive on neurons and most other cell types
CMB-087820 **8c**	CHD	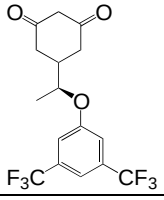	MTD >5000 mg/kg, in vitro half life ~60 min., 13% lifespan extension in ALS mice, poor brain penetration (few % of blood level)
CMB-087822 **9c**	CHD	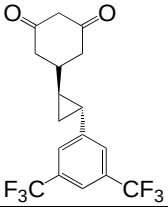	MTD = 1280 mg/kg

In Vivo *C. elegans* Model Studies

Pharmacological and genetic approaches were integrated using Morimoto's previously described *C. elegans* model for ALS.[2] *C. elegans* has several characteristics that make it ideal for drug studies, including a short lifecycle, small size, and ease of culturing in liquid. Furthermore, decades of genetic, and neurobiological

and antiparasitic drug studies in *C. elegans* provide a strong foundation for use of this organism in experiments designed to uncover pathways involved in a compound's mechanism of action. The Morimoto *C. elegans* ALS models express wild type and three mutant SOD1 variants (G85R, G93A, and 127X) in body wall muscle cells. The ability to employ dynamic imaging in live animals allows the visualization of the SOD1 protein in the muscle cells. While WT SOD1 protein remains soluble, all three mutant SOD1 proteins form aggregates in early development. Expression of these aggregation-prone proteins caused a decrease in motility (25-30% compared to wild type), indicating toxicity. Taking advantage of these phenotypes, our compounds were tested to determine if they could suppress protein aggregation and toxicity in the *C. elegans* model. If the compounds reduced aggregation and toxicity significantly, genetic approaches could be employed to identify pathways of drug action.

To determine whether the compounds protect cells against the toxic effects of aggregated variants of SOD1, each lead compound and several of their analogues were tested for their ability to restore motility in the *C. elegans* model. Since the lead compounds reduced cytotoxicity in PC12 cells expressing mutant G93A SOD1, the *C. elegans* model expressing G93A was utilized to test whether the compounds improve motor performance. Motility of animals was calculated by capturing movies using SimplePCI. Using ImageJ, the position of all animals was determined and animals were tracked. The length of the track was calculated as the sum of the lengths of all movement vectors. The average speed (pixels per frame) was the sum of all movement vectors divided by the total number of vectors (tracks). Speeds were converted from pixels per frame into body lengths per sec (BLPS). G93A expressing animals were treated with three different concentrations of compounds, 10 μM, 100 μM, and 1.5 mM. In some cases, addition of the drug at high concentrations yielded toxicity. The highest concentration that was not toxic to the animals was selected for motility tests. Geldanamycin (GA), a compound that inhibits the chaperone HSP90 and induces expression of other chaperones, restored motility to near wild type levels, as anticipated (the speed of wild type is 0.071+/-0.008 BLPS, G93A is 0.044+/-0.002, and the speed of geldanamycin treated animals is 0.061+/-0.005) (Figure 20). The test compounds did not perform as well as geldanamycin, reaching speeds of 0.053 BLPS, but the compounds did provide protection in the cytotoxicity screen by partially suppressing the motility defect. Therefore, the ability of a subset of compounds to reduce aggregation of G93A was tested. A small decrease in overall aggregation of G93A was observed, reflecting the small improvement in motility. However, with the goal of utilizing genetic manipulations, these differences in aggregation and toxicity are not robust enough to employ genetic screens to dissect the mechanism of drug action.

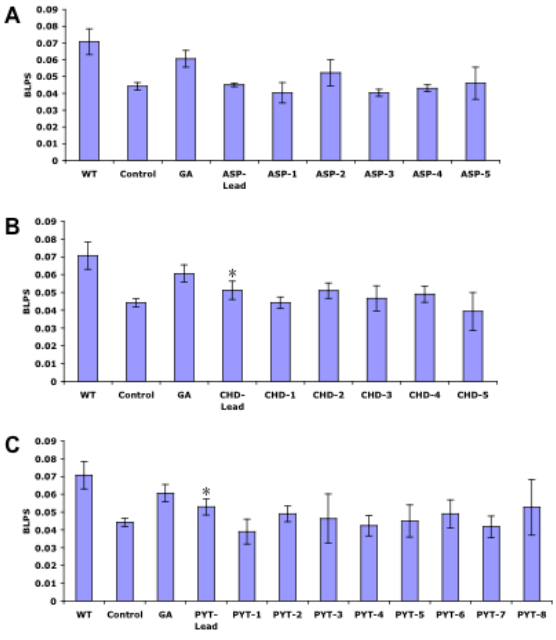

Figure 20. Compounds reduce the toxicity associated with expression of G93A in body wall muscle cells. The ASP (A), CHD (B) and PYT (C) scaffolds and their analogs were tested for suppression of the motility defect caused by G93A. The body length per sec (BLPS) of wild type animals is 0.071+/-0.008. G93A expressing animals move at a rate of 0.044+/-0.002; the speed of geldanamycin treated animals was 0.061+/-0.005. The largest improvement for each scaffold was ASP-2 (0.052+/-0.008), CHD-Lead (0.051+/-0.005) and the PYT-Lead (0.051+/-0.005). Those with $p<0.05$ are highlighted (*).

Previous efforts focused on the *C. elegans* ALS models that express wild type and three mutant SOD1 variants (G85R, G93A, and 127X) in body wall muscle cells. While WT SOD1 protein remains soluble, all three mutant SOD1 proteins form aggregates in early development. Expression of these aggregation-prone proteins causes a decrease in motility (25-30% compared to wild type), indicating toxicity. Taking advantage of these phenotypes, we tested whether **1a, 7,** and **11** could suppress protein aggregation and toxicity in the *C. elegans* model. If the compounds reduced aggregation and toxicity significantly, we could employ genetic approaches to identify pathways of drug action. We found that the test compounds did not perform as well as geldanamycin, but the compounds did provide protection in the cytotoxicity screen by partially suppressing the motility defect of G93A expressing animals. Therefore, we tested for the ability of **1a, 7,** and **11** to reduce aggregation. A small decrease in overall aggregation of G93A was observed, reflecting the

small improvement in motility. However, with the goal of utilizing genetic manipulations, these differences in aggregation and toxicity are not robust enough to employ genetic screens to dissect the mechanism of drug action.

Approaches to Target Identification

In Vivo Neurotoxicity and Gene Profiling Studies

To provide a better understanding of the mechanism of action of these novel analogs, we undertook neurotoxicity and gene profiling studies in both G93A and G85R models of ALS. We have performed gene array studies that have provided leads consistent with disease mechanisms. These findings have led to further experimental studies using 3-nitropropionic acid as a mitochondrial inhibitor resulting in mitochondrial dysfunction. We have furthered these experiments, completing conformational studies in the G93A mice.

We began our query with CMB-021805 by looking at changes in a general neurotoxicity PCR array, profiling the expression of 84 key genes involved in drug and chemical-induced neurotoxic responses (SABiosciences) using both G93A and G85R ALS mouse models. Quantifiable gene expression changes that occur prior to gross morphological changes allow an earlier identification and determination of neurotoxicity and the more specific mechanisms behind it. The organization of genes by their predicted direction of expression change allows for a more exact data analysis. Using real-time PCR, we analyzed the expression of a focused panel of genes involved in neurotoxicity. Our results provided a number of hits, the greatest of which were close to a four-fold change and associated with mitochondrial protection (superoxide dismutase 2, SOD2; angiopoietin-like 4, Angptl4; and Fas ligand TNF superfamily, FasL) (Table 3 and Figure 21). Increased SOD2 is especially interesting, as we have previously reported that crossing experiments with SOD2 overexpressors

Table 3. Fas ligand (TNF superfamily, member 6) APT1LG1, CD178, CD95L, Fas-L, Fas-Ligand, Faslg, Tnfsf6, gld, superoxide dismutase 2, mitochondrial MGC6144, MnSOD, Sod-2.

				Fold Change
C09	Fasl	0.000722858	0.000181719	3.977880675
F09	Sod2	0.023947187	0.006407601	3.737309388
A02	Angptl4	0.000103076	0.000028752	3.585066798
D11	Il10	0.000033534	0.000012343	2.716972569
A08	Bdnf	0.002624030	0.001020859	2.570412675
B01	Casp7	0.163345657	0.068109507	2.398279828
B10	Col12a1	0.000029601	0.000012515	2.365262
F11	Tnfrsf10b	0.000089733	0.000042095	2.131693472
F03	Pou1f1	0.000018096	0.000009035	2.002774511
F08	Slc16a3	0.000204729	0.000102933	1.988940337

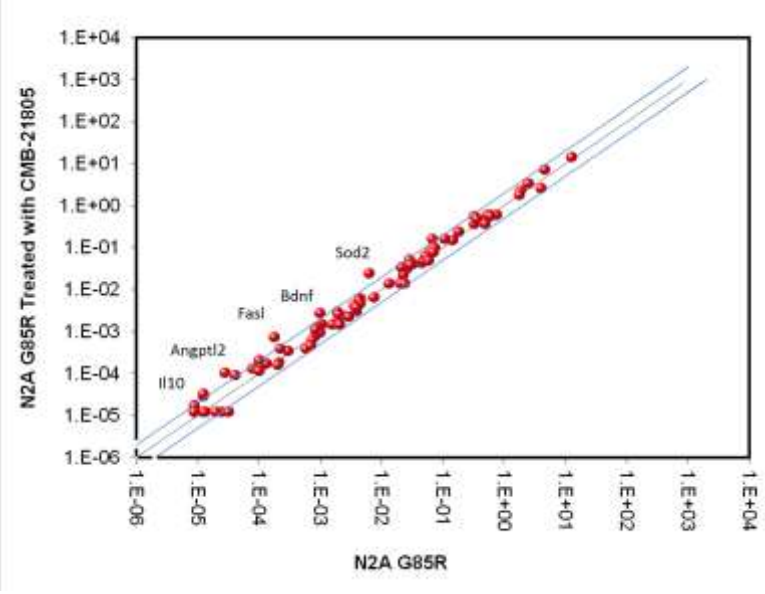

Figure 21. Scatter plot of select genes associated with neuroprotection in the N2a mutant G85R cell line

and G93A mice is neuroprotective and leads to increased survival.[3] The next group, with three-fold change, included brain-derived neurotrophic factor (BDNF) and interleukin 10 (Il10), an anti-inflammatory cytokine, both of which are involved in neuroprotection and relevant to the disease process in ALS. There were another half dozen genes that were down regulated and associated with apoptosis. These findings provide evidence to suggest that mitochondrial neuroprotection might be involved as one mechanism of action for CMB-021805. As such, we next used a model of mitochondrial derangement, administering 3-nitropropionic acid (a selective inhibitor of the mitochondrial electron transport chain), with concomitant administration of CMB-021805, to determine whether any further evidence of neuroprotection was associated within the mitochondrial pathway. We used SABiosciences PCR array profile analysis, monitoring genes, including regulators and mediators of mitochondrial molecular transport, not only the metabolites needed for the electron transport chain and oxidative phosphorylation, but also the ions required for maintaining the mitochondrial membrane polarization, which are potentially important for ATP synthesis. This array's genes also target and translocate previously translated and folded proteins across and/or into the outer and/or inner mitochondrial membranes and even into the mitochondrial matrix. Indeed, CMB-021805 not only slowed neuronal (N2a G85R) cell death after 3-nitropropionic acid administration, but it also provided a gene array profile, indicating mitochondrial improvement (Figure 22). In this experiment, those mitochondrial-associated genes that were down regulated

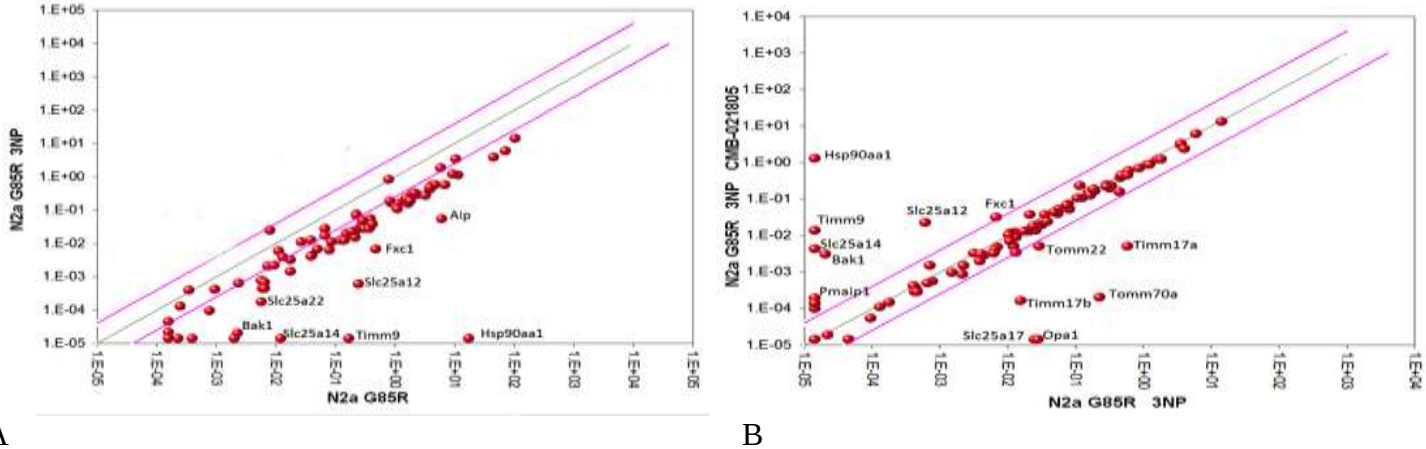

A B

Figure 22. Scatter plots of N2a G85R cells treated with 3-nitropropionic acid resulting in the down-regulation of mitochondrial associated genes (A) that were reversed by the administration of CMB-021805.

by 3-nitropropionic acid (e.g., aryl-hydrocarbon receptor-interacting protein, Aip; BCL2-antagonist/killer 1, Bak1; fractured callus expressed transcript 1, Fxc1; heat shock protein 90, alpha (cytosolic), class A member 1, Hsp90, and solute carrier family 25, Scl25 genes) were all significantly upregulated by the administration of CMB-021805. These findings suggest that CMB-021805 is neuroprotective by improving mitochondrial

function.

Lastly, to help provide evidence for confirmation of the gene changes with respect to CMB-021805, we analyzed the expression of SOD2 and BDNF in Western analyses from *in vivo* experiments in G93A ALS mice. Mice were given continuous daily intraperitoneal injections of CMB-021805 (20 mg/kg) for two weeks and euthanized. The brain was immediately quenched and analyzed. Consistent with the G85R studies, there was significant increased expression of SOD2 and BDNF in the brains of treated mice in comparison to untreated G93A mice. The levels of each protein reached that observed in wild type mice (Figure 23).

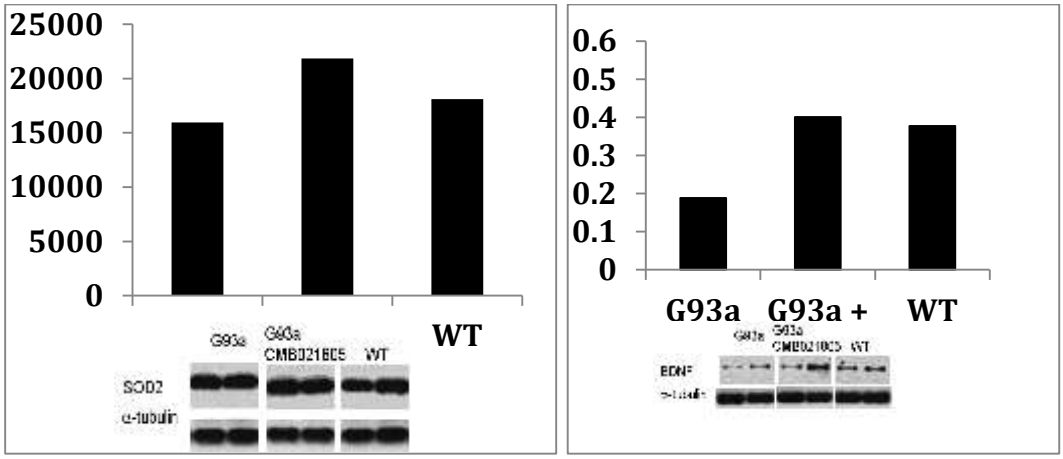

A B

Figure 23. Western analysis of SOD2 (A) and BDNF (B) in G93A mice treated with CMB-021805.

Attempts at target identification via pharmacological and functional screening

Compound **1** (R_1 = R_2 = H) was sent to NIMH Psychoactive Drug Screening Program at the University of North Carolina, where pharmacological and functional screening is carried out on a large number of CNS receptors, channels, and transporters. The only CNS protein in the tested panel affected by this compound was GPCR metabotrophic glutamate receptor 5 ($mGluR_5$), which was antagonized 65% at 10 uM concentration. Antagonists of this receptor have been shown to be therapeutic in ALS.[4] However, when a variety of known $mGluR_5$ and other mGluR receptor antagonists were screened in our cell-based assay, none showed any activity (Table 4). It is apparent that our assay is not sensitive to this class of receptors, and it is therefore highly unlikely that $mGluR_5$ antagonism is the primary mechanism for the activity of this compound.

Table 4. Effect of metabotrophic glutamate receptor antagonism on our cell-based assay

Structure	Name	Target	Potency (IC_{50})	Neuroprotection (EC_{50})
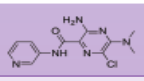	ACDPP	mGluR5	Ki = 295 nM	>32 uM
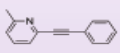	MPEP	mGluR5	36 nM	>32 uM
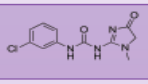	Fenobam	mGluR5	87 nM	>32 uM
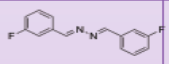	DFB	mGluR5	3-5 fold potentiation	>32 uM
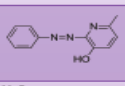	SIB	mGluR5	0.4 uM	>32 uM
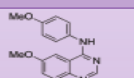	LY 456236	mGluR1	143 nM	>32 uM
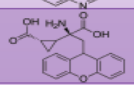	LY 341495	mGluR2/ mGluR3	2.3 nM 1.3 nM	>32 uM

Approaches to Identify the Target of Activity via in vivo studies

Our most promising novel compound, CMB-021805 (**11**), arose from the pyrimidine 2,4,6-trione chemical scaffold. Compound **11** shows superior biological performance as a disease-modifying therapeutic candidate, with excellent drug qualities, very low toxicity, superb oral and blood absorption, and good blood-brain barrier penetration.[5] We have furthered these experiments, completing confirming studies in G93A SOD1 mice. To provide a better understanding of the biological activity of these novel analogues, we have expanded our previous findings associated with the biological effects of compound **11**. We have identified actions of **11** that, in addition to anti protein-aggregation properties, improve brain-derived neurotrophic factor, reduces oxidative stress, modulates aberrant nucleosomal dynamics, and significantly ameliorates mitochondrial dysfunction. Moreover, **11** is highly neuroprotective in both *in vitro* and *in vivo* model systems of ALS. In both clinically presymptomatic and symptomatic therapeutic trials in ALS mice, **11** had dose-dependent benefits, slowing functional motor performance decline, and markedly ameliorating the neuropathological phenotype observed in ALS mice after clinical disease expression. Consistent with the improved clinical and pathological phenotype, we have also found that **11** is neuroprotective against altered signaling cascades in ALS mice. These data suggest that **11** has salient pleiotropic properties that may provide efficacy in ALS patients.

We performed a Western analysis for markers of mitochondrial function and biogenesis (SOD2, PGC-1a, and TFAM) and mitochondrial dynamics fission (Drp1) and fusion (Mfn1) proteins, and found that they were markedly changed in mutant G85R N2a cells, compared with wild type control cells (Figure 24). While SOD2, PGC-1a, and TFAM were significantly reduced, Drp1 and Mfn1 were significantly increased. The levels of Drp1 and Mfn1 in wild type N2a cells were not significantly different, confirming previous studies that both fission and fusion of mitochondria are at equilibrium under normal conditions. These findings are consistent with the hypothesis that mitochondrial dynamics are disrupted in ALS. Mutant G85R N2a cells treated with **11** showed significantly increased levels of SOD2, PGC-1a, and TFAM, while normalizing Drp1 and Mfn1 to wild type levels (Figure 24). In addition, oxidative stress may mediate mitochondrial dysfunction and, as such, we administered **11** to N2a mutant G85R cells, resulting in improved cell viability by 25%, as measured using a colorimetric assay (MTS) (Figure 24). We induced oxidative stress and serum deprivation in N2a G85R cells using hydrogen peroxide (500 mM), as this oxidative stressor is a potential pathophysiological mechanism in ALS. Cell death was significantly increased in untreated cells, while **11** administration resulted in significant protection (Figure 24).

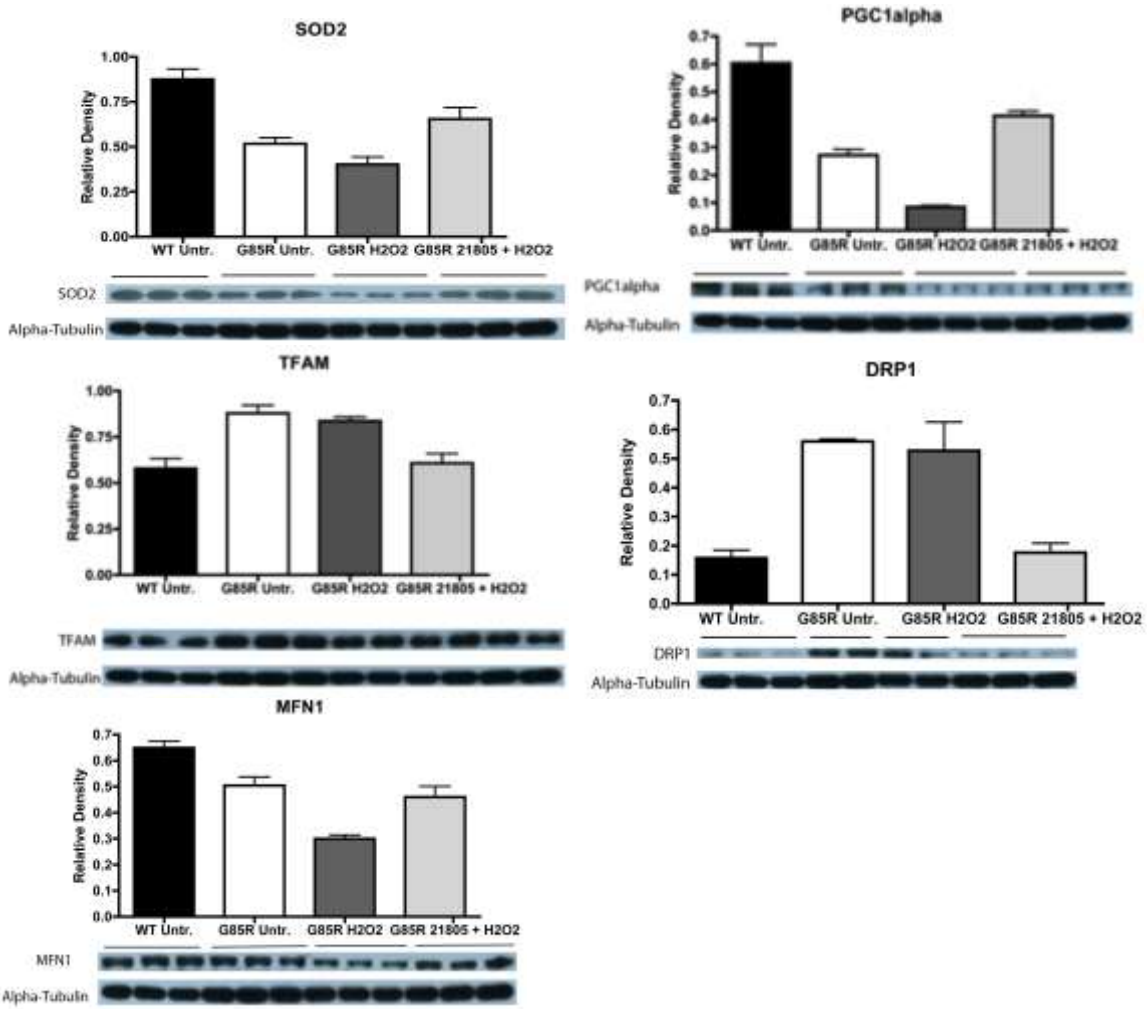

Figure 24. Western blots for markers of mitochondrial function and biogenesis (SOD2, PGC-1a, and TFAM) and mitochondrial dynamics fission (Drp1) and fusion (Mfn1) proteins, and show that they were markedly changed in mutant G85R N2a cells, as compared with wild type control cells and **11** treated cells. Compound **11** also protected G85R mutant SOD cells from oxidative stress using hydrogen peroxide.

Recent studies suggest that transcriptional dysregulation may play a role in the pathogenesis of ALS. Transcription is regulated by complex interactions between many proteins, many of which are regulated by covalent modifications, such as acetylation, methylation, and phosphorylation. There is strong evidence that hypoacetylation is found in both ALS patients and in ALS mice. We have observed that hypoacetylation and hypermethylation are present in N2a G85R cells, in comparison to wild type N2a cells, and that treatment with **11** normalizes the altered chromatin remodeling (Figure 25). Compound **11**, therefore, acts to normalize nucleosomal dynamics in regulation transcription.

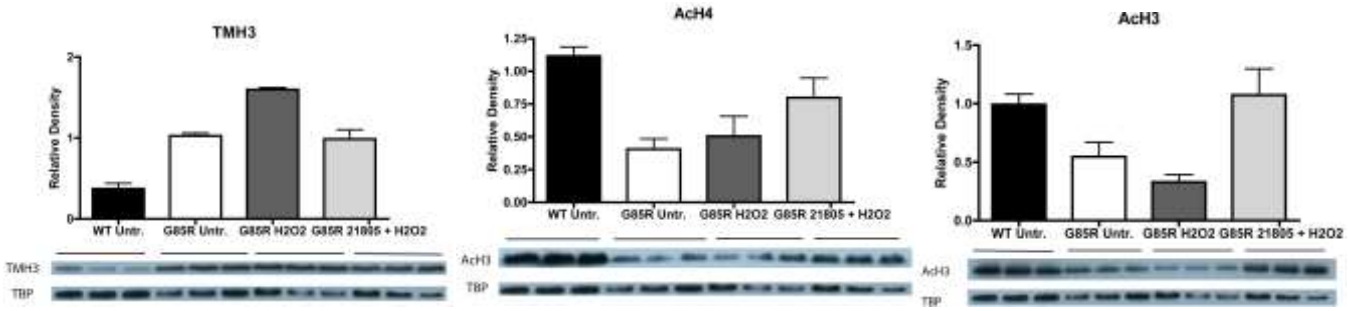

Figure 25. Chromatin Dynamics N2a G85R treated untreated **11**. Trimethyl histone 3 (TMH3) and acetylated histones 3 and 4 (AcH3 and AcH4) are altered in the G85R cells and further exacerbated by oxidative stress. Compound **11** treatment ameliorates both methylation and acetylation alterations.

Consistent with the N2a G85R mutant SOD findings, treatment of mutant G93A mice with **11** produces normalized levels of PGC-1a, TFAM, Drp1, and Mfn1 (Figure 26).

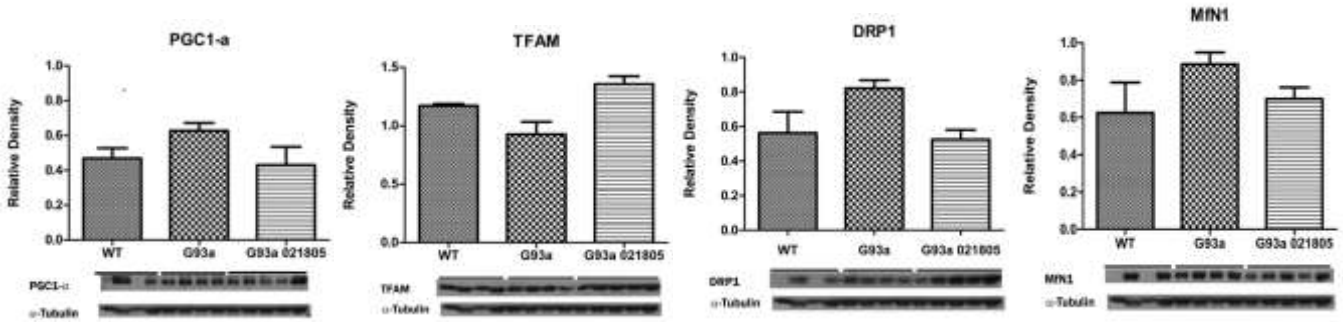

Figure 26. Compound **11** treatment in G93A mice was neuroprotective and improved mitochondrial dysfunction, normalizing levels of mitochondrial proteins.

Protein chip array studies

Protein chip arrays can be used to rapidly test large numbers of human proteins for their ability to bind to compounds of interest.[6] A recent study of this type successfully identified the target of D156844, a compound currently in development for the treatment of spinal muscular atrophy (SMA).[7] Similar to our studies, this chemical scaffold had been identified and optimized using a non-target based cellular assay, suggesting that this experiment was a good model for our own work.

Studies of this type work best with high potency compounds that will provide adequate binding to proteins on the chip. Cell-based assay potency in the 1 uM range is generally considered the minimum potency needed for detection. In addition, the compound probe needs to have aqueous solubility and other physical characteristics to make it compatible with the chip methodology. Of particular importance is low general non-specific protein binding to provide clear detection of binding over background. Lastly, compound labeling is needed with either 1) a low energy isotope such as tritium or ^{125}I (so that the radio decay remains localized to a specific address on the chip) at high specific activity (e.g., >10 Ci/mmol for tritium) to permit detection or 2) a fluorescent tag with adequate quantum yield to allow clear detection of binding on the chip. We considered a variety of compounds among the three scaffolds as candidates for this experiment. Considerations included the disadvantage of a fluorescent tag, which would produce a chemical probe different from the compound producing biological effects of interest, and the ability to isotopically label compound to adequate specific activity. Several compounds were initially explored, but we were able to label only one of these, CMB-021805, to an adequate specific activity. CMB-021805 has a cell based assay potency of 1.68 µM, at or above the minimum level required for a successful protein chip study.[8]

CMB-021805 (**11**) was synthesized with iodine at the para-position of the two phenyl rings by the Silverman group and was sent to the CRO Vitrax for tritium exchange of the iodine atoms. A specific activity of 31.7 Ci/mmol was obtained and, unlike other candidate compounds investigated for radiolabeling, the radiolabel did not exchange out upon standing. Chip studies were performed at Invitrogen under contract. An initial pilot experiment was carried out to determine the background binding of ^{3}H CMB-021805 to 1) determine whether active signals could be detected above background and 2) to optimize conditions for binding studies. As shown in Figure 27, [^{3}H]-CMB-021805 produces moderate non-specific binding, making it difficult to detect binding of [^{3}H]-estradiol spiked into the mixture. Further studies showed that the addition of 1% casein blocked background binding, but not the [^{3}H]-estradiol signals. A full-scale experiment with over 9000 proteins was therefore carried out.

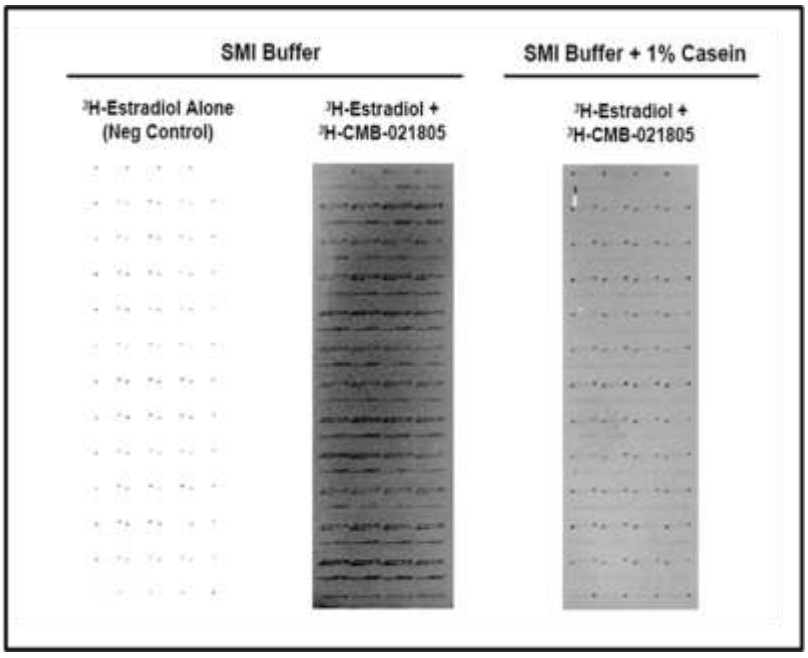

Figure 27. Assay to define and optimize conditions for screening protein arrays, which employs [^{3}H]-estradiol as an internal binding control. [^{3}H]-CMB-021805 produced moderate non-specific binding, making it difficult to detect binding of [^{3}H]-estradiol spiked into the mixture. The addition of 1% casein blocked background binding but not the detection of the [^{3}H]-estradiol signals.

Because of the potentially marginal properties of CMB-021805, relatively generous criteria were chosen to define actives, so as to insure that interactions of interest would not be missed despite the relatively high background produced by the compound:

1) A Z–score of greater than 3.0.

2) A replicate spot intra-assay coefficient of variation of less than 50% for the corresponding protein.

3) An inter-assay coefficient of variation of variation of less than 50% for the corresponding protein.

Some compounds require NaCl to interact with their corresponding protein target *in vitro*, while other compounds only interact in the absence of salt. Still other compounds interact both with and without salt. The experiment was therefore conducted in duplicate in the presence and in the absence of 150 mM NaCl. A total of 42 candidate interacting proteins were detected in the absence of NaCl using the above criteria (Table 5). In the second half of the study, 33 candidate interacting proteins were detected in the presence of 150 mM NaCl

Table 5. Candidate interacting proteins meeting statistical criteria identified in the absence of NaCl.

Database ID	Ultimate ORF ID	Signal. Used	Z-Factor	Z-Score	CI P-Value	Assay	Inter-Assay CV	Replicate Spot CV	Neg Signal. Used	Hits In Other Services	Description
NM_004329.1		1246	0.39	5.08	1.76E-02	SMI #2	25%	5%	122	1	Bone morphogenetic protein receptor type-1A
BC019015.2	IOH12089	1190	0.43	4.80	1.88E-02	SMI #2	15%	3%	116	6	mediator complex subunit 29 (MED29)
BC044612.1	IOH26756	1161	0.28	4.65	2.27E-02	SMI #2	17%	10%	-27	3	glycoprotein M6A (GPM6A)
NM_000861.2	IOH29722	1114	0.31	4.41	2.16E-02	SMI #2	25%	2%	-51	1	histamine receptor H1 (HRH1), transcript variant 4
NM_004724.2	IOH42575	1110	0.34	4.38	2.55E-02	SMI #2	31%	11%	-3	0	ZW10, kinetochore associated, homolog (Drosophila) (ZW10)
NM_016440.1		1051	0.30	4.08	2.60E-02	SMI #2	28%	5%	195	1	Serine/threonine-protein kinase VRK3
NM_015161.1	IOH11244	970	0.18	4.07	3.58E-02	SMI #1	7%	7%	15	1	ADP-ribosylation factor-like 6 interacting protein 1 (ARL6IP1)
BC005177.1	IOH4713	1029	0.42	3.97	2.85E-02	SMI #2	3%	8%	8	2	transmembrane protein 51 (TMEM51)
NM_002802.1	IOH3591	1025	0.34	3.95	2.85E-02	SMI #2	16%	7%	80	3	proteasome (prosome, macropain) 26S subunit, ATPase, 1 (PSMC1)
PHC0076		1025	0.01	3.95	3.48E-02	SMI #2	21%	18%	109	1	interleukin 7 (IL7)
NM_005669.3	IOH45648	946	0.28	3.94	3.95E-02	SMI #1	15%	9%	-31	0	Receptor expression-enhancing protein 5
NM_021101.3	IOH10602	1002	-0.11	3.83	3.94E-02	SMI #2	7%	22%	103	0	claudin 1 (CLDN1)
NM_004779.4	IOH27767	988	-0.05	3.76	3.54E-02	SMI #2	0%	14%	33	0	CCR4-NOT transcription complex, subunit 8 (CNOT8)
NM_005922.1		983	0.25	3.73	2.84E-02	SMI #2	15%	1%	-27	0	Mitogen-activated protein kinase kinase kinase 4
BC000314.1	IOH3485	966	-0.11	3.65	4.34E-02	SMI #2	21%	22%	23	1	Reticulon-1
BC030530.1	IOH21699	965	-0.46	3.64	4.57E-02	SMI #2	16%	24%	-126	0	synovial apoptosis inhibitor 1, synoviolin (SYVN1)
NM_001017417.1	IOH54734	885	0.27	3.61	4.34E-02	SMI #1	9%	6%	142	1	cancer/testis antigen family 45, member A1 (CT45A1), mRNA.
BC007014.1	IOH7141	954	-0.42	3.58	4.75E-02	SMI #2	14%	25%	76	0	tumor necrosis factor, alpha-induced protein 8 (TNFAIP8)
NM_004955.1	IOH3983	951	-0.27	3.56	4.63E-02	SMI #2	31%	23%	123	3	solute carrier family 29 (nucleoside transporters), member 1 (SLC29A1), nuclear gene encoding mitochondrial protein, transcript variant 5
NM_000850.2	IOH9886	944	0.08	3.53	3.31E-02	SMI #2	3%	5%	88	6	glutathione S-transferase M4 (GSTM4), transcript variant 1
NM_023015.3	IOH41890	866	0.02	3.50	5.22E-02	SMI #1	9%	13%	48	0	integrator complex subunit 3 (INTS3)
NM_024754.2	IOH12500	937	0.39	3.50	3.34E-02	SMI #2	11%	4%	69	0	pentatricopeptide repeat domain 2 (PTCD2)
NM_006746.1	IOH22321	862	-0.10	3.48	5.53E-02	SMI #1	0%	16%	113	2	sex comb on midleg-like 1 (Drosophila) (SCML1), transcript variant 2
BC003555.1	IOH4980	854	0.33	3.44	4.42E-02	SMI #1	7%	2%	55	1	nucleolar complex associated 2 homolog (S. cerevisiae) (NOC2L)
BC015596.1	IOH29335	926	0.43	3.44	3.32E-02	SMI #2	14%	2%	146	0	chromosome 21 open reading frame 51 (C21orf51)
NM_001006946.1	IOH54992	914	-0.55	3.38	5.27E-02	SMI #2	22%	25%	11	0	Syndecan-1
NM_016584.2	IOH39400	902	-1.17	3.32	8.57E-02	SMI #2	3%	44%	1	0	interleukin 23, alpha subunit p19 (IL23A)
NM_174909.1	IOH14735	901	-0.21	3.31	4.99E-02	SMI #2	13%	20%	55	1	transmembrane protein 167 (TMEM167)
NM_005805.2	IOH40112	897	0.16	3.29	3.84E-02	SMI #2	25%	6%	-54	2	26S proteasome non-ATPase regulatory subunit 14
NM_024009.1	IOH11015	826	0.28	3.29	5.15E-02	SMI #1	14%	6%	96	0	gap junction protein, beta 3, 31kDa (GJB3), transcript variant 1
BC006969.1	IOH7343	888	-0.51	3.24	5.63E-02	SMI #2	16%	25%	68	0	dynein, cytoplasmic 2, light intermediate chain 1, mRNA (cDNA clone MGC:12166 IMAGE:3828551), complete cds
NM_004701.2	IOH41218	818	0.17	3.24	5.88E-02	SMI #1	18%	12%	21	3	cyclin B2 (CCNB2)
NM_152285.1	IOH21698	885	0.25	3.23	4.26E-02	SMI #2	29%	10%	62	5	arrestin domain containing 1 (ARRDC1)
NM_016433.3	IOH57161	878	0.24	3.19	3.72E-02	SMI #2	33%	1%	-36	0	Glycolipid transfer protein
NM_138820.1	IOH4234	877	-0.29	3.19	5.27E-02	SMI #2	19%	20%	19	0	HIG1 domain family, member 2A (HIGD2A)
NM_002930.1	IOH54792	875	0.18	3.18	3.99E-02	SMI #2	15%	5%	124	0	GTP-binding protein Rit2
NM_181270.1	IOH58636	802	-0.16	3.15	6.07E-02	SMI #1	16%	11%	141	2	CKLF-like MARVEL transmembrane domain-containing protein 1
NM_017735.3	IOH40508	867	0.03	3.14	4.74E-02	SMI #2	15%	13%	45	0	Tetratricopeptide repeat protein 27
XM_096472.2	IOH42996	866	0.32	3.13	4.16E-02	SMI #2	11%	6%	185	0	hypothetical LOC143678 (LOC143678)
NM_018019.1	IOH4211	865	-0.20	3.12	4.97E-02	SMI #2	15%	15%	110	2	mediator complex subunit 9 (MED9)
NM_024071.2	IOH3850	781	-1.08	3.04	1.57E-01	SMI #1	11%	50%	7	0	zinc finger, FYVE domain containing 21 (ZFYVE21)
P2999		849	0.22	3.04	4.42E-02	SMI #2	24%	6%	13	1	v-akt murine thymoma viral oncogene homolog 1 (AKT1), transcript variant 3

(Table 6). A comparison of the two lists showed that there were 18 candidate interacting proteins in common. Invitrogen had previously conducted this experiment with nine other chemical compound probes. In the course of this work they discovered that some proteins are 'sticky' and interact non-specifically with many structurally diverse compounds. The second column from the right shows the number of times each protein on the list had been identified in prior studies. A large number of prior identifications suggests that the current interaction might not be specific.

In summary, after removing duplicates, there were a total of 57 hits that met the criteria for activity. An initial analysis of these data indicates the following:

- Approximately 20% of the candidate interacting proteins are kinases or other proteins that have nucleotide binding sites. This may simply reflect the fact that such proteins are overrepresented as a result of early decisions taken in the design of the chips.
- Approximately 10% of the candidate interacting proteins are proteins involved in transcription or RNA processing. Genes identified in familial ALS have suggested that the disease may result from defects in RNA processing or transport.[9]
- There are multiple chaperones on the chip so, consistent with prior findings, the lack of chaperone hits suggests that CMB-021805 does not have a direct action on chaperones.
- Approximately 10% of the candidate interacting proteins belong to the greater ubiquitin proteasome family of proteins. This group fits well with the biological effects of CMB-021805, since stimulation of the ubiquitin proteasome system would be expected to accelerate the removal of misfolded proteins. Of particular interest in this group is the proteasome ATPase, PSMC1. PSMC1 (also called Rpt2) has been reported to regulate the opening of the core particle channel of the proteasome.[10] If activated by a small molecule, PSMC1 could potentially accelerate the removal of misfolded proteins. This protein was identified both with and

without NaCl and with better statistics in the presence of 150 mM NaCl, suggesting that salt might stabilize the interaction. However, PSMC1 has previously been detected three times in unrelated studies, suggesting that it may be a generally sticky protein.

Table 6. Candidate interacting proteins meeting statistical criteria identified in the presence of 150 mM NaCl

Database ID	Ultimate ORF ID	Signal. Used	Z-Factor	Z-Score	CI P-Value	Assay	Inter-Assay CV	Replicate Spot CV	Neg Signal. Used	Hits In Other Services	Description
BC019015.2	IOH12089	1467	0.25	5.62	2.04E-02	NaCl #2	24%	10%	116	6	mediator complex subunit 29 (MED29)
NM_002802.1	IOH3591	1377	0.48	5.17	2.12E-02	NaCl #2	26%	4%	80	3	proteasome (prosome, macropain) 26S subunit, ATPase, 1 (PSMC1)
BC000314.1	IOH3485	1217	-0.38	4.38	4.24E-02	NaCl #2	19%	23%	23	1	Reticulon-1
NM_000850.2	IOH9886	1202	0.17	4.30	3.52E-02	NaCl #2	3%	12%	88	6	glutathione S-transferase M4 (GSTM4), transcript variant 1
NM_021101.3	IOH10602	1074	0.46	4.24	2.92E-02	NaCl #1	2%	2%	103	0	claudin 1 (CLDN1)
NM_032907.3	IOH56973	1072	0.24	4.23	3.16E-02	NaCl #1	8%	6%	16	1	Ubiquitin-like protein 7
BC047393.1	IOH26537	1152	-0.18	4.05	4.38E-02	NaCl #2	30%	18%	-41	1	ring finger and CHY zinc finger domain containing 1 (RCHY1)
PV4819		1143	0.15	4.01	3.90E-02	NaCl #2	10%	11%	49	4	MAP/microtubule affinity-regulating kinase 3 (MARK3)
BC046214.1	IOH26987	1137	0.52	3.98	3.21E-02	NaCl #2	31%	0%	2	1	M-phase phosphoprotein 8 (HSMPP8)
NM_152285.1	IOH21698	1010	-0.16	3.89	4.55E-02	NaCl #1	21%	17%	62	5	arrestin domain containing 1 (ARRDC1)
NM_032341.1	IOH7525	1077	0.02	3.68	4.56E-02	NaCl #2	34%	11%	5	6	DDI1, DNA-damage inducible 1, homolog 2 (S. cerevisiae) (DDI2)
BC044612.1	IOH26756	1072	-0.51	3.66	6.06E-02	NaCl #2	11%	23%	-27	3	glycoprotein M6A (GPM6A)
NM_018019.1	IOH4211	1068	-0.20	3.63	4.46E-02	NaCl #2	11%	9%	110	2	mediator complex subunit 9 (MED9)
NM_015161.1	IOH11244	1060	-0.35	3.60	5.45E-02	NaCl #2	13%	17%	15	1	ADP-ribosylation factor-like 6 interacting protein 1 (ARL6IP1)
NM_004329.1		1059	-0.28	3.59	4.74E-02	NaCl #2	23%	10%	122	1	Bone morphogenetic protein receptor type-1A
NM_004724.2	IOH42575	946	0.30	3.53	4.09E-02	NaCl #1	4%	3%	-3	0	ZW10, kinetochore associated, homolog (Drosophila) (ZW10)
NM_016440.1		906	0.02	3.31	5.23E-02	NaCl #1	0%	9%	195	1	Serine/threonine-protein kinase VRK3
NM_000975.2	IOH1740	1001	0.12	3.30	4.95E-02	NaCl #2	10%	5%	25	1	ribosomal protein L11 (RPL11)
NM_004955.1	IOH3983	998	-0.17	3.29	6.53E-02	NaCl #2	12%	18%	123	3	solute carrier family 29 (nucleoside transporters), member 1 (SLC29A1), nuclear gene encoding mitochondrial protein, transcript variant 5
NM_181270.1	IOH58636	992	-0.24	3.26	5.96E-02	NaCl #2	9%	13%	141	2	CKLF-like MARVEL transmembrane domain-containing protein 1
BC002559.1	IOH4053	990	0.07	3.25	5.05E-02	NaCl #2	8%	5%	-16	3	YTH domain family, member 2 (YTHDF2)
NM_024754.2	IOH12500	976	0.04	3.18	5.67E-02	NaCl #2	10%	8%	69	0	pentatricopeptide repeat domain 2 (PTCD2)
NM_052848.1	IOH13249	975	0.08	3.17	5.90E-02	NaCl #2	25%	10%	51	1	coiled-coil domain containing 97 (CCDC97)
NM_144620.1	IOH13940	975	-0.03	3.17	5.64E-02	NaCl #2	15%	8%	40	0	leucine rich repeat containing 39 (LRRC39)
NM_006701.2	IOH3749	973	0.24	3.17	4.94E-02	NaCl #2	27%	1%	59	1	thioredoxin-like 4A (TXNL4A)
NM_152255.1	IOH39607	973	-1.70	3.16	1.75E-01	NaCl #2	15%	49%	-9	0	proteasome (prosome, macropain) subunit, alpha type, 7 (PSMA7),
NM_152789.1	IOH21683	875	-0.45	3.14	6.18E-02	NaCl #1	23%	13%	20	3	family with sequence similarity 133, member B (FAM133B), transcript
NM_004691.3	IOH57018	968	0.20	3.14	5.50E-02	NaCl #2	1%	6%	153	4	V-type proton ATPase subunit d 1
BC005177.1	IOH4713	872	-1.44	3.12	1.23E-01	NaCl #1	1%	39%	8	2	transmembrane protein 51 (TMEM51)
BC028141.1	IOH21529	868	-0.05	3.10	6.57E-02	NaCl #1	9%	14%	25	2	mixed lineage kinase domain-like (MLKL)
NM_001017417.1	IOH54734	960	-0.69	3.10	7.50E-02	NaCl #2	18%	19%	142	1	cancer/testis antigen family 45, member A1 (CT45A1), mRNA.
NM_000861.2	IOH29722	863	-0.02	3.07	5.74E-02	NaCl #1	22%	7%	-51	1	histamine receptor H1 (HRH1), transcript variant 4
NM_020679.1	IOH21880	943	0.21	3.02	6.03E-02	NaCl #2	28%	7%	129	3	MIF4G domain containing (MIF4GD)

A total of 42 candidate interacting proteins were detected in the absence of NaCl, 33 candidate interacting proteins were detected in the presence of 150 mM NaCl. There were 18 candidate interacting proteins that appeared in both studies producing a total of 57 protein hits. Most of these hits are likely to be artifacts. We therefore contracted Invitrogen to carry out a follow up experiment to try to distinguish which of the candidate interacting proteins are interacting specifically and which non-specifically with **11**. CMB-086887 (**13**) is an analogue that differs from CMB-021805 by only a single methyl group but is inactive in our protein aggregation assay. By repeating the chip experiment with [^{3}H]-CMB-021805 in the presence of **13** as a blocking cold competitor, non-specific interactions should be largely competed off by **13**.

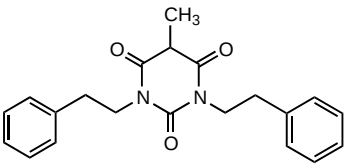

13

However, because **13** is inactive, specific interactions should not be affected. This experiment was conducted in two parts. Stocks of the 9000 protein chip array used in the first experiment had been exhausted and, because array sets are not identical, it was therefore necessary to perform the **13** competition experiment twice using two different array sets in order to cover all the hits from the first experiment. This experimental design turned out to be provident. First, the cold competitor, unfortunately, had little effect on binding in any part of the study. The competitor effects for proteins hit in both the original and the initial follow up study are shown in Table 7. The effects are small, varied, and may not be meaningful. We do not know why this occurred, but one possibility is that despite the fact that the competitor is structurally very similar to **11**, it might bind in a different way. Secondly, actives were defined as showing binding that is greater than three standard deviations

above the mean. Assuming that the data show a normal distribution, one would expect approximately 9 hits to be produced per chip set via statistical fluctuation alone. In addition, these data may not be mean distributed. Chip proteins show variation in general stickiness, and many proteins have been shown to be highly sticky, binding to multiple chemically unrelated probes. This would suggest that the data may not be normally distributed with a bias toward enhanced binding and thus could produce a larger number of artifacts.

Table 7. Results of follow-up study with **11**

Gene	**Annotation**	**% Competition***
Syndecan-1	heparin sulfate cell surface receptor	0%
rpn14	26S proteasome non-ATPase regulatory subunit	4%
ARRDC1	arrestin domain containing 1	9%
MARK3	MAP kinase associated protein	13%
V-type ATPase	V-type proton ATPase subunit – acidifies vacuole	13%
CCDC97	coil-coil domain protein	15%
VRK3	Serine threonine kinase	17%
v-akt homolog 1	AKT1 homolog, kinase, cell survival protein	19%
BMP receptor 1A	cytokine receptor	19%
MED29	associated with RNA polymerase	23%
GST M4	glutathione S transferase	30%

*Maximum observed

Irrespective of the poor performance of the competitor, 44 hits were observed in the first competitor experiment of which 12 were repeats from the first experiment. It is therefore highly likely that the other 45 hits from the first experiment, since they were not repeatable, were artifacts. The second competitor experiment produced 58 hits, only 16 of which were repeats from the first study, and it is, therefore, highly likely that the other 42 hits were non-reproducible artifacts. Examining the three experiments in aggregate, a total of 29 hits were observed at least twice with some of these showing activity three times. This is, in part, a result of the fact that not every protein was present on each of the two types of arrays used, so, as a result, some of the proteins were only tested twice. In addition, a total of 91 additional proteins, all of which were tested at least twice, were hit only a single time. We are at this point considering all non-repeatable hits to be artifacts. Table 8 provides a list of the proteins that showed binding in multiple experiments along with the number of times they were tested.

Table 8. Proteins that showed binding in multiple experiments

Hit in more than one assay			**Protein is present in Lot = x: Not present = 0**					
Phase 1 Hit	1st Phase 2 Hit	2nd Phase 2 Hit	Phase 1 Lot HA20261	Phase 2a Lot HA20266	Phase 2b Lot HA20275	Description	Activity	Hit with other Probes
X		X	x	0	x	Reticulon-1	2/2	1
X		X	x	0	x	YTH domain family, member 2 (YTHDF2)	2/2	3
X	X	X	x	x	x	mediator complex subunit 29, associated with RNA polymerase (MED29)	3/3	6
	X	X	x	x	x	SGT1, suppressor of G2 allele of SKP1 like 1 (S. cerevisiae) (SUGT1L1)	2/3	1
	X	X	x	x	x	chromosome 10 open reading frame 118 (C10orf118)	2/3	2
X		X	x	0	x	glycoprotein M6A (GPM6A)	2/2	3
X	X	X	x	x	x	glutathione S-transferase M4 (GSTM4), transcript variant 1	3/3	6
X		X	x	x	x	histamine receptor H1 (HRH1), transcript variant 4	2/3	1
X	X		x	x	x	Syndecan-1, heparin sulfte surface receptor	2/3	0
X		X	x	0	x	proteasome (prosome, macropain) 26S subunit, ATPase, 1 (PSMC1)	2/2	3
	X	X	x	x	x	39S ribosomal protein L12, mitochondrial	2/3	1
	X	X	x	x	x	Bifunctional purine biosynthesis protein PURH	2/3	2
X	X		x	x	x	Bone morphogenetic protein receptor type-1A	2/3	1
X	X	X	x	x	x	V-type proton ATPase subunit d 1 (acidifies vacuole)	3/3	4
	X	X	x	x	x	tumor protein p53 inducible protein 3 (TP53I3), transcript variant 1	2/3	1
X		X	x	0	x	solute carrier family 29 (nucleoside transporters), member 1 (SLC29A1), nuclear gene encoding mitochondrial protein, transcript variant 5	2/2	3
X	X	X	x	x	x	26S proteasome non-ATPase regulatory subunit 14	3/3	2
	X	X	x	x	x	Rho-related GTP-binding protein Rho6	2/3	4
	X	X	x	x	x	paroxysmal nonkinesigenic dyskinesia (PNKD), transcript variant 1	2/3	5
X	X		x	x	x	Serine/threonine-protein kinase VRK3	2/3	1
X		X	x	x	x	DDI1, DNA-damage inducible 1, homolog 2 (S. cerevisiae) (DDI2)	2/3	6
X		X	x	x	x	Ubiquitin-like protein 7	2/3	1
X		X	x	x	x	leucine rich repeat containing 39 (LRRC39)	2/3	3
X	X	X	x	x	x	arrestin domain containing 1 (ARRDC1)	3/3	5
X	X	X	x	x	x	family with sequence similarity 133, member B (FAM133B), transcript variant 1	3/3	1
X	X	X	x	x	x	v-akt murine thymoma viral oncogene homolog 1 (AKT1), transcript variant 3, kinase	3/3	1
	X	X	x	x	x	Dual specificity tyrosine-phosphorylation-regulated kinase 1A	2/3	0
X	X	X	x	x	x	MAP/microtubule affinity-regulating kinase 3 (MARK3)	3/3	4
X	X		x	x	x	coiled coil domain containing 97 (CCDC97)	2/3	1

Color coding: Red - tested three times and active three times; Yellow - tested three times and active two times; Blue - tested two times and active two times

Proteins that repeated every time tested (i.e., 3/3 or 2/2), are arguably more robust actives than those that were inactive in one experiment (i.e., 2/3). During prior research at Invitrogen their protein chips have been probed with 9 different chemically unrelated compounds. It was this work that demonstrated that some proteins appear to be generally 'sticky'; that is they seem to have a propensity to bind compounds non-specifically. Some of the proteins that were hit in our study, for example MED29, GSTM4 and DD1, previously were found to bind to a variety of unrelated compounds (in these cases 6 out of 9 tested). Therefore, it can be argued that the interaction between these proteins and **11** is likely to be non-specific. Lastly, the annotations indicate that some of the proteins that bind **11** are involved in protein dynamics. Thus, it would be reasonable that a small molecule acting on such a protein would influence protein misfolding and aggregation. An example of one such protein is PMSC1, 26S proteasome subunit that is involved in regulating proteasome activity.

A hit that is of particular interest is the 26S proteasome non-ATPase regulatory subunit 14 (rpn14). Interaction with **11** appears both with and without salt, was found to be active in 3 out of 3 tests and, while the inactive competitor **13** data are suspect due to generally poor performance, it was one of the hits least affected by the inactive competitor (see Table 7). The rpn14 protein is not a component of the mature proteasome, but rather appears to be a negative regulator of 26S proteasome assembly.[11] Inhibition of rpn14 would be expected to reduce protein aggregation; inhibiting an inhibitor should increase proteasome activity, clearing out protein aggregates. The crystal structure of rpn14 was recently reported,[12] so it was therefore possible to produce a model for the binding of **11** to rpn14. Figure 28 shows that there are three reasonable pockets for **11** binding to rpn14.

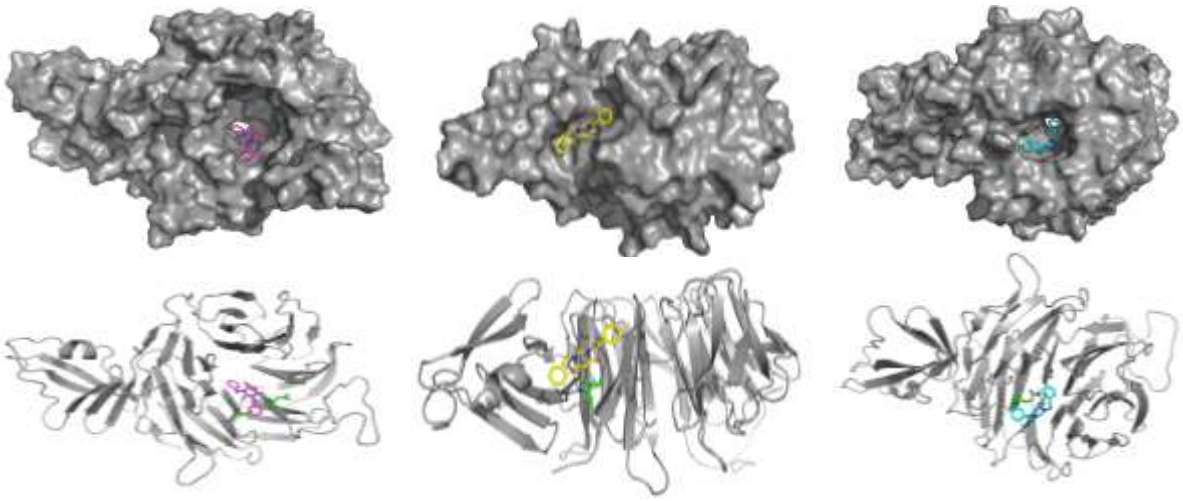

Figure 28. Docking poses of **11** into the crystal structure of rpn14

Genome transcriptional profiling was carried out in the Morimoto lab with CMB-021805 (using HeLa cells) and CMB-003299 (using PC12 cells). Of the 57 hits from the protein array studies (*vide supra*), both claudin 1 and bone morphogenetic protein receptor type-1A (affected both in the presence and absence of NaCl in the gene array study) were altered in these profiling studies as well. CMB-021805 (**11**) reduced the level of the bone morphogenetic protein receptor type-1A (2.5 fold down regulation) while CMB-003299 (ASP) increased the level of claudin 1 (1.6 fold upregulation). Also, syndecan-1 levels increased (1.4 fold upregulation) when CMB-003299 was added. The fact that these hits were observed in two independent, unbiased approaches, suggests biological relevance. The expression levels of the remaining 54 candidates from the protein array studies did not change significantly. Delineation of the target for these molecules also might accelerate progress on the design of ALS therapeutics.

Heat shock response and proteasomal activity

On the basis of the cell-based assay used during preliminary studies we hypothesized that neuroprotective activity would involve modulation of protein folding/refolding, direct inhibition of protein aggregation, or increased protein degradation.[13,14] Hence, initial experiments were carried out to understand the effect of these molecules on the heat shock response and proteasomal activity. Proteasomal activity was assessed using PC12 cells expressing a ubiquitin-tagged yellow fluorescent protein (Ubi-YFP). Treatment with proteasome inhibitor MG-132 resulted in the accumulation of the Ubi-YFP and a corresponding increase in fluorescent signal (untreated = 0.12 AU; MG-132 treated = 0.32 AU, Figure 29A-B). Co-treatment with 1st generation ASPs (CMB-3299 or CMB-3319, Figure 29C) reduced fluorescence to levels equivalent to untreated control experiments. Therefore, ASPs are capable of reversing MG-132 mediated proteasomal inhibition. On its own, this result could indicate direct interaction between ASPs and MG-132. However, our in vivo studies have clearly demonstrated that ASPs possess disease-modifying efficacy in a disease model that does not involve MG-132.[15] On the basis of these considerations, we hypothesize that enhanced proteasomal activity plays an important role in the neuroprotective activity of ASPs.

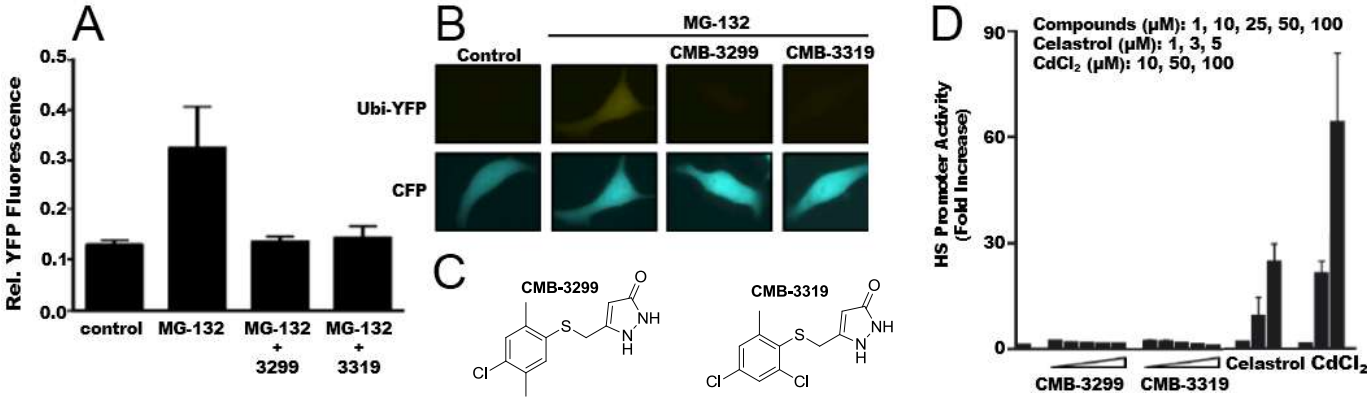

Figure 29. Pyrazolone mechanism of action studies: impact on protein degredation and heat shock response
A-B) Ability of ASP (25 μM) to enhance protein degradation in the presence of the proteasome inhibitor MG-132 (10 nM). Co-expression of a cyan fluorescence protein (CFP) control reporter was unaffected. **C**) Structures of ASP analogs. **D**) ASPs do not induce a heat shock response in a HeLa cell based assay that monitors a Hsp70 promoter-luciferase reporter. Positive controls (celastrol and $CdCl_2$) resulted in a significant increase in heat shock

Induction of the heat shock response (HSR) leads to expression of molecular chaperones and other cell-protective pathways to protect nascent chain synthesis and folding, to prevent misfolding and aggregation, and to promote recovery from stress-induced damage.[13,14,16] Enhanced proteasomal activity is an integral mechanism by which the HSR provides neuroprotection. Therefore, it was speculated that ASPs may enhance proteasomal activity via induction of the HSR. Several ASP analogs were tested for their impact on the HSR using a HeLa cell based assay previously developed by the Morimoto lab, which monitors a Hsp70 promoter-luciferase reporter (results for representative analogs are shown in Figure 29D). No HSR activation was observed, even at concentrations 10-fold higher than the EC_{50} values for neuroprotection. This result establishes that enhanced protein degradation elicited by ASP is independent of HSR induction.

Figure 30. Resin bound BASP cell lysate pull-down experiment

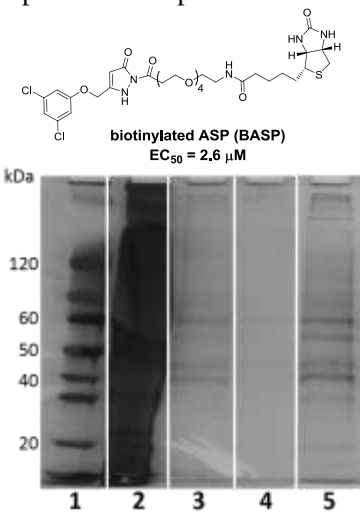

1- Ladder
2- ^{G93}SOD1 lysate (10 uL)
3- Neutravidin resin + lysate (30 uL)
4- 1 h incubation with **CMB-087229** then resin bound **BASP** (30 uL)

In Vitro Pull Down Experiments for Target Identification

Target identification studies were carried out to define the protein target(s) of ASPs and fully understand their mechanism of action. This work involved the use of two complementary techniques: 1) affinity bait experiments employing a resin bound biotinylated ASP (BASP), lysate pull-down, SDS PAGE, and proteomic analysis; and 2) photoaffinity labeling experiments in whole cell culture, in situ functionalization with chemical biology reporters, SDS PAGE, fluorimaging, affinity purification, and proteomic identification.

Affinity bait experiments employing a biotinylated ASP probe.

A biotinylated ASP (**BASP**) was synthesized as described previously.[17] The **BASP** was immobilized on neutravidin bound agarose resin under saturating conditions and incubated with PC12 cell lysate from ^{G93A}SOD1 cells.[18] Nonspecific protein binding was removed by sequential washing with a prepared washing solution (4% DMSO in PBS) followed by elution of the proteins in SDS buffer after denaturation by heating (70 °C, 10 min). The eluted proteins were analyzed by SDS-PAGE and visualized by silver staining (Figure 30). Several bands were observed in the resin bound **BASP** pull-down sample (Figure 30, lane 5). The presence of similar bands in the **BASP** pull-down compared to the neutravidin resin background control (compare lane 5 and lane 3) indicates that the **BASP** bound resin was not entirely saturated by the **BASP**, which led to nonspecific binding of background

biotinylated proteins present in the lysate. The new bands in lane 5 disappeared upon pre-incubation with **CMB-087229** (compare lane 4 and lane 5). Replicate **BASP** pull-down experiments employed in-gel digestion of the 20-150 kDa region (via several 25 kDa sectional excisions) of the SDS PAGE gel or in-solution digestion followed by proteomic analysis by LC-MS/MS. Potential protein targets presented by the database were analyzed by sequence matching probability score, mass, and known biological function.[19] Additional relevance criteria were set as: 1) sequence probability of 99.9% was required for a protein to be considered a hit; 2) the biological function of the protein needed to have a strong relevance to the observed bioactivity.

Proteomic analysis identified the presence of dozens of proteins, some of which had particular relevance to our mechanism of action. Multiple proteasome related proteins and peptide fragments were identified, including: non-ATPase 26S proteasome regulatory subunit 7 (PSMC7); 26S regulator subunit 8 [PSMC5]; 26S regulator subunit 6B (PSMC4); 26S non-ATPase proteasome regulatory subunit 4 (PSMD4, a.k.a. rpn14); 26S non-ATPase regulatory subunit 3 (PSMD3); 26S non-ATPase proteasome regulatory subunit 2 (PSMD2). Additionally, multiple subunits of the T-complex protein 1 (TCP-1), subunits zeta (58 kDa), eta (59 kDa), gamma (61 kDa), alpha (60 kDa), theta (60 kDa), delta (58 kDa), epsilon (60 kDa), and beta (57 kDa) were revealed. TCP-1 is a molecular chaperone that plays a crucial role in the folding of tubulin, actin, and a host of other cytosolic proteins including mutant Huntingtin.[20,21] It has been proposed that TCP-1 interacts with the proteasome and facilitates the degradation of TCP-1 substrates that have misfolded; the TCP-1 complex functions in assisting protein degradation through interaction with the proteasome.[22] These results demonstrate that proteasomal subunits bind to ASPs with relatively strong affinity in cell lysate.

Biotin affinity probe experiments employing cell lysates have been shown to have applications in target ID in the past; however, the inherent poor cell permeability of the biotin moiety limits the utility of the **BASP** in more relevant whole cell experiments. A more desirable paradigm for target ID involves the use of a cell permeable probe to examine the interactions between ligands and target proteins within dynamic biological systems.

Photoaffinity Labeling using a PhotoReactive Alkynyl Pyrazolone Probe (PRAPP)

Probe Design. Design and synthesis of a photoaffinity probe can be one of the major challenges associated with photoaffinity labeling studies and small molecule target ID. Several photoaffinity labeling approaches have been described.[23] Generally, activity-based probes are designed to have the following characteristics: 1) similar efficacy as the lead; 2) a reactive functionality for labeling interacting proteins; 3) appropriate physiochemical properties to allow cell permeation and aqueous solubility; and 4) a conjugation site for modification with chemical biology reporters. A combination of the desire to incorporate these properties and a wealth of SAR data from our previous investigations made it possible to predict *a priori* which chemical probe would be suitable for our specific application. We chose to incorporate a photoreactive moiety at the terminal aryl position and an alkynyl conjugation site off of the tertiary nitrogen of the **CMB-087839** scaffold (Figure 31). A perfluoroaryl azide was chosen as the photolabeling group because it fit seamlessly into our SAR,

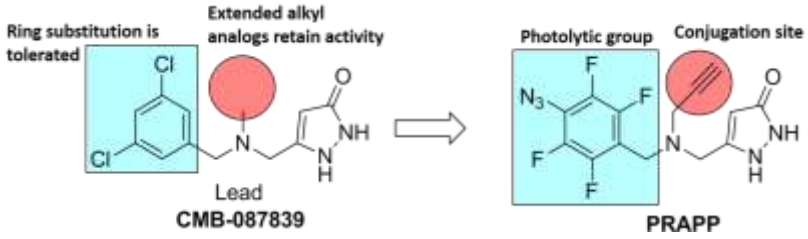

Figure 31. Probe design rationale

and UV activation of perfluoroaryl azides yields high labeling efficiency compared to unsubstituted aryl azides and other photolytic moieties.[23,24] Furthermore, perfluoroarylazides are capable of indiscriminately inserting into any type of residue, including chemically "inert" aliphatic C-H bonds, which makes this moiety appropriate when little information on binding residues is available.

Synthesis and Evaluation. Synthesis of the desired **PRAPP** was problematic and required the use of a novel synthetic route (Scheme 1). Related analogues and SAR controls were accessible via our previously described

Scheme 1.[a] Synthesis of the PRAPP

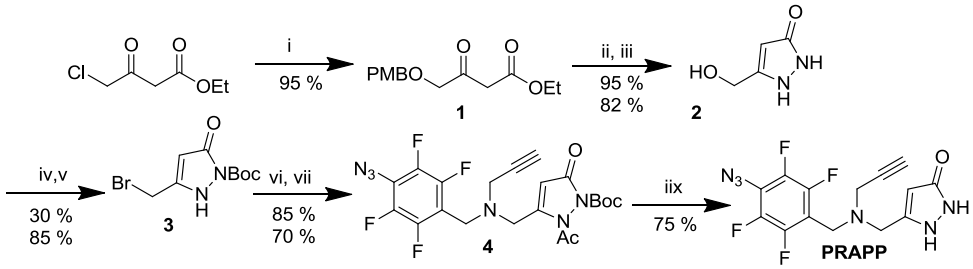

[a] Reagents and conditions: i) NaH, 0 °C, 1 h, then *p*-methoxybenzyl alcohol, 12 h; ii) NH_2NH_2, EtOH, 5 min; iii) TFA, CH_2Cl_2, 1 h,; iv) Boc_2O, $NaHCO_3$, CH_2Cl_2; v) CBr_4, $P(Ph_3)$; vi) Ac_2O, DMAP, CH_2Cl_2, 1 h; vii) N-(4-azido-2,3,5,6-tetrafluorobenzyl)prop-2-yn-1-amine, $NaHCO_3$, CH_2Cl_2; iix) TFA, CH_2Cl_2.

route.[25] The PRAPP library (Figure 32) was evaluated for ability to ameliorate MG-132 induced cellular toxicity in PC-12 ^{G93A}SOD1 cells.[26] All analogues possessed at least equipotent activity compared to the 1st generation control (**CMB-003299,** Figure 32). Importantly, the **PRAPP** (EC_{50} = 0.19 µM) demonstrated better potency than the lead. It is also noteworthy that pentafluorophenyl containing **IS-1-53** gave the best significant activity.

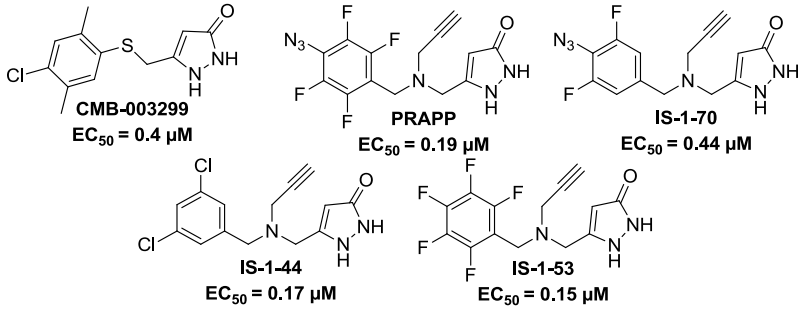

Figure 32. Focused PRAPP library. EC_{50} values are based on 12-point dose−response experiments. Assay workflow: ^{G93A}SOD1 cells + analyte for 4 h → + MG132 (400 nM) 48 h → measure viability using fluorescent probe (Calcein-AM). Values were normalized to DMSO control and represent the mean average of duplicate experiments. S.D ± 0.02 µM for untreated control.

Photolysis Characterization

Following observations of neuroprotective activity by the PRAPP, elementary photoactivation studies were carried out. Literature precedents led to the examination of photolysis at two wavelengths (312 nm and 360 nm).[23,24] Short term irradiation (< 30 min) of each of these wavelengths is generally considered to have minimal detrimental impact on biological systems. The PRAPP (100 µM) was irradiated with UV light for varying periods of time (2, 5, 10, 15, and 30 min), and disappearance was monitored by HPLC-UV-Vis_{278nm} analysis (Figure 33). Following 10 min irradiation at 312 nm, the PRAPP was completely consumed, with a photolysis $t_{1/2}$ ~ 2.3 min. In similar experiments, photolysis following irradiation with 360 nm light for 10 min was found to be negligible (~95 % remaining [data not shown]). On the basis of these results, subsequent photolabeling studies involved 10 min irradiation with 312 nm UV light.

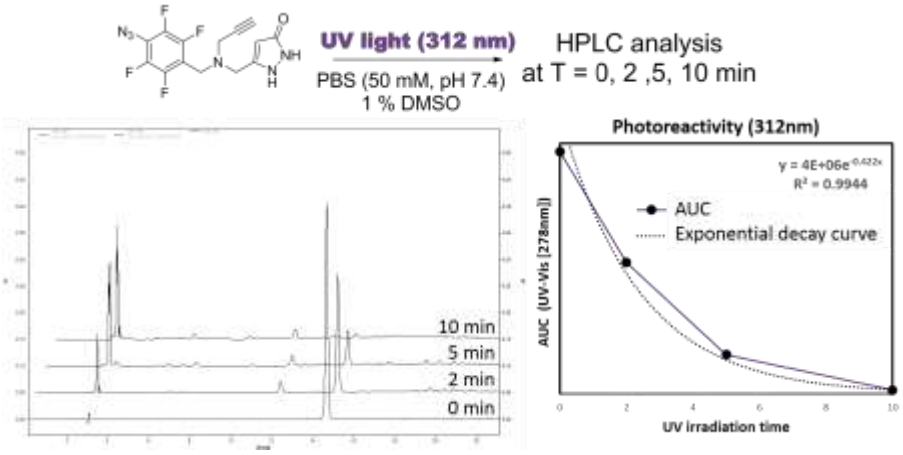

Figure 33. PRAPP rate of photoactivation at 312 nm. The PRAPP (100 µM) was dissolved in PBS (50 mM, pH 7.4) and irradiated with UV light (312 nm, 6W, 4 cm). Photolysis was monitored by HPLC-UV-Vis$_{278nm}$.

Photoaffinity labeling Studies in Whole Cell Culture. Identifying ligand-protein interactions within dynamic biological systems is exceedingly challenging and the ultimate goal of most successful target ID projects. The **PRAPP** was confirmed to be neuroprotective, and conditions for photolysis were characterized. The approach for whole cell photoaffinity labeling followed the schematic shown in Figure 34. At the appropriate time-point

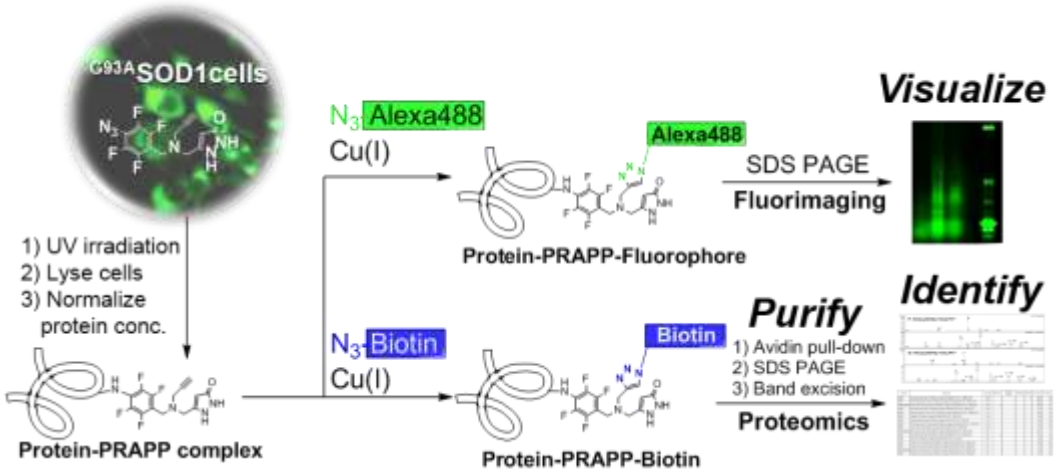

Figure 34. PRAPP Methodology Overview

(2 h, 2.5 h, or 24 h) culture media was replaced, and cells were irradiated with UV light for 10 min. The cells were then lysed, protein concentrations normalized, and the resulting protein concentrates conjugated with appropriate chemical biology functionalities. Cu (I)-catalyzed "click" conjugation was used to incorporate two complementary reporters: 1) a fluorescent azido-rhodamine (N_3-Alexa488) for visualization of protein modification via fluorimaging after SDS PAGE; and 2) an azido-biotin (N_3-PEG_4-biotin) for affinity purification, SDS PAGE, band excision, tryptic digest, and proteomic analysis. Similar protein modification was seen from experiments after 2 h incubation in the absence of MG-132 and 24 h experiments with MG-132 (Figure 35 shows results from the 2 h timepoint). One distinct protein band was observed at ~25 kDa based on a

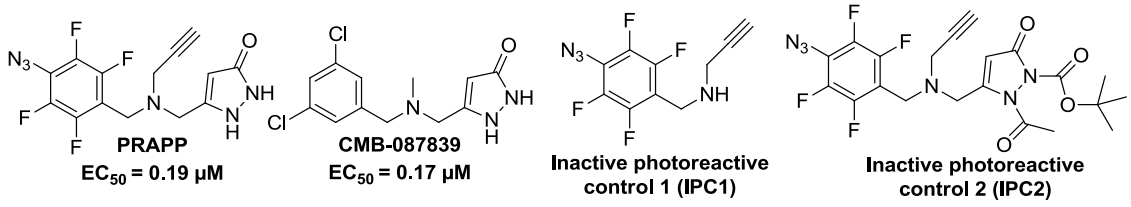

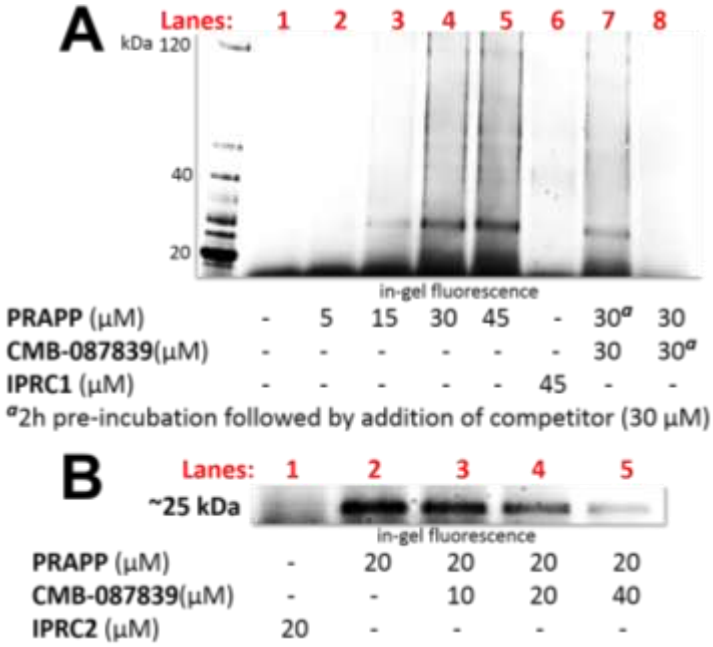

Figure 35. **Photoaffinity labeling in whole cell culture using PRAPP. A**) in-gel fluorescence from SDS PAGE of photoaffinity labeling following 2 h incubations in ^{G93A}SOD1 cell culture. **B**) photoaffinity labeling from co-incubations of PRAPP and CMB-087839. Two inactive photoaffinity labeling controls were used (**IPRC1-2**).

concentration dependent increase in in-gel fluorescence (Figure 35A, lanes 2-5). This band was not present in control experiments employing two inactive photoaffinity labeling controls (Figure 35A, lane 6 and Figure 35B, lane 1), without UV light induced photolysis (not shown), and in the absence of the **PRAPP** (Figure 35A, lane 1). Pre-incubation of the **PRAPP** for 2 h followed by addition of the equipotent **CMB-087839** and incubation for an additional 30 min resulted in decreased fluorescent intensity compared to the **PRAPP** alone (compare Figure 35A, lane 7 and lane 4). Alternatively, pre-incubation with **CMB-087839** completely blocks **PRAPP** modification (Figure 35A lane 8). Co-incubation with **CMB-087839** and the **PRAPP** results in a concentration dependent decrease in band intensity (Figure 35B lanes 3-5). On the basis of these results, the normalized protein concentrates were conjugated to an azido-biotin for affinity purification followed by SDS PAGE, band excision (20-30 kDa) and proteomic identification.

Proteomic analysis led to the identification of 24 proteins with 99.9% certainty. Approximately one third of these proteins were associated with hspb1 (a.k.a. HSP27 in humans or HSP25 in rats), a small heat shock protein (25 kDa in rats) that was identified with ~36% sequence coverage and the highest ID score based on iterative proteomic ID criteria (i.e., unique peptide fragments, % sequence coverage, peptide-spectrum matches). On the basis of the high % sequence coverage compared to other proteins that were identified (most other proteins were identified with < 15% coverage), it is reasonable to assume that HSP27 is present in high abundance within this gel band. Multiple proteasomal subunits were also identified, although none of these coincided with those identified in the biotin affinity bait experiments described above.

HSP27 is a small ATP-independent heat shock protein and molecular chaperone. Hsp27 has been the subject of intense research efforts recently but is still relatively poorly understood. It was observed that Hsp27 large oligomers, which are in dynamic equilibrium with those of smaller sizes, have ATP-independent "holdase" chaperone activity. Following cellular stress, it stores misfolded polypeptides in large oligomeric complexes. Subsequently, the stored misfolded polypeptides are either processed for refolding by ATP-dependent chaperones (i.e., Hsp70 and co-chaperones) or transported to the proteasome for degradation. Under physiological conditions, Hsp27 exists in large oligomeric complexes (500-800 kDa) and is regulated via phosphorylation by kinases (particularly MAPKAP kinases 2 and 3). Phosphorylation causes a shift in Hsp27 equilibrium from large

oligomeric species to dimers or monomers. This equilibrium shift has been shown to be important for neuroprotective activity.[27] Hsp27 is known to have neuroprotective effects, including disease modifying effects in an ALS model.[28] Furthermore, Hsp27 overexpression results in enhanced proteasome activation. Dimeric and monomeric Hsp27 species directly interact with the proteasome.[29] It is important to note that Hsp27 has a cellular mechanism for rapid response to cellular stress (minutes) and does not necessarily require induction of the HSR to act upon misfolded proteins.

During the course of our target ID studies we have used multiple chemical biology techniques to understand the direct binding partners of ASPs in a biological system. Photoaffinity labeling studies demonstrated that binding interactions exist between a small ATP-independent Hsp, HSP27, and the **PRAPP**. A mechanism of action involving HSP27 elicited enhancement in proteasomal activity is supported by our results from biotin-affinity bait experiments and examination of proteasomal activity in cell-based studies. Because of its integral functions in cellular survival, HSP27 modulators are desirable for a broad range of therapeutic indications, including cancer therapy and as neuroprotective agents. There are few reports of HSP27 small molecule modulators in the literature, and the accounts that do exist rely upon mechanisms that act through induction of the HSR to increase HSP27 expression (e.g., sulforaphane).[30] Our observations of ASPs as novel small molecule modulators of HSP27 that are capable of enhancing proteasomal activity in the absence of HSR induction could aid future directions in drug development.

KEY RESEARCH ACCOMPLISHMENTS

- Synthesized new classes of analogues related to the ASP and CHD structures, both with good activity
- Identified a possible explanation for why the CHD analogue did not exhibit lifespan extension in the ALS mouse and have prepared two compounds that address that problem
- Repeated ALS mouse experiments with CMB-021805 (PYT) under different dosing regimens and found an even greater life extension of 31% (previously our best was 26%).
- Carried out gene profiling in both G93A and G85R models of ALS and have gene array evidence for which proteins may be involved in the mechanism of action of CMB-021805, namely those involved in mitochondrial functioning
- Two protective proteins, superoxide dismutase 2 (SOD2), and brain-derived neurotrophic factor (BDNF), were found to be upregulated by CMB-021805.
- Protein chip array studies were carried out with CMB-021805, and a total of 57 different proteins were shown to be affected, some requiring the presence of NaCl and others not. Of the 57 proteins, 18 were affected both in the presence and absence of NaCl.
- An active ASP analog has been modified with a tether to a biotin in preparation for protein pull-down experiments to identify to what protein(s) the ASP compound binds.
- Identified a new class of active AXP compounds with X = nitrogen in place of oxygen; these can also be used for target pull-down experiments
- Identified another new class of active compounds with a basic nitrogen so salt forms are stable for increased solubility
- Elucidated the SAR of the AXP class of compounds, demonstrating that N^2-H of the pyrazolone ring is absolutely essential for activity
- The most potent AXP was sent for pharmacological and functional screening, and only one protein was affected, namely, metabotrophic glutamate receptor 5 ($mGluR_5$)
- $mGluR_5$ antagonists, however, are not active in our screen
- Additional sites on the AXP compounds were identified for attachment to agarose beads for protein pull-down experiments
- A new CHD compound was separated into enantiomers, found to be active, had good ADME properties, and was highly nontoxic (MTD >5g/kg)
- The more potent CHD enantiomer produced a 13% increase in the lifespan of the ALS mouse relative to the control

- MTD studies were carried out on nine novel compounds; three of them had MTD > 5g/kg; three had MTD 1280 mg/kg; two were irritants; one had MTD 100 mg/kg
- Mechanisms of action studies of our best PYT compound showed anti protein aggregation properties, improved brain-derived neurotrophic factor, reduced oxidative stress, modulated aberrant nucleosomal dynamics, and ameliorated mitochondrial dysfunction, and was neuroprotective
- Protein chip array studies were repeated with a competitor molecule to differentiate false positives; 29 hits were observed, but one, 26S proteasome non-ATPase regulatory subunit 14 (rpn14), appears promising
- Induction of a heat shock response does not appear to be the mechanism of these compounds
- From affinity bait experiments, activation of the proteasome is a possible mechanism for, at least, the PYTs.
- Photoaffinity labeling experiments have identified HSP27 as a possible target for, at least, the ASPs

REPORTABLE OUTCOMES:

Manuscripts (Complete Bibliography)

Benmohamed, R., Arvanites, A.C., Kim. J., Ferrante, R.J., Silverman, R.B., Morimoto, R.I. and Kirsch, D.R., Identification of Compounds Protective Against G93A SOD1 toxicity for the Treatment of Amyotrophic Lateral Sclerosis. *Amyotroph. Lat. Scler.* **2011**, *12*, 87-96. PMCID: PMC21073276

Chen, T, Benmohamed, R., Arvanites, A.C., Ranaivo, H.R., Morimoto, R.I., Ferrante, R.J., Watterson, D.M., Kirsch, D.R., and Silverman, R.B. Arylsulfanyl Pyrazolones Block Mutant SOD1-G93A Aggregation. Potential Application for the Treatment of Amyotrophic Lateral Sclerosis, *Bioorg. Med. Chem.* **2011**, *19*, 613-622. PMCID: PMC3014451

Xia, G., Benmohamed, R., Kim, J., Arvanites, A.C., Morimoto, R.I. Ferrante, R. J., Kirsch, D.R., and Silverman, R.B. Pyrimidine-2,4,6-trione Derivatives and Their Inhibition of Mutant SOD1-dependent Protein Aggregation. Toward a Treatment for Amyotrophic Lateral Sclerosis, *J. Med. Chem.* **2011**, *54*, 2409-2421. PMCID: PMC3074252

Zhang, W.; Benmohamed, R.; Arvanites, A. C.; Morimoto, R. I.; Ferrante, R. J.; Kirsch, D. R.; Silverman, R. B. Cyclohexane 1,3-diones and their inhibition of mutant SOD1-dependent protein aggregation and toxicity in PC12 cells. *Bioorg. Med. Chem.* **2012**, *20*, 1029-1045. PMCID: PMC3259267

Chen, T.; Benmohamed, R.; Kim, J.; Smith, K.; Amante, D.; Morimoto, R. I.; Kirsch, D. R.; Ferrante, R. J.; Silverman, R. B. ADME-Guided Design and Synthesis of Aryloxanyl Pyrazolone Derivatives to Block Mutant SOD1 Cytotoxicity and Protein Aggregation: Potential Application for the Treatment of Amyotrophic Lateral Sclerosis. *J. Med. Chem.* **2012**, *55*, 515-527. PMCID: PMC22191331

Zhang, Y.; Silverman, R. B. Direct amination of γ-halo-β-ketoesters with anilines. *J. Org. Chem.* **2012**, *77*, 3462-3467. PMCID: PMC3321089

Zhang, Y.; Benmohamed, R.; Zhang, W.; Kim, J.; Edgerly, C.; Zhu, Y.; Morimoto, R. I.; Ferrante, R. J.; Kirsch, D. R.; Silverman, R. B. Chiral cyclohexane 1,3-diones as inhibitors of mutant SOD1-dependent protein aggregation for the treatment of ALS. *ACS Med. Chem. Lett.* **2012**, *3*, 584-585. PMCID: PMC3402085

Trippier, P.; Benmohamed, R.; Kirsch, D. R.; Silverman, R. B. Substituted pyrazolones require N2 hydrogen bond donating ability to protect against cytotoxicity from protein aggregation of mutant super-oxide dismutase 1. *Bioorg. Med. Chem. Lett*. **2012**, *22*, 6647-6650. PMCID: PMC23021992

Zhang, Y.; Silverman, R. B. A novel synthesis of 1-aryl-3-piperidone derivatives. *Tetrahedron Lett.* **2013**, *54*, 573-575. PMCID: PMC3541782

Zhang, Y.; Benmohamed, R.; Huang, H.; Chen, T.; Voisine, C.; Morimoto, R. I.; Kirsch, D. R.; Silverman, R. B. Arylazanylpyrazolone derivatives as inhibitors of mutant SOD1-dependent protein aggregation for the treatment of amyotrophic lateral sclerosis, *J. Med. Chem.* **2013**, *56*, 2665-2675. PMCID: PMC3627359

Trippier, P. C.; Zhang, Y.; Benmohamed, R.; Moran, J.; Kirsch, D. R.; Morimoto, R. I.; Silverman, R. B. Proteasome activation: a new therapeutic strategy for the potential treatment of amyotrophic lateral sclerosis and other neurodegenerative diseases, submitted.

Kim, J.; Amante, D. J.; Edgerly, C.; Cipicchio, P. M.; Bennett, E. R.; Lauver, M. A.; Callear, A. P.; Benmohamed, R.; Xia, G.; Kirsch, D. R.; Friedlander, R. M.; Morimoto, R. I.; Silverman, R. B.; Ferrante, R. J. Pyrimidine-2,4,6-trione treatment as a therapeutic strategy for amyotrophic lateral sclerosis, submitted.

Patents

Kirsch, D.R., Benmohamed, R., Arvanites, A.C., Morimoto, R.I., Silverman, R.B. and Chen, T. Treatment of Amyotrophic Lateral Sclerosis. PCT/US09/06237 – November 20, 2009

Kirsch, D.R. and Benmohamed, R. Butaclamol for the Treatment of Amyotrophic Lateral Sclerosis. PCT/US10/32651 – April 27, 2010

Kirsch, D.R., Arvanites, A.C. Benmohamed, R., Morimoto, R.I., Silverman, R.B. and Xia, G. Pyrimidine-2,4,6-triones for the Treatment of Amyotrophic Lateral Sclerosis. PCT/US10/33714 – May 5, 2010

Kirsch, D.R., Arvanites, A.C. Benmohamed, R., Morimoto, R.I., Silverman, R.B. and Zhang, W. Cyclohexane-1,3-diones for the Treatment of Amyotrophic Lateral Sclerosis. PCT/US10/54747 – October 29, 2010

The following national stage applications were filed based on earlier PCT filings:

Inventions	Country of Filing	Application No.	Title	Inventors
2009-072	United States	13/318,429	Pyrimidine-2,4,6-Triones for Use in the Treatment of Amyotrophic Lateral Sclerosis	Donald R. Kirsch; Radhia Benmohamed; Anthony C. Arvanites; Richard I. Morimoto; Richard B. Silverman; Guoyao Xia
2009-072	Europe	EP 10772761.2	Pyrimidine-2,4,6-Triones for Use in the Treatment of Amyotrophic Lateral Sclerosis	Donald R. Kirsch;Radhia Benmohamed;Anthony C. Arvanites;Richard I. Morimoto;Richard B. Silverman;Guoyao Xia
2009-098	United States	13/504,893	Cyclohexane-1,3-Diones for Use in the Treatment of Amyotrophic Lateral Sclerosis	Donald R. Kirsch;Radhia Benmohamed;Anthony C. Arvanites;Richard B. Silverman;Richard I. Morimoto;Wei Zhang

Presentations

Paul C. Trippier, Tian Chen, Radhia Benmohammed, Donald R. Kirsch, Robert J. Ferrante, Richard I. Morimoto and Richard B. Silverman; *Pyrazolone containing small molecules exhibit activity in a G93A-SOD1 mouse model of Amyotrophic Lateral Sclerosis.* Abstracts of papers, 42nd ACS Central Regional Meeting, Indianapolis, IN, USA. June 8-10, (**2011**), CRM-429.

Richard B. Silverman, *Protein Aggregation and the Development of Therapeutics for Amyotrophic Lateral Sclerosis.* Gordon Research Conference on Medicinal Chemistry (New London, NH), Aug. 2011; ALS

Association Chicago Investigators Workshop and Symposium (Chicago) Oct. 2011; Les Turner ALS Foundation 2nd Annual Symposium (Chicago, IL) May 2012.

CONCLUSIONS

We have identified new structures within the three general classes of compounds (PYT, ASP, and CHD) that have improved potency and pharmacokinetic properties, and ALS mouse trials using several of these compounds have resulted in 13-31% extension of life. At 10 mg/kg BID, CMB-021805, gave a 31% life extension, **which is above any reported mouse trial extension of life**. Our results also showed that CMB-021805 significantly improved the motor performance and rescued body weight loss. All of the compounds tested in vivo have high maximum tolerated dose levels (320 mg/kg to 5 g/kg), suggesting low toxicity. Our findings were confirmed using neuropathological analyses, and we have met the specific aims of the study. In addition, we have provided *in vivo* data on the mechanism of action associated with CMB-021805, suggesting that the neuroprotective effect may be associated with improved mitochondrial function. Two types of mechanism of action experiments, using protein pull-down methods, have identified activation of the proteasome and interaction with HSP27 as possible mechanisms for, at least, the ASP class of compounds. These data may also provide biomarkers for use in human clinical trials.

References

[1] Haidet-Phillips, A. M.; Hester, M. E.; Miranda, C. J.; Meyer, K.; Braun, L.; Frakes, A.; Song, S.; Likhite, S.; Murtha, M. J.; Foust, K. D.; Rao, M.; Eagle, A.; Kammesheidt, A.; Christensen, A.; Mendell, J. R.; Burghes, A. H.; Kaspar, B. K. Astrocytes from familial and sporadic ALS patients are toxic to motor neurons. *Nat. Biotechnol.* **29**, 824-828 (2011).

[2] Gidalevitz, T., Krupinski, T., Garcia, S., Morimoto, R. I. Destabilizing protein polymorphisms in the genetic background direct phenotypic expression of mutant SOD1 toxicity. *PLoS Genet* **5**, e1000399 (2009).

[3] Andreassen, O. A. *et al.*, Partial deficiency of manganese superoxide dismutase exacerbates a transgenic mouse model of amyotrophic lateral sclerosis. *Ann. Neurol.* **47**, 447-455 (2000).

[4] Vermeiren, C.; de Hemptinne, I.; Vanhoutte, N.; Tilleux, S.; Maloteaux, J.-M.; Hermans, E. Loss of metabotropic glutamate receptor-mediated regulation of glutamate transport in chemically activated astrocytes in a rat model of amyotrophic lateral sclerosis. *J. Neurochem.* **96**(3), 719-731 (2006).

[5] G. Xia; Benmohamed, R.; Kim, J.; Arvanites, A. C.; Morimoto, R. I.; Ferrante, R. J.; Kirsch, D. R.; Silverman, R. B. Pyrimidine-2,4,6-trione Derivatives and Their Inhibition of Mutant SOD1-dependent Protein Aggregation. Toward a Treatment for Amyotrophic Lateral Sclerosis (ALS). *J. Med. Chem.* **54**, 2409-2421 (2011).

[6] B. Schweitzer, P. Predki, M. Snyder, Microarrays to characterize protein interactions on a whole-proteome scale. *Proteomics* **3**, 2190-2199 **(**2003).

[7] J. Singh *et al.*, DcpS as a therapeutic target for spinal muscular atrophy. *ACS Chem. Biol.* **3**, 711-722 (2008).

[8] G. Xia *et al.*, Pyrimidine-2,4,6-trione derivatives and their inhibition of mutant SOD1-dependent protein aggregation. Toward a treatment for amyotrophic lateral sclerosis *J. Med. Chem.* **54**, 2409-2421 (2011).

[9] D. Baumer, O. Ansorge, M. Almeida, K. Talbot, The role of RNA processing in the pathogenesis of motor neuron degeneration. *Expert Rev. Mol. Med.* **12**, e21/1-e21/22 (2010).

[10] A. Kohler *et al.*, The substrate translocation channel of the proteasome. *Biochimie* **83**, 325-332 (2001).

[11] (a) Park et al., Proteasomal ATPASE-associated factor 1 negatively regulates proteasome activity by interacting with progteasomal ATPases, *Mol. Cell Biol.* **25**, 3842-3845 (2005). (b) Lassot et al., The proteasome regulates HIV-1 transcription by both proteolytic and nonproteolytic mechanisms. *Mol. Cell* **25**, 369-383 (2007).

[12] Kim et al., Crystal structrure of yeast Rpn14, a chaperone of the 19 S regulatory particle of the proteasome. *J. Biol Chem.* **285**, 15159-15166 (2010).

[13] Morimoto, R. I., Proteotoxic stress and inducible chaperone networks in neurodegenerative disease and aging. *Genes & development* **22**, 1427-1438 (2008).

[14] Calamini, B.; Silva, M. C.; Madoux, F.; Hutt, D. M.; Khanna, S.; Chalfant, M. A.; Saldanha, S. A.; Hodder, P.; Tait, B. D.; Garza, D.; Balch, W. E.; Morimoto, R. I. Small-molecule protease regulators for protein conformational diseases. *Nat. Chem. Biol.* **8**, 185-196 (2012).
[15] Chen, T.; Benmohamed, R.; Kim, J.; Smith, K.; Amante, D.; Morimoto, R. I.; Kirsch, D. R.; Ferrante, R. J.; Silverman, R. B. ADME-guided design and synthesis of aryloxanyl pyrazolone derivatives to block mutant SOD1 cytotoxicity and protein aggregation: Potential application for the treatment of amyotrophic lateral sclerosis. *J. Med. Chem.* **55**, 515-527 (2012).
[16] Morimoto, R. I. The heat shock response: systems of biology of proteotoxic stress in aging and disease. *Cold Spring Harbor Symposia on Quantitative Biology* **76**, 91-99 (2011).
[17] Trippier, P. C.; Benmohammed, R.; Kirsch, D. R.; Silverman, R. B. Substituted pyrazolones require N2 hydrogen bond donating ability to protect against cytotoxicity from protein aggregation of mutant super-oxide dismutase 1. *Bioorg. Med. Chem. Lett.* **22**, 6647-6650 (2012).
[18] Matsumoto, G.; Stojanovic, A.; Holmberg, C. I.; Kim, S.; Morimoto, R. I. Structural properties and neuronal toxicity of amyotrophic lateral sclerosis-associated Cu/Zn superoxide dismutase 1. *J. Cell. Biol.* **171**, 75-85 (2005).
[19] Aebersold, R.; Mann, M. Mass-spectometry-based proteomics. *Nature* **422**, 198-207 (2003).
[20] Spiess, C.; Meyer, A. S.; Reissmann, S.; Frydman, J. Mechanism of the eukaryotic chaperonin: protein unfolding in the chamber of secrets. *Trends Cell. Biol.* **14**, 598-604 (2004).
[21] Kitamura, A.; Kubota, H.; Pack, C. G.; Matsumoto, G.; Hirayama, S.; Takahashi, Y.; Kimura, H.; Kinjo, M.; Morimoto, R. I.; Nagata, K. Cytosolic chaperonin prevents polyglutamine toxicity with altering the aggregation state. *Nat. Cell Biol.* **8**, 1163-1169 (2006).
[22] Guerrero, C.; Milenkovic, T.; Przulj, N.; Kaiser, P.; Huang, L. Characterization of the proteasome interaction network using *Proc. Natl. Acad. Sci. USA* **105**, 13333-13338 (2008).
[23] Brunner, J. New photolabeling and crosslinking methods. *Ann. Rev. Biochem.* **62**, 483-514 (1993).
[24] MacKinnon, A. L.; Taunton, J. Target identification by diazirine photo-cross-linking and click chemistry. In *Curr. Protoc. Chem. Biol.* John Wiley & Sons, Inc.: 2009.
[25] Zhang, Y.; Silverman, R. B. Direct amination of gamma-halo-beta-ketoesters with anilines. *The J. Org. Chem.* **77**, 3462-3467 (2012).
[26] Zhang, Y.; Benmohamed, R.; Huang, H.; Chen, T.; Voisine, C.; Morimoto, R. I.; Kirsch, D. R.; Silverman, R. B. Arylazanylpyrazolone derivatives as inhibitors of mutant SOD1-dependent protein aggregation for the treatment of amyotrophic lateral sclerosis. *J. Med. Chem.* **56**, 2665-2675 (2013).
[27] Benn, S. C.; Perrelet, D.; Kato, A. C.; Scholz, J.; Decosterd, I.; Mannion, R. J.; Bakowska, J. C.; Woolf, C. J. Hsp27 upregulation and phosphorylation is required for injured sensory and motor neuron survival. *Neuron* **36**, 45-56 (2002).
[28] Sharp, P. S.; Akbar, M. T.; Bouri, S.; Senda, A.; Joshi, K.; Chen, H.-J.; Latchman, D. S.; Wells, D. J.; de Belleroche, J. Protective effects of heat shock protein 27 in a model of ALS occur in the early stages of the disease progression. *Neurobiol. Dis.* **30**, 42-55 (2008).
[29] Parcellier, A.; Schmitt, E.; Gurbuxani, S.; Seigneurin-Berny, D.; Pance, A.; Chantôme, A.; Plenchette, S.; Khochbin, S.; Solary, E.; Garrido, C. HSP27 is a ubiquitin-binding protein involved in I-kBα proteasomal degradation. *Mol. Cell. Biol.* **23**, 5790-5802 (2003).
[30] Gan, N.; Wu, Y.-C.; Brunet, M.; Garrido, C.; Chung, F.-L.; Dai, C.; Mi, L. Sulforaphane activates heat shock response and enhances proteasome activity through Up-regulation of Hsp27. *J. Biol. Chem.* **285**, 35528-35536 (2010).

Paid Personnel (over the course of the award)

Silverman Laboratory:

Dr. Yinan Zhang, Postdoctoral Fellow
Dr. Paul Tripper, Postdoctoral Fellow
Dr. Gavin Xia, Postdoctoral Fellow
Tian Chen, Graduate Student

Morimoto Laboratory:

Dr. Cindy Voisine. Postdoctoral Fellow

Ferrante Laboratory:

Dr. Robert Ferrante, Ph.D.
Daniel Amante, Technician
Dr. Jin Ho Kim, Research Associate
Molly Lauver, Research Specialist

Cambria Pharmaceuticals:

Dr. Donald Kirsch (later consultant after closure of Cambria Pharmaceuticals)
Radhia Benmohamed, Scientist I

Bioorganic & Medicinal Chemistry Letters 22 (2012) 6647–6650

Contents lists available at SciVerse ScienceDirect

Bioorganic & Medicinal Chemistry Letters

journal homepage: www.elsevier.com/locate/bmcl

Substituted pyrazolones require N^2 hydrogen bond donating ability to protect against cytotoxicity from protein aggregation of mutant superoxide dismutase 1

Paul C. Trippier [a], Radhia Benmohammed [b], Donald R. Kirsch [b], Richard B. Silverman [a,c,*]

[a] Department of Chemistry, Northwestern University, Evanston, IL, USA
[b] Cambria Pharmaceuticals, Cambridge, MA, USA
[c] Department of Molecular Biosciences, Chemistry of Life Processes Institute, Center for Molecular Innovation and Drug Discovery, Northwestern University, Evanston, IL, USA

ARTICLE INFO

Article history:
Received 28 June 2012
Revised 14 August 2012
Accepted 28 August 2012
Available online 7 September 2012

Keywords:
Amyotrophic lateral sclerosis
Superoxide dismutase 1
Neuroprotection
Pyrazolone
Pharmacophore

ABSTRACT

Amyotrophic lateral sclerosis (ALS) is a debilitating and fatal neurodegenerative disease. Although the cause remains unknown, misfolded protein aggregates are seen in neurons of sporadic ALS patients, and familial ALS mutations, including mutations in superoxide dismutase 1 (SOD1), produce proteins with an increased propensity to misfold and aggregate. A structure activity relationship of a lead scaffold exhibiting neuroprotective activity in a G93A-SOD1 mouse model for ALS has been further investigated in a model PC12 cellular assay. Synthesis of biotinylated probes at the N^1 nitrogen of the pyrazolone ring gave compounds (**5d**–**e**) that retained activity within 10-fold of the proton-bearing lead compound (**5a**) and were equipotent with a sterically less cumbersome N^1-methyl substituted analogue (**5b**). However, when methyl substitution was introduced at N^1 and N^2 of the pyrazolone ring, the compound was inactive (**5c**). These data led us to investigate further the pharmacophoric nature of the pyrazolone unit. A range of N^1 substitutions were tolerated, leading to the identification of an N^1-benzyl substituted pyrazolone (**5m**), equipotent with **5a**. Substitution at N^2 or excision of N^2, however, removed all activity. Therefore, the hydrogen bond donating ability of the N^2–H of the pyrazolone ring appears to be a critical part of the structure, which will influence further analogue synthesis.

Amyotrophic lateral sclerosis (ALS), commonly known as Lou Gehrig's disease, is a progressive and ultimately fatal neurodegenerative disease, with a worldwide prevalence of approximately 2 per 100,000. The disease generally first presents between 40 and 60 years of age; loss of motor neurons controlling voluntary actions results in progressive muscle paralysis and death attributed to respiratory failure, typically within 3–5 years of diagnosis.[1]

Currently, the only approved drug for ALS, riluzole, extends median survival by only 2–3 months.[2] Clearly, there is a need for new therapeutics; however, progress has been impeded because the underlying pathology of the disease remains unknown. There is strong evidence[3] that one pathophysiological mechanism in particular, that of toxic protein misfolding and/or aggregation, may trigger motor neuron dysfunction and loss. Mutations in familial ALS (FALS) patients that promote protein misfolding and aggregation include Cu/Zn superoxide dismutase type 1 (SOD1),[4] UBQLN2,[5] TAR DNA binding protein (TDP-43),[6] fused in sarcoma/translated in liposarcoma (FUS/TLS),[7] and angiogenin (ANG)[8] and, in addition, TDP-43 aggregates are seen in motor neurons of sporadic ALS (SALS) patients.[9]

The clinical phenotype and pathology of SALS, which accounts for 90% of all ALS cases, are indistinguishable from those of the familial form.[10] It has therefore been possible to make significant advances in studying the pathology of ALS through the investigation of the familial form of the disease,[11] which accounts for only approximately 10% of all cases, 20% of which are caused by missense mutations in the gene encoding for the enzyme SOD1. Recent studies[12] have now linked FALS to SALS through common SOD1 containing astrocytes, demonstrating that SOD1 is a viable target for both FALS and SALS, providing further impetus to the identification of compounds active in mutant SOD1 disease models.

We previously described[13] a high throughput screening method for the identification of compounds active in a PC12 cell model in which protein aggregation and cell death depended on the expression of G93A SOD1. One of the chemical scaffolds identified

Abbreviations: ALS, amyotrophic lateral sclerosis; FALS, familial amyotrophic lateral sclerosis; SALS, sporadic amyotrophic lateral sclerosis; SOD1, Cu/Zn superoxide dismutase 1.

* Corresponding author at: Department of Chemistry, Northwestern University, 2145 Sheridan Road, Evanston, IL 60208-3113, USA. Tel.: +1 847 491 5653; fax: +1 847 491 7713.

E-mail addresses: Agman@chem.northwestern.edu, r-silverman@northwestern.edu (R.B. Silverman).

0960-894X/$ - see front matter © 2012 Elsevier Ltd. All rights reserved.
http://dx.doi.org/10.1016/j.bmcl.2012.08.114

in this screen was the arylsulfanylpyrazolones.[14] Although ineffective as a potential therapeutic because of the metabolic instability of the sulfanyl linker, this scaffold has served as a valuable lead for detailed structure–activity relationship (SAR) studies,[15] resulting in **5a** (Scheme 1, Table 1), which has an EC_{50} = 0.067 μM in our G93A-SOD1 cell assay and is active in a mutant SOD1 mouse model of ALS. Methylation of **5a** to **5b** (Table 1) or conjugation with biotin (**5d**) gave compounds with similar EC_{50} values, but dimethylation to **5c** gave an inactive compound. This intriguing result led us to investigate the cause for the inactivity of **5c** relative to much more sterically-demanding active compounds, such as **5b** and **5d**. Here, we describe the SAR profile of the pyrazolone ring; substitution, excision, and replacement of one or both of the two nitrogen atoms is described, and the pharmacophoric nature of the N^2-position is demonstrated.

The synthetic route delineated in Scheme 1 was modified in step iv to include the addition of suitably substituted hydrazine reagents, providing access to a wide range of N^1-substituted pyrazolone analogues (Table 1). Phenyl, heteroaryl, alkyl, and acyl-substituted pyrazolones were synthesized and their activities determined.

Alkyl substitution at the N^1-position of the pyrazolone ring is tolerated, albeit with an approximately 10-fold reduction in cell activity compared to **5a**. All of the N^1-substituted compounds were active except for **5f**, **5j**, **5k**, and **5o**. Steric hindrance, apparently, plays little or no role in the activity of the compounds synthesized; compounds with methyl (**5b**, EC_{50} = 0.67 μM), biotin (**5d**, EC_{50} = 0.56 μM) and tetraethyleneglycol-linked biotin (**5e**, EC_{50} = 0.67 μM) all display the same activity over a substituent length from 1 to 24 atoms including, in the case of biotin compounds **5d** and **5e**, the presence of a bulky tetrahydro-1*H*-thieno(3,4-*d*)imidazol-2(3*H*)-one ring.

The inactivity of **5f** is intriguing because it is small and not bulky. As an explanation for this lack of activity, we considered the possibility that the compound exists in a bicyclic structure with the hydroxyl hydrogen bonded to the N^2 position, thereby forming a six-membered intramolecular hydrogen-bonded ring and blocking the hydrogen bond donating ability of the N^2 position. To support this hypothesis, the hydroxypropyl-substituted compound (**5g**) was synthesized from known 3-hydrazinylpropan-1-ol.[16] The corresponding hydrogen bonding in **5g** would lead to an unfavorable seven-membered ring, which therefore would not be expected to form, allowing the hydrogen bond donating ability of the N^2 position to be unobstructed. In agreement with this hypothesis, **5g** was active (EC_{50} = 0.34 μM). The stability of the proposed six-membered hydrogen bonded ring has been

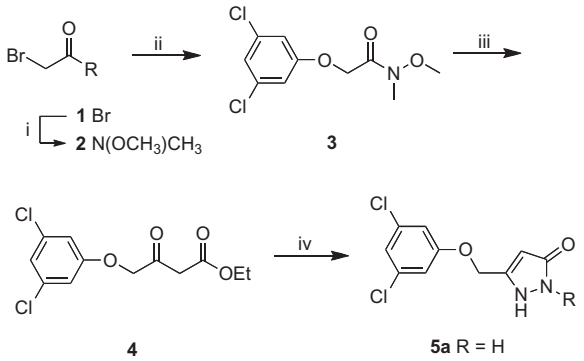

Reactants and conditions: i) TEA, (Me)N(OMe).HCl, DCM (65%); ii) 3,5-dichlorophenol, NaOEt, EtOH, heat (47%); iii) LiHMDS, EtOAc, THF,-78 °C (56%); iv) NH_2NHR, EtOH, RT (28%).

Scheme 1. Synthesis of lead compound **5a** via Weinreb amide intermediate **3**.

Table 1
SAR studies of substitution of the pyrazolone ring

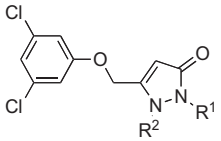

Compound	R^1	R^2	EC_{50} (μM)
a	H	H	0.067
b	Me	H	0.67
c	Me	Me	>32[a]
d	Biotin	H	0.56
e	Peg4–Biotin	H	0.67
f	CH_2CH_2OH	H	>32
g	$CH_2CH_2CH_2OH$	H	0.34
h	Ph	H	1.03
i	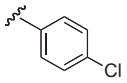	H	1.73
j	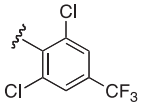	H	>32
k	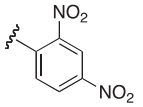	H	>32
l	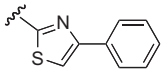	H	1.00
m	Bn	H	0.13
n	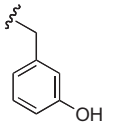	H	0.36
o	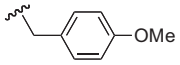	H	>32
p	CHO	H	0.49
q	Ac	H	0.27
r	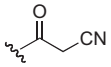	H	0.42
s	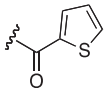	H	0.31
t	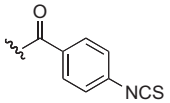	H	0.33
u	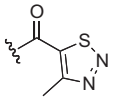	H	1.71
v	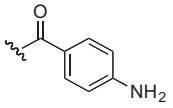	H	0.93
w	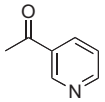	H	1.32

[a] >32 μM indicated EC_{50} not reached at the highest concentration used. All values are reported as the mean average of three determinations. Average Z′ factor value = 0.5.

estimated to be 20 kJ/mol[17] (4.8 kcal/mol) and 29 kJ/mol (6.9 kcal/mol),[18] which could account for the large difference in

activity between **5f** and **5g**. Explanations relating to solubility, cell permeability, or bioavailability are unlikely, given the one methylene difference from that of **5g**.

An alternative possibility regarding the importance of hydrogen bonding for activity is that the tautomeric enol form of the pyrazolone is the active form, and it is the enol hydroxyl that is essential for activity. If that were the case, there are two tautomeric forms, one that retains the N^1–H and one that retains the N^2–H (both still having the enol OH) (Fig. 1). If the OH were the important H-bond donor, the activity would not be affected if the compound were methylated at N^1 or N^2. In a related series of compounds from our group,[19] the N^1-methylated analogue was active, but the N^2-methylated analogue was not active. If the enol OH were relevant, both of those methylated compounds would have been active.

An increase in electron-withdrawing ability should have an important effect on activity because of its decrease in the pK_a of N^2–H and corresponding promotion of hydrogen bond donation ability. Suprisingly, phenyl substitution at N^1 attenuated the activity of the pyrazolone (**5h**, EC_{50} = 1.03 μM), allowing further characterization of the relatively expansive pocket environment the N^1 substituents inhabit. A further decrease in activity of analogue **5i** and total loss of activity with N^1-phenyl analogues **5j** and **5k**, containing multiple strong electron-withdrawing substituents was observed. An explanation for the reduced activity seen with **5h** and **5i** may be the steric bulk of the introduced phenyl ring, which impedes the N^2 position and prevents hydrogen bond donation. The lack of activity of **5j** and **5k** may be attributed to steric crowding by the ortho substituents, which completely block the hydrogen bond donating ability at N^2, further supporting our assertion that this position represents an important pharmacophore of the pyrazolone moiety. These results support the importance of N^2–H in its activity, presumably some hydrogen-bonding interaction with a target that is essential for activity. The N^1-phenylthiazole substituted analogue (**5l**) is equipotent (EC_{50} = 1.00 μM) with phenyl substituted pyrazolone **5h**, illustrating that five-membered aromatics and bulky bicyclics are tolerated at this position.

The moderate activity displayed by phenyl substitution, coupled with the relatively large steric pocket that N^1 substituents inhabit, suggested the synthesis of a benzyl-substituted pyrazolone, providing steric relief from the phenyl moiety by the methylene spacer. Compound **5m** was the most potent of the substituted pyrazolones yet synthesized, having an EC_{50} = 0.13 μM, essentially equivalent to that of **5a** (EC_{50} = 0.067 μM) within the reproducibility of the assay.[13] Substitution around the benzyl ring attenuates bioactivity; *meta*-hydroxybenzyl analogue **5n** exhibits an almost three-fold reduction in potency (EC_{50} = 0.36 μM). Introduction of a *para*-methoxyl substituent (**5o**) renders the compound inactive. It is not clear why the *para*-methoxyl functionality exerts a deactivating effect.

Acyl substitution appears to be well tolerated. Pyrazolones **5p**–**5t** have comparable EC_{50} values, and **5u**–**5w** are comparable but about one-third less potent. To aid in future target identification studies of these compounds phenylisothiocyanate **5t** was prepared. It was anticipated that this compound would act as a covalent linker, forming a bond with a suitably disposed residue within the target of action active site for use in subsequent affinity chromatography experiments. This was among the most potent of the acyl-substituted pyrazolones. Appendage of a biotin or affinity gel moiety to **5t** will determine if this approach will be successful in a protein pull-down experiment.

To further establish the pharmacophoric nature of the N^2 hydrogen bond donor group, a series of pyrazolone ring analogues was synthesized, which replaced N^2 and other positions around the pyrazolone ring with heteroatoms and/or methylene groups. Lactone **9** was obtained from the nucleophilic coupling of known bromo-substituted lactone **8**[20] and 3,5-dichlorophenol (Scheme 2) in analogy with compounds **5a**–**w**. The lactone, lacking the hydrogen bond donor ability of the pyrazolone nitrogen at N^2, was inactive in the assay, providing further evidence for the importance of the N^2 position for bioactivity.

Replacement of the pyrazolone ring with a cyclopentanone ring (**13**) was achieved through an analogous coupling of known iodide **12**[21] with 3,5-dichlorophenol (Scheme 3) to produce a compound devoid of both nitrogen atoms of the pyrazolone ring and of biological activity.

The isoxazol-3(2*H*)-one analogue (**17**) was synthesized (Scheme 4) using a modified procedure.[22] The lithium acetylide of propargyl bromide was treated with ethyl chloroformate to yield bromotetrolate **15**; addition of an aqueous methanolic solution of hydroxylamine and careful control of pH afforded bromomethylisoxazole **16**. Subsequent addition of 3,5-dichlorophenol provided **17**, which, lacking the crucial N^2 hydrogen bond donating group, displayed no activity.

Another ring system lacking the N^2 hydrogen bond donor is illustrated by benzyl protected unsaturated pyrolidinone **22** (Scheme 5). This was obtained by reduction of commercially available pyrrolidinone ester **18** to form alcohol **19**, followed by mesylation and nucleophilic addition of a bromide ion to furnish bromide **20** in good yield (42%) relative to the alternative Appel reaction (PBr_3, pyridine; 2% yield); addition of 3,5-dichlorophenol to **20** provided pyrrolidinone **21**. Subsequent addition of phenylselenyl bromide to the prepared enolate and selenoxide elimination provided unsaturated pyrrolidinone **22**, identical to the most potent analogue (**5m**) except lacking the crucial N^2–H. Again, both **21** and **22**, possessing no N^2 hydrogen bond donor, had no activity (EC_{50} = >32 μM).

In conclusion, we have shown that the N^2 pyrazolone position is essential for the cellular activity of this class of compounds. While other factors such as cell membrane penetration may play a role in the activity patterns of some of these compounds, a sufficient degree of evidence has been accumulated to support the hypothesis that the hydrogen bond donating N^2–H group is pharmacophoric in these compounds. SAR data have provided further information on the interactions of **5a** and its analogues. Steric considerations are of little importance around the pyrazolone N^1 area, suggesting a large open pocket or corridor within the target structure. Placement of a benzyl group β to the pyrazolone N^1 (**5m**) enhances its

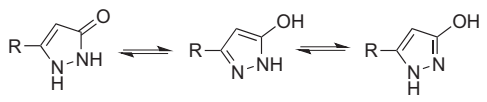

Figure 1. Tautomeric forms of the pyrazolones.

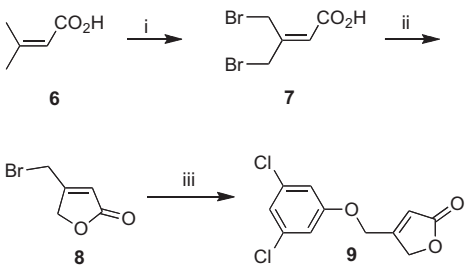

Reagents and Conditions: i) NBS, CCl_4, Benzoyl peroxide, reflux (98%); ii) 5% NaOH (61%); iii) NaOEt, EtOH, reflux (14%)

Scheme 2. Synthesis of lactone analogue **9**.

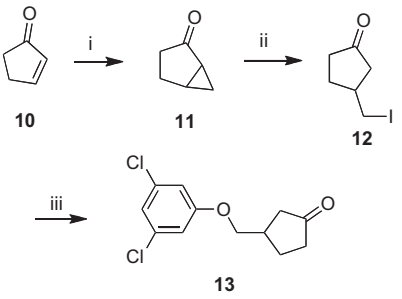

Reagents and Conditions: i) Me_3SOI, DMSO, NaH (33%); ii) Me_3SiCl, NaI, MeCN, RT (39%); iii) 3,5-dichlorophenol, NaOEt, EtOH, reflux (27%)

Scheme 3. Synthesis of cyclopentanone **13**.

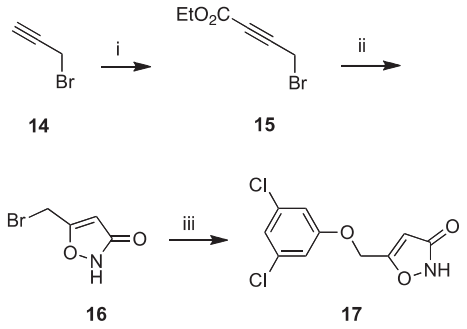

Reagents and Conditions: i) a, ^{n}BuLi, THF, Et_2O, -40 °C; b, Ethyl chloroformate (11%); ii) NH_2OH, MeOH, -35 °C - RT (47%); iii) 3,5-dichlorophenol, NaOEt, EtOH, 70 °C (20%)

Scheme 4. Synthesis of 3-bromo-4,5-dihydroisoxazole analogue **17**.

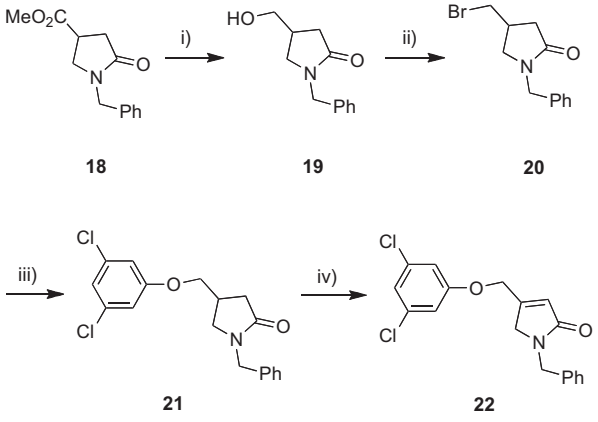

Reagents and Conditions: i) $LiBH_4$, THF, RT (99%); ii) PBr_3, Py, DCM (2%) or MsCl, NEt_3 then LiBr (42%); iii) 3,5-dichlorophenol, NaOEt, DMF, reflux (24%); iv) a) LDA, PhSeBr, THF, -78°C, b) H_2O_2, H_2O, DCM (27%).

Scheme 5. Synthesis of protected pyrolidinone analogue **22**.

potency, suggesting the presence, within the target, of a hydrophobic pocket, possibly containing aromatic residues. The importance of the N^2–H group to participate in hydrogen bond donating interactions with the biological target serves to promote this scaffold as both a lead compound for further therapeutic investigation and as a probe compound to potentially identify the biological target for these compounds.

Acknowledgments

We thank the National Institutes of Health (Grant 1R43NS057849), the ALS Association (TREAT program), and the Department of Defense (Grant AL093052) for funding.

Supplementary data

Supplementary data associated with this article can be found, in the online version, at http://dx.doi.org/10.1016/j.bmcl.2012.08.114.

References and notes

1. Rothstein, J. D. *Anal. Neurol.* **2009**, *65*, S3.
2. Bensimon, G.; Lacomblez, L.; Meininger, V. N. *Engl. J. Med.* **1994**, *330*, 585.
3. Brown, R. H., Jr.; Robberecht, W. *Semin. Neurol.* **2001**, *21*, 131.
4. Kerman, A.; Liu, H. N.; Croul, S.; Bilbao, J.; Rogaeva, E.; Zinman, L.; Robertson, J.; Chakrabartty, A. *Acta Neuropathol.* **2010**, *119*, 335.
5. Deng, H. X.; Chen, W.; Hong, S. T.; Boycott, K. M.; Gorrie, G. H.; Siddique, N.; Yang, Y.; Fecto, F.; Shi, Y.; Zhai, H.; Jiang, H.; Hirano, M.; Rampersaud, E.; Jansen, G. H.; Donkervoort, S.; Bigio, E. H.; Brooks, B. R.; Ajroud, K.; Sufit, R. L.; Haines, J. L.; Mugnaini, E.; Pericak-Vance, M. A.; Siddique, T. *Nature* **2011**, *477*, 211.
6. Sreedharan, J.; Blair, I. P.; Tripathi, V. B.; Hu, X.; Vance, C.; Rogelj, B.; Ackerley, S.; Durnall, J. C.; Williams, K. L.; Buratti, E.; Baralle, F.; de Belleroche, J.; Mitchell, J. D.; Leigh, P. N.; Al-Chalabi, A.; Miller, C. C.; Nicholson, G.; Shaw, C. E. *Science* **2008**, *319*, 1668.
7. Kwiatkowski, T. J., Jr.; Bosco, D. A.; Leclerc, A. L.; Tamrazian, E.; Vanderburg, C. R.; Russ, C.; Davis, A.; Gilchrist, J.; Kasarskis, E. J.; Munsat, T.; Valdmanis, P.; Rouleau, G. A.; Hosler, B. A.; Cortelli, P.; de Jong, P. J.; Yoshinaga, Y.; Haines, J. L.; Pericak-Vance, M. A.; Yan, J.; Ticozzi, N.; Siddique, T.; McKenna-Yasek, D.; Sapp, P. C.; Horvitz, H. R.; Landers, J. E.; Brown, R. H., Jr. *Science* **2009**, *323*, 1205.
8. Greenway, M. J.; Andersen, P. M.; Russ, C.; Ennis, S.; Cashman, S.; Donaghy, C.; Patterson, V.; Swingler, R.; Kieran, D.; Prehn, J.; Morrison, K. E.; Green, A.; Acharya, K. R.; Brown, R. H., Jr.; Hardiman, O. *Nat. Genet.* **2006**, *38*, 411.
9. Chen-Plotkin, A. S.; Lee, V. M.-Y.; Trojanowski, J. Q. *Nat. Rev. Neurol.* **2010**, *6*, 211.
10. Bruijn, L. I.; Houseweart, M. K.; Kato, S.; Anderson, K. L.; Anderson, S. D.; Ohama, E.; Reaume, A. G.; Scott, R. W.; Cleveland, D. W. *Science* **1851**, *1998*, 281.
11. Pasinelli, P.; Brown, R. H., Jr. *Nat. Rev. Neurol.* **2006**, *7*, 710.
12. Haidet-Phillips, A. M.; Hester, M. E.; Miranda, C. J.; Meyer, K.; Braun, L.; Frakes, A.; Song, S.; Likhite, S.; Murtha, M. J.; Foust, K. D.; Rao, M.; Eagle, A.; Kammesheidt, A.; Christensen, A.; Mendell, J. R.; Burghes, A. H.; Kaspar, B. K. *Nat. Biotechnol.* **2011**, *29*, 824.
13. Benmohamed, R.; Arvanites, A. C.; Kim, J.; Ferrante, R. J.; Silverman, R. B.; Morimoto, R. I.; Kirsch, D. R. *Amyotroph Lateral Scler.* **2011**, *12*, 87.
14. Chen, T.; Benmohamed, R.; Arvanites, A. C.; Ralay Ranaivo, H.; Morimoto, R. I.; Ferrante, R. J.; Watterson, D. M.; Kirsch, D. R.; Silverman, R. B. *Bioorg. Med. Chem.* **2011**, *19*, 613.
15. Chen, T.; Benmohamed, R.; Kim, J.; Smith, K.; Amante, D.; Morimoto, R. I.; Kirsch, D. R.; Ferrante, R. J.; Silverman, R. B. *J. Med. Chem.* **2012**, *55*, 515.
16. Muehlebach, M.; Boeger, M.; Cederbaum, F.; Cornes, D.; Friedmann, A. A.; Glock, J.; Niderman, T.; Stoller, A.; Wagner, T. *Bioorg. Med. Chem.* **2009**, *17*, 4241.
17. Porath, B.; Rademacher, P.; Boese, R.; Blaser, D. Z. *Naturforsch.* **2002**, *57*, 365.
18. Ferguson, L. N. *The modern structural theory of organic chemistry*; Prentice-Hall: Englewood Cliffs, NJ, 1963. p. 128.
19. Zhang, Y.; Kirsch, D.R.; Silverman, R.B. Manuscript in preparation.
20. Liu, G. Z.; Xu, H. W.; Chen, G. W.; Wang, P.; Wang, Y. N.; Liu, H. M.; Yu, D. Q. *Bioorg. Med. Chem.* **2010**, *18*, 1626.
21. Dieter, R. K.; Pounds, S. *J. Org. Chem.* **1982**, *47*, 3174.
22. Orth, R.; Bottcher, T.; Sieber, S. A. *Chem. Commun.* **2010**, *46*, 8475.

Tetrahedron Letters 54 (2013) 573–575

Contents lists available at SciVerse ScienceDirect

Tetrahedron Letters

journal homepage: www.elsevier.com/locate/tetlet

A novel synthesis of 1-aryl-3-piperidone derivatives

Yinan Zhang, Richard B. Silverman *

Department of Chemistry, Chemistry of Life Processes Institute, Center for Molecular Innovation and Drug Design, Northwestern University, 2145 Sheridan Road, Evanston, Illinois 60208-3113, USA

ARTICLE INFO

Article history:
Received 19 October 2012
Revised 20 November 2012
Accepted 21 November 2012
Available online 29 November 2012

Key words:
3-Piperidone
Synthesis
Morita–Baylis–Hillman
Ring-closing metathesis
Heterocycles

ABSTRACT

A novel method to construct the 1-aryl-3-piperidone scaffold is described here. Starting from 3,5-dichloroaniline, a seven-step synthesis, without the use of protecting groups, generates the desired 3-piperidone ring in an overall yield of 30% through a key Morita–Baylis–Hillman reaction and ring-closing metathesis, providing an easy access to diverse and useful heterocycles.

The piperidine ring is an ubiquitous structure present in many natural alkaloids[1] and drug candidates;[2] therefore, its synthesis attracts much interest from organic chemists (Fig. 1). Of the piperidine derivatives, 3-piperidone is an important intermediate because of its easy conversion to other functional groups using various methods for the construction of bioactive heterocycles. For example, the transformation of a 4-carboethoxy-3-piperidone to pyrimidinone RO3203546, a selective α-1 antagonist,[3] and the rearrangement of a 2-methyl-3-piperidone to a 2-acetylpyrrolidine[4] proceed from 3-piperidone intermediates.

A typical procedure to 3-piperidones employs an intramolecular Claisen condensation of two branched esters of a tertiary amine to form a cyclic β-ketoester, followed by decarboxylation.[5] However, the extra deprotection step, as well as the moderate to low yield in the Claisen condensation, limits its application. Herein we report a novel route to construct 1-aryl-3-piperidone-4-carboxylate analogues without the use of protecting groups.

As a part of an ongoing project in our group to discover a therapeutic for amyotrophic lateral sclerosis (ALS),[6] the synthesis of the 3-piperidone, 1-(3,5-dichlorophenyl)-4-carboethoxy-3-piperidone (**6**), was a high priority. Initially we tried diethyl carbonate and Mander's reagent,[7] which was successful in our synthesis of the isomeric 1-aryl-4-piperidone-3-carboxylate **2**, but those reagents gave no β-ketoester from 3-piperidone **5** (Scheme 1). A Dieckmann condensation of diester **3** was shown to be an effective alternative route, but that reaction also failed when applied to **7**. Possibly, the intramolecular enolate attack does not occur because the planar aniline structure (**7**) reduces the flexibility of the ester chain and causes a loss of its ability to condense with the other ester. Several other attempts, including the use of a strong lithium base, intramolecular Claisen condensation between the corresponding Weinreb amide and an ester and a Buchwald amination of the corresponding phenyl bromide and 3-piperidone, also failed.

Since two possible bond-breaking positions around the β-ketoester moiety (**6**, a and b, Fig. 2) were fruitless, our focus shifted to position c. Given the wide utilization of Grubbs catalysts to mediate ring closing metathesis reactions,[8] we decided to replace the single bond at position c with a double bond. The double bond might isomerize from position c to b, which would provide the β-ketoester from the isomeric allylic alcohol in one step. Retrosynthetically, **6** could be derived from **8**, which could come from another key synthon **9** through a Morita–Baylis–Hillman (MBH) nucleophilic addition,[9] and **9** could be made from commercially available **10**.

The selective reactions of ethyl bromoacetate and allyl bromide with the aniline were performed under standard conditions (Scheme 2) in good yields.

Subsequent conversion to **8** was achieved via DIBAL reduction and then the MBH nucleophilic attack of acrylate mediated by DABCO. Standard conditions for ring-closing metathesis with 5% Grubbs II catalyst produced cyclic allyl alcohol **12** in near quantitative yields; the product yield decreased if the loading amount of Grubbs catalyst was reduced (see Supplementary data). With **12** on hand, several redox isomerization reactions of allyl alcohols to carbonyl compounds were explored, including Pd/C, $Ru(PPh_3)_2Cl_2$,[10] and $Cp^*Ru(CH_3CN)_3PF_6$.[11] However, no desired isomeric product was observed. Therefore, **12** was converted to **6** by hydrogenolysis of

* Corresponding author. Tel.: +1 847 491 5653; fax: +1 847 491 7713.
E-mail address: Agman@chem.northwestern.edu (R.B. Silverman).

0040-4039/$ - see front matter © 2012 Elsevier Ltd. All rights reserved.
http://dx.doi.org/10.1016/j.tetlet.2012.11.085

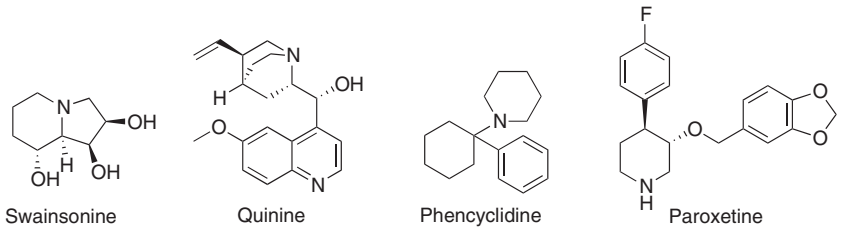

Figure 1. Examples of piperidine-containing alkaloids and drugs.

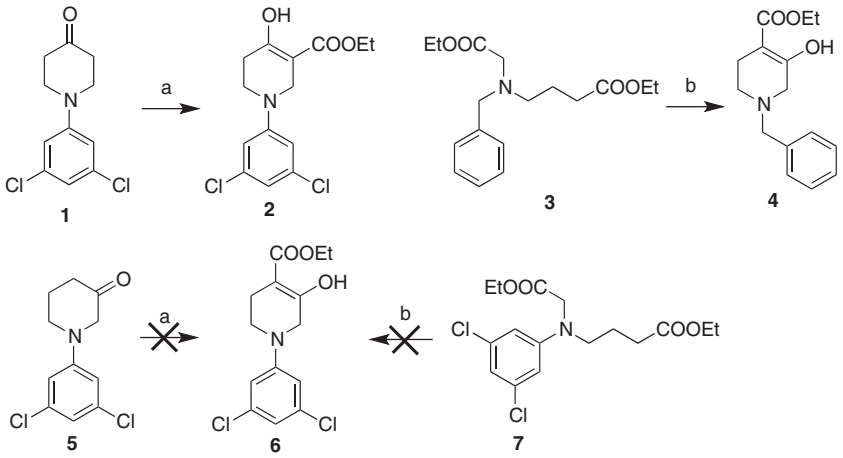

Scheme 1. Reagents and conditions: (a) $(EtO)_2CO$ or CNCOOMe, NaH, MeOH, toluene, 80 °C, 3 h, 24%; (b) NaH, toluene, reflux, 4 h, 52%.[3]

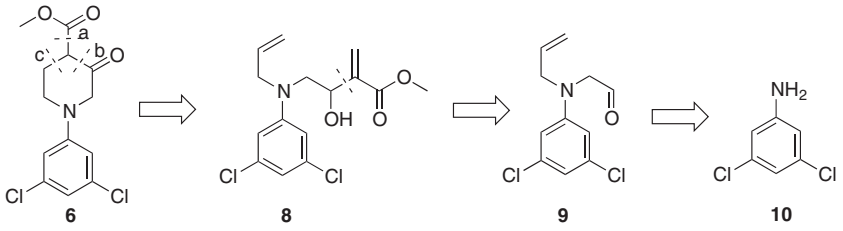

Figure 2. Retrosynthetic analysis of 3-piperidone analogue.

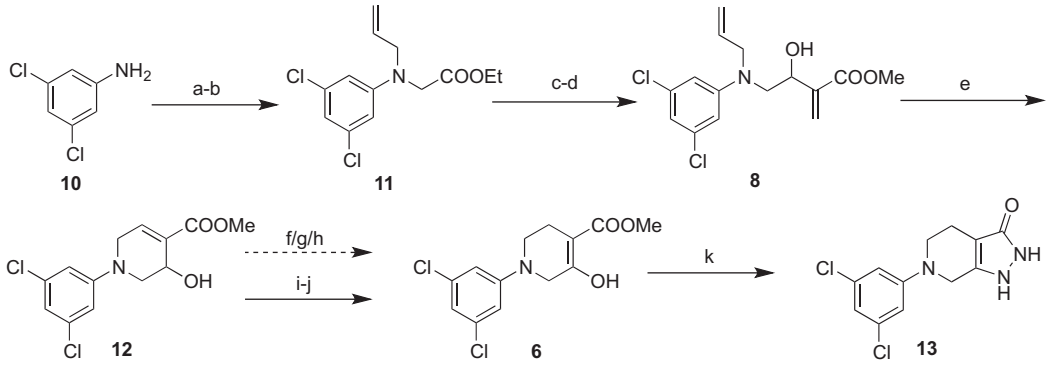

Scheme 2. Reagents and conditions: (a) $BrCH_2COOEt$, DIPEA, 90 °C, 24 h, 88%; (b) K_2CO_3, NaI, allyl bromide, CH_3CN, reflux, 2 days, 83%; (c) DIBAL, DCM, −78 °C, 1 h, 86%; (d) DABCO, methyl acrylate, room temp, 3 days, 71%; (e) 5 mol % Grubbs II, DCM, reflux, 5 h, 96%; (f) 5 mol % Pd/C, MeOH, reflux, 16 h; (g) 5 mol % $Ru(PPh_3)_2Cl_2$ toluene, K_2CO_3, 100 °C, 16 h; (h) $Cp^*Ru(CH_3CN)_3PF_6$, K_2CO_3, CH_3CN, 80 °C, 1 h; (i) Pd/C, EtOAc, 1 atm H_2, room temp, 16 h; (j) Dess-Martin periodinane, DCM, room temp, 1 h, 70% for two steps; (k) NH_2NH_2, EtOH, room temp, 16 h, 74%.

the double bond followed by Dess–Martin periodinane oxidation of the alcohol in good yields, giving **6** in an overall yield of 30% for the seven steps. Compound **6** was readily converted to our desired pyrazolone analogue **13** with hydrazine.

The 3-piperidinone analogue (**6**) is a useful intermediate for the synthesis of a variety of heterocycles, such as pyrimidinones,[3] quinuclidinones,[12] cyclohexanediamines[13] and benzomorphans.[14] Furthermore, medium size ring derivatives, such as azepanone and azocanone analogues, could be attainable from homoallylic or γ-propionate anilines using standard RCM conditions.[15]

In conclusion, a novel synthesis of 1-aryl-3-piperidone-4-carboxylates has been accomplished without the need for protecting groups. This method should be highly applicable for the synthesis of a variety of diverse heterocyclic compounds.

Acknowledgments

We thank the National Institutes of Health (Grant 1R43NS057849), the ALS Association (TREAT program) and the Department of Defense (AL093052), for their generous support of this research project.

Supplementary data

Supplementary data associated with this article can be found, in the online version, at http://dx.doi.org/10.1016/j.tetlet.2012.11.085.

References and notes

1. O'Hagan, D. *Nat. Prod. Rep.* **2000**, *17*, 435–446.
2. (a) Hu, L. Y.; Ryder, T. R.; Rafferty, M. F.; Feng, M. R.; Lotarski, S. M.; Rock, D. M.; Sinz, M.; Stoehr, S. J.; Taylor, C. P.; Weber, M. L.; Bowersox, S. S.; Miljanich, G. P.; Millerman, E.; Wang, Y. X.; Szoke, B. G. *J. Med. Chem.* **1999**, *42*, 4239–4249; (b) Becker, C. K.; Caroon, J. M.; Melville, C. R.; Padilla, F.; Pfister, J. R.; Zhang, X. WO 02/053558 A1, 2002.; (c) Large, C. H.; Bison, S.; Sartori, I.; Read, K. D.; Gozzi, A.; Quarta, D.; Antolini, M.; Hollands, E. *J. Pharmacol. Exp. Ther.* **2011**, *338*, 100–113.
3. Connolly, T. J.; Matchett, M.; Sarma, K. *Org. Process Res. Dev.* **2005**, *9*, 80–87.
4. Zhao, S.; Jeon, H.-B.; Nadkarni, D. V.; Sayre, L. M. *Tetrahedron* **2006**, *62*, 6361–6369.
5. Scalone, M.; Waldmeier, P. *Org. Process Res. Dev.* **2003**, *7*, 418–425.
6. (a) Chen, T.; Benmohamed, R.; Kim, J.; Smith, K.; Amante, D.; Morimoto, R. I.; Ferrante, R. J.; Kirsch, D.; Silverman, R. B. *J. Med. Chem.* **2012**, *55*, 515–527; (b) Zhang, Y.; Silverman, R. B. *J. Org. Chem.* **2012**, *77*, 3462–3467.
7. Mander, L. N.; Sethi, S. P. *Tetrahedron Lett.* **1983**, *24*, 5425–5428.
8. For review and recent examples of RCM application in heterocyclic synthesis (a) Vougioukalakis, G. C.; Grubbs, R. H. *Chem. Rev.* **2010**, *110*, 1746–1783; (b) Dondas, H. A.; Clique, B.; Cetinkaya, B.; Grigg, R.; Kilner, C.; Morris, J.; Sridharan, V. *Tetrahedron* **2005**, *61*, 10652–10666; (c) Polshettiwar, V.; Varma, R. S. *J. Org. Chem.* **2008**, *73*, 7417–7419; (d) Sattely, E. S.; Alexander Cortez, G.; Moebius, D. C.; Schrock, R. R.; Hoveyda, A. H. *J. Am. Chem. Soc.* **2005**, *127*, 8526–8533.
9. (a) Basavaiah, D.; Reddy, B. S.; Badsara, S. S. *Chem. Rev.* **2010**, *110*, 5447–5674; (b) Masson, G.; Housseman, C.; Zhu, J. *Angew. Chem., Int. Ed.* **2007**, *46*, 4614–4628.
10. Basavaiah, D.; Muthukumaran, K. *Synth. Commun.* **1999**, *29*, 713–719.
11. (a) Fagan, P. J.; Ward, M. D.; Clabrese, J. C. *J. Am. Chem. Soc.* **1989**, *111*, 1698–1719; (b) Bouziane, A.; Carboni, B.; Bruneau, C.; Carreaux, F.; Renaud, J. *Tetrahedron* **2008**, *64*, 11745–11750.
12. Da Silva Goes, A. J.; Cave, C.; d'Angelo, J. *Tetraheron Lett.* **1998**, *39*, 1939–1940.
13. Wang, J.-X.; Zhang, Y.-B.; Liu, M.-L.; Wang, B.; Chai, Y.; Li, S.-J.; Guo, H.-Y. *Eur. J. Med. Chem.* **2011**, *46*, 2421–2426.
14. Khartulyari, A. S.; Maier, M. E. *Eur. J. Org. Chem.* **2007**, 317–324.
15. Chattopadhyay, S. K.; Karmakar, S.; Biswas, T.; Majumdar, K. C.; Rahaman, H.; Roy, B. *Tetrahedron* **2007**, *63*, 3919–3952.

Journal of Medicinal Chemistry

Perspective

pubs.acs.org/jmc

Target- and Mechanism-Based Therapeutics for Neurodegenerative Diseases: Strength in Numbers

Paul C. Trippier,[†,§] Kristin Jansen Labby,[†,∥] Dustin D. Hawker,[†] Jan J. Mataka,[†,⊥] and Richard B. Silverman*[,†,‡]

[†]Department of Chemistry, Northwestern University, 2145 Sheridan Road, Evanston, Illinois 60208-3113, United States

[‡]Department of Molecular Biosciences, Chemistry of Life Processes Institute, Center for Molecular Innovation and Drug Discovery, Northwestern University, Evanston, Illinois, United States

ABSTRACT: The development of new therapeutics for the treatment of neurodegenerative pathophysiologies currently stands at a crossroads. This presents an opportunity to transition future drug discovery efforts to target disease modification, an area in which much still remains unknown. In this Perspective we examine recent progress in the areas of neurodegenerative drug discovery, focusing on some of the most common targets and mechanisms: *N*-methyl-D-aspartic acid (NMDA) receptors, voltage gated calcium channels (VGCCs), neuronal nitric oxide synthase (nNOS), oxidative stress from reactive oxygen species, and protein aggregation. These represent the key players identified in neurodegeneration and are part of a complex, intertwined signaling cascade. The synergistic delivery of two or more compounds directed against these targets, along with the design of small molecules with multiple modes of action, should be explored in pursuit of more effective clinical treatments for neurodegenerative diseases.

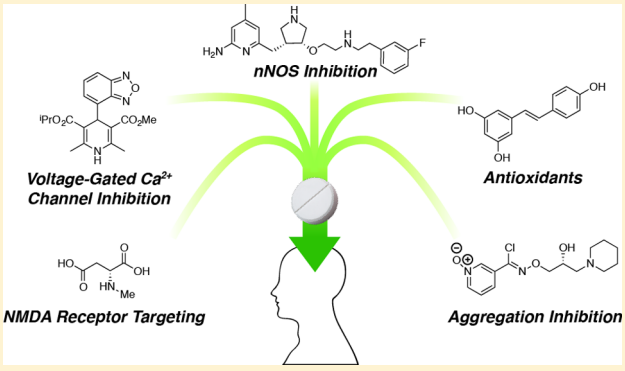

1. INTRODUCTION

Neurodegenerative disease is an encompassing term for a set of over 600 diseases in which the nervous system progressively and irreversibly deteriorates. The single greatest risk factor for the development of neurodegenerative disease is advancing age, with associated mitochondrial DNA mutation and oxidative stress damage,[1] illustrated by the fact that the majority of these diseases are late-onset. Alzheimer's disease (AD), the most prevalent of the neurodegenerative diseases, affects approximately 15 million people worldwide. Estimates expect the number of sufferers to triple in the U.S.[2] and Europe[3] by 2050, figures that are repeated for most other forms of neurodegeneration, including Parkinson's disease (PD) and Huntington's disease (HD).

The most common forms of neurodegenerative diseases are AD, PD, HD, and amyotrophic lateral sclerosis (ALS) (or in Europe, motor neurone disease, MND).[4] Specific aspects of these diseases, including protein aggregation, genetic mutations, and pathophysiology, are discussed in this Perspective. Extensive literature exists detailing each of the pathways highlighted, as well as for the many other neurodegenerative diseases. The interested reader is directed to those excellent reviews and references cited within this manuscript.

A commonality of the neurodegenerative diseases is that they are not diseases attributed to a single gene or even multiple genes; they are far more complicated, involving a myriad of known and unknown signaling cascades, misfolded proteins, protofibril formation, ubiquitin−proteasome dysfunction, oxidative and nitrosative stress, mitrochondrial injury, and many more events.[5] Our current understanding of neuroscience has enabled the identification of some key genes involved, but since many cases are seemingly sporadic, we know that mechanisms of neurodegeneration are more than just genetic.[6] While they vary in symptoms, neurodegenerative diseases have many pathologic overlaps (Figure 1). In this Perspective, we focus on the major components of this shared pathway: *N*-methyl-D-aspartic acid (NMDA) receptors, voltage gated calcium channels (VGCCs), neuronal nitric oxide synthase (nNOS), oxidative stress from reactive oxygen species (ROS), and protein aggregation.

NMDA receptors are ligand-gated, voltage-dependent ion channels that respond to the neurotransmitters glutamate and NMDA. NMDA receptor activation leads to Ca^{2+} influx into postsynaptic cells, which continues signal potentiation by activating signaling cascades. Overstimulation of NMDA receptors has been implicated in neurodegeneration, in addition to other disease states, and therefore NMDA receptors have been greatly investigated as a drug target (section 2). Ca^{2+} influx is also regulated by VGCCs. As discussed in section 3, one specific channel, $Ca_v1.3$, has been identified to play a role in the progression of PD, and therefore, selective antagonism of $Ca_v1.3$ is hypothesized to be potentially neuroprotective in early or presymptomatic stages of PD. Among many other responses, increased intracellular Ca^{2+} concentration

Received: October 29, 2012
Published: March 4, 2013

dx.doi.org/10.1021/jm3015926 | *J. Med. Chem.* 2013, 56, 3121−3147

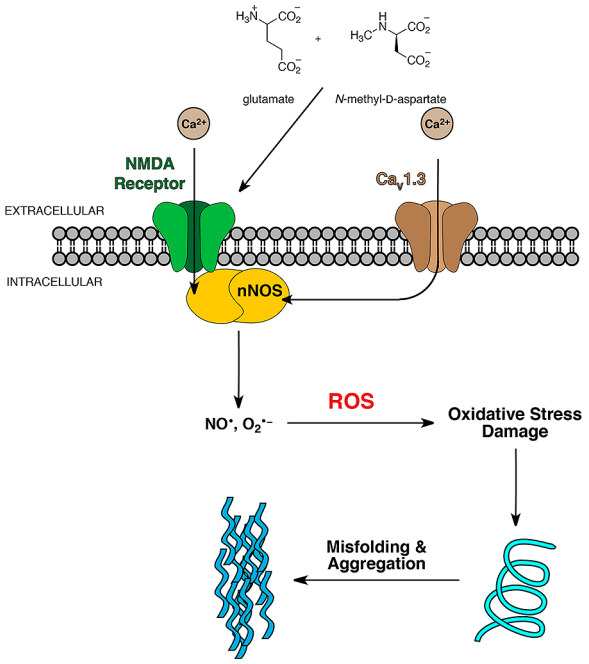

Figure 1. Common targets and mechanisms associated with many neurodegenerative diseases that are highlighted in this Perspective.

activates nNOS. Overactivation of nNOS produces high intracellular levels of nitrite and superoxide, which react to form ROS including peroxynitrite. This oxidative stress within the cell causes damage to DNA and lipids and causes protein modifications. Overactivation of nNOS has also been implicated in neurodegeneration, and therefore, inhibitors of nNOS are sought-after as potential therapeutics (section 4). Additionally antioxidant therapeutics are designed to directly prevent cellular damage from oxidative species (section 5). Lastly, protein aggregation is a hallmark of AD and PD, and while it may result from modifications by ROS, other mechanisms, such as mutations, are thought to be involved in protein aggregates observed in AD and PD. Progress toward developing antiaggregation therapeutics is examined in section 6.

A separate, but crucially important, pathophysiological pathway that contributes to neurodegeneration is inflammation and immune response.[7,8] Many of the most relevant immunological molecules are produced within the brain, and this leads to the observation that systemic immune responses affect brain function and contribute to neurodegeneration.[9] This pathway of inflammation and immune response is intricately connected with several, if not all, of the individual targets discussed in this Perspective. Space does not permit an all-encompassing review of this subject, and the reader is directed to the excellent review articles referenced herein. Expanding research continues to link this key pathophysiological pathway to the individual targets discussed in this Perspective, as briefly highlighted below.

Highly regulated by the immune system, the kynurenine pathway is an enzymatic cascade that converts tryptophan to serotonin but also to several other neuroactive compounds. Misregulation of this pathway results in increased or decreased production of these metabolites and contributes to a neurodegenerative effect.[10] Kynurenic acid is a competitive antagonist for the NMDA, kainite, and AMPA receptors and forms the structural scaffold for drug discovery efforts mentioned in section 2. Independent of the antagonistic effect of kynurenic acid is the observation that it is an effective free radical scavenger and can therefore display antioxidant properties similar to those of compounds discussed in section 5.[11]

Further connections from inflammation and immune response to antioxidants and nNOS inhibitors exist via a family of proteins known as toll-like receptors (TLRs). Evidence is increasing for the role of TLRs in sterile inflammation observed in neurodegenerative diseases, such as PD and AD.[12] These receptors play an important role in innate immunity because they recognize conserved motifs found in microorganisms. They are expressed in large numbers in various cells within the central nervous system (CNS) and serve to activate microglia. Microglia, the immune cells of the brain, are activated by distress signals from nearby cells. A side effect of this activation is the release of toxic factors, such as nitric oxide (section 4) and ROS (section 5), resulting in increased neuronal damage. TLRs are also being explored as targets for the treatment of neurodegenerative diseases.[13] Furthermore, polyphenols, discussed in section 5 and acting predominantly as antioxidants, also have activity crossover to the inflammation and inflammatory response; these compounds are known to modulate neuroinflammation by inhibiting the expression of inflammatory genes and the level of intracellular antioxidants.[14] Neuroinflammation commonly occurs as a result of oxidative and excitotoxic damage to neurons, and because of mitochondrial dysfunction, it is linked to protein aggregation.[15] It is therefore envisioned that drugs that combat neuroinflammation might also combat neurodegenerative disease progression.

However, while anti-inflammatory agents may be required to treat neurodegenerative diseases, they may not be sufficient on their own but may be effective as part of a combination therapy.[16] Such a combination might include targeting proinflammatory factors, such as tumor necrosis factor α and Fas ligand. One compound, revlimid, has been reported to modestly reduce these proinflammatory cytokines and to show some neuroprotection in an ALS mouse model.[17] Use of revlimid in a combinatorial approach with selected antiaggregation agents discussed in section 6 or potentially any of the agents in this Perspective may increase the neuroprotective effects from "modest" results with a single therapeutic compound to "significant" results with a combination of two or more compounds.

The thesis that AD, PD, HD, and ALS, although distinct disorders, share a common mechanism that progresses neuron death along a "neurodegenerative spectrum" has been advanced by numerous researchers.[18,19]

Recent advances have increased our understanding of the processes underlying neurodegeneration.[20−23] Drug candidates that target single or dual processes have been advanced to the clinic, but they only provide relief of symptoms, not of the underlying causes (which still remain unknown). Modulation of multiple targets along the same biological pathway could potentially lead to disease modification rather than just control of symptoms. The widely accepted definition of a disease modifying drug is "an agent that alters the underlying pathophysiology of the disease in question and demonstrates meaningful reduction in the rate of decline or progression to a defined milestone".[24] In a complex pathway with many drug targets, such as those contributing to neurodegenerative diseases, a drug with a single-target mechanism of action cannot always correct that pathway. The synergistic delivery of a "cocktail" of two or more drugs may deliver enhanced potency in the treatment of neurodegenerative diseases by potentially leading to disease modification.

dx.doi.org/10.1021/jm3015926 | J. Med. Chem. 2013, 56, 3121−3147

Polypharmacy, the synergistic combination of two or more drugs acting on different targets, has been successful in treating other diseases such as hyperlipidemia (high blood cholesterol). The combination of simvastatin (a 3-hydroxy-3-methylglutaryl-coenzyme A (HMG-CoA) reductase inhibitor) and ezetimibe (an inhibitor of dietary cholesterol uptake) is marketed as Vytorin.[25] This combination therapy works by preventing the body from making its own cholesterol while also inhibiting the absorption of cholesterol from dietary intake. A drug that inhibits only one source of cholesterol is less effective at lowering overall levels, as cholesterol is still produced by the second source. This disease-modifying therapy reduces overall cholesterol levels by targeting both sources. Other disease-modifying synergistic drug combinations have been utilized for the treatment of cancer,[26] hepatitis C virus,[27] and HIV/AIDS,[28] supporting the potential strategy of treating other complex diseases in a similar manner.

Alternatively, a single therapeutic agent could be designed to interact at two different targets. An example of a dual-acting drug that is disease-modifying is duloxetine (Cymbalta), used in the treatment of depression. This compound inhibits both serotonin and norepinephrine reuptake in the CNS.[29] Inhibition of the reuptake of both neurotransmitters increases overall levels of the two compounds, known to play an important role in mood. A deficit in either neurotransmitter can cause depression; therefore, increasing levels of both provides a disease-modifying therapy to counteract this deficit.[30] An example relevant to the disease pathway outlined in Figure 1 is the polycyclic caged amine compound NGP1-01 (**18**) (section 2), which blocks both the NMDA receptor and L-type calcium channel with resulting neuroprotective effects. Blocking only one of these targets allows the continued influx of Ca^{2+} ions from the other. As excess Ca^{2+} ion concentration is implicated in excitotoxicity, this would be analogous to trying to stop a bucket leaking from two holes by only stoppering one. Preventing an increase in overall Ca^{2+} ion concentration, and thereby excitotoxicity, could be considered disease-modifying over simply reducing the concentration.

Additionally, a multifaceted strategy would further probe the pathophysiological pathway(s) of neurodegeneration and confirm the intricate connectivity that has been proposed between therapeutic targets. Therapeutics developed for one type of neurodegenerative disease, when delivered in combination, may transfer their therapeutic potential to a different disease state, thereby exploiting and expanding the neurodegenerative therapeutic arsenal. Such combination therapy would also have advantages in drug delivery and dosing. Delivery of a significant dose of an inhibitor of $Ca_v1.3$-type calcium channels is hindered by concerns of selectivity over other Ca_v channels and resultant off-target toxicity. Dosing a lower concentration of such an inhibitor in conjunction with a modulator of another target on the pathophysiological pathway would allow for the inhibition of two targets that alone may provide no therapeutic response. This approach would provide the opportunity to use drugs that are active but only have low efficacy because of selectivity problems. As a result, the potential to tune inhibitory responses rather than outright blockage would allow for the use of small molecules previously discarded as nonefficacious.

This Perspective examines the state-of-the-art small molecule therapeutics available for each of the neurodegenerative disease targets depicted in Figure 1. A combination of these molecules or the design of new compounds bearing active moieties that target two or more of the pathophysiological hallmarks of neurodegenerative diseases might be expected to bring about a new era in neuroscience drug discovery while efforts continue toward further elucidation of the underlying causes of neurodegeneration.

2. ALTERATION OF NMDA RECEPTOR FUNCTION

NMDA receptors, named after their selective agonist, *N*-methyl-D-aspartate, are ionotropic receptors that mediate glutamatergic neurotransmission. These receptors, as well as α-amino-3-hydroxy-5-methyl-4-isoxazolepropionic acid (AMPA) receptors, kainate cation channel receptors, and metabotropic receptors, respond to glutamate, the major excitatory transmitter in the brain.[31,32] The NMDA receptors have long been studied as potential therapeutic targets because of the numerous CNS functions in which they have been implicated, both in normal physiological function and in disease states.[32,33] However, the numerous roles they play in normal neurological function have led to disappointing clinical outcomes in the development of new drugs as a result of adverse side effects.[32,34] Another complicating factor for the lack of successful therapeutic intervention through modification of NMDA receptor function lies in the permeability of Ca^{2+} through the channel; excessive ion influx results in excitotoxicity that can lead to neuronal cell death.[35,36]

The NMDA receptor has a relatively complex tetrameric subunit organization, and the subunit combination varies in different regions of the brain. This subunit heterogeneity presents additional challenges in drug design, since each subunit has distinct functional and pharmacological properties. Seven NMDA receptor subunits have been identified: a GluN1 subunit, four different GluN2 subunits (GluN2A−D), and two GluN3 subunits (GluN3A,B). The intact receptor consists of two GluN1 subunits and two GluN2 subunits. Glutamate binds to the GluN2 subunit, but for the receptor to be functional, glycine must simultaneously bind to the GluN1 subunit as a coagonist.[37] However, studies involving the CA1 region of rat hippocampus tissue slices have shown that synaptic NMDA receptors, which are important in long-term potentiation and NMDA-induced neurotoxicity, utilize D-serine as coagonist, whereas extrasynaptic NMDA receptors have a preferential affinity for glycine.[38] The intracellular portion of the transmembrane domains connect to a postsynaptic signaling complex known as the postsynaptic density, which contains PSD-95, enzymes such as nNOS and kinases, and other signaling and scaffolding proteins (Figure 2).[39,40] Excitotoxicity, including the excessive stimulation of NMDA receptors, has long been hypothesized to play a role in the etiology of neurodegenerative disorders such as PD[41] and HD[42,43] and may contribute, at least in part, to neuronal loss in AD[44] and other dementias, ALS,[36,45−47] and possibly multiple sclerosis and prion disease.[48]

Earlier work on NMDA receptor antagonists has focused on designing compounds targeting four regions of the receptor: the glutamate and the glycine agonist binding domain (ABD) sites, the channel pore, and the N-terminal domain (NTD) region between GluN1 and GluN2B.[49] Among the earliest glutamate competitive antagonists to be developed was phosphonic acid (*R*)-AP5 (**1**), which showed strong selectivity for NMDA receptors over kainate and AMPA receptors.[50,51] The introduction of rigidity with a piperazine ring provided another phosphonic glutamate site antagonist (**2**), which relieved parkinsonian symptoms and improved locomotion in animal models of PD when coadministered with L-DOPA,

dx.doi.org/10.1021/jm3015926 | J. Med. Chem. 2013, 56, 3121−3147

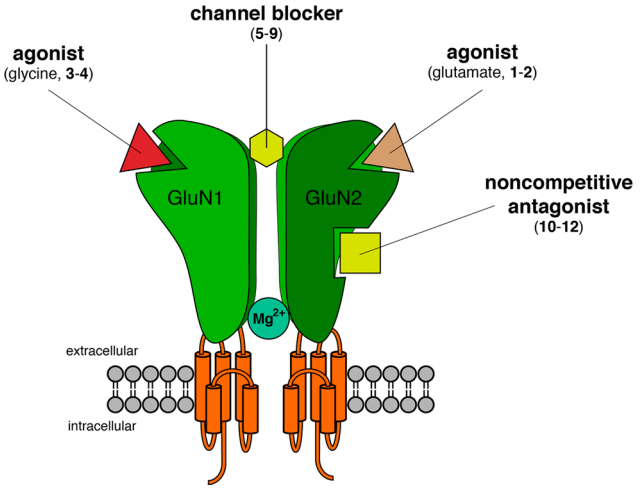

Figure 2. NMDA receptor showing agonist and antagonist binding site domains.

although it was not effective when given alone.[52] A drawback of the phosphonic acid class of antagonists is that their polarity makes passage through the blood–brain barrier (BBB) and intestinal membranes difficult.[53] Another problem with these competitive antagonists is that they generally demonstrate poor subunit selectivity.[31] The differences in potency between NMDA and glutamate between the different GluN2 subtypes are less than 4-fold, and an analysis of key residues in the binding pocket shows the presence of a highly conserved binding site.[54] Glycine site competitive antagonist 7-chlorokynurenate (**3**) did prevent NMDA-induced striatal lesions in an animal model as well as in vitro, but the compound targeted kainite receptors as well as NMDA receptors. In addition, the protection afforded by the compound could not be surmounted by coadministration of glycine but instead by increasing the dose of NMDA, calling into question its actual mechanism of action.[55] Since glycine acts at all NMDA subtypes, there may be an issue of tolerability of compounds targeting the glycine binding site, in addition to the higher doses of either glutamate or glycine antagonists that would be needed to surmount the competition with the endogenous ligands for their respective binding sites.[39] However, since glycine antagonists act at the GluN1 subunit, they may be associated with fewer side effects, although in the case of 7-chlorokynurenate (**3**), there has been the added issue of poor BBB penetration.[53,54] A series of 3-amino-1-hydroxypyrrolidin-2-one (HA-966, **4**) analogues were synthesized to overcome the limitations of poor solubility and BBB penetration.[53]

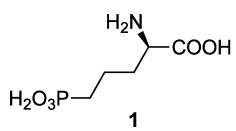

1

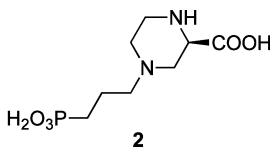

2

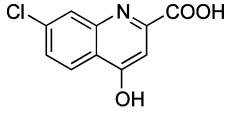

3

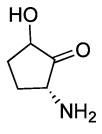

4

NMDA channel pore blockers, in particular amantadine (**5**) and its derivative memantine (**6**), have been developed for therapeutic use in inhibiting excitotoxicity. One of the earlier NMDA pore blockers to be advanced was dizocilpine (**7**), a high-affinity, uncompetitive antagonist.[56] Coadministration of dizocilpine with L-DOPA completely prevented the progressive reduction in the duration of the L-DOPA response occurring with chronic L-DOPA therapy in parkinsonian rats.[57] However, use of dizocilpine has been associated with severe side effects, such as coma,[58] and in one study actually exacerbated the symptoms of MPTP-induced parkinsonism when administered to a monkey.[59]

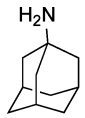

5

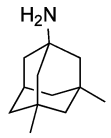

6

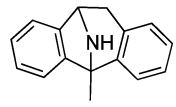

7

Amantadine (**5**) is an FDA approved drug that has been widely used in the treatment of PD. The predominant inhibitory mechanism of action of amantadine results from increasing the rate of channel closed states when the drug is bound in the channel of NMDA receptors.[60] In a retrospective study of PD patients attending a single clinic, improved survival was associated with amantadine use.[61] Amantadine, as well as the NMDA channel pore blocker dextromethorphan (**8**), also improved L-DOPA-associated motor response complications when given as an adjuvant to L-DOPA therapy.[62,63] However, a systematic Cochrane review of randomized controlled trials for amantadine concluded that because of a lack of evidence, it was not possible to determine whether amantadine is a safe and effective treatment for L-DOPA-induced dyskinesias in PD patients. The report also noted that in one study, 8 out of 18 participants had side effects, including confusion and worsening of hallucinations.[64] In an unrelated study, NMDA channel blocker remacemide (**9**), as adjunct therapy with L-DOPA, was not found to significantly improve motor fluctuation symptoms, although the compound was found to be safe and tolerable.[65]

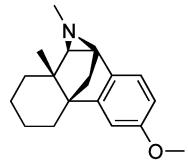

8

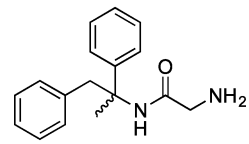

9

Memantine (**6**), another NMDA antagonist, is classified as an uncompetitive, open-channel blocker. The drug was patented by Eli Lilly & Co. in 1968 and was marketed by the German pharmaceutical company Merz to treat PD. The drug has a relatively fast off-rate from channel binding, which contributes to the drug's low affinity for the channel pore and, as a result, its clinical efficacy and tolerability. As a result, after several clinical trials, memantine was approved by the European Union in 2002 and the FDA in 2003 for the treatment of moderate to severe Alzheimer's disease.[66] One analysis concluded that the safety profile of memantine makes it particularly suitable for its use in elderly patients, since it is associated with a low overall rate of adverse events and a low potential for drug–drug interactions (because of a low extent of metabolism and protein binding, particularly to cytochrome P450 enzymes).[67] A recent review adds that for the treatment of moderate to severe AD, memantine should be offered either as a monotherapy or in conjunction with an acetylcholinesterase inhibitor but that the

dx.doi.org/10.1021/jm3015926 | J. Med. Chem. 2013, 56, 3121–3147

use of memantine as a first-line therapy for mild to moderate AD is not supported by current data. Further, insufficient data exist to make a recommendation for its use in PD dementia.[68] A paradoxical feature of the action of memantine is that a higher concentration of memantine is needed to alleviate mild dementia than to counteract the damage associated with moderate-to-severe dementia. This apparent incongruity has been explained by the on-rate for channel blockage by memantine being increased by increasing the drug's concentration, which leads to a greater proportion of channels being blocked.[66] To increase the neuroprotective efficacy of memantine, a second-generation derivative has been designed to incorporate a nitric oxide moiety, which should bind to the sulfhydryl group of a cysteine residue in the channel pore that has been found to down-regulate NMDA receptor activity.[58,69]

Much work remains for the design of therapeutic agents that can modulate NMDA receptors without adversely affecting normal cellular processes regulated by these channels. One more recent approach toward accomplishing this goal would be to design ligands that are subunit-specific and serve as noncompetitive antagonists.[31] The first subunit-selective NMDA receptor antagonist was ifenprodil (**10**), which inhibits Glu2B-containing receptors with a 200- to 400-fold selectivity over receptors containing Glu2A, Glu2C, and Glu2D subunits and with an IC_{50} of 0.34 μM for the GluN1/Glu2B receptor.[31,70] The difficulty in designing noncompetitive antagonists for the Glu2B subunit, which may be therapeutically relevant for a number of disorders, is that they also act at other receptors and channels, leading to side effects, causing a subefficacious lowering of the dose.[71,72] To improve selectivity, ifenprodil analogue **11**[73] and traxoprodil (CP-101,606, **12**)[74] were designed. Analogue **11** was found to be more effective than **10** in preventing toxicity to cortical neurons that mimic ischemic brain damage when exposed to glutamate (IC_{50} of 0.4 versus 3.5 μM, respectively).[73] Compounds **10**–**12** have antiparkinsonian activity in animal models. In a study of the use of **12** in counteracting dyskinesia and parkinsonism, it was found to reduce the maximum severity of L-DOPA-induced dyskinesia by approximately 30%, although many of the subjects in the study experienced dissociation, abnormal thinking, and amnesia. Compound **12** did not reduce parkinsonism in the study; however, the antidyskinetic effects were maximal at a lower dose, and the adverse effects were found to be dose-responsive.[75]

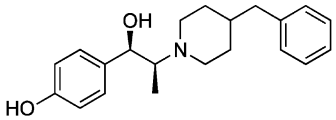

10

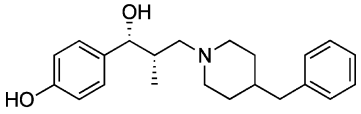

11

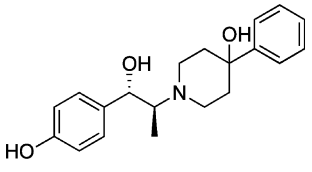

12

Among the recently identified voltage-independent negative allosteric modulators of NMDA receptors is **13**, one of the quinazoline-4-one derivatives advanced by Traynelis and co-workers.[76] Compound **13** had approximately 50-fold selectivity for recombinant GluN2C/D-containing receptors over GluN2A/B-containing receptors, low micromolar potency, and a novel mechanism that requires binding of glutamate to the GluN2 subunit but not glycine binding to the GluN1 subunit. The GluN2C/D over GluNA/B subunit selectivity of **13** was determined from ABD residues adjacent to the transmembrane helices.[77] Differing subunit selectivity profiles for negative allosteric modulation were also seen in a recent series of naphthalene and phenanthrene derivatives.[78] 9-Iodophenanthrene-3-carboxylic acid (UBP512, **14**) inhibited only GluN1/GluN2C and GluN1/GluN2D receptors, while 6-bromocoumarin-3-carboxylic acid (UBP608, **15**) inhibited GluN1/GluN2A receptors (23-fold) over GluN1/GluN2D, with IC_{50} values in the micromolar range. Consistent with their characterization as allosteric modulators, these compounds were found to be voltage-independent and not competitive with glutamate and glycine agonists. The site of action for **14** and related compounds is thought to be at the dimer interface between the ABDs, and the NTD was not found to be necessary for inhibitory activity.[78] Another negative allosteric antagonist, dihydropyrazoloquinoline **16**, inhibited GluN2C- and GluN2D-containing NMDA receptors over recombinant GluN2A- and GluN2B-containing receptors, with at least 50-fold difference in IC_{50} values. The selectivity was attributed to residues in the membrane-proximal lower lobe of the GluN2 ABD.[79]

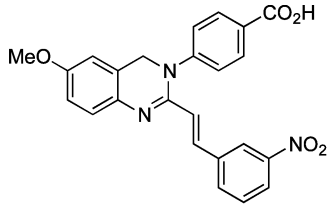

13

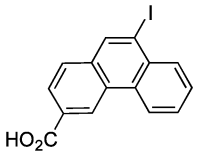

14

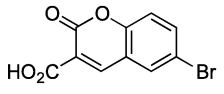

15

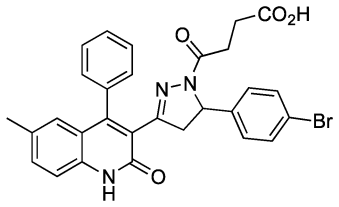

16

Bettini and co-workers reported several sulfonamide derivatives from high-throughput screening that were selective antagonists at GluN1/GluN2A over GluN1/GluN2B.[80] Addition of 1 mM glycine, but not 1 mM L-glutamate, overcame the inhibitory effects of the two most promising compounds. It was subsequently determined that one of the compounds, **17**, binds to a novel allosteric site at the dimer interface between the GluN1

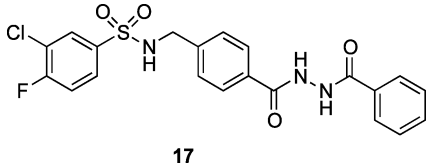

17

dx.doi.org/10.1021/jm3015926 | J. Med. Chem. 2013, 56, 3121–3147

and GluN2 ABDs, thereby reducing glycine potency (IC_{50} = 0.1−0.32 μM).

To exploit the subunit selectivity of these newer pharmacological tools for therapeutic advantage, it will be necessary to map the relative contribution of each subunit to its function both in normal cellular processes and in disease states. Recently, it was found that the NMDA receptor subtype specificity of three crucial channel properties (Mg^{2+} blockage, relative Ca^{2+} permeability, and single-channel conductance) were all determined primarily at a single GluN2 subunit residue in the transmembrane region.[81] However, because of the challenges involved in obtaining highly selective antagonists, there is still relatively little known about the function and therapeutic potential of the different subunits of the NMDA receptors.[49] One confounding issue in this regard is the subunit composition of the NMDA receptor, since two different GluN2 subunits may be present rather than only the binary combination of GluN1 and one type of GluN2 (or GluN3) subunit, in different regions of the brain.[82] By use of recombinant heterotrimeric GluN1/GluN2A/GluN2B and GluN1/GluN2A/GluN2C receptors with Zn^{2+} and ifenprodil antagonism, it was found that each ligand produced only partial inhibition and that maximal inhibition was only achieved with both copies of each GluN2 subunit in the receptor.[83] This finding suggested a potential limitation in using ifenprodil and its derivatives, since both GluN1/GluN2B and heterotrimeric GluN1/GluN2A/GluN2B receptors will be inhibited, possibly affecting subunit-specific control of normal neurological processes.

Other considerations may enter into the design of NMDA therapeutic antagonists, such as whether the agents will preferentially target synaptic or extrasynaptic NMDA receptors and the GluN2 subunit composition at those receptor sites. Work on the mechanism of action of memantine has shown that it preferentially targets extrasynaptic over synaptic NMDA receptors in a hippocampal autaptic neuronal preparation. In this study, the synaptic and extrasynaptic NMDA receptors in mature neurons differed in subunit composition, with the GluN2A receptors predominating at the synaptic receptors and the GluN2B subunits at the extrasynaptic receptors.[84] When cultured primary striatal or cortical neurons from rat were transfected with the gene coding for mutant huntingtin, a protein with polyglutamine repeat residues implicated in the pathogenesis of HD, and treated with D-APV, memantine, or ifenprodil, there was a significant decrease in the number of neurons expressing aggregated mutant-protein macroinclusions.[85] Further studies using a transgenic YAC128 mouse HD model showed that at high concentration of memantine both synaptic and extrasynaptic NMDA-mediated currents were blocked, worsening neurodegeneration. At low concentration of memantine the extrasynaptic receptors were predominately blocked, leading to a neuroprotective effect (reduction of striatal volume loss and motor learning deficits at 12 months post-treatment) from the largely unaffected synaptic activity.[85] Milnerwood et al. reported a similar reversal in intracellular signaling and motor learning deficits when the extrasynaptic NMDA receptors of YAC128 HD mice were pharmacologically blocked with a low dose of memantine, thus providing further evidence for a new therapeutic approach to combating HD.[86,87]

In view of the complex interplay of factors affecting NMDA receptor function, an integrative approach involving the modulation of receptor-associated pathways in the disease state may constitute a viable therapeutic strategy for neurodegenerative disorders. Since an excessive influx of Ca^{2+} ion into neurons is an important factor in the excitotoxic process, blockade of NMDA receptors could potentially be offset by the presence of L-type voltage-gated calcium channels.[88] Thus, design of therapeutic agents that can jointly antagonize both targets may be a desirable goal, and at least one such compound (**18**) has been developed.[89−91] Dimebon (latrepirdine) (**19**), an antihistamine compound used clinically in Russia for many years, has demonstrated efficacy in phase II clinical trials for AD and HD,[92] although a phase III trial for use in mild-to-moderate AD gave disappointing results.[93] Dimebon was found to inhibit both NMDA receptors (IC_{50} = 10 μM) and L-type calcium channels (IC_{50} = 50 μM) in cultured neurons, possibly accounting, at least in part, for its mechanism of action.[92,94,95] Blockage of NMDA-induced currents was different from that of memantine, suggesting a different site of action for dimebon at the NMDA receptor.[95]

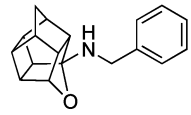

18

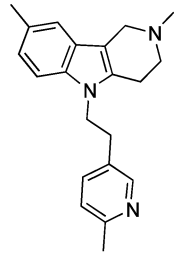

19

Influx of calcium via NMDA receptors can induce necrotic or apoptotic cell death, depending on the degree of glutamate stimulation, with the cellular fate influenced by the effect of the resultant intracellular calcium concentration on the mitochondria.[96] A therapeutic approach targeting the apoptotic pathway had mixed results when compounds shown to be effective both in vitro and in animal models for several neurodegenerative disorders were tested in human clinical trials.[97−99]

Another strategy for counteracting neuronal excitotoxicity might involve coadministration of an NMDA antagonist with an inhibitor of glutamate release. One potential candidate, riluzole (**20**), has been approved for use in treating the symptoms of ALS, although with limited success.[48] In addition to its role as an inhibitor for glutamate release, riluzole also protects neurons against NMDA-induced toxicity.[100−102] A clinical trial for use of riluzole in early PD showed that it was well tolerated in patients but with no significant difference relative to the placebo group.[103] Similarly, a 3-year randomized controlled study showed no neuroprotective or beneficial symptomatic effect of riluzole in HD.[104] An alternative to inhibiting glutamate release might be to use an agonist, such as ceftriaxone (**21**), for stimulation of glutamate uptake transporters. Ceftriaxone, a third-generation cephalosporin antibiotic, was found to be a potent modulator of glutamate transport through NF-κB-mediated excitatory amino acid transporter-2 (EAAT2) in primary human fetal astrocytes[105] and was in a clinical trial for ALS.[48]

Another important facet of an integrative therapeutic strategy to combat neurodegenerative diseases is the role that metabotropic glutamate receptors (mGluR) may play in the neural excitotoxicity process. An advantage of additionally targeting the mGlu receptors is that they can modulate the activity of voltage-gated calcium channels while not affecting fast excitatory synaptic transmission.[106] Pharmacological blockade of $mGlu_5$ receptors has led to reduced neuronal death in animal

dx.doi.org/10.1021/jm3015926 | J. Med. Chem. 2013, 56, 3121−3147

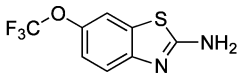

20

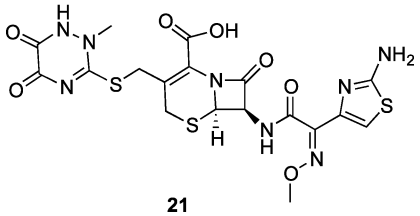

21

models of PD and ALS, and negative allosteric modulators for this receptor, as well as selective $mGlu_3$ receptor agonists, have been in clinical development.[107] A recent perspective provides an excellent overview of this subject.[108]

3. VOLTAGE-GATED CALCIUM CHANNELS

In the central nervous system, calcium's conductance properties are principally mediated by two types of receptors: ligand[109] and voltage-gated channels.[110] While NMDA receptors are involved in the total calcium load in neurons, smaller, but still significant, calcium contributions are mediated primarily through voltage-gated calcium channels.[111] Voltage-gated calcium channels (VGCCs) are expressed on the plasma membrane and open in response to depolarizing stimuli (events that lower the resting potential of neurons). In most physiological environments, VGCCs shuttle calcium from the extracellular space into the intracellular space. The accessory subunit and conducting pore (α_1-subunit) that constitutes VGCCs is the portion of the channel that conducts calcium, gives rise to the biochemical and biophysical properties in identified channels, and is the major site of pharmacological action. To date, 10 types of α_1-subunits have been identified, normally classified into five subtypes: L-type ($Ca_v1.1$, 1.2, 1.3, 1.4), P/Q-type ($Ca_v2.1$), N-type ($Ca_v2.2$), R-type ($Ca_v2.3$), and T-type ($Ca_v3.1$, 3.2, 3.3).[112]

$Ca_v1.1$, $Ca_v1.2$, $Ca_v1.3$, and $Ca_v1.4$ α_1-subunits, constituting the family of L-type calcium channels (LTCCs), are central players in neuronal calcium dynamics in both physiological and pathophysiological states. α_1-Subunits constituting $Ca_v1.1$ and $Ca_v1.4$ LTCCs are predominantly expressed outside the central nervous system, in skeletal muscle and the retina, respectively.[109] Functional $Ca_v1.2$ and $Ca_v1.3$ LTCCs are found in cardiovascular[113] and nervous tissue, respectively,[114] and play central roles as pharmacological targets in antiarrhythmia and antihypertension therapeutics. 1,4-Dihydropyridines (DHPs), phenylalkylamines (PAAs), and benzodiazepines (BZAs) are among the most common LTCC channel antagonists.[115,116]

$Ca_v1.3$ LTCCs have been identified as playing a role in the progression of Parkinson's disease by allowing uncompensated calcium loading in dopaminergic (DA) neurons in the substantia nigra pars compacta (SNc), which subsequently places a heavy and unsustainable metabolic burden on these neurons. It has been shown that by antagonism of these channels nonselectively with isradipine (**22**), a potent LTCC inhibitor, SNc DA neurons exhibit less metabolic stress and are protected in multiple PD animal models.[117] Selective antagonism of $Ca_v1.3$ LTCC is therefore hypothesized to be potentially neuroprotective in early or presymptomatic stages of PD.

While promising, isradipine is nonselective. It is also a potent $Ca_v1.2$ LTCC inhibitor. Therefore, long-term use of isradipine

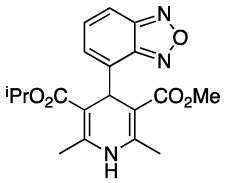

22

as a treatment for PD might result in hypotension or peripheral edema. Even if this does not result directly from isradipine use, it is known that during the course of PD, hypotension is common, thereby exacerbating this undesirable side effect.[118] Moreover, the nonselective nature of DHP inhibition of both neuronal types of LTCCs, $Ca_v1.2$ and $Ca_v1.3$, makes dosing regimens of isradipine, or other nonselective DHPs that might be disease-modifying in PD or other neurodegenerative diseases, an impossibility because the efficacious dose may have a serious effect on the therapeutic index of this strategy.[119] None of the Ca_v1 antagonists in the clinic preferentially select for $Ca_v1.3$ channels.[114,120] Thus, the search for more isoform-selective $Ca_v1.3$ LTCC antagonists has garnered recent attention.

Chang et al. described[121] a comprehensive structure–activity-relationship (SAR) study of modifications to the structurally simple, active DHP nifedipine[122] (**23**). A collection of 124 chemically diverse 4-substituted 1,4-dihydropyridines was generated; however, little selectivity of $Ca_v1.3$ over $Ca_v1.2$ was obtained. The most selective compounds generated (**24** and **25**) possessed $Ca_v1.3$ selectivities of only 2.2- and 2.4-fold, respectively, and both demonstrated only micromolar potencies. Observations from the SAR study showed an activity pattern for 4-substituted 1,4-dihydropyridines of substituted phenyl > thienyl > furyl > pyridyl > napthyl > alkyl (cyclic alkyl), with substitution of the phenyl ring at the 2-position being the most potent and at the 4-position the least potent. Complete loss of activity was observed when the pyridyl nitrogen was methylated or replaced with oxygen. These data implied that the generation of a high $Ca_v1.3$ selective DHP may be unlikely, and attention was focused on the generation of new scaffolds.

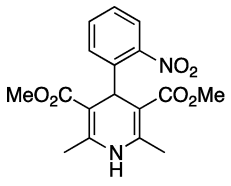

23

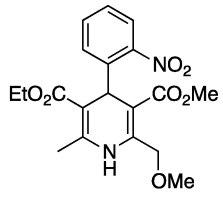

24

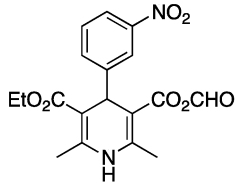

25

Compounds that show $Ca_v1.3$ LTCC inhibition, however selective, must maintain good pharmacokinetic properties and structure components with good potential for passing through the BBB. A high-throughput screen was initialized by the Silverman laboratory to identify novel $Ca_v1.3$ selective LTCC

dx.doi.org/10.1021/jm3015926 | J. Med. Chem. 2013, 56, 3121–3147

inhibitors by use of a calcium-sensing fluorescent imaging plate reader (FLIPR) assay. Over 60 000 molecules from a variety of commercial and government libraries were screened for activity with no hits resulting. In parallel with this screen Xia et al. described a series of symmetric pyrimidine-2,4,6-triones (PYT) investigated for applications in antiaggregation ALS models, possessing good pharmacokinetic properties and BBB penetration.[123] About 200 of these compounds and other scaffolds from the Silverman lab that were active in antiaggregation assays were tested, and the first PYT $Ca_v1.3$-selective antagonists were realized, although most of the compounds screened showed $Ca_v1.2$ selectivity. The lead compound was modified, providing the first highly selective $Ca_v1.3$ antagonist (**26**).[124]

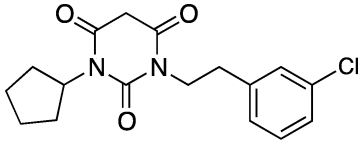

26

4. NEURONAL NITRIC OXIDE SYNTHASE INHIBITORS

As shown in the Figure 1 cellular cascade, activation of the NMDA receptor leads to calcium influx, which activates many downstream proteins, including nNOS.[125] The signaling molecule, nitric oxide (NO), is a free radical that is produced by nitric oxide synthases (NOSs) from substrate L-arginine, molecular oxygen, and NADPH. There are three isoforms of NOS: neuronal NOS (nNOS), which produces NO as a neurotransmitter; endothelial NOS (eNOS), which produces NO to signal the relaxation of smooth muscle cells in blood vessels; inducible NOS (iNOS), which produces a burst of NO in response to invading pathogens. The prominent role of NO in the nervous system leads to the possibility of improper regulation of NO and therefore various disease pathologies. High levels of NO have been implicated in neurodegenerative diseases including ALS and PD.[126] NO itself is a reactive molecule that leads to the formation of other oxidative species such as superoxide and peroxynitrite. Also, nitrated protein aggregates, which are highly toxic to neurons, are found in patients with neurodegenerative diseases. S-Nitrosylation of proteins is a common feature of Lewy bodies and intraneuronal protein aggregates found in PD.[127] Increased nitrosative stress may also compromise the ubiquitin degradation system, which, when impaired, cannot properly degrade proteins, leading to aggregation.[125] Parkin, an E3 ubiquitin ligase implicated in PD, has been shown to be S-nitrosylated, which impairs its function and leads to increased protein aggregation.[128−130] S-Nitrosylation of Hsp90 compromises its protection abilities as a chaperone and leads to increased aggregation.[131] NO stress can also compromise mitochondrial function. Electrons leak from the electron transport chain (ETC) to react with NO, forming peroxynitrite ($ONOO^-$), which damages lipids, proteins, and DNA.[132] S-Nitrosylation of prosurvival and proapoptotic proteins, p21, Ras, and Bcl-2 alters their activity.[132] Two of the isoforms of NOS, nNOS and eNOS, are constitutively expressed and activated by an increase in intracellular calcium concentration. Calcium binds to calmodulin, a small protein, and this complex binds and activates these NOSs.[133]

NOS inhibitors as potential therapeutics have been sought since the discovery of NO's signaling role in the late 1980s. Since crystal structure information was not yet available, early inhibitors began as arginine analogues, shown in Table 1 (**27**−**33**).[134] These inhibitors, however, lacked selectivity. Selectivity has proven to be difficult to achieve over the past 20 years because of the high homology of the isoforms, especially in the active site. *N*-Nitro-L-arginine (L-NNA, **27**) does show some selectivity, about 250-fold for nNOS over iNOS, but essentially no selectivity for nNOS over eNOS.[135] Because of the important role of eNOS in vascular regulation, this poor selectivity over eNOS leads to hypertension in animals.[136] L-NNA (**27**), L-NMA (**28**), and L-NAME (**29**) are commonly used in both in vitro and in vivo pharmacology experiments because of their stability, commercial availability, low toxicity, and solubility. Thiocitrulline and methylated thiocitrulline analogues have also been explored, but selectivity over eNOS has been difficult to achieve.[134]

Using L-NNA as a starting point, Silverman and co-workers developed several series of nNOS-selective dipeptides (see Table 2). This approach takes advantage of the potency of the arginine analogue scaffolds but also provides compounds that can potentially extend out of the heme binding pocket in an attempt to interrogate the isozymes for selective contacts away from the active site. Residue differences between isoforms include the following: S585 in nNOS is N370 in iNOS but is S356 in eNOS; D597 nNOS is N368 in eNOS.

Early dipeptide esters (**34**) achieved impressive selectivity over iNOS,[137] while more optimization led to **35**, which is highly selective over eNOS (1500-fold).[138] Modifications of the peptide scaffold included acetylation, benzyloxycarbonylation, amide methylation or conversion to peptoids, in an attempt to protect against metabolic degradation but led to drops in selectivity.[139] Exploration of conformationally rigid analogues of **34** led to highly potent, selective dipeptide amides **36**,[140] **37**,[141] and **38**,[142] but these compounds have limited BBB permeability because of their tricationic structures.

As crystal structures of NOS became available,[143,144] nNOS inhibitors moved away from the arginine mimetic scaffold. The Silverman group switched their strategy to de novo design using a pharmacophoric approach they developed termed "fragment hopping".[145,146] This led to a potent, nNOS selective aminopyridine scaffold (±**39**). Optimization led to potent, selective nNOS inhibitors (±**40**), and replacement of a nitrogen atom with an oxygen atom increased bioavailability (**41**).[145] Furthermore, (±)-**40** was shown to prevent hypoxia-ischemia-induced death in a rabbit model of cerebral palsy.[147] Upon maternal administration, (±)-**40** and an analogue were able to distribute readily to the fetal brain, inhibit NOS activity, and decrease NO concentration in vivo, to be nontoxic, without detrimental cardiovascular effects, and to show a remarkable protection of fetal rabbit kits from the HI induced phenotype of cerebral palsy. The rabbit kits from saline-treated dams had a large incidence of fetal/neonatal deaths (16/34, 47%) but *no deaths* (0/49) were observed from animals treated with (±)-**40** and its analogue. Of the kits from saline-treated dams that came to term (18/34), severe neurobehavioral abnormalities occurred in 12/18 (67%) compared to only 7/49 (14%) in those from dams treated with the inhibitors. Furthermore, the inhibitor-treated animals exhibited a remarkably larger number (83%) of normal kits; only 9% (3/34) of the kits from saline-treated dams were born normal.

Crystal structures of single enantiomers **41** and **42** revealed a surprising difference in binding mode.[148] Previous crystal structures show aminopyridines bind NOS with the aminopyridine head over the heme, but the (*R*,*R*) stereochemistry of **42** induces a flipped binding mode with the fluorophenyl tail

dx.doi.org/10.1021/jm3015926 | J. Med. Chem. 2013, 56, 3121−3147

Table 1. Structures, Potencies, and Selectivities of Arginine Analogues[e]

					Selectivity	
	Name	R_1	R_2	$K_{i\ rat\ nNOS}$(μM)	nNOS/eNOS[a]	nNOS/iNOS[b]
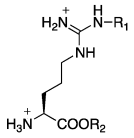						
27	L-NNA	NO_2	H	0.015[c]	11	293
28	L -NMA	CH_3	H	0.2	4.5	65
29	L - NAME	CH_3	CH_3	-[d]	-	-
30	L -NAA	NH_2	H	0.3[c]	8.3	10
31	L -ALA		H	0.2[c]	35	11
32	L -NCPA		H	0.6	-	400
33	L -NPA	$CH_2CH_2CH_3$	H	0.55	18	145

[a] $K_{i\ bovine\ eNOS}/K_{i\ rat\ nNOS}$. [b] $K_{i\ murine\ iNOS}/K_{i\ rat\ nNOS}$. [c] Bovine nNOS, not rat nNOS. [d] L-NAME presumably is hydrolyzed to L-NMA intracellularly or in vivo. [e] Data reported from Erdal et al. and references within ref 134.

Table 2. Dipeptide Ester and Amide nNOS Inhibitors

			Selectivity	
R		$K_{i\ rat\ nNOS}$ (μM)	nNOS/eNOS[a]	nNOS/iNOS[b]
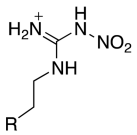				
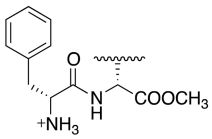	**34**[137]	1.9	2.6	1800
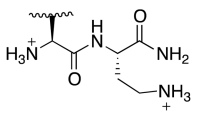	**35**[138]	0.13	1540	190
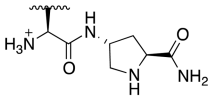	**36**[140]	0.10	1280	290
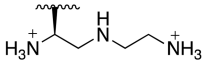	**37**[141]	0.12	2600	330
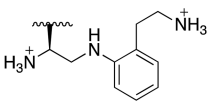	**38**[142]	0.05	2100	70

[a] $K_{i\ bovine\ eNOS}/K_{i\ rat\ nNOS}$. [b] $K_{i\ murine\ iNOS}/K_{i\ rat\ nNOS}$.

dx.doi.org/10.1021/jm3015926 | J. Med. Chem. 2013, 56, 3121−3147

binding over the heme. Moreover, this flipped binding mode is more potent; the K_i of **42** is 7.2 nM, which is lower than the K_i of **41** (116 nM) for nNOS.[149] Bioavailability of these inhibitors is poor as a result of the multiple cationic charges. A successful attempt to increase bioavailability and take advantage of the two binding pockets for the aminopyridine head led to **43**,[150] which displayed decreased nNOS selectivity. Compound **43** is a lead compound for designing future selective inhibitors of nNOS with increased bioavailability and a synthetically simple structure.

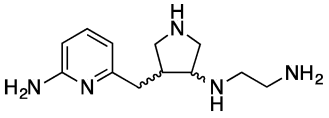

39

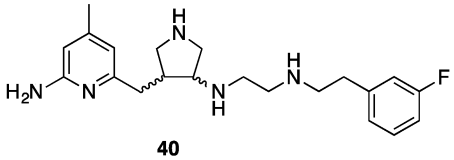

40

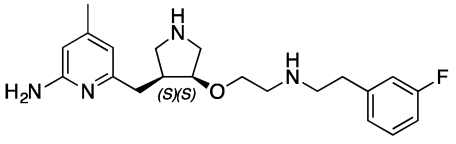

41

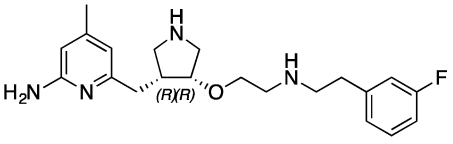

42

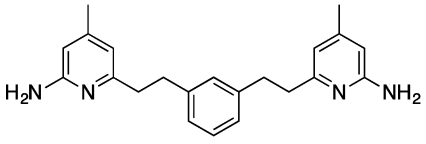

43

The aminopyridine moiety is a bioisostere of the guanidinium group of arginine. 2-Amino-4-methylpyridine (**44**) was found to be potent both in vitro and in vivo but is nonselective.[151] Simple substituted 2-aminopyridines were studied as NOS inhibitors but were found to be mostly selective for iNOS.[152] 6-Phenyl-2-aminopyridines were explored by Pfizer in the early 2000s as nNOS selective inhibitors. Compound **45** had an IC_{50} of 140 nM for human nNOS but only modest selectivity over eNOS (6 fold).[153] Compound **46** has an IC_{50} of 70 nM for human nNOS with 50- and 10-fold selectivity over eNOS and iNOS, respectively. The compound possessed a good pharmacokinetic profile and was well tolerated and effective in vivo.[154]

L-NIO (**47**) is an arginine analogue known to be a nonselective inactivator of NOS.[155] Compound **48**,[156] is an nNOS selective reversible inhibitor, unlike its homologue **49**,[157] which is iNOS selective and is an irreversible inhibitor. Compound **48** is selective for nNOS over eNOS (155-fold) and potent (IC_{50} human nNOS = 40 nM) but is not effective in vivo in rats.[156] nNOS selective carbamidines **50** and **51** were

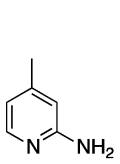

44

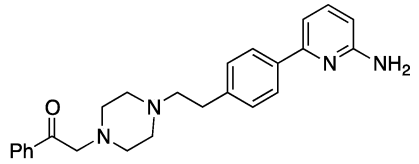

45

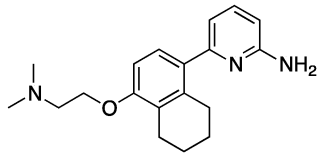

46

reported by Amoroso and co-workers;[158] computer modeling was used to rationalize that the selectivity of these bulky inhibitors is the result of the larger heme binding pocket of nNOS compared to that of eNOS and iNOS.

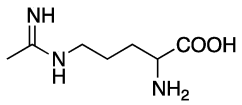

47

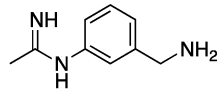

48

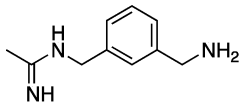

49

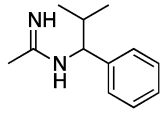

50

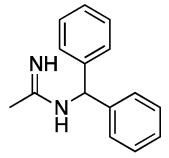

51

Another successful guanidine-mimetic moiety is the thiophene amidine (thienylcarbamidine) (**52**). Developed by AstraZeneca, **52** is a selective nNOS inhibitor with an IC_{50} of 0.035, 5.0, and 3.5 μM for human nNOS, iNOS, and eNOS, respectively.[159] It has been shown to effectively cross the BBB in animal studies and to be neuroprotective in ischemia models.[160] Crystal structures reveal that the amidine nitrogens hydrogen-bond to nNOS Glu592, much like arginine, while the thiophene sulfur lies 3.4 Å above the heme iron but does not coordinate as a sixth ligand.[161] NeurAxon has further explored the thienylcarbamidine functionality with **53** and **54**; these nNOS selective inhibitors are being developed for the treatment of migraine pain. Compound **53** is a dual-acting inhibitor of nNOS (IC_{50} of 0.44 μM) and agonist of the μ-opioid receptor (K_i of 5.4 nM), which is involved in pain.[162] Compound **54** is a potent, selective nNOS inhibitor without any cardiovascular effects and with a good side effect profile.[163]

A variety of other scaffolds have been explored as NOS inhibitors, but they are beyond the scope of this Perspective. They are described in detail in other excellent, recent review articles.[134,164,165] The compounds described above have all been active site inhibitors. Inhibitors that disrupt dimerization[166] and inhibitors that displace tetrahydrobiopterin[167] also have been explored as NOS inhibitors.

5. ANTIOXIDANTS AS THERAPEUTICS FOR NEURODEGENERATIVE DISORDERS

Misregulation of nNOS production can lead to oxidative stress, a hallmark of neurodegeneration. In addition to unregulated production of nitric oxide (NO) by nNOS, other reactive oxygen species (ROS) exist and have also been implicated in

dx.doi.org/10.1021/jm3015926 | J. Med. Chem. 2013, 56, 3121−3147

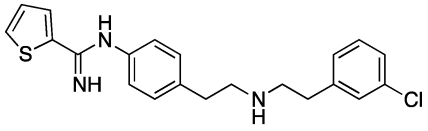

52
$IC_{50\ human\ nNOS}$ = 0.035 μM
selectivity nNOS/eNOS = 142
selectivity nNOS/iNOS = 100

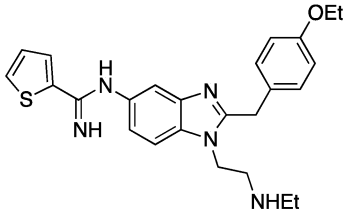

53
$IC_{50\ human\ nNOS}$ = 0.44 μM
selectivity nNOS/eNOS = 10
selectivity nNOS/iNOS = 125
$K_{i\ \mu\text{-opioid}}$ = 5.4 nm

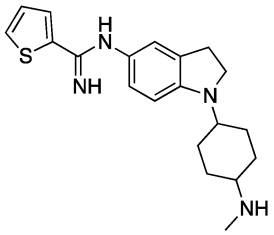

54
$IC_{50\ human\ nNOS}$ = 0.37 μM
selectivity nNOS/eNOS = 532
selectivity nNOS/iNOS = 224

neurodegeneration. A large number of ROS are free radicals or radical-generating derivatives of oxygen such as superoxide ($O_2^{\bullet-}$), hydroxyl radical ($^{\bullet}OH$), and hydrogen peroxide (H_2O_2). Cellular damage in the nervous system by free radical species has been implicated in AD,[168−173] PD,[174−177] HD,[178] and ALS.[179,180] Antioxidants are molecules that react with ROS to deactivate them and are of interest as potential therapeutics. Here, we present a summary of the major classes of antioxidants and their known or potential efficacy as treatments of neurodegenerative disease.

Compounds that can directly react with free radical species are referred to as direct antioxidants. These compounds do not generally rely on endogenous cellular mechanisms to wield their primary effect. The major classes of direct antioxidants include phenols, low-molecular-weight enzyme mimetics, and polyenes. Because of their ability to quench free radical species, direct antioxidants can halt the procession of potentially damaging radical chain reactions.

Free radical scavenging phenols, which rely on the facile ability of phenols to be oxidized to their corresponding quinones, can be divided into two categories: monophenolic and polyphenolic compounds. Monophenols vitamin E (α-tocopherol, **55**) and estrogens (**56**) have been repeatedly investigated for potential efficacy in treating a number of neurodegenerative diseases. Vitamin E has been shown to offer modest cognitive benefits in some AD patients;[181−183] however, other studies have shown no preventative benefit of vitamin E for AD development.[182−186] While no significant effects have been observed in PD,[187−190] or HD,[191] vitamin E was found to delay onset as well as slow the progression of ALS.[192,193] The use of estrogen replacement therapy (ERT) is also believed to play a preventative rather than therapeutic role in AD,[194−198] and it is likewise the case for PD,[199−201] which may be related to the increased disease prevalence observed in men over women.[202,203] Polyphenols, which include well-known compounds resveratrol (**57**) and curcumin (**58**), as well as a large family of flavonoids such as quercitin (**59**) and epicatechin (**60**), have already been extensively reviewed for their potential therapeutic properties.[204−207]

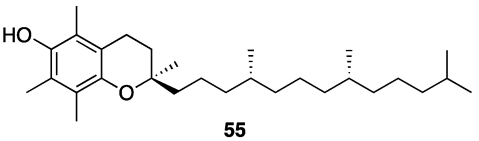

55

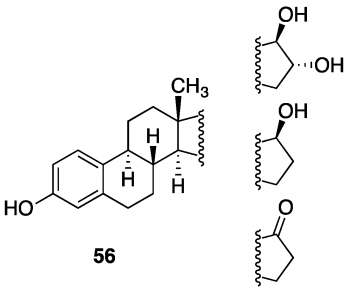

56

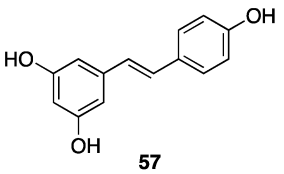

57

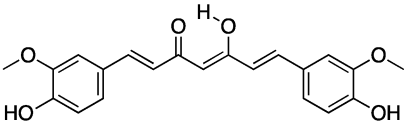

58

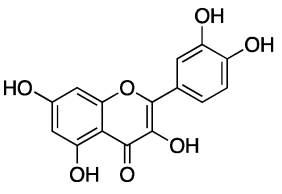

59

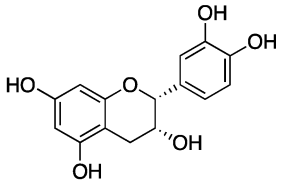

60

Under normal conditions, cellular antioxidant defense mechanisms are present to combat both metabolic and exogenous sources of ROS. These mechanisms include both small molecules and enzymes. The primary small molecule utilized is glutathione (GSH), a tripeptide possessing a sulfhydryl moiety capable of donating electrons to oxidized molecules, followed by regeneration via NADPH.[208,209] As for antioxidant enzymes, superoxide dismutase (SOD) converts $O_2^{\bullet-}$ into H_2O_2, which can then be rapidly reduced by catalase or glutathione peroxidase (GPx) to H_2O and O_2.[177,210,211] The metabolism of $O_2^{\bullet-}$ and H_2O_2 is critical because $O_2^{\bullet-}$ can react with NO to form peroxynitrite ($ONOO^-$), and H_2O_2 can react with Fe^{2+}

dx.doi.org/10.1021/jm3015926 | J. Med. Chem. 2013, 56, 3121−3147

to generate $^{\bullet}OH$ radicals, which are highly reactive species that are capable of lipid, protein, and DNA damage.[209,212] A study of potential low-molecular-weight mimics of SOD and GPx has identified a small number of potential therapeutics. The small, organoselenium compound ebselen (**61**) has exhibited notable activity as a GPx mimetic and $ONOO^-$ scavenger in vitro[213,214] and has shown significant beneficial effects in a primate model of PD.[215] Ebselen's catalytic ability can be initiated with or without the presence of ROS. In the presence of oxidative species, oxidation to the selenoxide (Se═O) followed by reduction via a thiol electron donor generates a reactive selenenic acid (Se−OH) that readily loses water and converts back to ebselen. Without the presence of ROS, oxidation of a free thiol forms a selenyl sulfide (Se−SR) leading to the production of a disulfide (RS−SR) and a selenol intermediate (Se−H). The selenol can be readily oxidized by ROS to form selenenic acid, which leads to regeneration of ebselen.[216] The organoselenium compound **62**, similar to ebselen, has shown even higher in vitro GPx-like activity and may also possess therapeutic potential for PD or other neurodegenerative disorders.[217,218] Organoselenium compound **62** is currently in clinical trials for cardiovascular indications.

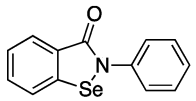

61

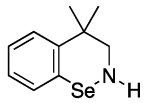

62

In addition to the therapeutic potential found in GPx mimetics, Mn-containing complexes have been found to be effective SOD mimetics. Metalloporphyrins **63** and **64** have been found to exhibit high SOD activity, catalase activity, as well as inhibition of lipid peroxidation.[219,220] The antioxidant activity of **63**, **64**, and similar metalloporphyrins has been extensively studied in a variety of models for oxidative neuronal damage.[221] Salen manganese complexes **65** and **66** are also SOD and catalase mimetics. These complexes have been shown to confer neuroprotection in both in vitro and in vivo models for PD.[222,223]

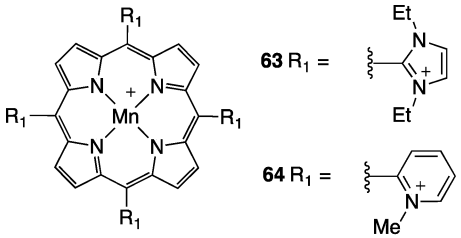

63 R_1 =

64 R_1 =

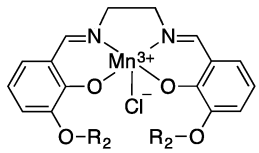

65 R_2 = Me
66 R_2 = Et

Polyene antioxidants primarily comprise carotenoids such as β-carotene (**67**), lycopene, retinol, and lutein and are typically of plant origin. These carotenoids are capable of scavenging singlet molecular oxygen ($^1O_2$) and peroxyl radicals forming stabilized radicals that can further react with ROS to halt radical chain reaction processes.[224] The rate constants for singlet oxygen quenching by carotenoids are on the order of 10^9 M^{-1} s^{-1}, which is near diffusion control.[225] Peroxyl radical scavenging is also efficient, especially under hypoxic conditions, and is important for the prevention of lipid peroxidation.[226] Carotenoids are an important part of the diet of animals because many carotenoids are metabolized to retinol (vitamin A), which cannot be synthesized endogenously. Retinoic acid (RA), an irreversibly oxidized form of retinol, is an important signaling molecule involved in embryonic growth and development. There have been a number of studies that suggest the therapeutic potential of RA for AD prevention,[227,228] but there has been no evidence to suggest a direct antioxidant effect of carotenoids being involved in neurodegenerative prevention. A more recent study, however, has shown that all-trans RA (ATRA, **68**) treatment invokes a decrease in brain Aβ deposition in an AD mouse model by inhibition of amyloid precursor protein processing.[229]

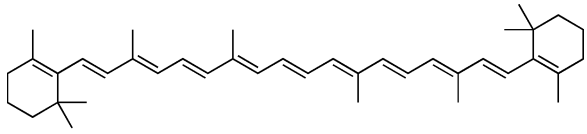

67

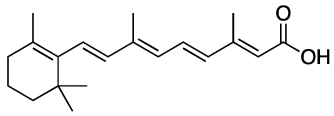

68

Indirect antioxidants are compounds that do not directly react with ROS but are involved in cellular management of oxidative species. Many of these compounds are essential cofactors required for cellular oxidative metabolism; however, a number of synthetic compounds have been identified that fall under this classification. These compounds act by easing the secondary metabolic burden of free radicals and therefore diminishing oxidative damage.

Quinones are a class of compounds, often derived from aromatic compounds, containing two carbonyl groups in an unsaturated six-membered carbon ring. The general label of vitamin K is applied to a number of related quinone compounds with a polyprenylated naphthoquinone ring structure. The primary role of vitamin K is to act as a necessary enzyme cofactor for a number of processes that include blood coagulation[230] and bone metabolism.[231] There is growing evidence, however, that vitamin K has important functions in the brain, and that a deficiency may contribute to the pathogenesis of AD.[232] Ubiquinone (**69**), also known as coenzyme Q_{10}, serves as an important cofactor, primarily in the electron transport chain during aerobic cellular respiration. Ubiquinone has been found to exert a protective effect against PD and HD[233,234] in addition to reducing intracellular Aβ deposition[235] and plaque pathology in AD mouse models.[236]

The mitochondrial-targeted ubiquinone analogues **70** and **71** have shown encouraging results for the treatment of age-related neurodegenerative disease.[237] Targeted delivery of these analogues is made possible by the cationic triphenylphosphonium group, which takes advantage of the potential gradient of the inner-mitochondrial membrane. Both have gone to clinical trials.[238]

Spin trapping compounds are labeled as such because of their ability to form adducts with free radicals via their nitrone functionality. Initially utilized in analytical chemistry, spin traps

dx.doi.org/10.1021/jm3015926 | J. Med. Chem. 2013, 56, 3121−3147

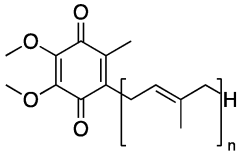

69

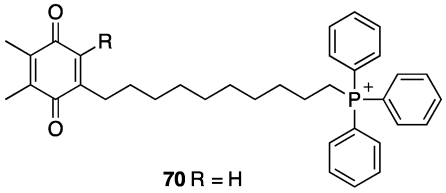

70 R = H
71 R = CH_3

have exhibited biological activity in a number of ROS implicated disease states.[239,240] Although spin traps are capable of directly quenching ROS, recent evidence suggests that they induce a number of endogenous antioxidants and enzymes involved in the attenuation of oxidative cellular damage.[241] *α*-Phenyl-*N*-*tert*-butylnitrone (PBN, **72**) has exhibited efficacy for the treatment of neurodegenerative diseases by affecting signal transduction pathways related to neuroinflammatory processes.[242,243] On the other hand, cerovive (**73**) was tested in stroke patients in clinical trials and failed to show efficacy, likely because of its poor pharmacokinetic properties.[244] The more lipophilic nitrones **74** and **75** have much higher radical scavenging potential over PBN and cerovive and have both exhibited neuroprotective efficacy in mouse models of PD.[245,246]

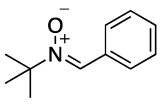

72

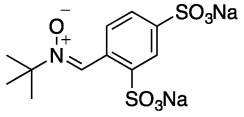

73

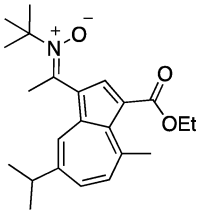

74

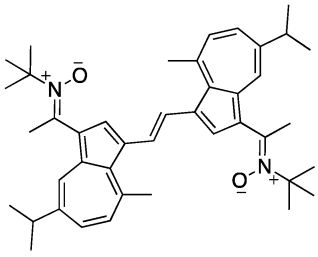

75

This final category of antioxidants is composed of a large and mixed group of compounds that are employed by the cell in the transport of reducing equivalents. Prominent examples include ascorbate (**76**), which has exhibited antioxidant activity in several in vitro studies,[247] and the previously mentioned GSH (**77**). A number of thiol precursors of GSH belong to this category as well. These include the dipeptide CysGly, which is used to generate GSH in neurons,[248] as well as cysteine precursors *N*-acetylcysteine (**78**) and procysteine (**79**).[249,250] Despite no known efficacy of these compounds for the treatment or prevention of neurodegenerative disease, brain levels of GSH are depleted by up to 30% in the elderly, suggesting a strong link to age-related disease.

The nuclear factor E2-related factor 2 (Nrf2) signaled gene expression in response to cellular stress must be considered

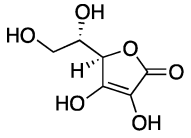

76

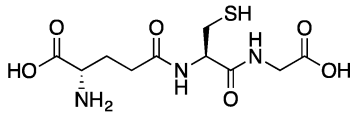

77

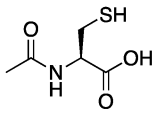

78

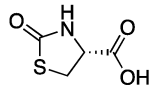

79

when discussing potential therapeutic effects of antioxidants. Nrf2 is a transcription factor responsible for the activation of a number of genes whose products are important in the reduction of cellular oxidative stress. These genes, which include glutathione-*S*-transferase (GST), coenzyme Q_{10}, NAD(P)H:quinone oxidoreductase, superoxide dismutase 1 (SOD1), and many others, contain a common promoter called the antioxidant response element (ARE). Under normal conditions, Nrf2 is bound to repressor protein Keap1 (Kelch ECH associating protein 1) and retained in the cytoplasm. In the Nrf2-Keap1-ARE expression pathway, Keap1 acts as a sensor for oxidative stress through oxidation of or electrophilic addition to its many cysteine residues.[251] Alteration of the cysteine residues of Keap1 disturbs Nrf2 binding, which allows Nrf2 to translocate into the nucleus. Once in the nucleus, Nrf2 heterodimerizes with members of the small Maf (sMaf) family of transcription factors, binds to the ARE, and ultimately leads to gene expression (Figure 3). An ever-growing number of

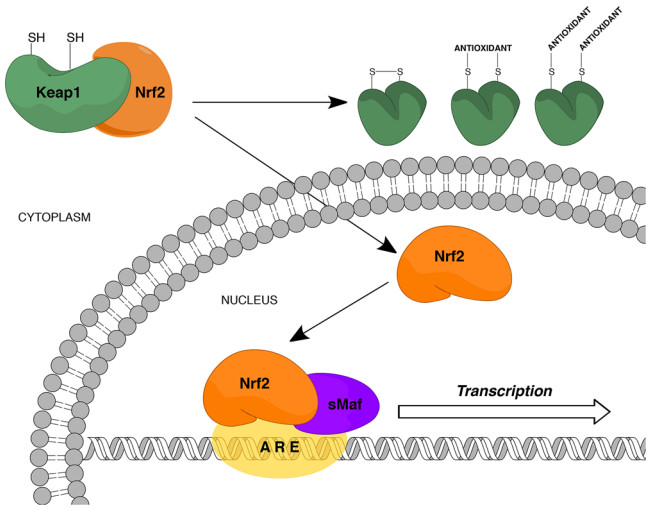

Figure 3. Mechanism of ARE-promoted gene expression by Nrf2. Disruption of the Keap1-Nrf2 complex allows for Nrf2 migration to the nucleus, where it joins with other transcription factors that bind to ARE regions of genes and initiate their transcription.

molecules able to induce Nrf2 signaling have been identified, including many previously mentioned antioxidants. These molecules, and the varying chemical characteristics that provide their activity, have previously been reviewed in great detail.[252,253]

The Nrf2 system has previously been the subject of reviews in regard to its potential as a therapeutic target.[254,255] Activation of Nrf2 has been observed to prevent apoptosis of

dx.doi.org/10.1021/jm3015926 | *J. Med. Chem.* 2013, 56, 3121−3147

motor neurons that were cocultured with the ALS model G93A-SOD1 mutant astrocytes. This prevention of apoptotic signaling is believed to be caused by glutathione-mediated NO detoxification.[256] Down-regulation of Nrf2 activated genes has also been observed in microarray analysis of mutant SOD transfected motor neuron-like Nsc34 cells.[257] It has also been shown that dietary sulforophane (**80**), a known Nrf2 signaling activator, protects against degeneration of dopaminergic neurons in a *Drosophila* PD model.[258] A study to assess the localization of Nrf2 in hippocampal neurons of AD indicated a loss of nuclear Nrf2 when compared to age-matched control individuals; however, cytoplasmic levels were the same between AD and control cases. This suggests impairment in nuclear trafficking and may limit Nrf2 activation as a potential AD treatment.[259] In an N171-82Q transgenic mouse model of HD, up-regulation of the Nrf2/ARE pathway by synthetic terpenoids **81** and **82** was found to rescue behavioral deficits, extend survival, and attenuate brain and peripheral pathology.[260]

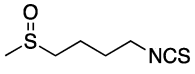

80

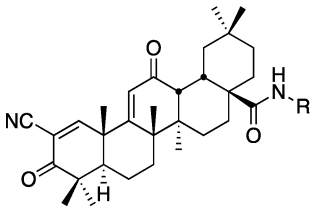

81 R = CH_2CH_3
82 R = CH_2CF_3

6. ANTIAGGREGATION AGENTS

One consequence of high levels of ROS is the damage and aggregation of proteins. Neurodegenerative diseases have been termed "protein aggregation diseases" because protein aggregation is another hallmark of these diseases. Aggregation consists of the formation of identical monomers of proteins self-associated into large oligomeric structures of reduced solubility that directly contribute to the onset and progression of the disease in question. Commonly implicated proteins (Table 3) include tau and amyloid-β in AD, α-synuclein in PD, huntingtin in HD, SOD1 in ALS, and others covering a range of diseases.[261] The aggregation process leads to formation of fibrils with defined morphologies or amorphous deposits or both. Here, we present an overview of therapeutic targets and a selection of molecules displaying antiaggregation properties. In this section we will concentrate on the most frequently studied protein targets for the development of antiaggregation inhibitors as listed in Table 3. Additional targets are known, and inhibitors are being actively developed; however, space precludes a detailed examination of all potential targets. Comprehensive introductions to the subjects of pathogenicity and potential targets,[262] and strategies for the design of antiaggregation inhibitors[263] that have been published previously, are excellent sources of in-depth coverage of the subject matter.

Inhibiting the accrual of misfolded forms of the proteins comprising aggregates is one commonly exploited approach for targeting many neurodegenerative diseases. Kinase inhibitors offer the advantage of allowing inhibition of the transformative process responsible for misfolding over inhibition of the production of the naturally occurring protein, which may be crucial to normal cellular function. Dual inhibition of glycogen synthase kinase 3 (GSK-3)[264] and cyclin-dependent kinase 5[265] is a promising strategy for tau-related diseases such as AD, when hyperphosphorylation of tau protein leads to malfunction and aggregation.[266] One such example of a dual-acting inhibitor for both kinases is the natural product hymenialdisine **83**, which has been the basis of intense SAR and analogue development to generate potential therapeutic candidates.[267] Similarly, GSK-3 has been implicated in the pathogenesis of a number of neurodegenerative diseases, such as ALS[268] and spinal muscular atrophy (SMA).[269] GSK-3 inhibitor VII (**84**) has been shown to significantly delay the onset of symptoms and extend the life span of a G93A-SOD1 mouse model of ALS.[270] BIP-135 (**85**) was found to prolong the median survival of the Δ7 SMA KO mouse model of SMA and elevate survival motor neuron levels in SMA patient-derived fibroblast cells.[269] Leucine-rich repeat kinase 2 (LRRK2) may regulate the propensity of α-synuclein to aggregate and, as a result, has garnered much attention as a target for a therapeutic intervention in PD.[271]

Table 3. Proteins Implicated in Misfolding Aggregation Diseases and Respective Targets for Aggregation Inhibitor Compound Design, As Discussed Herein

disease	aggregating protein	direct targets	indirect targets
Alzheimer's		BACE-1	HMG-CoA reductase inhibitors
	amyloid-β	α-secretase	protein kinases (GSK3, CDK5)
		γ-secretase	autophagy activators
		metal chelators	
	tau	physiological tau	
Parkinson's	α-synuclein		HMG-CoA reductase inhibitors
			protein kinases (LRRK2)
			autophagy activators
			heat shock protein
Huntington's	huntingtin	polyQ aggregates	HMG-CoA reductase inhibitors
			autophagy activators
			heat shock protein
amyotrophic lateral sclerosis	SOD1 and many others implicated		protein kinases (GSK3)
			autophagy activators
			heat shock protein

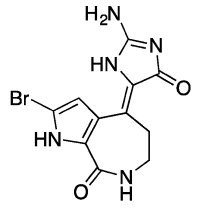

83

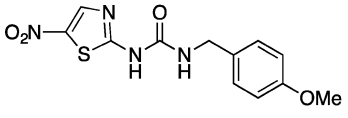

84

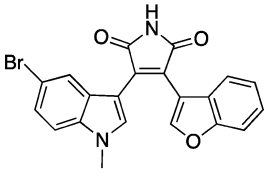

85

dx.doi.org/10.1021/jm3015926 | J. Med. Chem. 2013, 56, 3121−3147

Inhibition of tau aggregation has become an important strategy in targeting pathological tau. The use of small molecules to inhibit self-assembly of tau into oligomeric and/or polymeric species, including the well-defined fibrils comprising neurofibrillary tangles, has met with mixed success. Several compounds demonstrate activity in vitro; however, most also suffer from toxicity and/or limited CNS uptake issues.[272] A testament to the difficulty in designing tau inhibitors is the fact that one of the most promising structures is still one of the originally reported compounds having tau aggregation inhibition activity: methylene blue (**86**).[273] While methylene blue itself only possesses weak inhibitory activity, the compound provided a lead scaffold for derivatization. The dimethyl derivative, tolonium chloride, was found to exhibit 30-fold greater activity with a K_i of 69 nM, acting at almost equimolar concentrations with tau. Crucially, the compound did not inhibit the required tau−tubulin binding interaction. Interestingly the inhibitory activity was also observed in hyperphosphorylated tau, bringing into question the need to inhibit kinases to elicit a subsequent inhibition of tau aggregation. Recent advances have identified aminothienopyridazines (ATPZs) as a novel class of tau fibrilization inhibitors with efficacy in in vitro models and favorable druglike properties. Compound **87** represents the current lead structure, demonstrating good brain penetration, oral bioavailability, and nonspecific brain tissue binding. The compound is set to undergo long-term in vivo testing.[274] Refinement of in vitro models of tauopathy will also have a large impact on drug design targeting tau aggregation. A recently disclosed model using inducible hippocampal brain slices provides a more robust assay environment for further advances.[275]

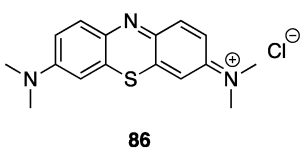

86

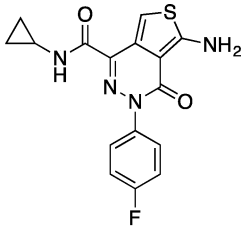

87

Accumulation of oligomeric β-amyloid peptides (Aβ) is characteristic of AD and is the primary agent in the pathogenesis of the disease. Aβ is generated from the amyloid precursor protein (APP) via two proteolytic enzymes, β-secretase and γ-secretase, responsible for the regulation of the first step in amyloidogenic APP metabolism and generation of Aβ, respectively. α-Secretase conducts an alternative proteolytic cleavage that prevents Aβ production and accumulation. Development of β-secretase (BACE-1) inhibitors has been hindered because of poor BBB permeability.[276] Recent efforts have moved away from peptide-based compounds to more lipophilic structures such as difluoride **88**, which demonstrated a 70% reduction of Aβ in beagle dog CSF up to 9 h after dosing.[277] Progression to phase I trials followed, showing for the first time a good correlation with preclinical and clinical efficacy. However, rat toxicology data indicated renal toxicity from an off-target interaction that has yet to be identified. The compound succeeded in demonstrating BACE to be a "druggable" target. Potent compounds inhibiting γ-secretase have been developed; however, inherent toxicity problems still remain as a challenge.[278] Avegacestat (**89**), a potent and selective γ-secretase inhibitor, succeeded in reducing brain levels of Aβ40 in wild-type rats by 59 ± 12% with a 30 mg/kg dose.[279] However, the compound has now been dropped from clinical studies by BMS. Modulation of α-secretase is an increasingly attractive target in AD therapy; activation is controlled by the protein phosphorylation signal transduction pathway of protein kinase C (PKC).[280] The known PKC activator bryostatin (**90**) promotes sAPP-α-secretase at subnanomolar levels;[281] analogue construction to refine pharmacological properties has garnered a great deal of attention in the literature.[282]

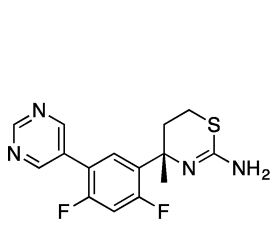

88

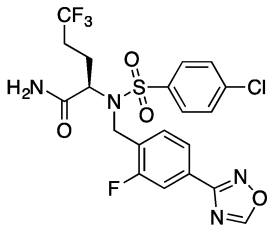

89

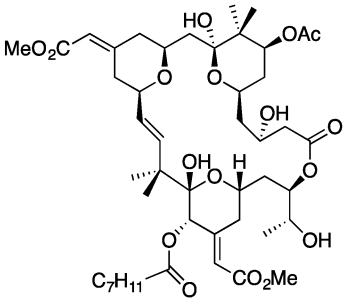

90

Twenty-five percent of the cholesterol present in humans is synthesized in the brain, where it performs many vital functions, such as myelin formation, structural composition of glial and neuronal membranes, and in neurotransmission. A link between cholesterol levels and the production of APP in Alzheimer's patients has been suggested by the use of statins, cholesterol-lowering drugs that inhibit 3-hydroxy-3-methylglutaryl coenzyme A (HMG-CoA) reductase, demonstrating a decreased prevalence of AD.[283] In particular, simvastatin showed a marked decrease of both cholesterol and Aβ in guinea pig CSF; however, translation to human patients only showed a small decrease, which may be attributed to the higher concentration of Aβ in plaque formed within the brain and therefore not available to transfer to CSF.[284] Interest in the link between cholesterol regulation and neurodegenerative diseases has grown considerably in recent years with implications ranging from AD[285] to PD,[286] HD,[287] and the prion diseases.[288] Attempts to identify new HMG-CoA reductase inhibitors and analogues of statins continue.[289]

There is increasing evidence that heat shock proteins (HSPs), molecular chaperones that control protein misfolding and aggregation, could counteract the pathological mechanisms that take place during AD, PD, and HD.[290] The HSPs can interfere with the misfolded disease-linked proteins, thereby preventing interactions that can lead to formation of toxic oligomers. Moreover, HSPs are expected to interfere with detrimental processes that occur during these diseases, such as oxidative stress, and act in support of the ubiquitin−proteasome degradation process. These factors combine to make HSP

dx.doi.org/10.1021/jm3015926 | J. Med. Chem. 2013, 56, 3121−3147

activators an important target in combating neurodegenerative disease.[291] Central to the hypothesis of targeting protein misfolding is heat shock transcription factor 1 (HSF1), the main activator of chaperone protein gene expression; activating HSF1 increases the amount of chaperone expression and, in turn, the rate of clearance of misfolded proteins.[292] The chaperone protein Hsp90 is responsible for protein folding regulation in many cells and, in addition, is known to bind to HSF1 and impede activation; therefore, Hsp90 inhibitors have therapeutic potential in many neurodegenerative diseases.[293] A representative example of a Hsp90 inhibitor, celastrol (**91**), which is isolated from a Chinese medicinal herb, is a potent inhibitor of Hsp90 acting by activation of HSF1;[294] however, the exact mode of action is poorly understood and is the subject of much investigation to aid in the development of this compound as a potential therapeutic.[295] Arimoclomol (**92**), a co-inducer of heat shock proteins, increases median survival in a G93A-SOD1 mouse model of ALS by 22%, illustrating the therapeutic potential of the HSP target in ALS.[296] In addition, the closely related protein Hsp70 is rapidly gaining interest as a target for many diseases, including those contributing to neurodegeneration.[297] In addition to HSP inhibitors, several other classes of compounds have been found to elicit an activation effect in autophagy and hence increase the rate of fibril clearance.[298] Among the most widely investigated of these compounds are rapamycin (**93**), which displays neuroprotective effects in many neurodegenerative diseases,[299] and the disaccharide trehalose (**94**), which has been shown to reverse aggregation caused by proteasome inhibition.[300] HSPs act as protein folding machinery and work in conjunction with the ubiquitin–proteasome system (UPS),[301] failure of which is thought to contribute to the pathogenesis of PD.[302]

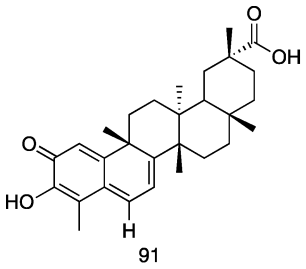

91

91

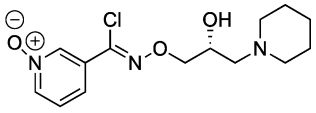

92

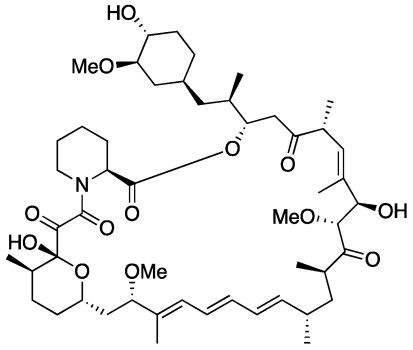

93

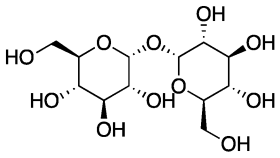

94

A myriad of additional approaches for therapeutic design and intervention in neurodegenerative disease have been proposed, and a comprehensive discussion is beyond the scope of this Perspective; however, several newly emerging areas will be discussed briefly. The use of chemical chaperones, small molecules having the ability to stabilize unfolded monomer conformations and/or to destabilize misfolded oligomers, has been widely explored.[303,304] An alternative approach involves the use of metal chelators, compounds that sequester physiological metal ions and, in so doing, block protein aggregation. Aβ, for example, shows ready binding to metals such as Zn^{2+} and Cu^{2+}, which induce nucleation and the formation of aggregate plaques. In addition, the interaction between redox active Cu^{2+} and Aβ can produce neurotoxic reactive oxygen species.[305] Recent developments have led to the synthesis of platiniferous chelators such as **95**, containing a Pt(bipyridine)-Cl_2 group as the Aβ binding portion.[306] Compounds of this type show almost complete reversal of Aβ aggregation in turbidimetry experiments conducted using Aβ40. Additional compounds, many of them peptidyl in structure, acting as β-sheet blockers have been investigated.[307]

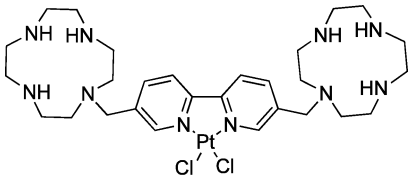

95

Direct inhibition of the oligomerization pathway has been shown to be possible with a number of small molecule inhibitors that disrupt soluble oligomers and interfere with larger structures; however, this approach does not take into account the accumulation of potentially toxic monomers. Such compounds include *N*-phenylanthranilic acid analogues (**96**), displaying activity against the Aβ peptide with an IC_{50} of 1 μM,[308] and benzothiazole **97**, with activity to prevent polyQ aggregates (the cause of Huntington's disease) in vitro with an IC_{50} of 1.2 μM.[309]

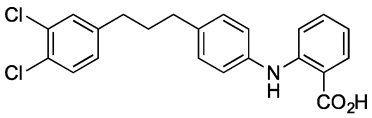

96

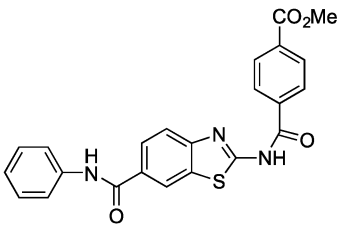

97

Despite a rich choice of targets of action, the use of anti-aggregation agents in the treatment of neurodegenerative diseases has been limited. Poor BBB penetration, off-target toxicity, distribution in target tissue, and poor kinase selectivity

dx.doi.org/10.1021/jm3015926 | J. Med. Chem. 2013, 56, 3121–3147

have limited the potential of this broad class of compounds. Developments continue to counteract these limitations, and further optimization has the potential to create an efficacious and clinically useful therapeutic. One such strategy is the development of compounds that interact at multiple targets across the antiaggregation target spectrum.

7. CONCLUSIONS

Modulation of one or more of the distinct physiological processes depicted in Figure 1 has been shown to be pathological in neurodegenerative diseases. Small molecule therapeutics have been developed to target each step of the process: voltage-gated calcium channels, NMDA receptors, neuronal nitric oxide synthase, oxidative stress from reactive oxygen species, and protein aggregation. In addition to their potential as therapeutics, small molecules targeting proteins involved in neurodegenerative pathways can provide insight into their roles and connections. Determining how targets interact with each other could reveal previously unknown pathways. However, after more than 100 years of intense research, all current therapies for neurodegeneration are still directed toward symptomatic relief, not disease-modifying effects.

In the development of small molecules to combat neurodegenerative diseases, a combination therapy approach such as those taken to treat cancer, to fight microorganisms, and to remedy hypertension should be considered. A multitarget therapeutic approach will combat the disease from many pathways, greatly enhancing the probability of disease modification. For example, inhibiting nNOS from producing species that generate ROS and inhibiting protein aggregation provide a dual mode of action by simultaneously reducing the underlying cause of protein misfolding and aggregation (oxidative stress damage) and combating the aggregation caused by ROS that survive to cause protein damage. Second, the potential synergy that may result from a drug combination may allow for the use of therapeutics at lower levels, allowing for the deployment of therapeutics that have small therapeutic windows, off-target effects, poor potency, or high toxicity, thereby expanding the arsenal of drugs available to fight these crippling, fatal diseases.

Successful dual-acting compounds are beginning to be reported; however, such compounds remain scarce in the literature and represent a minute proportion of the overall effort in drug discovery for neurodegeneration.[310] Examples designed to target two of the pathways depicted in Figure 1 include compound **18**, a dual NMDA and LTCC inhibitor discussed in section 2. Benzofuran-based compound **98** and analogues demonstrate activity in three pertinent targets for AD; they serve as acetylcholine esterase inhibitors, Aβ aggregation inhibitors, and inhibitors of Aβ_{25-35} peptide-induced ROS formation. The potential of these compounds to be disease modifying lies not just with their targets but also with their ability to combat one of the underlying generators of ROS in AD rather than simply inactivating individual species.[311] Imidazole **99** represents the most active compound of a library of analogues screened for nNOS inhibition activity. The compounds were designed as dual-target compounds; in addition to acting as nNOS inhibitors, the compounds are active antioxidants that scavenge free radicals and/or reduce lipid peroxidation.[312] While these compounds were designed as a possible therapeutic for cerebral ischemia, they would appear to be ideal compounds for screening in neurodegenerative disease drug discovery.

A final example is the combination of two therapeutic constructs by a linker chain. Huprine−tacrine heterodimers (**100**) simultaneously block the active and peripheral sites of acetylcholinesterase, resulting in high potency (approximately 1 nM). Additionally, the heterodimers interact at two targets in the pathway of Figure 1, acting as both self-aggregation inhibitors of Aβ (ranging from 39% to 67% inhibition) and BACE-1 inhibitors (5−7 μM). Interestingly, while both of these targets are AD specific, the compounds inhibit the aggregation of a prion peptide that plays a key role in the aggregation of the prion protein.[313]

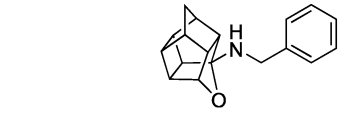

18

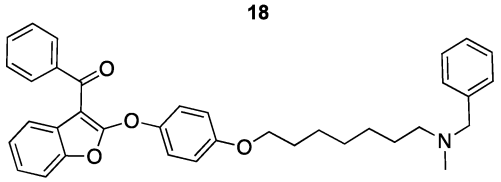

98

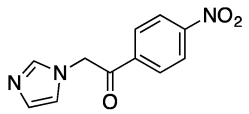

99

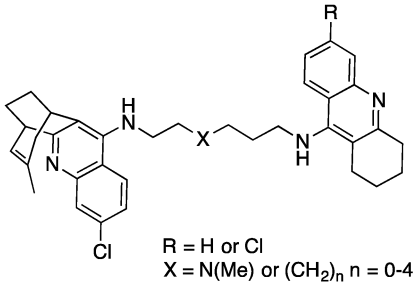

100

A multitarget approach would provide drug combinations and first-in-class molecular scaffolds to allow for the further probing and elucidation of the precise molecular networks and signaling cascades that underlie the nature of neurodegeneration. Given the fact that at present there is not yet a single therapy, let alone a combination of therapies, that significantly alters the progression of neurodegeneration, an understanding of the root causes for neurodegeneration, and the knowledge of the important pathways that should be altered to accomplish this, would be welcomed.

This Perspective, based on the commonalities within neurodegeneration (Figure 1), describes druggable targets of action and the compounds developed to interact with them. In so doing, we have covered many targets that are specific to one particular disease (e.g., BACE1 inhibitors for AD). It is our intent to bring to the attention of the reader possible target combinations and molecular scaffolds that, when combined, may advance the discovery of the ultimate goal in neuroscience drug discovery: a disease modifying therapeutic.

dx.doi.org/10.1021/jm3015926 | J. Med. Chem. 2013, 56, 3121−3147

AUTHOR INFORMATION

Corresponding Author

*Phone: 1-847-491-5653. Fax: 1-847-491-7713. E-mail: Agman@chem.northwestern.edu.

Present Addresses

[§]For P.C.T.: Department of Pharmaceutical Sciences, Texas Tech University Health Sciences Center, School of Pharmacy, Amarillo, TX 79106

[∥]For K.J.L.: Life Sciences Institute, University of Michigan, Ann Arbor, MI 48109

[⊥]For J.J.M.: Department of Chemistry, Northeastern Illinois University, Chicago, IL 60625

Notes

The authors declare no competing financial interest.

Biographies

Paul C. Trippier is Assistant Professor of Medicinal Chemistry in the School of Pharmacy at Texas Tech University Health Sciences Center, TX, and a member of the Center for Chemical Biology, Department of Chemistry and Biochemistry at Texas Tech University. Paul completed his doctorate with Professor Mark G. Moloney at The University of Oxford, U.K., working on the total synthesis and biological evaluation of bioactive natural products. He carried out postdoctoral work at the Welsh School of Pharmacy, Cardiff, U.K., with Professor Chris McGuigan, working on the design and synthesis of antiviral and anticancer compounds. In 2010 he moved to the laboratory of Professor Richard B. Silverman at Northwestern University, IL, working on the synthesis of compounds possessing neuroprotective activity and determination of their intracellular targets of action.

Kristin Jansen Labby recently completed her doctorate in Organic Chemistry in the laboratory of Richard B. Silverman at Northwestern University, IL. Her dissertation examined substrate analogues of neuronal nitric oxide synthase. She was a 2011−2012 National Science Foundation GK-12 fellow at Northwestern University. Kristin earned her Bachelors degree from the University of Wisconsin-Madison, WI, in 2007, working under the direction of Hans J. Reich in the Department of Chemistry as well as with Andrew F. Bent in the Department of Plant Pathology. She is currently a Postdoctoral Fellow in the Life Sciences Institute at the University of Michigan in the laboratory of Sylvie Garneau-Tsodikova, studying aminoglycoside modifying enzymes and their roles in antibiotic resistance in tuberculosis and other mycobacterium.

Dustin D. Hawker obtained his B.S. degree in Biochemistry from California Polytechnic State University, San Luis Obispo, CA, in 2007. In 2006 he was a Summer Undergraduate Research Fellow at California Institute of Technology in the laboratory of Harry B. Gray. He is currently a Ph.D. candidate in the laboratory of Richard B. Silverman at Northwestern University, IL, where his dissertation research is focused on the synthesis of novel substrates and inactivators of GABA aminotransferase.

Jan J. Mataka completed his doctoral work in 2002 under the direction of Professor David Crich at the University of Illinois at Chicago on the stereoselective formation of glycosyl sulfoxides, as well as the development of novel organic bases. Since then, he has been an instructor of chemistry at Northeastern Illinois University, teaching courses in general, organic, and more recently toxicological chemistry and pharmacology, in addition to teaching in the Urban Health Program at the University of Illinois at Chicago. Jan is a member of the National Academy of Clinical Biochemistry and currently is a Visiting Scholar in the laboratory of Richard B. Silverman at Northwestern University, IL, having worked on the development of inhibitors for neuronal nitric oxide synthase as a therapeutic target for Parkinson's disease.

Richard B. Silverman received his Ph.D. in organic chemistry from Harvard, MA, in 1974, did postdoctoral work in enzymology for 2 years at Brandeis University, MA, then joined the chemistry faculty at Northwestern University, IL. Since 2004, he has been the John Evans Professor of Chemistry. He is the inventor of Lyrica, marketed by Pfizer for epilepsy, neuropathic pain, and fibromyalgia. Recent awards include the 2009 Perkin Medal, ACS Medicinal Chemistry Hall of Fame (2009), E. B. Hershberg Award from the ACS (2011), Fellow of the ACS (2011), Sato Memorial International Award of the Japan Pharmaceutical Society (2012), Roland T. Lakey Award from Wayne State (2013), and the BMS-Smissman Award from the ACS (2013). He has published over 300 articles, holds 48 domestic and foreign patents, and has written four books.

ACKNOWLEDGMENTS

We are grateful to the National Institutes of Health (Grants GM049725 and DA030604) and the Department of Defense (Grant W81XWH-10-1-0536) for financial support of our work in neurodegenerative and neurological diseases. We thank Garry Cooper for assistance in writing the section on voltage-gated calcium channels.

ABBREVIATIONS USED

AD, Alzheimer's disease; PD, Parkinson's disease; HD, Huntington's disease; ALS, amyotrophic lateral sclerosis; Ca_v, voltage gated calcium channel; NMDA, *N*-methyl-D-aspartic acid; nNOS, neuronal nitric oxide synthase; ROS, reactive oxygen species; AMPA, α-amino-3-hydroxy-5-methyl-4-isoxazolepropionic acid; CNS, central nervous system; BBB, blood−brain barrier; ABD, agonist binding domain; NTD, N-terminal domain; L-DOPA, L-3,4-dihydroxyphenylalanine; mGluR, metabotropic glutamate receptor; VGCC, voltage gated calcium channel; DHP, 1,4-dihydroxypyridine; PAA, phenylalkylamine; BZA, benzodiazepine; DA, dopamine; SNc, substantia nigra pars compacta; SAR, structure−activity relationship; FLIPR, fluorescent imaging plate reader; PYT, pyrimidine-2,4,6-trione; NO, nitric oxide; NADPH, nicotinamide adenine dinucleotide phosphate; eNOS, endothelial nitric oxide synthase; iNOS, inducible nitric oxide synthase; nNOS, neuronal nitric oxide synthase; HSP90, heat shock protein 90; ETC, electron transport chain; $ONOO^-$, peroxynitrite; L-NNA, *N*-nitro-L-arginine; GSH, glutathione; SOD, superoxide dismutase; GPx, glutathione peroxidase; RA, retinoic acid; GSK-3, glycogen synthase kinase 3; SMA, spinal muscular atrophy; LRRK2, leucine rich repeat kinase 2; Aβ, β-amyloid; APP, amyloid precursor protein; BACE-1, β-secretase; CSF, cerebrospinal fluid; PKC, protein kinase C; HMG-CoA, 3-hydroxy-3-methylglutaryl-coenzyme A; HSP, heat shock protein; HSF1, heat shock factor protein 1; ETC, electron transport chain

REFERENCES

(1) Lin, M. T.; Beal, M. F. Mitochondrial dysfunction and oxidative stress in neurodegenerative diseases. *Nature* **2006**, *443*, 787−795.

(2) Hebert, L. E.; Scherr, P. A.; Bienias, J. L.; Bennett, D. A.; Evans, D. A. Alzheimer disease in the US population: prevalence estimates using the 2000 census. *Arch. Neurol.* **2003**, *60*, 1119−1122.

(3) Wancata, J.; Musalek, M.; Alexandrowicz, R.; Krautgartner, M. Number of dementia sufferers in Europe between the years 2000 and 2050. *Eur. Psychiatry* **2003**, *18*, 306−313.

(4) Forman, M. S.; Trojanowski, J. Q.; Lee, V. M. Y. Neurodegenerative diseases: a decade of discoveries paves the way for therapeutic breakthroughs. *Nat. Med.* **2004**, *10*, 1055−1063.
(5) Bossy-Wetzel, E.; Schwarzenbacher, R.; Lipton, S. A. Molecular pathways to neurodegeneration. *Nat. Med.* **2004**, *10* (Suppl.), S2−S9.
(6) Pardo, L. M.; van Duijn, C. M. In search of genes involved in neurodegenerative disorders. *Mutat. Res.* **2005**, *592*, 89−101.
(7) Amor, S.; Puentes, F.; Baker, D.; van der Valk, P. Inflammation in neurodegenerative diseases. *Immunology* **2010**, *129*, 154−169.
(8) Glass, C. K.; Saijo, K.; Winner, B.; Marchetto, M. C.; Gage, F. H. Mechanisms underlying inflammation in neurodegeneration. *Cell* **2010**, *140*, 918−934.
(9) Czirr, E.; Wyss-Coray, T. The immunology of neurodegeneration. *J. Clin. Invest.* **2012**, *122*, 1156−1163.
(10) Schwarcz, R.; Bruno, J. P.; Muchowski, P. J.; Wu, H. Q. Kynurenines in the mammalian brain: when physiology meets pathology. *Nat. Rev. Neurosci.* **2012**, *13*, 465−477.
(11) Lugo-Huitron, R.; Blanco-Ayala, T.; Ugalde-Muniz, P.; Carrillo-Mora, P.; Pedraza-Chaverri, J.; Silva-Adaya, D.; Maldonado, P. D.; Torres, I.; Pinzon, E.; Ortiz-Islas, E.; Lopez, T.; Garcia, E.; Pineda, B.; Torres-Ramos, M.; Santamaria, A.; La Cruz, V. P. On the antioxidant properties of kynurenic acid: free radical scavenging activity and inhibition of oxidative stress. *Neurotoxicol. Teratol.* **2011**, *33*, 538−547.
(12) Hanisch, U. K.; Johnson, T. V.; Kipnis, J. Toll-like receptors: roles in neuroprotection? *Trends Neurosci* **2008**, *31*, 176−182.
(13) Drouin-Ouellet, J.; Cicchetti, F. Inflammation and neurodegeneration: the story "retolled". *Trends Pharmacol. Sci.* **2012**, *33*, 542−551.
(14) Aquilano, K.; Baldelli, S.; Rotilio, G.; Ciriolo, M. R. Role of nitric oxide synthases in Parkinson's disease: a review on the antioxidant and anti-inflammatory activity of polyphenols. *Neurochem. Res.* **2008**, *33*, 2416−2426.
(15) Frank-Cannon, T. C.; Alto, L. T.; McAlpine, F. E.; Tansey, M. G. Does neuroinflammation fan the flame in neurodegenerative diseases? *Mol. Neurodegener.* **2009**, *4*, 47.
(16) Mosley, R. L.; Gendelman, H. E. Control of neuroinflammation as a therapeutic strategy for amyotrophic lateral sclerosis and other neurodegenerative disorders. *Exp. Neurol.* **2010**, *222*, 1−5.
(17) Neymotin, A.; Petri, S.; Calingasan, N. Y.; Wille, E.; Schafer, P.; Stewart, C.; Hensley, K.; Beal, M. F.; Kiaei, M. Lenalidomide (Revlimid) administration at symptom onset is neuroprotective in a mouse model of amyotrophic lateral sclerosis. *Exp. Neurol.* **2009**, *220*, 191−197.
(18) Greenfield, S.; Vaux, D. J. Parkinson's disease, Alzheimer's disease and motor neurone disease: identifying a common mechanism. *Neuroscience* **2002**, *113*, 485−492.
(19) Calne, D. B.; Mcgeer, E.; Eisen, A.; Spencer, P. Alzheimers-disease, Parkinsons-disease, and Motoneuron disease—abiotropic interaction between aging and environment. *Lancet* **1986**, *2*, 1067−1070.
(20) Cooper-Knock, J.; Kirby, J.; Ferraiuolo, L.; Heath, P. R.; Rattray, M.; Shaw, P. J. Gene expression profiling in human neurodegenerative disease. *Nat. Rev. Neurol.* **2012**, *8*, 518−530.
(21) Cramer, P. E.; Cirrito, J. R.; Wesson, D. W.; Lee, C. Y.; Karlo, J. C.; Zinn, A. E.; Casali, B. T.; Restivo, J. L.; Goebel, W. D.; James, M. J.; Brunden, K. R.; Wilson, D. A.; Landreth, G. E. ApoE-directed therapeutics rapidly clear beta-amyloid and reverse deficits in AD mouse models. *Science* **2012**, *335*, 1503−1506.
(22) Graff, J.; Rei, D.; Guan, J. S.; Wang, W. Y.; Seo, J.; Hennig, K. M.; Nieland, T. J.; Fass, D. M.; Kao, P. F.; Kahn, M.; Su, S. C.; Samiei, A.; Joseph, N.; Haggarty, S. J.; Delalle, I.; Tsai, L. H. An epigenetic blockade of cognitive functions in the neurodegenerating brain. *Nature* **2012**, *483*, 222−226.
(23) Jellinger, K. A. Recent advances in our understanding of neurodegeneration. *J. Neural Transm.* **2009**, *116*, 1111−1162.
(24) Salloway, S.; Mintzer, J.; Weiner, M. F.; Cummings, J. L. Disease-modifying therapies in Alzheimer's disease. *Alzheimer's Dementia* **2008**, *4*, 65−79.
(25) Zimmermann, G. R.; Lehar, J.; Keith, C. T. Multi-target therapeutics: when the whole is greater than the sum of the parts. *Drug Discovery Today* **2007**, *12*, 34−42.
(26) De Raedt, T.; Walton, Z.; Yecies, J. L.; Li, D.; Chen, Y.; Malone, C. F.; Maertens, O.; Jeong, S. M.; Bronson, R. T.; Lebleu, V.; Kalluri, R.; Normant, E.; Haigis, M. C.; Manning, B. D.; Wong, K. K.; Macleod, K. F.; Cichowski, K. Exploiting cancer cell vulnerabilities to develop a combination therapy for ras-driven tumors. *Cancer Cell* **2011**, *20*, 400−413.
(27) McHutchison, J. G.; Manns, M.; Patel, K.; Poynard, T.; Lindsay, K. L.; Trepo, C.; Dienstag, J.; Lee, W. M.; Mak, C.; Garaud, J. J.; Albrecht, J. K. Adherence to combination therapy enhances sustained response in genotype-1-infected patients with chronic hepatitis C. *Gastroenterology* **2002**, *123*, 1061−1069.
(28) Ho, D. D. Time to hit HIV, early and hard. *N. Engl. J. Med.* **1995**, *333*, 450−451.
(29) Kihara, T.; Ikeda, M. Effects of duloxetine, a new serotonin and norepinephrine uptake inhibitor, on extracellular monoamine levels in rat frontal cortex. *J. Pharmacol. Exp. Ther.* **1995**, *272*, 177−183.
(30) Delgado, P. L.; Moreno, F. A. Role of norepinephrine in depression. *J. Clin. Psychiatry* **2000**, *61* (Suppl. 1), 5−12.
(31) Traynelis, S. F.; Wollmuth, L. P.; McBain, C. J.; Menniti, F. S.; Vance, K. M.; Ogden, K. K.; Hansen, K. B.; Yuan, H.; Myers, S. J.; Dingledine, R. Glutamate receptor ion channels: structure, regulation, and function. *Pharmacol. Rev.* **2010**, *62*, 405−496.
(32) Lipton, S. A.; Rosenberg, P. A. Excitatory amino-acids as a final common pathway for neurologic disorders. *N. Engl. J. Med.* **1994**, *330*, 613−622.
(33) Lynch, D. R.; Guttmann, R. P. Excitotoxicity: perspectives based on *N*-methyl-D-aspartate receptor subtypes. *J. Pharmacol. Exp. Ther.* **2002**, *300*, 717−723.
(34) Waxman, E. A.; Lynch, D. R. *N*-Methyl-D-aspartate receptor subtypes: multiple roles in excitotoxicity and neurological disease. *Neuroscientist* **2005**, *11*, 37−49.
(35) Hartley, D. M.; Kurth, M. C.; Bjerkness, L.; Weiss, J. H.; Choi, D. W. Glutamate receptor-induced $^{45}Ca^{2+}$ accumulation in cortical cell culture correlates with subsequent neuronal degeneration. *J. Neurosci.* **1993**, *13*, 1993−2000.
(36) Rothstein, J. D. Excitotoxicity hypothesis. *Neurology* **1996**, *47*, 19S−26S.
(37) Hedegaard, M. K.; Hansen, K. B.; Andersen, K. T.; Bräuner-Osborne, H.; Traynelis, S. F. Molecular pharmacology of human NMDA receptors. *Neurochem. Int.* **2012**, *61*, 601−609.
(38) Papouin, T.; Ladepeche, L.; Ruel, J.; Sacchi, S.; Labasque, M.; Hanini, M.; Groc, L.; Pollegioni, L.; Mothet, J. P.; Oliet, S. H. Synaptic and extrasynaptic NMDA receptors are gated by different endogenous coagonists. *Cell* **2012**, *150*, 633−646.
(39) Kemp, J. A.; McKernan, R. M. NMDA receptor pathways as drug targets. *Nat. Neurosci.* **2002**, *5*, 1039−1042.
(40) Paoletti, P.; Neyton, J. NMDA receptor subunits: function and pharmacology. *Curr. Opin. Pharmacol.* **2007**, *7*, 39−47.
(41) Beal, M. F. Aging, energy, and oxidative stress in neurodegenerative diseases. *Ann. Neurol.* **1995**, *38*, 357−366.
(42) Coyle, J. An animal model for Huntington's disease. *Biol. Psychiatry* **1979**, *14*, 251−276.
(43) Fan, M. M. Y.; Raymond, L. A. *N*-Methyl-D-aspartate (NMDA) receptor function and excitotoxicity in Huntington's disease. *Prog. Neurobiol.* **2007**, *81*, 272−293.
(44) Good, P. F.; Werner, P.; Hsu, A.; Olanow, C. W.; Perl, D. P. Evidence of neuronal oxidative damage in Alzheimer's disease. *Am. J. Pathol.* **1996**, *149*, 21−28.
(45) Plaitakis, A. Glutamate dysfunction and selective motor neuron degeneration inamyotrophic lateral sclerosis: a hypothesis. *Ann. Neurol.* **1990**, *28*, 3−8.
(46) Rothstein, J. D.; Martin, L. J.; Kuncl, R. W. Decreased glutamate transport by the brain and spinal cord in amyotrophic lateral sclerosis. *N. Engl. J. Med.* **1992**, *326*, 1464−1468.
(47) Rothstein, J. Excitotoxicity and neurodegeneration in amyotrophic lateral sclerosis. *Clin. Neurosci.* **1996**, *3*, 348−359.

(48) Kalia, L. V.; Kalia, S. K.; Salter, M. W. NMDA receptors in clinical neurology: excitatory times ahead. *Lancet Neurol.* **2008**, *7*, 742−755.
(49) Monaghan, D. T.; Irvine, M. W.; Costa, B. M.; Fang, G.; Jane, D. E. Pharmacological modulation of NMDA receptor activity and the advent of negative and positive allosteric modulators. *Neurochem. Int.* **2012**, *61*, 581−592.
(50) Evans, R.; Francis, A.; Jones, A.; Smith, D.; Watkins, J. The effects of a series of omega-phosphonic alpha-carboxylic amino acids on electrically evoked and excitant amino acid-induced responses in isolated spinal cord preparations. *Br. J. Pharmacol.* **1982**, *75*, 65−75.
(51) Ogden, K. K.; Traynelis, S. F. New advances in NMDA receptor pharmacology. *Trends Pharmacol. Sci.* **2011**, *32*, 726−733.
(52) Löschmann, P. A.; Lange, K.; Kunow, M.; Rettig, K. J.; Jähnig, P.; Honore, T.; Turski, L.; Wachtel, H.; Jenner, P.; Marsden, C. Synergism of the AMPA-antagonist NBQX and the NMDA-antagonist CPP with L-dopa in models of Parkinson's disease. *J. Neural Transm.: Parkinson's Dis. Dementia Sect.* **1991**, *3*, 203−213.
(53) Veender, J. R.; Nair, S. N.; Lehmann, J. C. NMDA receptors: the first decade. *Expert Opin. Invest. Drugs* **1994**, *3*, 341−354.
(54) Bräuner-Osborne, H.; Egebjerg, J.; Nielsen, E. O.; Madsen, U.; Krogsgaard-Larsen, P. Ligands for glutamate receptors: design and therapeutic prospects. *J. Med. Chem.* **2000**, *43*, 2609−2645.
(55) Lehmann, J. C.; Wood, P. L. 7-Chlorokynurenate prevents NMDA-induced and kainate-induced striatal lesions. *Brain Res.* **1993**, *620*, 1−6.
(56) Wong, E.; Kemp, J. A.; Priestley, T.; Knight, A. R.; Woodruff, G. N.; Iversen, L. L. The anticonvulsant MK-801 is a potent *N*-methyl-D-aspartate antagonist. *Proc. Natl. Acad. Sci. U.S.A.* **1986**, *83*, 7104−7108.
(57) Marin, C.; Papa, S.; Engber, T. M.; Bonastre, M.; Tolosa, E.; Chase, T. MK-801 prevents levodopa-induced motor response alterations in parkinsonian rats. *Brain Res.* **1996**, *736*, 202−205.
(58) Chen, H. S. V.; Lipton, S. A. The chemical biology of clinically tolerated NMDA receptor antagonists. *J. Neurochem.* **2006**, *97*, 1611−1626.
(59) Crossman, A.; Peggs, D.; Boyce, S.; Luquin, M.; Sambrook, M. Effect of the NMDA antagonist MK-801 on MPTP-induced parkinsonism in the monkey. *Neuropharmacology* **1989**, *28*, 1271−1273.
(60) Blanpied, T. A.; Clarke, R. J.; Johnson, J. W. Amantadine inhibits NMDA receptors by accelerating channel closure during channel block. *J. Neurosci.* **2005**, *25*, 3312−3322.
(61) Uitti, R.; Rajput, A.; Ahlskog, J.; Offord, K.; Schroeder, D.; Ho, M.; Prasad, M.; Rajput, A.; Basran, P. Amantadine treatment is an independent predictor of improved survival in Parkinson's disease. *Neurology* **1996**, *46*, 1551−1556.
(62) Metman, V. L.; Dotto, D. P.; Natte, R.; Van den Munckhof, P.; Chase, T. Dextromethorphan improves levodopa-induced dyskinesias in Parkinson's disease. *Neurology* **1998**, *51*, 203−206.
(63) Metman, L. V.; Del Dotto, P.; LePoole, K.; Konitsiotis, S.; Fang, J.; Chase, T. N. Amantadine for levodopa-induced dyskinesias: a 1-year follow-up study. *Arch. Neurol.* **1999**, *56*, 1383−1386.
(64) Crosby, N.; Deane, K.; Clarke, C. Amantadine for dyskinesia in Parkinson's disease. *Cochrane Database Syst. Rev.* **2003**, *2*, 1−14.
(65) Shoulson, I.; Penney, J.; McDermott, M.; Schwid, S.; Kayson, E.; Chase, T.; Fahn, S.; Greenamyre, J.; Lang, A.; Siderowf, A. A randomized, controlled trial of remacemide for motor fluctuations in Parkinson's disease. *Neurology* **2001**, *56*, 455−462.
(66) Lipton, S. A. Paradigm shift in neuroprotection by NMDA receptor blockade: memantine and beyond. *Nat. Rev. Drug Discovery* **2006**, *5*, 160−170.
(67) Ferris, S. H. Evaluation of memantine for the treatment of Alzheimer's disease. *Expert Opin. Pharmacother.* **2003**, *4*, 2305−2313.
(68) Herrmann, N.; Li, A.; Lanctoot, K. Memantine in dementia: a review of the current evidence. *Expert Opin. Pharmacother.* **2011**, *12*, 787−800.
(69) Lipton, S. A. Pathologically activated therapeutics for neuroprotection. *Nat. Rev. Neurosci.* **2007**, *8*, 803−808.
(70) Williams, K. Ifenprodil discriminates subtypes of the *N*-methyl-D-aspartate receptor: selectivity and mechanisms at recombinant heteromeric receptors. *Mol. Pharmacol.* **1993**, *44*, 851−859.
(71) Tahirovic, Y. A.; Geballe, M.; Gruszecka-Kowalik, E.; Myers, S. J.; Lyuboslavsky, P.; Le, P.; French, A.; Irier, H.; Choi, W.; Easterling, K. Enantiomeric propanolamines as selective *N*-methyl-D-aspartate 2B receptor antagonists. *J. Med. Chem.* **2008**, *51*, 5506−5521.
(72) Mosley, C. A.; Myers, S. J.; Murray, E. E.; Santangelo, R.; Tahirovic, Y. A.; Kurtkaya, N.; Mullasseril, P.; Yuan, H.; Lyuboslavsky, P.; Le, P. Synthesis, structural activity-relationships, and biological evaluation of novel amide-based allosteric binding site antagonists in NR1A/NR2B *N*-methyl-D-aspartate receptors. *Bioorg. Med. Chem.* **2009**, *17*, 6463−6480.
(73) Fischer, G.; Mutel, V.; Trube, G.; Malherbe, P.; Kew, J.; Mohacsi, E.; Heitz, M.; Kemp, J. Ro 25-6981, a highly potent and selective blocker of *N*-methyl-D-aspartate receptors containing the NR2B subunit. Characterization in vitro. *J. Pharmacol. Exp. Ther.* **1997**, *283*, 1285−1292.
(74) Taniguchi, K.; Shinjo, K.; Mizutani, M.; Shimada, K.; Ishikawa, T.; Menniti, F. S.; Nagahisa, A. Antinociceptive activity of CP-101,606, an NMDA receptor NR2B subunit antagonist. *Br. J. Pharmacol.* **1997**, *122*, 809−812.
(75) Nutt, J. G.; Gunzler, S. A.; Kirchhoff, T.; Hogarth, P.; Weaver, J. L.; Krams, M.; Jamerson, B.; Menniti, F. S.; Landen, J. W. Effects of a NR2B selective NMDA glutamate antagonist, CP-101,606, on dyskinesia and parkinsonism. *Mov. Disord.* **2008**, *23*, 1860−1866.
(76) Mosley, C. A.; Acker, T. M.; Hansen, K. B.; Mullasseril, P.; Andersen, K. T.; Le, P.; Vellano, K. M.; Bräuner-Osborne, H.; Liotta, D. C.; Traynelis, S. F. Quinazolin-4-one derivatives: a novel class of noncompetitive NR2C/D subunit-selective *N*-methyl-D-aspartate receptor antagonists. *J. Med. Chem.* **2010**, 5476−5490.
(77) Hansen, K. B.; Traynelis, S. F. Structural and mechanistic determinants of a novel site for noncompetitive inhibition of GluN2D-containing NMDA receptors. *J. Neurosci.* **2011**, *31*, 3650−3661.
(78) Costa, B. M.; Irvine, M. W.; Fang, G.; Eaves, R. J.; Mayo-Martin, M. B.; Skifter, D. A.; Jane, D. E.; Monaghan, D. T. A novel family of negative and positive allosteric modulators of NMDA receptors. *J. Pharmacol. Exp. Ther.* **2010**, *335*, 614−621.
(79) Acker, T. M.; Yuan, H.; Hansen, K. B.; Vance, K. M.; Ogden, K. K.; Jensen, H. S.; Burger, P. B.; Mullasseril, P.; Snyder, J. P.; Liotta, D. C. Mechanism for noncompetitive inhibition by novel GluN2C/D *N*-methyl-D-aspartate receptor subunit-selective modulators. *Mol. Pharmacol.* **2011**, *80*, 782−795.
(80) Bettini, E.; Sava, A.; Griffante, C.; Carignani, C.; Buson, A.; Capelli, A. M.; Negri, M.; Andreetta, F.; Senar-Sancho, S. A.; Guiral, L. Identification and characterization of novel NMDA receptor antagonists selective for NR2A-over NR2B-containing receptors. *J. Pharmacol. Exp. Ther.* **2010**, *335*, 636−644.
(81) Retchless, B. S.; Gao, W.; Johnson, J. W. A single GluN2 subunit residue controls NMDA receptor channel properties via intersubunit interaction. *Nat. Neurosci.* **2012**, *15*, 406−413.
(82) Neyton, J.; Paoletti, P. Relating NMDA receptor function to receptor subunit composition: limitations of the pharmacological approach. *J. Neurosci.* **2006**, *26*, 1331−1333.
(83) Hatton, C. J.; Paoletti, P. Modulation of triheteromeric NMDA receptors by N-terminal domain ligands. *Neuron* **2005**, *46*, 261−274.
(84) Xia, P.; Chen, H. V.; Zhang, D.; Lipton, S. A. Memantine preferentially blocks extrasynaptic over synaptic NMDA receptor currents in hippocampal autapses. *J. Neurosci.* **2010**, *30*, 11246−11250.
(85) Okamoto, S.; Pouladi, M. A.; Talantova, M.; Yao, D.; Xia, P.; Ehrnhoefer, D. E.; Zaidi, R.; Clemente, A.; Kaul, M.; Graham, R. K. Balance between synaptic versus extrasynaptic NMDA receptor activity influences inclusions and neurotoxicity of mutant huntingtin. *Nat. Med.* **2009**, *15*, 1407−1413.
(86) Hardingham, G. E.; Bading, H. Synaptic versus extrasynaptic NMDA receptor signalling: implications for neurodegenerative disorders. *Nat. Rev. Neurosci.* **2010**, *11*, 682−696.

(87) Levine, M. S.; Cepeda, C.; André, V. M. Location, location, location: contrasting roles of synaptic and extrasynaptic NMDA receptors in Huntington's disease. *Neuron* **2010**, *65*, 145−147.
(88) Surmeier, D. J.; Guzman, J. N.; Sanchez-Padilla, J.; Goldberg, J. A. The origins of oxidant stress in Parkinson's disease and therapeutic strategies. *Antioxid. Redox Signaling* **2011**, *14*, 1289−1301.
(89) Youdim, M.; Buccafusco, J. CNS targets for multi-functional drugs in the treatment of Alzheimer's and Parkinson's diseases. *J. Neural Transm.* **2005**, *112*, 519−537.
(90) Youdim, M. B. H.; Geldenhuys, W. J.; Van der Schyf, C. J. Why should we use multifunctional neuroprotective and neurorestorative drugs for Parkinson's disease? *Parkinsonism Relat. Disord.* **2007**, *13*, S281−S291.
(91) Geldenhuys, W. J.; Youdim, M. B. H.; Carroll, R. T.; Van der Schyf, C. J. The emergence of designed multiple ligands for neurodegenerative disorders. *Prog. Neurobiol.* **2011**, 347−359.
(92) Wu, J.; Li, Q.; Bezprozvanny, I. Evaluation of Dimebon in cellular model of Huntington's disease. *Mol. Neurodegener.* **2008**, *3*, 15.
(93) Jones, R. W. Dimebon disappointment. *Alzheimer's Res. Ther.* **2010**, *2*, 25.
(94) Lermontova, N.; Redkozubov, A.; Shevtsova, E.; Serkova, T.; Kireeva, E.; Bachurin, S. Dimebon and tacrine inhibit neurotoxic action of β-amyloid in culture and block L-type Ca^{2+} channels. *Bull. Exp. Biol. Med.* **2001**, *132*, 1079−1083.
(95) Grigor'ev, V.; Dranyi, O.; Bachurin, S. Comparative study of action mechanisms of dimebon and memantine on AMPA-and NMDA-subtypes glutamate receptors in rat cerebral neurons. *Bull. Exp. Biol. Med.* **2003**, *136*, 474−477.
(96) Blandini, F. An update on the potential role of excitotoxicity in the pathogenesis of Parkinson's disease. *Funct. Neurol.* **2010**, *25*, 65−71.
(97) Waldmeier, P.; Bozyczko-Coyne, D.; Williams, M.; Vaught, J. L. Recent clinical failures in Parkinson's disease with apoptosis inhibitors underline the need for a paradigm shift in drug discovery for neurodegenerative diseases. *Biochem. Pharmacol.* **2006**, *72*, 1197−1206.
(98) Kim, H. S.; Suh, Y. H. Minocycline and neurodegenerative diseases. *Behav. Brain Res.* **2009**, *196*, 168−179.
(99) X Sureda, F.; Junyent, F.; Verdaguer, E.; Auladell, C.; Pelegri, C.; Vilaplana, J.; Folch, J.; Maria Canudas, A.; Beas Zarate, C.; Pallas, M. Antiapoptotic drugs: a therapeutic strategy for the prevention of neurodegenerative diseases. *Curr. Pharm. Des.* **2011**, *17*, 230−245.
(100) Malgouris, C.; Daniel, M.; Doble, A. Neuroprotective effects of riluzole on *N*-methyl-D-aspartate- or veratridine-induced neurotoxicity in rat hippocampal slices. *Neurosci. Lett.* **1994**, *177*, 95−99.
(101) Doble, A. The pharmacology and mechanism of action of riluzole. *Neurology* **1996**, *47*, 233S−241S.
(102) Bryson, H. M.; Fulton, B.; Benfield, P. Riluzole. A review of its pharmacodynamic and pharmacokinetic properties and therapeutic potential in amyotrophic lateral sclerosis. *Drugs* **1996**, *52*, 549−563.
(103) Jankovic, J.; Hunter, C. A double-blind, placebo-controlled and longitudinal study of riluzole in early Parkinson's disease. *Parkinsonism Relat. Disord.* **2002**, *8*, 271−276.
(104) Landwehrmeyer, G. B.; Dubois, B.; de Yébenes, J. G.; Kremer, B.; Gaus, W.; Kraus, P. H.; Przuntek, H.; Dib, M.; Doble, A.; Fischer, W. Riluzole in Huntington's disease: a 3-year, randomized controlled study. *Ann. Neurol.* **2007**, *62*, 262−272.
(105) Lee, S. G.; Su, Z. Z.; Emdad, L.; Gupta, P.; Sarkar, D.; Borjabad, A.; Volsky, D. J.; Fisher, P. B. Mechanism of ceftriaxone induction of excitatory amino acid transporter-2 expression and glutamate uptake in primary human astrocytes. *J. Biol. Chem.* **2008**, *283*, 13116−13123.
(106) Nicoletti, F.; Bruno, V.; Copani, A.; Casabona, G.; Knöpfel, T. Metabotropic glutamate receptors: a new target for the therapy of neurodegenerative disorders? *Trends Neurosci.* **1996**, *19*, 267−271.
(107) Caraci, F.; Battaglia, G.; Sortino, M. A.; Spampinato, S.; Molinaro, G.; Copani, A.; Nicoletti, F.; Bruno, V. Metabotropic glutamate receptors in neurodegeneration/neuroprotection: Still a hot topic? *Neurochem. Int.* **2012**, *61*, 559−565.
(108) Gregory, K. J.; Dong, E. N.; Meiler, J.; Conn, P. J. Allosteric modulation of metabotropic glutamate receptors: structural insights and therapeutic potential. *Neuropharmacol.* **2011**, *60*, 66−81.
(109) Striggow, F.; Ehrlich, B. E. Ligand-gated calcium channels inside and out. *Curr. Opin. Cell. Biol.* **1996**, *8*, 490−495.
(110) Zamponi, G. W. *Voltage-Gated Calcium Channels*; Kluwer Academic: New York, 2005.
(111) Berridge, M. J. Neuronal calcium signaling. *Neuron* **1998**, *21*, 13−26.
(112) Catterall, W. A.; Striessnig, J.; Snutch, T. P.; Perez-Reyes, E. International Union of Pharmacology. XL. Compendium of voltage-gated ion channels: calcium channels. *Pharmacol. Rev.* **2003**, *55*, 579−581.
(113) Eisenberg, M. J.; Brox, A.; Bestawros, A. N. Calcium channel blockers: an update. *Am. J. Med.* **2004**, *116*, 35−43.
(114) Striessnig, J.; Koschak, A.; Sinnegger-Brauns, M. J.; Hetzenauer, A.; Nguyen, N. K.; Busquet, P.; Pelster, G.; Singewald, N. Role of voltage-gated L-type Ca^{2+} channel isoforms for brain function. *Biochem. Soc. Trans.* **2006**, *34*, 903−909.
(115) Helton, T. D.; Xu, W.; Lipscombe, D. Neuronal L-type calcium channels open quickly and are inhibited slowly. *J. Neurosci.* **2005**, *25*, 10247−10251.
(116) Epstein, B. J.; Vogel, K.; Palmer, B. F. Dihydropyridine calcium channel antagonists in the management of hypertension. *Drugs* **2007**, *67*, 1309−1327.
(117) Chan, C. S.; Guzman, J. N.; Ilijic, E.; Mercer, J. N.; Rick, C.; Tkatch, T.; Meredith, G. E.; Surmeier, D. J. "Rejuvenation" protects neurons in mouse models of Parkinson's disease. *Nature* **2007**, *447*, 1081−1086.
(118) Brevetti, G.; Bonaduce, D.; Breglio, R.; Perna, S.; Simonelli, P.; Marconi, R.; Campanella, G. Parkinson's disease and hypotension: 24-hour blood pressure recording in ambulant patients. *Clin. Cardiol.* **1990**, *13*, 474−478.
(119) Sinnegger-Brauns, M. J.; Huber, I. G.; Koschak, A.; Wild, C.; Obermair, G. J.; Einzinger, U.; Hoda, J. C.; Sartori, S. B.; Striessnig, J. Expression and 1,4-dihydropyridine-binding properties of brain L-type calcium channel isoforms. *Mol. Pharmacol.* **2009**, *75*, 407−414.
(120) Xu, W.; Lipscombe, D. Neuronal Ca(V)1.3alpha(1) L-type channels activate at relatively hyperpolarized membrane potentials and are incompletely inhibited by dihydropyridines. *J. Neurosci.* **2001**, *21*, 5944−5951.
(121) Chang, C. C.; Cao, S.; Kang, S.; Kai, L.; Tian, X.; Pandey, P.; Dunne, S. F.; Luan, C. H.; Surmeier, D. J.; Silverman, R. B. Antagonism of 4-substituted 1,4-dihydropyridine-3,5-dicarboxylates toward voltage-dependent L-type Ca^{2+} channels Ca V 1.3 and Ca V 1.2. *Bioorg. Med. Chem.* **2010**, *18*, 3147−3158.
(122) Sorkin, E. M.; Clissold, S. P.; Brogden, R. N. Nifedipine. A review of its pharmacodynamic and pharmacokinetic properties, and therapeutic efficacy, in ischaemic heart disease, hypertension and related cardiovascular disorders. *Drugs* **1985**, *30*, 182−274.
(123) Xia, G.; Benmohamed, R.; Kim, J.; Arvanites, A. C.; Morimoto, R. I.; Ferrante, R. J.; Kirsch, D. R.; Silverman, R. B. Pyrimidine-2,4,6-trione derivatives and their inhibition of mutant SOD1-dependent protein aggregation. Toward a treatment for amyotrophic lateral sclerosis. *J. Med. Chem.* **2011**, *54*, 2409−2421.
(124) Kang, S.; Cooper, G.; Dunne, S. F.; Dusel, B.; Luan, C. H.; Surmeier, D. J.; Silverman, R. B. Ca(V)1.3-selective L-type calcium channel antagonists as potential new therapeutics for Parkinson's disease. *Nat. Commun.* **2012**, *3*, 1146.
(125) Nakamura, T.; Lipton, S. A. Cell death: protein misfolding and neurodegenerative diseases. *Apoptosis* **2009**, *14*, 455−468.
(126) Chung, K. K. K.; David, K. K. Emerging roles of nitric oxide in neurodegeneration. *Nitric Oxide* **2010**, *22*, 290−295.
(127) Giasson, B. I.; Duda, J. E.; Murray, I. V.; Chen, Q.; Souza, J. M.; Hurtig, H. I.; Ischiropoulos, H.; Trojanowski, J. Q.; Lee, V. M. Oxidative damage linked to neurodegeneration by selective alpha-synuclein nitration in synucleinopathy lesions. *Science* **2000**, *290*, 985−989.

(128) Chung, K. K. K.; Thomas, B.; Li, X.; Pletnikova, O.; Troncoso, J. C.; Marsh, L.; Dawson, V. L.; Dawson, T. M. S-Nitrosylation of parkin regulates ubiquitination and compromises parkin's protective function. *Science* **2004**, *304*, 1328−1331.
(129) Yao, D. D.; Gu, Z. Z.; Nakamura, T. T.; Shi, Z.-Q. Z.; Ma, Y. Y.; Gaston, B. B.; Palmer, L. A. L.; Rockenstein, E. M. E.; Zhang, Z. Z.; Masliah, E. E.; Uehara, T. T.; Lipton, S. A. S. Nitrosative stress linked to sporadic Parkinson's disease: S-nitrosylation of parkin regulates its E3 ubiquitin ligase activity. *Proc. Natl. Acad. Sci. U.S.A.* **2004**, *101*, 10810−10814.
(130) Dawson, V. L.; Dawson, T. M. Nitric oxide in neurodegeneration. *Prog. Brain Res.* **1998**, *118*, 215−229.
(131) Martínez-Ruiz, A.; Villanueva, L.; González de Orduña, C.; López-Ferrer, D.; Higueras, M. A.; Tarín, C.; Rodríguez-Crespo, I.; Vázquez, J.; Lamas, S. S-Nitrosylation of Hsp90 promotes the inhibition of its ATPase and endothelial nitric oxide synthase regulatory activities. *Proc. Natl. Acad. Sci. U.S.A.* **2005**, *102*, 8525−8530.
(132) Tsang, A. H. K.; Chung, K. K. K. Oxidative and nitrosative stress in Parkinson's disease. *Biochim. Biophys. Acta* **2009**, *1792*, 643−650.
(133) Daff, S. NO synthase: structures and mechanisms. *Nitric Oxide* **2010**, *23*, 1−11.
(134) Erdal, E. P.; Litzinger, E. A.; Seo, J.; Zhu, Y.; Ji, H.; Silverman, R. B. Selective neuronal nitric oxide synthase inhibitors. *Curr. Top. Med. Chem.* **2005**, *5*, 603−624.
(135) Furfine, E. S.; Harmon, M. F.; Paith, J. E.; Garvey, E. P. Selective inhibition of constitutive nitric oxide synthase by L-NG-nitroarginine. *Biochemistry* **1993**, *32*, 8512−8517.
(136) Yamamoto, K.; Shimamura, K.; Sekiguchi, F.; Sunano, S. Effects of NG-nitro-L-arginine on the blood pressure of spontaneously hypertensive rats with different degrees of hypertension. *Clin. Exper. Hypertens.* **2001**, *23*, 533−544.
(137) Silverman, R. B.; Huang, H.; Marletta, M. A.; Martásek, P. Selective inhibition of neuronal nitric oxide synthase by N^{ω}-nitroarginine- and phenylalanine-containing dipeptides and dipeptide esters. *J. Med. Chem.* **1997**, *40*, 2813−2817.
(138) Huang, H.; Martásek, P.; Roman, L. J.; Masters, B. S. S.; Silverman, R. B. N^{ω}-Nitroarginine-containing dipeptide amides. Potent and highly selective inhibitors of neuronal nitric oxide synthase. *J. Med. Chem.* **1999**, *42*, 3147−3153.
(139) Huang, H.; Martásek, P.; Roman, L. J.; Silverman, R. B. Synthesis and evaluation of peptidomimetics as selective inhibitors and active site probes of nitric oxide synthases. *J. Med. Chem.* **2000**, *43*, 2938−2945.
(140) Gómez-Vidal, J. A.; Martásek, P.; Roman, L. J.; Silverman, R. B. Potent and selective conformationally restricted neuronal nitric oxide synthase inhibitors. *J. Med. Chem.* **2004**, *47*, 703−710.
(141) Hah, J.-M.; Roman, L. J.; Martásek, P.; Silverman, R. B. Reduced amide bond peptidomimetics. (4*S*)-*N*-(4-Amino-5-[aminoakyl]aminopentyl)-*N*′-nitroguanidines, potent and highly selective inhibitors of neuronal nitric oxide synthase. *J. Med. Chem.* **2001**, *44*, 2667−2670.
(142) Hah, J.-M.; Martásek, P.; Roman, L. J.; Silverman, R. B. Aromatic reduced amide bond peptidomimetics as selective inhibitors of neuronal nitric oxide synthase. *J. Med. Chem.* **2003**, *46*, 1661−1669.
(143) Crane, B. R.; Arvai, A. S.; Gachhui, R.; Wu, C.; Ghosh, D. K.; Getzoff, E. D.; Stuehr, D. J.; Tainer, J. A. The structure of nitric oxide synthase oxygenase domain and inhibitor complexes. *Science* **1997**, *278*, 425−431.
(144) Raman, C. S.; Li, H.; Martásek, P.; Král, V.; Masters, B. S. S.; Poulos, T. L. Crystal structure of constitutive endothelial nitric oxide synthase: a paradigm for pterin function involving a novel metal center. *Cell* **1998**, *95*, 939−950.
(145) Ji, H.; Li, H.; Martásek, P.; Roman, L. J.; Poulos, T. L.; Silverman, R. B. Discovery of highly potent and selective inhibitors of neuronal nitric oxide synthase by fragment hopping. *J. Med. Chem.* **2009**, *52*, 779−797.
(146) Ji, H.; Stanton, B. Z.; Igarashi, J.; Li, H.; Martásek, P.; Roman, L. J.; Poulos, T. L.; Silverman, R. B. Minimal pharmacophoric elements and fragment hopping, an approach directed at molecular diversity and isozyme selectivity. Design of selective neuronal nitric oxide synthase inhibitors. *J. Am. Chem. Soc.* **2008**, *130*, 3900−3914.
(147) Ji, H.; Tan, S.; Igarashi, J.; Li, H.; Derrick, M.; Martásek, P.; Roman, L. J.; Vásquez-Vivar, J.; Poulos, T. L.; Silverman, R. B. Selective neuronal nitric oxide synthase inhibitors and the prevention of cerebral palsy. *Ann. Neurol.* **2009**, *65*, 209−217.
(148) Delker, S. L.; Ji, H.; Li, H.; Jamal, J.; Fang, J.; Xue, F.; Silverman, R. B.; Poulos, T. L. Unexpected binding modes of nitric oxide synthase inhibitors effective in the prevention of a cerebral palsy phenotype in an animal model. *J. Am. Chem. Soc.* **2010**, *132*, 5437−5442.
(149) Ji, H.; Delker, S. L.; Li, H.; Martásek, P.; Roman, L. J.; Poulos, T. L.; Silverman, R. B. Exploration of the active site of neuronal nitric oxide synthase by the design and synthesis of pyrrolidinomethyl 2-aminopyridine derivatives. *J. Med. Chem.* **2010**, *53*, 7804−7824.
(150) Xue, F.; Fang, J.; Delker, S. L.; Li, H.; Martásek, P.; Roman, L. J.; Poulos, T. L.; Silverman, R. B. Symmetric double-headed aminopyridines, a novel strategy for potent and membrane-permeable inhibitors of neuronal nitric oxide synthase. *J. Med. Chem.* **2011**, *54*, 2039−2048.
(151) Faraci, W. S.; Nagel, A. A.; Verdries, K. A.; Vincent, L. A.; Xu, H.; Nichols, L. E.; Labasi, J. M.; Salter, E. D.; Pettipher, E. R. 2-Amino-4-methylpyridine as a potent inhibitor of inducible NO synthase activity in vitro and in vivo. *Br. J. Pharmacol.* **1996**, *119*, 1101−1108.
(152) Hagmann, W. K.; Caldwell, C. G.; Chen, P.; Durette, P. L.; Esser, C. K.; Lanza, T. J.; Kopka, I. E.; Guthikonda, R.; Shah, S. K.; MacCoss, M.; Chabin, R. M.; Fletcher, D.; Grant, S. K.; Green, B. G.; Humes, J. L.; Kelly, T. M.; Luell, S.; Meurer, R.; Moore, V.; Pacholok, S. G.; Pavia, T.; Williams, H. R.; Wong, K. K. Substituted 2-aminopyridines as inhibitors of nitric oxide synthases. *Bioorg. Med. Chem. Lett.* **2000**, *10*, 1975−1978.
(153) Lowe, J. A.; Qian, W.; Volkmann, R. A.; Heck, S.; Nowakowski, J.; Nelson, R.; Nolan, C.; Liston, D.; Ward, K.; Zorn, S.; Johnson, C.; Vanase, M.; Faraci, W. S.; Verdries, K. A.; Baxter, J.; Doran, S.; Sanders, M.; Ashton, M.; Whittle, P.; Stefaniak, M. A new class of selective and potent inhibitors of neuronal nitric oxide synthase. *Bioorg. Med. Chem. Lett.* **1999**, *9*, 2569−2572.
(154) Lowe, J. A.; Qian, W.; Drozda, S. E.; Volkmann, R. A.; Nason, D.; Nelson, R. B.; Nolan, C.; Liston, D.; Ward, K.; Faraci, S.; Verdries, K.; Seymour, P.; Majchrzak, M.; Villalobos, A.; White, W. F. Structure−activity relationships of potent, selective inhibitors of neuronal nitric oxide synthase based on the 6-phenyl-2-aminopyridine structure. *J. Med. Chem.* **2004**, *47*, 1575−1586.
(155) McCall, T. B.; Feelisch, M.; Palmer, R. M.; Moncada, S. Identification of *N*-iminoethyl-L-ornithine as an irreversible inhibitor of nitric oxide synthase in phagocytic cells. *Br. J. Pharmacol.* **1991**, *102*, 234−238.
(156) Collins, J. L.; Shearer, B. G.; Oplinger, J. A.; Lee, S.; Garvey, E. P.; Salter, M.; Duffy, C.; Burnette, T. C.; Furfine, E. S. *N*-Phenylamidines as selective inhibitors of human neuronal nitric oxide synthase: structure−activity studies and demonstration of in vivo activity. *J. Med. Chem.* **1998**, *41*, 2858−2871.
(157) Garvey, E. P.; Oplinger, J. A.; Furfine, E. S.; Kiff, R. J.; Laszlo, F.; Whittle, B. J.; Knowles, R. G. 1400W is a slow, tight binding, and highly selective inhibitor of inducible nitric-oxide synthase in vitro and in vivo. *J. Biol. Chem.* **1997**, *272*, 4959−4963.
(158) Maccallini, C.; Patruno, A.; Lannutti, F.; Ammazzalorso, A.; De Filippis, B.; Fantacuzzi, M.; Franceschelli, S.; Giampietro, L.; Masella, S.; Felaco, M.; Re, N.; Amoroso, R. N-Substituted acetamidines and 2-methylimidazole derivatives as selective inhibitors of neuronal nitric oxide synthase. *Bioorg. Med. Chem. Lett.* **2010**, *20*, 6495−6499.
(159) Reif, D. W.; McCarthy, D. J.; Cregan, E.; Macdonald, J. E. Discovery and development of neuronal nitric oxide synthase inhibitors. *Free Radical Biol. Med.* **2000**, *28*, 1470−1477.
(160) O'Neill, M. J.; Murray, T. K.; McCarty, D. R.; Hicks, C. A.; Dell, C. P.; Patrick, K. E.; Ward, M. A.; Osborne, D. J.; Wiernicki, T.

R.; Roman, C. R.; Lodge, D.; Fleisch, J. H.; Singh, J. ARL 17477, a selective nitric oxide synthase inhibitor, with neuroprotective effects in animal models of global and focal cerebral ischaemia. *Brain Res.* **2000**, *871*, 234−244.
(161) Fedorov, R.; Vasan, R.; Ghosh, D. K.; Schlichting, I. Structures of nitric oxide synthase isoforms complexed with the inhibitor AR-R17477 suggest a rational basis for specificity and inhibitor design. *Proc. Natl. Acad. Sci. U.S.A.* **2004**, *101*, 5892−5897.
(162) Renton, P.; Green, B.; Maddaford, S. P.; Rakhit, S.; Andrews, J. S. Novel dual action neuronal nitric oxide synthase inhibitors with μ-opioid agonist activity. *ACS Med. Chem. Lett.* **2012**, *3*, 227−231.
(163) Annedi, S. C.; Ramnauth, J.; Maddaford, S. P.; Renton, P.; Rakhit, S.; Mladenova, G.; Dove, P.; Silverman, S.; Andrews, J. S.; Felice, M. D.; Porreca, F. Discovery of *cis*-*N*-(1-(4-(methylamino)-cyclohexyl)indolin-6-yl)thiophene-2-carboximidamide: a 1,6-disubstituted indoline derivative as a highly selective inhibitor of human neuronal nitric oxide synthase (nNOS) without any cardiovascular liabilities. *J. Med. Chem.* **2012**, *55*, 943−955.
(164) Maddaford, S.; Annedi, S. C.; Ramnauth, J.; Rakhit, S. Advancements in the development of nitric oxide synthase inhibitors. *Annu. Rep. Med. Chem.* **2009**, *44*, 27−50.
(165) Serafim, R. A.; Primi, M. C.; Trossini, G. H.; Ferreira, E. I. Nitric oxide: state of the art in drug design. *Curr. Med. Chem.* **2012**, *19*, 386−405.
(166) Payne, J. E.; Bonnefous, C.; Symons, K. T.; Nguyen, P. M.; Sablad, M.; Rozenkrants, N.; Zhang, Y.; Wang, L.; Yazdani, N.; Shiau, A. K.; Noble, S. A.; Rix, P.; Rao, T. S.; Hassig, C. A.; Smith, N. D. Discovery of dual inducible/neuronal nitric oxide synthase (iNOS/nNOS) inhibitor development candidate 4-(2-cyclobutyl-1*H*-imidazo-[4,5-*b*]pyrazin-1-yl)methyl)-7,8-difluoroquinolin-2(1*H*)-one (KD7332). Part 2: Identification of a novel, potent, and selective series of benzimidazole-quinolinone iNOS/nNOS dimerization inhibitors that are orally active in pain models. *J. Med. Chem.* **2010**, *53*, 7739−7755.
(167) Matter, H.; Kumar, H. S. A.; Fedorov, R.; Frey, A.; Kotsonis, P.; Hartmann, E.; Fröhlich, L. G.; Reif, A.; Pfleiderer, W.; Scheurer, P.; Ghosh, D. K.; Schlichting, I.; Schmidt, H. H. H. W. Structural analysis of isoform-specific inhibitors targeting the tetrahydrobiopterin binding site of human nitric oxide synthases. *J. Med. Chem.* **2005**, *48*, 4783−4792.
(168) Behl, C. Alzheimer's disease and oxidative stress: implications for novel therapeutic approaches. *Prog. Neurobiol.* **1999**, *57*, 301−323.
(169) Christen, Y. Oxidative stress and Alzheimer disease. *Am. J. Clin. Nutr.* **2000**, *71*, 621S−629S.
(170) Harman, D. A hypothesis on the pathogenesis of Alzheimer's disease. *Ann. N. Y. Acad. Sci.* **1996**, *786*, 152−168.
(171) Joseph, J.; Shukitt-Hale, B.; Denisova, N. A.; Martin, A.; Perry, G.; Smith, M. A. Copernicus revisited: amyloid beta in Alzheimer's disease. *Neurobiol. Aging* **2001**, *22*, 131−146.
(172) Markesbery, W. R.; Carney, J. M. Oxidative alterations in Alzheimer's disease. *Brain Pathol.* **1999**, *9*, 133−146.
(173) Prasad, K. N.; Hovland, A. R.; Cole, W. C.; Prasad, K. C.; Nahreini, P.; Edwards-Prasad, J.; Andreatta, C. P. Multiple antioxidants in the prevention and treatment of Alzheimer disease: analysis of biologic rationale. *Clin. Neuropharmacol.* **2000**, *23*, 2−13.
(174) Beal, M. F. Experimental models of Parkinson's disease. *Nat. Rev. Neurosci.* **2001**, *2*, 325−334.
(175) Blum, D.; Torch, S.; Lambeng, N.; Nissou, M.; Benabid, A. L.; Sadoul, R.; Verna, J. M. Molecular pathways involved in the neurotoxicity of 6-OHDA, dopamine and MPTP: contribution to the apoptotic theory in Parkinson's disease. *Prog. Neurobiol.* **2001**, *65*, 135−172.
(176) Foley, P.; Riederer, P. Influence of neurotoxins and oxidative stress on the onset and progression of Parkinson's disease. *J. Neurol.* **2000**, *247* (Suppl. 2), II82−II94.
(177) Gerlach, M.; Riederer, P. Animal models of Parkinson's disease: an empirical comparison with the phenomenology of the disease in man. *J. Neural Transm.* **1996**, *103*, 987−1041.
(178) Browne, S. E.; Ferrante, R. J.; Beal, M. F. Oxidative stress in Huntington's disease. *Brain Pathol.* **1999**, *9*, 147−163.
(179) Pedersen, W. A.; Fu, W.; Keller, J. N.; Markesbery, W. R.; Appel, S.; Smith, R. G.; Kasarskis, E.; Mattson, M. P. Protein modification by the lipid peroxidation product 4-hydroxynonenal in the spinal cords of amyotrophic lateral sclerosis patients. *Ann. Neurol.* **1998**, *44*, 819−824.
(180) Sayre, L. M.; Smith, M. A.; Perry, G. Chemistry and biochemistry of oxidative stress in neurodegenerative disease. *Curr. Med. Chem.* **2001**, *8*, 721−738.
(181) Grodstein, F.; Chen, J.; Willett, W. C. High-dose antioxidant supplements and cognitive function in community-dwelling elderly women. *Am. J. Clin. Nutr.* **2003**, *77*, 975−984.
(182) Laurin, D.; Masaki, K. H.; Foley, D. J.; White, L. R.; Launer, L. J. Midlife dietary intake of antioxidants and risk of late-life incident dementia: the Honolulu-Asia aging study. *Am. J. Epidemiol.* **2004**, *159*, 959−967.
(183) Petersen, R. C.; Thomas, R. G.; Grundman, M.; Bennett, D.; Doody, R.; Ferris, S.; Galasko, D.; Jin, S.; Kaye, J.; Levey, A.; Pfeiffer, E.; Sano, M.; van Dyck, C. H.; Thal, L. J. Vitamin E and donepezil for the treatment of mild cognitive impairment. *N. Engl. J. Med.* **2005**, *352*, 2379−2388.
(184) Hayden, K. M.; Welsh-Bohmer, K. A.; Wengreen, H. J.; Zandi, P. P.; Lyketsos, C. G.; Breitner, J. C. Risk of mortality with vitamin E supplements: the Cache County study. *Am. J. Med.* **2007**, *120*, 180−184.
(185) Luchsinger, J. A.; Tang, M. X.; Shea, S.; Mayeux, R. Antioxidant vitamin intake and risk of Alzheimer disease. *Arch. Neurol.* **2003**, *60*, 203−208.
(186) Sinha, K.; Chaudhary, G.; Gupta, Y. K. Protective effect of resveratrol against oxidative stress in middle cerebral artery occlusion model of stroke in rats. *Life Sci.* **2002**, *71*, 655−665.
(187) The Parkinson Study Group. Effects of tocopherol and deprenyl on the progression of disability in early Parkinson's disease. *N. Engl. J. Med.* **1993**, *328*, 176−183.
(188) Kieburtz, K.; McDermott, M.; Como, P.; Growdon, J.; Brady, J.; Carter, J.; Huber, S.; Kanigan, B.; Landow, E.; Rudolph, A.; Saint-Cyr, J.; Stern, Y.; Tennis, M.; Thelen, J.; Shoulson, I.; Parkinson Study Group. The effect of deprenyl and tocopherol on cognitive performance in early untreated Parkinson's disease. *Neurology* **1994**, *44*, 1756−1759.
(189) Mihatsch, W.; Russ, H.; Gerlach, M.; Riederer, P.; Przuntek, H. Treatment with antioxidants does not prevent loss of dopamine in the striatum of MPTP-treated common marmosets: preliminary observations. *J. Neural Transm.: Parkinson's Dis. Dementia Sect.* **1991**, *3*, 73−78.
(190) Perry, T. L.; Yong, V. W.; Hansen, S.; Jones, K.; Bergeron, C.; Foulks, J. G.; Wright, J. M. Alpha-tocopherol and beta-carotene do not protect marmosets against the dopaminergic neurotoxicity of *N*-methyl-4-phenyl-1,2,3,6-tetrahydropyridine. *J. Neurol. Sci.* **1987**, *81*, 321−331.
(191) Peyser, C. E.; Folstein, M.; Chase, G. A.; Starkstein, S.; Brandt, J.; Cockrell, J. R.; Bylsma, F.; Coyle, J. T.; McHugh, P. R.; Folstein, S. E. Trial of D-alpha-tocopherol in Huntington's disease. *Am. J. Psychiatry* **1995**, *152*, 1771−1775.
(192) Desnuelle, C.; Dib, M.; Garrel, C.; Favier, A. A double-blind, placebo-controlled randomized clinical trial of alpha-tocopherol (vitamin E) in the treatment of amyotrophic lateral sclerosis. ALS Riluzole-Tocopherol Study Group. *Amyotrophic Lateral Scler. Other Mot. Neuron Disord.* **2001**, *2*, 9−18.
(193) Gurney, M. E.; Cutting, F. B.; Zhai, P.; Doble, A.; Taylor, C. P.; Andrus, P. K.; Hall, E. D. Benefit of vitamin E, riluzole, and gabapentin in a transgenic model of familial amyotrophic lateral sclerosis. *Ann. Neurol.* **1996**, *39*, 147−157.
(194) Asthana, S.; Baker, L. D.; Craft, S.; Stanczyk, F. Z.; Veith, R. C.; Raskind, M. A.; Plymate, S. R. High-dose estradiol improves cognition for women with AD: results of a randomized study. *Neurology* **2001**, *57*, 605−612.

(195) Carlson, M. C.; Zandi, P. P.; Plassman, B. L.; Tschanz, J. T.; Welsh-Bohmer, K. A.; Steffens, D. C.; Bastian, L. A.; Mehta, K. M.; Breitner, J. C. Hormone replacement therapy and reduced cognitive decline in older women: the Cache County study. *Neurology* **2001**, *57*, 2210−2216.
(196) Henderson, V. W.; Paganini-Hill, A.; Miller, B. L.; Elble, R. J.; Reyes, P. F.; Shoupe, D.; McCleary, C. A.; Klein, R. A.; Hake, A. M.; Farlow, M. R. Estrogen for Alzheimer's disease in women: randomized, double-blind, placebo-controlled trial. *Neurology* **2000**, *54*, 295−301.
(197) Mulnard, R. A.; Cotman, C. W.; Kawas, C.; van Dyck, C. H.; Sano, M.; Doody, R.; Koss, E.; Pfeiffer, E.; Jin, S.; Gamst, A.; Grundman, M.; Thomas, R.; Thal, L. J. Estrogen replacement therapy for treatment of mild to moderate Alzheimer disease: a randomized controlled trial. Alzheimer's disease cooperative study. *JAMA, J. Am. Med. Assoc.* **2000**, *283*, 1007−1015.
(198) Wang, P. N.; Liao, S. Q.; Liu, R. S.; Liu, C. Y.; Chao, H. T.; Lu, S. R.; Yu, H. Y.; Wang, S. J.; Liu, H. C. Effects of estrogen on cognition, mood, and cerebral blood flow in AD: a controlled study. *Neurology* **2000**, *54*, 2061−2066.
(199) Blanchet, P. J.; Fang, J.; Hyland, K.; Arnold, L. A.; Mouradian, M. M.; Chase, T. N. Short-term effects of high-dose 17beta-estradiol in postmenopausal PD patients: a crossover study. *Neurology* **1999**, *53*, 91−95.
(200) Fernandez, H. H.; Lapane, K. L. Estrogen use among nursing home residents with a diagnosis of Parkinson's disease. *Mov. Disord.* **2000**, *15*, 1119−1124.
(201) Tsang, K. L.; Ho, S. L.; Lo, S. K. Estrogen improves motor disability in parkinsonian postmenopausal women with motor fluctuations. *Neurology* **2000**, *54*, 2292−2298.
(202) Baldereschi, M.; Di Carlo, A.; Rocca, W. A.; Vanni, P.; Maggi, S.; Perissinotto, E.; Grigoletto, F.; Amaducci, L.; Inzitari, D. Parkinson's disease and parkinsonism in a longitudinal study: two-fold higher incidence in men. ILSA Working Group. Italian longitudinal study on aging. *Neurology* **2000**, *55*, 1358−1363.
(203) Mayeux, R.; Marder, K.; Cote, L. J.; Denaro, J.; Hemenegildo, N.; Mejia, H.; Tang, M. X.; Lantigua, R.; Wilder, D.; Gurland, B.; Hauser, A. The frequency of idiopathic Parkinson's disease by age, ethnic group, and sex in northern Manhattan, 1988−1993. *Am. J. Epidemiol.* **1995**, *142*, 820−827.
(204) Aggarwal, B. B.; Harikumar, K. B. Potential therapeutic effects of curcumin, the anti-inflammatory agent, against neurodegenerative, cardiovascular, pulmonary, metabolic, autoimmune and neoplastic diseases. *Int. J. Biochem. Cell Biol.* **2009**, *41*, 40−59.
(205) Richard, T.; Pawlus, A. D.; Iglesias, M. L.; Pedrot, E.; Waffo-Teguo, P.; Merillon, J. M.; Monti, J. P. Neuroprotective properties of resveratrol and derivatives. *Ann. N. Y. Acad. Sci.* **2011**, *1215*, 103−108.
(206) Heim, K. E.; Tagliaferro, A. R.; Bobilya, D. J. Flavonoid antioxidants: chemistry, metabolism and structure−activity relationships. *J. Nutr. Biochem.* **2002**, *13*, 572−584.
(207) Pietta, P. G. Flavonoids as antioxidants. *J. Nat. Prod.* **2000**, *63*, 1035−1042.
(208) Dickinson, D. A.; Forman, H. J. Cellular glutathione and thiols metabolism. *Biochem. Pharmacol.* **2002**, *64*, 1019−1026.
(209) Owuor, E. D.; Kong, A. N. Antioxidants and oxidants regulated signal transduction pathways. *Biochem. Pharmacol.* **2002**, *64*, 765−770.
(210) Filomeni, G.; Rotilio, G.; Ciriolo, M. R. Cell signalling and the glutathione redox system. *Biochem. Pharmacol.* **2002**, *64*, 1057−1064.
(211) Paolicchi, A.; Dominici, S.; Pieri, L.; Maellaro, E.; Pompella, A. Glutathione catabolism as a signaling mechanism. *Biochem. Pharmacol.* **2002**, *64*, 1027−1035.
(212) Fridovich, I. Superoxide anion radical ($O_2^{-\bullet}$), superoxide dismutases, and related matters. *J. Biol. Chem.* **1997**, *272*, 18515−18517.
(213) Masumoto, H.; Sies, H. The reaction of 2-(methylseleno)-benzanilide with peroxynitrite. *Chem. Res. Toxicol.* **1996**, *9*, 1057−1062.
(214) Parnham, M.; Sies, H. Ebselen: prospective therapy for cerebral ischaemia. *Expert Opin. Invest. Drugs.* **2000**, *9*, 607−619.
(215) Moussaoui, S.; Obinu, M. C.; Daniel, N.; Reibaud, M.; Blanchard, V.; Imperato, A. The antioxidant ebselen prevents neurotoxicity and clinical symptoms in a primate model of Parkinson's disease. *Exp. Neurol.* **2000**, *166*, 235−245.
(216) Aitken, J. B.; Lay, P. A.; Duong, T. T.; Aran, R.; Witting, P. K.; Harris, H. H.; Lai, B.; Vogt, S.; Giles, G. I. Synchrotron radiation induced X-ray emission studies of the antioxidant mechanism of the organoselenium drug ebselen. *J. Biol. Inorg. Chem.* **2012**, *17*, 589−598.
(217) d'Alessio, P.; Moutet, M.; Coudrier, E.; Darquenne, S.; Chaudiere, J. ICAM-1 and VCAM-1 expression induced by TNF-alpha are inhibited by a glutathione peroxidase mimic. *Free Radical Biol. Med.* **1998**, *24*, 979−987.
(218) Moutet, M.; d'Alessio, P.; Malette, P.; Devaux, V.; Chaudiere, J. Glutathione peroxidase mimics prevent TNFalpha- and neutrophil-induced endothelial alterations. *Free Radical Biol. Med.* **1998**, *25*, 270−281.
(219) Batinic-Haberle, I.; Benov, L.; Spasojevic, I.; Fridovich, I. The ortho effect makes manganese(III) meso-tetrakis(*N*-methylpyridinium-2-yl)porphyrin a powerful and potentially useful superoxide dismutase mimic. *J. Biol. Chem.* **1998**, *273*, 24521−24528.
(220) Bowler, R. P.; Sheng, H.; Enghild, J. J.; Pearlstein, R. D.; Warner, D. S.; Crapo, J. D. A catalytic antioxidant (AEOL 10150) attenuates expression of inflammatory genes in stroke. *Free Radical Biol. Med.* **2002**, *33*, 1141−1152.
(221) Patel, M.; Day, B. J. Metalloporphyrin class of therapeutic catalytic antioxidants. *Trends Pharmacol. Sci.* **1999**, *20*, 359−364.
(222) Peng, J.; Mao, X. O.; Stevenson, F. F.; Hsu, M.; Andersen, J. K. The herbicide paraquat induces dopaminergic nigral apoptosis through sustained activation of the JNK pathway. *J. Biol. Chem.* **2004**, *279*, 32626−32632.
(223) Peng, J.; Stevenson, F. F.; Doctrow, S. R.; Andersen, J. K. Superoxide dismutase/catalase mimetics are neuroprotective against selective paraquat-mediated dopaminergic neuron death in the substantial nigra: implications for Parkinson disease. *J. Biol. Chem.* **2005**, *280*, 29194−29198.
(224) Young, A. J.; Lowe, G. M. Antioxidant and prooxidant properties of carotenoids. *Arch. Biochem. Biophys.* **2001**, *385*, 20−27.
(225) Di Mascio, P.; Kaiser, S.; Sies, H. Lycopene as the most efficient biological carotenoid singlet oxygen quencher. *Arch. Biochem. Biophys.* **1989**, *274*, 532−538.
(226) Burton, G. W.; Ingold, K. U. beta-Carotene: an unusual type of lipid antioxidant. *Science* **1984**, *224*, 569−573.
(227) Goodman, A. B.; Pardee, A. B. Evidence for defective retinoid transport and function in late onset Alzheimer's disease. *Proc. Natl. Acad. Sci. U.S.A.* **2003**, *100*, 2901−2905.
(228) Goodman, A. B. Retinoid receptors, transporters, and metabolizers as therapeutic targets in late onset Alzheimer disease. *J. Cell. Physiol.* **2006**, *209*, 598−603.
(229) Ding, Y.; Qiao, A.; Wang, Z.; Goodwin, J. S.; Lee, E. S.; Block, M. L.; Allsbrook, M.; McDonald, M. P.; Fan, G. H. Retinoic acid attenuates beta-amyloid deposition and rescues memory deficits in an Alzheimer's disease transgenic mouse model. *J. Neurosci.* **2008**, *28*, 11622−11634.
(230) Mann, K. G. Biochemistry and physiology of blood coagulation. *Thromb. Haemostasis* **1999**, *82*, 165−174.
(231) Price, P. A. Role of vitamin-K-dependent proteins in bone metabolism. *Annu. Rev. Nutr.* **1988**, *8*, 565−583.
(232) Allison, A. C. The possible role of vitamin K deficiency in the pathogenesis of Alzheimer's disease and in augmenting brain damage associated with cardiovascular disease. *Med. Hypotheses* **2001**, *57*, 151−155.
(233) Beal, M. F.; Shults, C. W. Effects of coenzyme Q10 in Huntington's disease and early Parkinson's disease. *BioFactors* **2003**, *18*, 153−161.
(234) Bhat, V.; Weiner, W. J. Parkinson's disease. Diagnosis and the initiation of therapy. *Minerva Med.* **2005**, *96*, 145−154.
(235) Yang, X.; Yang, Y.; Li, G.; Wang, J.; Yang, E. S. Coenzyme Q10 attenuates beta-amyloid pathology in the aged transgenic mice with Alzheimer presenilin 1 mutation. *J. Mol. Neurosci.* **2008**, *34*, 165−171.

(236) Yang, X.; Dai, G.; Li, G.; Yang, E. S. Coenzyme Q10 reduces beta-amyloid plaque in an APP/PS1 transgenic mouse model of Alzheimer's disease. *J. Mol. Neurosci.* **2010**, *41*, 110−113.
(237) Skulachev, V. P. Mitochondria-targeted antioxidants as promising drugs for treatment of age-related brain diseases. *J. Alzheimer's Dis.* **2012**, *28*, 283−289.
(238) Szeto, H. H.; Schiller, P. W. Novel therapies targeting inner mitochondrial membrane—from discovery to clinical development. *Pharm. Res.* **2011**, *28*, 2669−2679.
(239) Floyd, R. A.; Hensley, K. Nitrone inhibition of age-associated oxidative damage. *Ann. N. Y. Acad. Sci.* **2000**, *899*, 222−237.
(240) Floyd, R. A.; Hensley, K.; Bing, G. Evidence for enhanced neuro-inflammatory processes in neurodegenerative diseases and the action of nitrones as potential therapeutics. *J. Neural Transm., Suppl.* **2000**, 387−414.
(241) Das, A.; Gopalakrishnan, B.; Voss, O. H.; Doseff, A. I.; Villamena, F. A. Inhibition of ROS-induced apoptosis in endothelial cells by nitrone spin traps via induction of phase II enzymes and suppression of mitochondria-dependent pro-apoptotic signaling. *Biochem. Pharmacol.* **2012**, *84*, 486−497.
(242) Floyd, R. A.; Hensley, K.; Jaffery, F.; Maidt, L.; Robinson, K.; Pye, Q.; Stewart, C. Increased oxidative stress brought on by pro-inflammatory cytokines in neurodegenerative processes and the protective role of nitrone-based free radical traps. *Life Sci.* **1999**, *65*, 1893−1899.
(243) Floyd, R. A.; Hensley, K.; Forster, M. J.; Kelleher-Andersson, J. A.; Wood, P. L. Nitrones, their value as therapeutics and probes to understand aging. *Mech. Ageing Dev.* **2002**, *123*, 1021−1031.
(244) Shuaib, A.; Lees, K. R.; Lyden, P.; Grotta, J.; Davalos, A.; Davis, S. M.; Diener, H. C.; Ashwood, T.; Wasiewski, W. W.; Emeribe, U. NXY-059 for the treatment of acute ischemic stroke. *N. Engl. J. Med.* **2007**, *357*, 562−571.
(245) Klivenyi, P.; Matthews, R. T.; Wermer, M.; Yang, L.; MacGarvey, U.; Becker, D. A.; Natero, R.; Beal, M. F. Azulenyl nitrone spin traps protect against MPTP neurotoxicity. *Exp. Neurol.* **1998**, *152*, 163−166.
(246) Yang, L.; Calingasan, N. Y.; Chen, J.; Ley, J. J.; Becker, D. A.; Beal, M. F. A novel azulenyl nitrone antioxidant protects against MPTP and 3-nitropropionic acid neurotoxicities. *Exp. Neurol.* **2005**, *191*, 86−93.
(247) Padayatty, S. J.; Katz, A.; Wang, Y.; Eck, P.; Kwon, O.; Lee, J. H.; Chen, S.; Corpe, C.; Dutta, A.; Dutta, S. K.; Levine, M. Vitamin C as an antioxidant: evaluation of its role in disease prevention. *J. Am. Coll. Nutr.* **2003**, *22*, 18−35.
(248) Dringen, R.; Pfeiffer, B.; Hamprecht, B. Synthesis of the antioxidant glutathione in neurons: supply by astrocytes of CysGly as precursor for neuronal glutathione. *J. Neurosci.* **1999**, *19*, 562−569.
(249) Dringen, R.; Hamprecht, B. *N*-Acetylcysteine, but not methionine or 2-oxothiazolidine-4-carboxylate, serves as cysteine donor for the synthesis of glutathione in cultured neurons derived from embryonal rat brain. *Neurosci. Lett.* **1999**, *259*, 79−82.
(250) Cudkowicz, M. E.; Sexton, P. M.; Ellis, T.; Hayden, D. L.; Gwilt, P. R.; Whalen, J.; Brown, R. H., Jr. The pharmacokinetics and pharmaco-dynamics of procysteine in amyotrophic lateral sclerosis. *Neurology* **1999**, *52*, 1492−1494.
(251) Dinkova-Kostova, A. T.; Holtzclaw, W. D.; Cole, R. N.; Itoh, K.; Wakabayashi, N.; Katoh, Y.; Yamamoto, M.; Talalay, P. Direct evidence that sulfhydryl groups of Keap1 are the sensors regulating induction of phase 2 enzymes that protect against carcinogens and oxidants. *Proc. Natl. Acad. Sci. U.S.A.* **2002**, *99*, 11908−11913.
(252) Surh, Y. J.; Kundu, J. K.; Na, H. K. Nrf2 as a master redox switch in turning on the cellular signaling involved in the induction of cytoprotective genes by some chemopreventive phytochemicals. *Planta Med.* **2008**, *74*, 1526−1539.
(253) Magesh, S.; Chen, Y.; Hu, L. Q. Small molecule modulators of Keap1-Nrf2-ARE pathway as potential preventive and therapeutic agents. *Med. Res. Rev.* **2012**, *32*, 687−726.
(254) Calkins, M. J.; Johnson, D. A.; Townsend, J. A.; Vargas, M. R.; Dowell, J. A.; Williamson, T. P.; Kraft, A. D.; Lee, J. M.; Li, J.; Johnson, J. A. The Nrf2/ARE pathway as a potential therapeutic target in neurodegenerative disease. *Antioxid. Redox Signaling* **2009**, *11*, 497−508.
(255) Jung, K. A.; Kwak, M. K. The Nrf2 system as a potential target for the development of indirect antioxidants. *Molecules* **2010**, *15*, 7266−7291.
(256) Vargas, M. R.; Pehar, M.; Cassina, P.; Beckman, J. S.; Barbeito, L. Increased glutathione biosynthesis by Nrf2 activation in astrocytes prevents p75(NTR)-dependent motor neuron apoptosis. *J. Neurochem.* **2006**, *97*, 687−696.
(257) Kirby, J.; Halligan, E.; Baptista, M. J.; Allen, S.; Heath, P. R.; Holden, H.; Barber, S. C.; Loynes, C. A.; Wood-Allum, C. A.; Lunec, J.; Shaw, P. J. Mutant SOD1 alters the motor neuronal transcriptome: implications for familial ALS. *Brain* **2005**, *128*, 1686−1706.
(258) Trinh, K.; Moore, K.; Wes, P. D.; Muchowski, P. J.; Dey, J.; Andrews, L.; Pallanck, L. J. Induction of the phase II detoxification pathway suppresses neuron loss in *Drosophila* models of Parkinson's disease. *J. Neurosci.* **2008**, *28*, 465−472.
(259) Ramsey, C. P.; Glass, C. A.; Montgomery, M. B.; Lindl, K. A.; Ritson, G. P.; Chia, L. A.; Hamilton, R. L.; Chu, C. T.; Jordan-Sciutto, K. L. Expression of Nrf2 in neurodegenerative diseases. *J. Neuropathol. Exp. Neurol.* **2007**, *66*, 75−85.
(260) Stack, C.; Ho, D.; Wille, E.; Calingasan, N. Y.; Williams, C.; Liby, K.; Sporn, M.; Dumont, M.; Beal, M. F. Triterpenoids CDDO-ethyl amide and CDDO-trifluoroethyl amide improve the behavioral phenotype and brain pathology in a transgenic mouse model of Huntington's disease. *Free Radical Biol. Med.* **2010**, *49*, 147−158.
(261) Ross, C. A.; Poirier, M. A. Protein aggregation and neurodegenerative disease. *Nat. Med.* **2004**, *10* (Suppl.), S10−S17.
(262) Aguzzi, A.; O'Connor, T. Protein aggregation diseases: pathogenicity and therapeutic perspectives. *Nat. Rev. Drug Discovery* **2010**, *9*, 237−248.
(263) Bartolini, M.; Andrisano, V. Strategies for the inhibition of protein aggregation in human diseases. *ChemBioChem* **2010**, *11*, 1018−1035.
(264) Schneider, A.; Mandelkow, E. Tau based treatment strategies in neurodegenerative diseases. *Neurotherapeutics* **2008**, *5*, 443−457.
(265) Shelton, S. B.; Johnson, G. V. Cyclin-dependent kinase-5 in neurodegeneration. *J. Neurochem.* **2004**, *88*, 1313−1326.
(266) Hanger, D. P.; Anderton, B. H.; Noble, W. Tau phosphorylation: the therapeutic challenge for neurodegenerative disease. *Trends Mol. Med.* **2009**, *15*, 112−119.
(267) Meijer, L.; Thunnissen, A. M. W. H.; White, A. W.; Garnier, M.; Nikolic, M.; Tsai, L. H.; Walter, J.; Cleverley, K. E.; Salinas, P. C.; Wu, Y. Z.; Biernat, J.; Mandelkow, E.; Kim, S. H.; Pettit, G. R. Inhibition of cyclin-dependent kinases, GSK-3beta and CK1 by hymenialdisine, a marine sponge constituent. *Chem. Biol.* **2000**, *7*, 51−63.
(268) Palomo, V.; Perez, D. I.; Gil, C.; Martinez, A. The potential role of glycogen synthase kinase 3 inhibitors as amyotrophic lateral sclerosis pharmacological therapy. *Curr. Med. Chem.* **2011**, *18*, 3028−3034.
(269) Chen, P. C.; Gaisina, I. N.; El-Khodor, B. F.; Ramboz, S.; Makhortova, N. R.; Rubin, L. L.; Kozikowski, A. P. Identification of a maleimide-based glycogen synthase kinase-3 (GSK-3) inhibitor, BIP-135, that prolongs the median survival time of Delta 7 SMA KO mouse model of spinal muscular atrophy. *ACS Chem. Neurosci.* **2012**, *3*, 5−11.
(270) Koh, S. H.; Kim, Y.; Kim, H. Y.; Hwang, S.; Lee, C. H.; Kim, S. H. Inhibition of glycogen synthase kinase-3 suppresses the onset of symptoms and disease progression of G93A-SOD1 mouse model of ALS. *Exp. Neurol.* **2007**, *205*, 336−346.
(271) Lin, X.; Parisiadou, L.; Gu, X. L.; Wang, L.; Shim, H.; Sun, L.; Xie, C.; Long, C. X.; Yang, W. J.; Ding, J.; Chen, Z. Z.; Gallant, P. E.; Tao-Cheng, J. H.; Rudow, G.; Troncoso, J. C.; Liu, Z.; Li, Z.; Cai, H. Leucine-rich repeat kinase 2 regulates the progression of neuropathology induced by Parkinson's-disease-related mutant alpha-synuclein. *Neuron* **2009**, *64*, 807−827.

(272) Ballatore, C.; Brunden, K. R.; Trojanowski, J. Q.; Lee, V. M.; Smith, A. B., 3rd; Huryn, D. M. Modulation of protein−protein interactions as a therapeutic strategy for the treatment of neurodegenerative tauopathies. *Curr. Top. Med. Chem.* **2011**, *11*, 317−330.
(273) Wischik, C. M.; Edwards, P. C.; Lai, R. Y.; Roth, M.; Harrington, C. R. Selective inhibition of Alzheimer disease-like tau aggregation by phenothiazines. *Proc. Natl. Acad. Sci. U.S.A.* **1996**, *93*, 11213−11218.
(274) Ballatore, C.; Crowe, A.; Piscitelli, F.; James, M.; Lou, K.; Rossidivito, G.; Yao, Y.; Trojanowski, J. Q.; Lee, V. M.; Brunden, K. R.; Smith, A. B., 3rd. Aminothienopyridazine inhibitors of tau aggregation: evaluation of structure−activity relationship leads to selection of candidates with desirable in vivo properties. *Bioorg. Med. Chem.* **2012**, *20*, 4451−4461.
(275) Messing, L.; Decker, J. M.; Joseph, M.; Mandelkow, E.; Mandelkow, E. M. Cascade of tau toxicity in inducible hippocampal brain slices and prevention by aggregation inhibitors. *Neurobiol. Aging* **2013**, *34*, 1343−1354.
(276) Ghosh, A. K.; Brindisi, M.; Tang, J. Developing beta-secretase inhibitors for treatment of Alzheimer's disease. *J. Neurochem.* **2012**, *120*, 71−83.
(277) May, P. C.; Dean, R. A.; Lowe, S. L.; Martenyi, F.; Sheehan, S. M.; Boggs, L. N.; Monk, S. A.; Mathes, B. M.; Mergott, D. J.; Watson, B. M.; Stout, S. L.; Timm, D. E.; Smith Labell, E.; Gonzales, C. R.; Nakano, M.; Jhee, S. S.; Yen, M.; Ereshefsky, L.; Lindstrom, T. D.; Calligaro, D. O.; Cocke, P. J.; Greg Hall, D.; Friedrich, S.; Citron, M.; Audia, J. E. Robust central reduction of amyloid-beta in humans with an orally available, non-peptidic beta-secretase inhibitor. *J. Neurosci.* **2011**, *31*, 16507−16516.
(278) D'Onofrio, G.; Panza, F.; Frisardi, V.; Solfrizzi, V.; Imbimbo, B. P.; Paroni, G.; Cascavilla, L.; Seripa, D.; Pilotto, A. Advances in the identification of γ-secretase inhibitors for the treatment of Alzheimer's disease. *Expert Opin. Drug Discovery* **2012**, *7*, 19−37.
(279) Gillman, K. W.; Starrett, J. E.; Parker, M. F.; Xie, K.; Bronson, J. J.; Marcin, L. R.; McElhone, K. E.; Bergstrom, C. P.; Mate, R. A.; Williams, R.; Meredith, J. E.; Burton, C. R.; Barten, D. M.; Toyn, J. H.; Roberts, S. B.; Lentz, K. A.; Houston, J. G.; Zaczek, R.; Albright, C. F.; Decicco, C. P.; Macor, J. E.; Olson, R. E. Discovery and evaluation of BMS-708163, a potent, selective and orally bioavailable gamma-secretase inhibitor. *ACS Med. Chem. Lett.* **2010**, *1*, 120−124.
(280) Panza, F.; Solfrizzi, V.; Frisardi, V.; Capurso, C.; D'Introno, A.; Colacicco, A. M.; Vendemiale, G.; Capurso, A.; Imbimbo, B. P. Disease-modifying approach to the treatment of Alzheimer's disease: from alpha-secretase activators to gamma-secretase inhibitors and modulators. *Drugs Aging* **2009**, *26*, 537−555.
(281) Khan, T. K.; Nelson, T. J.; Verma, V. A.; Wender, P. A.; Alkon, D. L. A cellular model of Alzheimer's disease therapeutic efficacy: PKC activation reverses Abeta-induced biomarker abnormality on cultured fibroblasts. *Neurobiol. Dis.* **2009**, *34*, 332−339.
(282) Wender, P. A.; Baryza, J. L.; Brenner, S. E.; DeChristopher, B. A.; Loy, B. A.; Schrier, A. J.; Verma, V. A. Design, synthesis, and evaluation of potent bryostatin analogs that modulate PKC translocation selectivity. *Proc. Natl. Acad. Sci. U.S.A.* **2011**, *108*, 6721−6726.
(283) Simons, M.; Keller, P.; Dichgans, J.; Schulz, J. B. Cholesterol and Alzheimer's disease: Is there a link? *Neurology* **2001**, *57*, 1089−1093.
(284) Simons, M.; Schwarzler, F.; Lutjohann, D.; von Bergmann, K.; Beyreuther, K.; Dichgans, J.; Wormstall, H.; Hartmann, T.; Schulz, J. B. Treatment with simvastatin in normocholesterolemic patients with Alzheimer's disease: a 26-week randomized, placebo-controlled, double-blind trial. *Ann. Neurol.* **2002**, *52*, 346−350.
(285) Puglielli, L.; Tanzi, R. E.; Kovacs, D. M. Alzheimer's disease: the cholesterol connection. *Nat. Neurosci.* **2003**, *6*, 345−351.
(286) Roy, A.; Pahan, K. Prospects of statins in Parkinson disease. *Neuroscientist* **2011**, *17*, 244−255.
(287) Valenza, M.; Cattaneo, E. Emerging roles for cholesterol in Huntington's disease. *Trends Neurosci.* **2011**, *34*, 474−486.
(288) Bate, C.; Tayebi, M.; Williams, A. Sequestration of free cholesterol in cell membranes by prions correlates with cytoplasmic phospholipase A2 activation. *BMC Biol.* **2008**, *6*, 8.
(289) Tobert, J. A. Lovastatin and beyond: the history of the HMG-CoA reductase inhibitors. *Nat. Rev. Drug Discovery* **2003**, *2*, 517−526.
(290) Arawaka, S.; Machiya, Y.; Kato, T. Heat shock proteins as suppressors of accumulation of toxic prefibrillar intermediates and misfolded proteins in neurodegenerative diseases. *Curr. Pharm. Biotechnol.* **2010**, *11*, 158−166.
(291) Wyttenbach, A.; Arrigo, A. P. The Role of Heat Shock Proteins during Neurodegeneration in Alzheimer's, Parkinson's and Huntington's Disease. In *Heat Shock Proteins in Neural Cells*; Richter-Landsberg, C., Ed.; Springer and R. G. Landes: Georgetown, TX, U.S., 2009; p 125.
(292) Neef, D. W.; Jaeger, A. M.; Thiele, D. J. Heat shock transcription factor 1 as a therapeutic target in neurodegenerative diseases. *Nat. Rev. Drug Discovery* **2011**, *10*, 930−944.
(293) Luo, W.; Sun, W.; Tadone, T.; Rodina, A.; Chiosis, G. Heat shock protein 90 in neurodegenerative diseases. *Mol. Neurodegener.* **2010**, *5*, 24.
(294) Trott, A.; West, J. D.; Klaic, L.; Westerheide, S. D.; Silverman, R. B.; Morimoto, R. I.; Morano, K. A. Activation of heat shock and antioxidant responses by the natural product celastrol: transcriptional signatures of a thiol-targeted molecule. *Mol. Biol. Cell* **2008**, *19*, 1104−1112.
(295) Klaic, L.; Trippier, P. C.; Mishra, R. K.; Morimoto, R. I.; Silverman, R. B. Remarkable stereospecific conjugate additions to the Hsp90 inhibitor celastrol. *J. Am. Chem. Soc.* **2011**, *133*, 19634−19637.
(296) Kieran, D.; Kalmar, B.; Dick, J. R.; Riddoch-Contreras, J.; Burnstock, G.; Greensmith, L. Treatment with arimoclomol, a coinducer of heat shock proteins, delays disease progression in ALS mice. *Nat. Med.* **2004**, *10*, 402−405.
(297) Evans, C. G.; Chang, L.; Gestwicki, J. E. Heat shock protein 70 (Hsp70) as an emerging drug target. *J. Med. Chem.* **2010**, *53*, 4585−4602.
(298) Fleming, A.; Noda, T.; Yoshimori, T.; Rubinsztein, D. C. Chemical modulators of autophagy as biological probes and potential therapeutics. *Nat. Chem. Biol.* **2011**, *7*, 9−17.
(299) Bove, J.; Martinez-Vicente, M.; Vila, M. Fighting neurodegeneration with rapamycin: mechanistic insights. *Nat. Rev. Neurosci.* **2011**, *12*, 437−452.
(300) Casarejos, M. J.; Solano, R. M.; Gomez, A.; Perucho, J.; de Yebenes, J. G.; Mena, M. A. The accumulation of neurotoxic proteins, induced by proteasome inhibition, is reverted by trehalose, an enhancer of autophagy, in human neuroblastoma cells. *Neurochem. Int.* **2011**, *58*, 512−520.
(301) Dennissen, F. J.; Kholod, N.; van Leeuwen, F. W. The ubiquitin proteasome system in neurodegenerative diseases: Culprit, accomplice or victim? *Prog. Neurobiol.* **2012**, *96*, 190−207.
(302) Luo, G.-R.; Chen, S.; Le, W.-D. Are heat shock proteins therapeutic target for Parkinson's disease? *Int. J. Biol. Sci.* **2007**, *3*, 20−26.
(303) Zhao, J. H.; Liu, H. L.; Lin, H. Y.; Huang, C. H.; Fang, H. W.; Chen, S. S.; Ho, Y.; Tsai, W. B.; Chen, W. Y. Chemical chaperone and inhibitor discovery: potential treatments for protein conformational diseases. *Perspect. Med. Chem.* **2008**, *1*, 39−48.
(304) Ali, Y. O.; Kitay, B. M.; Zhai, R. G. Dealing with misfolded proteins: examining the neuroprotective role of molecular chaperones in neurodegeneration. *Molecules* **2010**, *15*, 6859−6887.
(305) Cuajungco, M. P.; Faget, K. Y.; Huang, X.; Tanzi, R. E.; Bush, A. I. Metal chelation as a potential therapy for Alzheimer's disease. *Ann. N. Y. Acad. Sci.* **2000**, *920*, 292−304.
(306) Wang, X.; Wang, X.; Zhang, C.; Jiao, Y.; Guo, Z. Inhibitory action of macrocyclic platiniferous chelators on metal-induced Ab aggregation. *Chem. Sci.* **2012**, *3*, 1304−1312.
(307) Wisniewski, T.; Sadowski, M. Preventing beta-amyloid fibrillization and deposition: beta-sheet breakers and pathological chaperone inhibitors. *BMC Neurosci.* **2008**, *9* (Suppl. 2), S5.

(308) Simons, L. J.; Caprathe, B. W.; Callahan, M.; Graham, J. M.; Kimura, T.; Lai, Y.; LeVine, H., 3rd; Lipinski, W.; Sakkab, A. T.; Tasaki, Y.; Walker, L. C.; Yasunaga, T.; Ye, Y.; Zhuang, N.; Augelli-Szafran, C. E. The synthesis and structure−activity relationship of substituted *N*-phenyl anthranilic acid analogs as amyloid aggregation inhibitors. *Bioorg. Med. Chem. Lett.* **2009**, *19*, 654−657.
(309) Heiser, V.; Engernann, S.; Brocker, W.; Dunkel, I.; Boeddrich, A.; Waelter, S.; Nordhoff, E.; Lurz, R.; Schugardt, N.; Rautenberg, S.; Herhaus, C.; Barnickel, G.; Bottcher, H.; Lehrach, H.; Wanker, E. E. Identification of benzothiazoles as potential polyglutamine aggregation inhibitors of Huntington's disease by using an automated filter retardation assay. *Proc. Natl. Acad. Sci. U.S.A.* **2002**, *99*, 16400−16406.
(310) Geldenhuys, W. J.; Van der Schyf, C. J. Designing drugs with multi-target activity: the next step in the treatment of neurodegenerative disorders. *Expert Opin. Drug Discovery* **2013**, *8*, 115−129.
(311) Rizzo, S.; Tarozzi, A.; Bartolini, M.; Da Costa, G.; Bisi, A.; Gobbi, S.; Belluti, F.; Ligresti, A.; Allara, M.; Monti, J. P.; Andrisano, V.; Di Marzo, V.; Hrelia, P.; Rampa, A. 2-Arylbenzofuran-based molecules as multipotent Alzheimer's disease modifying agents. *Eur. J. Med. Chem.* **2012**, *58*, 519−532.
(312) Sorrenti, V.; Salerno, L.; Di Giacomo, C.; Acquaviva, R.; Siracusa, M. A.; Vanella, A. Imidazole derivatives as antioxidants and selective inhibitors of nNOS. *Nitric Oxide* **2006**, *14*, 45−50.
(313) Galdeano, C.; Viayna, E.; Sola, I.; Formosa, X.; Camps, P.; Badia, A.; Clos, M. V.; Relat, J.; Ratia, M.; Bartolini, M.; Mancini, F.; Andrisano, V.; Salmona, M.; Minguillon, C.; Gonzalez-Munoz, G. C.; Rodriguez-Franco, M. I.; Bidon-Chanal, A.; Luque, F. J.; Munoz-Torrero, D. Huprine−tacrine heterodimers as anti-amyloidogenic compounds of potential interest against Alzheimer's and prion diseases. *J. Med. Chem.* **2012**, *55*, 661−669.

Journal of Medicinal Chemistry

Article

pubs.acs.org/jmc

Arylazanylpyrazolone Derivatives as Inhibitors of Mutant Superoxide Dismutase 1 Dependent Protein Aggregation for the Treatment of Amyotrophic Lateral Sclerosis

Yinan Zhang,[†] Radhia Benmohamed,[‡] He Huang,[†] Tian Chen,[†] Cindy Voisine,[§,∥] Richard I. Morimoto,[§] Donald R. Kirsch,[‡] and Richard B. Silverman*,[†]

[†]Department of Chemistry and Department of Molecular Biosciences, Chemistry of Life Processes Institute, Center for Molecular Innovation and Drug Discovery, Northwestern University, Evanston, Illinois 60208-3113, United States

[‡]Cambria Pharmaceuticals, Cambridge, Massachusetts 02142, United States

[§]Department of Molecular Biosciences, Rice Institute for Biomedical Research, Northwestern University, Evanston, Illinois 60208-3500, United States

Supporting Information

ABSTRACT: The arylsulfanylpyrazolone and aryloxanylpyrazolone scaffolds previously were reported to inhibit Cu/Zn superoxide dismutase 1 dependent protein aggregation and to extend survival in the ALS mouse model. However, further evaluation of these compounds indicated weak pharmacokinetic properties and a relatively low maximum tolerated dose. On the basis of an ADME analysis, a new series of compounds, the arylazanylpyrazolones, has been synthesized, and structure−activity relationships were determined. The SAR results showed that the pyrazolone ring is critical to cellular protection. The NMR, IR, and computational analyses suggest that phenol-type tautomers of the pyrazolone ring are the active pharmacophore with the arylazanylpyrazolone analogues. A comparison of experimental and calculated IR spectra is shown to be a valuable method to identify the predominant tautomer.

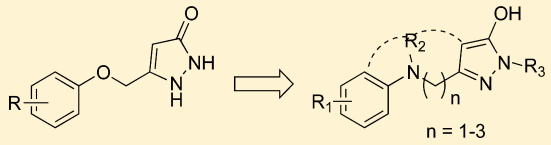

INTRODUCTION

Amyotrophic lateral sclerosis (ALS), a rapidly fatal neurodegenerative disease, is characterized by progressive loss of upper and/or lower neurons in the motor cortex, brainstem, and ventral spinal cord.[1] Although the incidence and prevalence of the disease are relatively low compared with other neurodegenerative diseases such as Parkinson's disease and Alzheimer's disease, it has the most rapid progression to death, in most cases within 3−5 years after diagnosis.[2] Moreover, an observed increased prevalence,[3] higher risk for military personnel,[4] and high cost for care in the late stages of ALS[5] result in extreme economic and emotional burdens to the patients and their families, nearly one-third of whom reside in the United States.[6] The sole FDA-approved drug riluzole, a presumptive antiglutamatergic agent, extends survival by only 2−3 months.[7]

Although the mechanistic basis of ALS and the cause of motor neuron death remain controversial, a cohort of susceptibility genes producing ALS have been identified from familial ALS patients,[8] such as fused in sarcoma, senataxin, TAR DNA binding protein (TDP-43), and UBQLN2. The discovery of the toxicity of mutant Cu/Zn superoxide dismutase 1 (SOD1) provides the first insight into potential causes for ALS[9] and contributes the most to our understanding of ALS pathology, which includes calcium mediated excitotoxicity, oxidative stress, mitochondrial dysfunction, and aberrant RNA processing.[10] Recent observations that mutant SOD1-expressing astrocytes are toxic to motor neurons in both familial and sporadic ALS,[11,12] together with the fact that SOD1 mediated protein misfolding and aggregation have proven to be associated with ALS pathogenesis,[13] suggest a possible therapeutic treatment involving protection against mutant SOD1-induced cytotoxicity. We therefore developed an assay using PC12 cells expressing G93A SOD1[14] and carried out a high-throughput screen to identify compounds that protected these cells from protein aggregation and toxicity.[15] One of the hit scaffolds was the arylsulfanylpyrazolones (ASPs), which exhibited good in vitro potency but was rapidly metabolized.[16] The metabolic hot spot was identified as the sulfur atom, which was readily oxidized. Conversion to the corresponding ether led to much more stable compounds, and one analogue extended the life of G93A ALS mice by 13.3% at 20 mg/kg.[17] A SAR study characterized the important parts of this class of compounds.[18] In a search of more potent and metabolically stable compounds, which also would allow diverse substitutions to carry out target identification studies, we synthesized the corresponding arylazanylpyrazolones (AAPs). These compounds are the focus of this paper (Figure 1).

RESULTS AND DISCUSSION

Chemistry. Two synthetic strategies were utilized to synthesize β-ketoesters, the critical intermediate for the construction of the pyrazolone ring. As shown in Scheme 1,

Received: January 17, 2013
Published: February 27, 2013

dx.doi.org/10.1021/jm400079a | J. Med. Chem. 2013, 56, 2665−2675

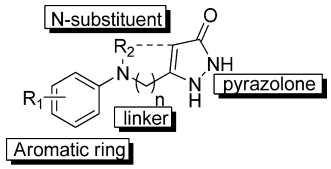

Figure 1. Substructures of AAP analogues.

the upper route started from the reaction of alkylanilines or sulfonylamides with ethyl bromoalkanoate. The ester intermediates reacted with the enolate of ethyl acetate, providing the anilino substituted β-ketoesters in moderate to high yields. The lower single-step route was carried out using an optimized methodology[19] based on the reaction of the aniline with ethyl 4-chloroacetoacetate, resulting in a series of anilino substituted β-ketoester intermediates with varied R and R′ substituents. All of the β-ketoester intermediates were transformed to pyrazolones in high yields with hydrazine.

An alternative synthetic route (Scheme 2) was designed for bulky R groups such as *tert*-butyl, phenyl, and benzyl, which gave low yields of anilino esters in the reaction above. By employment of ethyl diazoacetate, an NH insertion occurred to achieve the anilino esters in good yields,[20] which were used to generate the β-ketoester intermediates by attack of the enolate of ethyl acetate.

The N^1-methylpyrazolone analogue (**30**) was easily obtained by replacing hydrazine with methylhydrazine in the heterocycle formation (Scheme 3). The N^1-methylpyrazolones can be further modified to dimethyl- and trimethyl-substituted pyrazolone analogues (**32**−**34**). Although it has been reported that the condensation between methylhydrazine and a β-ketoester produces a mixture of N^1-alkyl and N^2-alkyl isomers,[21] no N^1-alkyl product was observed with our substrate. With the help of a method developed by Janin and co-workers,[22] our attempts to synthesize the N^2-alkyl product (**31**) were successful, as shown in Scheme 3. The β-ketoester intermediate was initially converted to N^1-2-hydroxylethyl-N^2-tosylpyrazolone derivative **35** in an 85% yield, which was then treated with sodium hydride to give key intermediate **36** containing a 2,3-dihydropyrazolo[3,2-*b*]oxazole ring. Alkylation with MeOTf and dihydrooxazole ring-opening with sodium iodide followed by elimination of hydrogen iodide led to N^1-vinyl-N^2-methylpyrazolone **37** in a 55% yield. Acid hydrolysis gave the desired N^1-methylpyrazolone analogue (**31**).

In Vitro Activity of Secondary and Tertiary AAPs. Compound **1** has an oral bioavailability of 27%, PK half-life of 3.6 h, and maximum tolerated dose of 75 mg/kg, which meet the standard minimal criteria for preclinical advancement.[23] However, some pharmacokinetic properties of **1** need improvement. For example, as indicated by the oral bioavailability,[17] the AUC/dose of **1** showed a distinct difference between iv (184 (ng·h/mL)/dose) and po (50 (ng·h/mL)/dose) administration. Given good aqueous solubility and cell permeability, one of the most likely causes for the difference between these two routes of administration is the first-pass clearance from hepatic and gut metabolism.[24] To increase metabolic stability and further diversify the structure, the ether oxygen was replaced by the isosteric amine functional group.

Two possible amines, secondary and tertiary AAP analogues, were initially screened in the protection assay (Figure 2) and for in vitro microsomal stability (Table 1) and Caco-2 permeability (Table 2). Introduction of the nitrogen led to a potency decrease in the cell-based protection assay; however, the tertiary arylazanyl analogue had a slightly better activity over the secondary arylazanyl analogue. The solubilities of **2** and **3** were good in aqueous media (≥150 μM), and no precipitation occurred at the highest concentration. The in vitro plasma half-life for both compounds was >60 min. Tertiary amine **3** exhibited a remarkable stability enhancement in human liver microsomes compared with the moderate half-lives and clearance rates of the ether and secondary amine analogues. Whereas **1** had excellent permeability and low efflux potential toward Caco-2, neither **2** nor **3** exhibited satisfactory Caco-2 permeability and both had high efflux potential, although **3** was superior to **2**.

These preliminary results suggest that the AAPs may not be an improvement over the aryloxanylpyrazolone series, but the tertiary amine analogue (**3**) showed improved human microsome stability, so a library of tertiary amine analogues was synthesized.

SAR of AAP Analogues. Compound activity was determined using the previously described cytotoxicity protection assay (Table 1, Supporting Information).[15] The variability of the EC_{50} values is about a factor of 2. As shown in Figure 1, the tertiary amine AAP scaffold contains four substructural moieties: aromatic ring, N-substituent, linker, and the pyrazolone. Structural modifications were conducted on each moiety. A variety of substituents in the aryl moiety was investigated using our previous synthetic method for amination of anilines and γ-halogen-β-ketoesters (Figure 3). In general, the potencies of these AAPs were slightly poorer than those of the ether counterparts (**1** vs **3**[25]). Our previous reports on arylsulfanyl-[16] and aryloxanylpyrazolones[17] (AXP) showed that the 3,5-dichloro substitution pattern in the aromatic ring gave greater potency over the other substitution patterns (about 5- to 10-fold enhancement). Here, neither the electronic properties (compounds **4**−**6**) nor the positions of substitution (compounds **9**−**11**) in the aromatic ring exhibited a large activity change, but the size of the substituents affected the activity in the following order: F < CN < OMe < Cl ∼ Br < di-Cl ∼ naphthalene. 2,4-Dichloro- and α-naphthyl substitutions in the aromatic ring moiety were the most effective.

Scheme 1. Synthetic Routes for Arylazanylpyrazolones

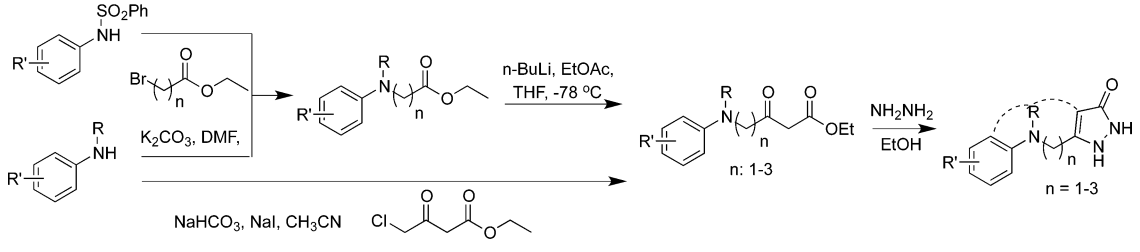

dx.doi.org/10.1021/jm400079a | J. Med. Chem. 2013, 56, 2665−2675

Scheme 2. Synthesis of β-Ketoester Intermediates with Bulky R Groups

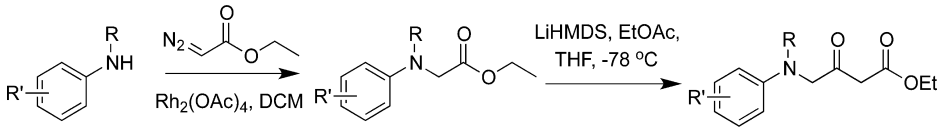

Scheme 3. Synthesis of Analogues Substituted on the Pyrazolone Moiety

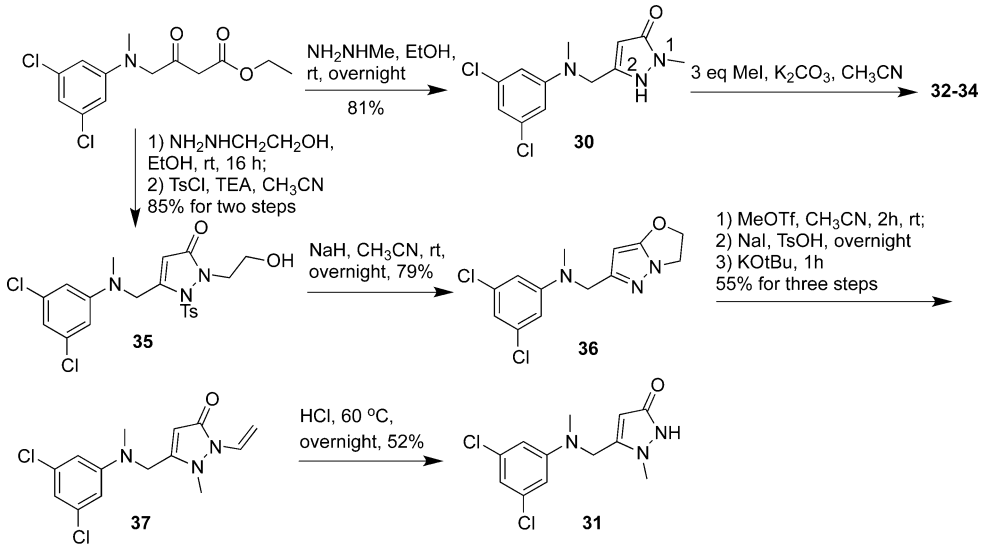

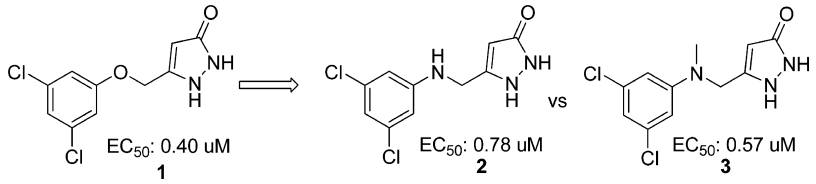

Figure 2. Conversion of ether linker to amine linker.

Table 1. In Vitro Microsomal Stability of 1-3[a]

	NADPH-dependent		NADPH-absent	
compd	CL_{int}[b] (mL min^{-1} kg^{-1})	$T_{1/2}$[c] (min)	CL_{int}[b] (mL min^{-1} kg^{-1})	$T_{1/2}$[c] (min)
		Human		
1	25	93	13	173
2	24	95	0	>180
3	0	>180	0	>180
		Mouse		
1	64	36	21	111
2	78	30	23	100
3	93	25	0	>180

[a]Data were obtained from Apredica. [b]Microsomal intrinsic clearance. [c]Half-life.

Table 2. In Vitro Caco-2 Permeability of 1−3[a]

compd	P_{app}(A→B)[b] (10^{-6} cm/s)	P_{app}(B→A)[b] (10^{-6} cm/s)	efflux ratio (B→A)/(A→B)
1	36.7	14.1	0.4
2	0.6	28.1	47.1
3	2.2	7.6	3.5

[a]Data were obtained from Apredica. [b]Apparent permeability.

With the aromatic ring substituents, linker, and pyrazolone held constant, a series of N-substituted AAPs was synthesized (Figure 4; these compounds were being synthesized prior to the measurements in Figure 3, so 3,5-dichloro was selected for aryl substitution). Although the range of potency changed by less than 4-fold, the ethyl analogue was the most potent and the potency decreased with an increase of the size of substituents in the following order: Et > *c*-Pr > *i*-Pr ∼ Bn > propargyl > *t*-Bu ∼ Ph; however, the smaller methyl analogue was comparable in potency to the cyclopropyl analogue. The propargyl analogue will be beneficial to our ongoing target identification studies, providing a terminal triple bond for reporter group attachment via click chemistry.[26]

An investigation of the linker between the aryl moiety and the pyrazolone also was carried out to determine the influence of length and shape. As shown in Figure 5, one carbon is the optimal length between the nitrogen and the pyrazolone moiety; longer linkers reduce the activity.

One useful modification to enhance the pharmacokinetic properties is a ring−chain transformation.[27] Four ring linkers were introduced to the AAP scaffold (**25**−**28**). The connection between the aryl group and the N-substituent (**25** and **26**) favored **26**. The linker between the N-substituent and the pyrazolone ring (**27** and **28**) has a preference for that described by **28**. The latter two compounds reveal that substitution at the 5-position of the pyrazolone does not affect potency.

Selected compounds were tested with cortical neurons, which is critical prior to the expensive and time-consuming ALS

dx.doi.org/10.1021/jm400079a | J. Med. Chem. 2013, 56, 2665−2675

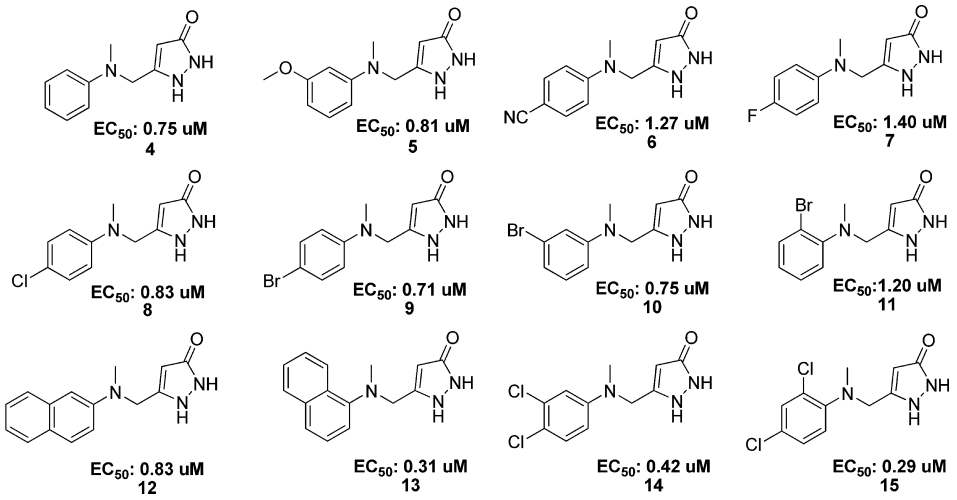

Figure 3. AAP analogues with different substituents in the aromatic moiety.

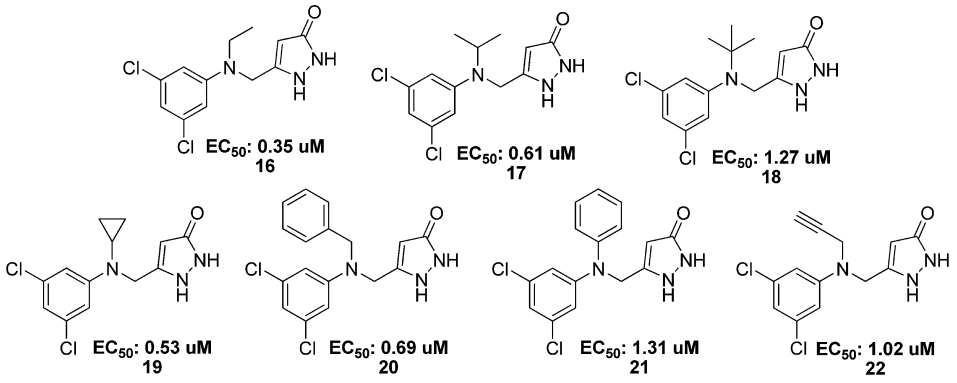

Figure 4. AAP analogues with different N-substituents.

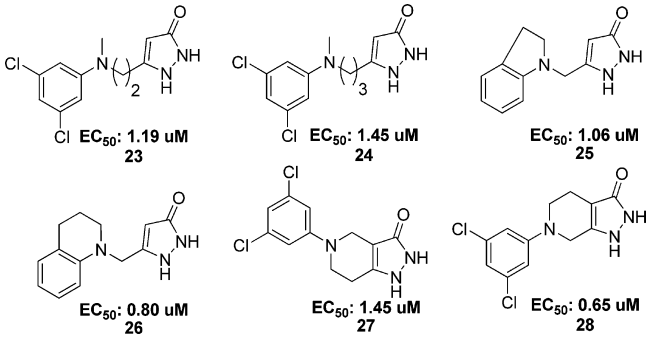

Figure 5. AAP analogues with different linkers.

mouse model studies.[28] Although long linker compound **24** and cyclic linker compound **27** are active in the PC12 assay, they are not active with cortical neurons. Compound **3** gave better results than the ether counterpart (**1**), recovering 100% neuronal activity at 10 μM (Supporting Information).

Pharmacophoric Nature of the Pyrazolone Ring. According to our previous studies, the pyrazolone ring is the key functional group for activity in all of the AXP scaffolds. The compounds without a pyrazolone or with *N,N′*-dimethyl substituted pyrazolone in the aryloxanyl series had no activity.[17] Given that there are three potential H-bonding donors/acceptors in the pyrazolone ring, a determination of their pharmacophoric nature is important. In our recent paper,[18] a putative explanation for the pyrazolone activity was the availability of the N^2-hydrogen (**3a**-type, Figure 7) for hydrogen bonding. To determine if the same moiety was essential for the AAP class of compounds, single N^2-nitrogen substituted pyrazolone analogue **31** and other substituted pyrazolone analogues were synthesized (Scheme 3). As shown in Figure 6, **29** and **30** were comparable in activity to parent

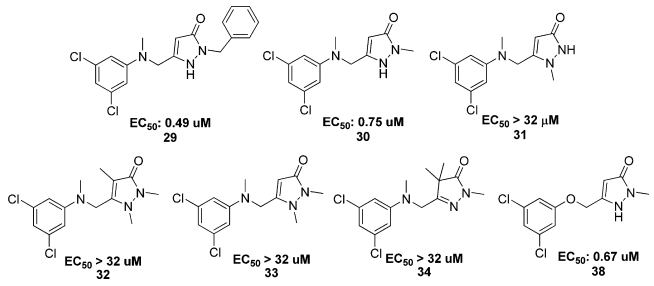

Figure 6. AAP analogues with different pyrazolone substitutions.

compound **3**, while compounds **31**–**34**, all of which do not have a N^2-H, were devoid of activity, demonstrating the significance of the N^2-H for activity in this series as well.

Several spectrometric analyses were carried out to determine if the pyrazolone structure shown in Figure 7 is the most prevalent. Because of a rapid equilibrium among the pyrazolone tautomers, the ^{13}C NMR spectrum of **3** gave a carbon signal with obscure bumps in the region of the pyrazolone and methylene group. However, clear ^{13}C NMR spectra of those

dx.doi.org/10.1021/jm400079a | J. Med. Chem. 2013, 56, 2665−2675

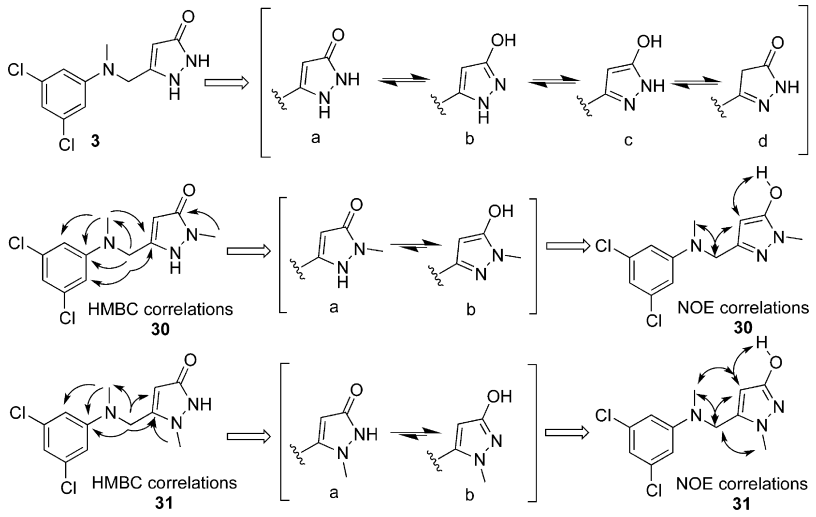

Figure 7. Tautomerism, HMBC, and NOE spectral results of compounds **3**, **30**, and **31**.

carbons in **30** and **31** suggested a predominant tautomer. HSQC, HMBC, and NOE spectra of **30** and **31** were then collected. The HSQC spectrum permitted the assignment of all of the protons with their bonding carbons. Analysis of the HMBC spectrum enabled the connectivity of the phenyl, the linker, and the pyrazolone moieties. The cross peaks between the phenol hydrogen and the 4-hydrogen of the pyrazolone in the NOE spectrum determined the spatial approach of these two neighboring hydrogens, which supported the predominant tautomer in **30** and **31** as the phenol form (**30b** and **31b**, Figure 7).

In an attempt to rationalize these observations, comprehensive theoretical calculations were performed on the four possible tautomers of **3** using density-functional theory (DFT); the predicted energy order was **3d** < **3b** < **3c** < **3a** in the gas phase (Table 3). The largest energy difference among

Table 3. Calculated Energies of the Tautomers of 3

tautomer	energy (au)	ΔE (kJ/mol)
3a	−1585.125 802	22.60
3b	−1585.129 852	11.97
3c	−1585.128 450	15.64
3d	−1585.134 409	0

all of the forms is 22.6 kJ/mol, which is an insufficient energy barrier to detect a preferred tautomeric form. Since the tautomerization of pyrazolone was first discovered by Knorr in 1895,[29] several reported calculations have predicted a similar prediction for the stability of the pyrazolone tautomers,[30] and calculations of similar structures predicted that the phenol forms are favored for 1- or 2-substituted pyrazolones in aprotic solvents,[20,31] as we observed.

To further characterize the predominant tautomeric form of the pyrazolone heterocycles in **30** and **31**, we performed quantum chemical calculations (Figure 8). The predominant conformation can be identified by comparing the experimental IR spectra with the predicted IR spectra of the different tautomers. All of the predicted spectra of keto tautomers have a similar high frequency at ∼1730 cm^{-1}, while the spectra of phenol-type tautomers have no absorption band in the same region. Hence, the frequency at ∼1730 cm^{-1}, the stretching vibration of the C═O bond, is an important band to differentiate these two tautomers. The experimental IR spectra do not contain a band at 1730 cm^{-1}. Furthermore, the most highly predictive bands for phenol forms are in good agreement with the experimental data. All of these results indicate that phenol forms of **30** and **31** are the more stable tautomers. Similar NOE and IR spectral observations for ether analogue **38**[32] suggest that the active pyrazolone tautomer in the AOP series also is the phenol form (see Supporting Information and Figure 8C).

On the basis of the above results, we conclude that the pyrazolone phenol-type tautomer is predominant in solution and in solid phase, but given that the target(s) is unknown, we cannot conclude definitively whether this tautomer is the pharmacophoric core responsible for the activity of all AAP and AOP analogues. If that tautomer is the active tautomer, then biological activity requires the following two criteria: (1) N^2 has unsubstituted sp^2 hybridization rather than sp^3 hybridization; (2) there is a phenol hydrogen, presumably as a H-bonding donor. The loss of activity by di- and trimethyl substituted derivatives also supports the hypothesis that both criteria must be met for activity.

CONCLUSION

Aryloxanyl analogues were previously identified as potential drug candidates exhibiting good potency, ADME properties, and equivalent or slightly better results with the ALS mouse model as did the FDA-approved drug riluzole. However, because of its structural limitations, the aryloxanyl analogues may not be suitable as a chemical probe for a biological target study and need further optimization to improve in vivo activity.

The AAP analogues showed superior properties relative to the corresponding ether derivative in potential structural diversity and in preliminary metabolic studies. Conclusions from the SAR study are as follows: (1) the size of the aryl moiety, rather than the electronic properties, is important for good potency; (2) potency decreases when the size of the N-substituents increase; as a potential chemical reporter, the alkynyl group is well tolerated; (3) one carbon is the optimum length for the linker; the linker can be linear or cyclic; (4) the pyrazolone moiety is the only critical pharmacophore of this structure for activity, which prefers the phenol-type tautomer in solution and solid phase, although it is not known if it binds to any targets in that form; (5) a comparison of the predicted and

dx.doi.org/10.1021/jm400079a | J. Med. Chem. 2013, 56, 2665−2675

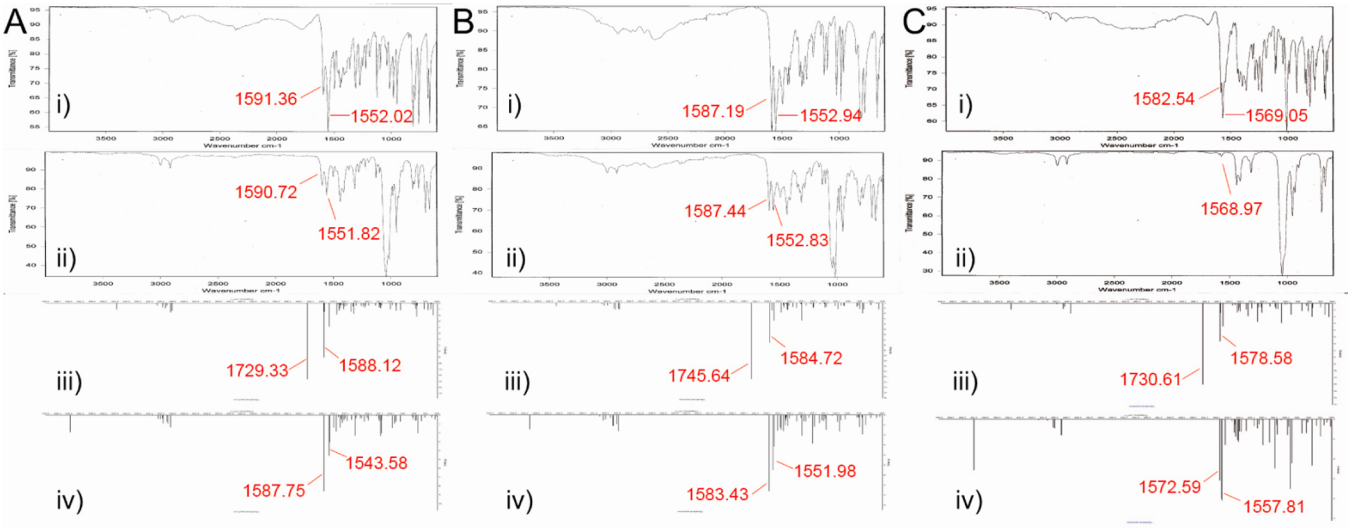

Figure 8. Experimental and calculated IR spectral comparison: (A) compound **30**; (B) compound **31**; (C) compound **38**; (i) experimental IR recorded in the solid phase; (ii) experimental IR recorded in DMSO solution; (iii) calculated IR of ketone-type tautomer (**30a**-like); (iv) calculated IR of phenol-type tautomer (**30b**-like). The stretching vibrations of the C═O bond (~1730 cm^{-1}) and skeletal vibrations of the aromatic rings (1600−1550 cm^{-1}) are given in red.

experimental IR spectra is useful to identify the predominant tautomer of a heterocyclic system.

These results support further development of AAP analogues as a reagent for target identification and as a novel drug candidate for the treatment of ALS.

EXPERIMENTAL SECTION

General Experimental Methods. All reactions were carried out with magnetic stirring and were monitored by thin-layer chromatography on precoated silica gel 60 F254 plates. Column chromatography was performed with silica gel 60 (230−400 mesh). Proton and carbon NMR spectra were recorded in deuterated solvents on a Bruker Ag500 (500 MHz) spectrometer. The chemical shifts were reported in δ (ppm) (^{1}H NMR: $CDCl_3$, δ 7.26 ppm; DMSO-d_6, δ 2.50 ppm. ^{13}C NMR: δ 77.23 ppm; DMSO-d_6, δ 39.52 ppm). The following abbreviations were used to define the multiplicities: s = singlet, d = doublet, t = triplet, q = quartet, p = pentet, m = multiplet. Electrospray mass spectra were obtained using an Agilent 1100 MSD instrument with methanol as the solvent in the positive ion mode. IR was recorded on a Bruker TENSOR FT-IR spectrometer. Elemental microanalysis was performed by Atlantic Microlab Inc. (Norcross, GA). The C, H, and N analyses were performed by combustion using automatic analyzers, and all of the compounds analyzed showed >95% purity. All reagents purchased from Aldrich, Alfa Aesar, and TCI were used without further purification unless stated otherwise.

General Procedure A for Nucleophilic Amination of Anilines and Bromoacetates. To a solution of K_2CO_3 (200 mol %) and the aniline (1.0 equiv) in DMF (2 mL/mmol) was added ethyl bromoacetate (150 mol %). The reaction mixture was stirred at room temperature or 80 °C for 16 h. The reaction solution was diluted with ethyl acetate, washed twice with water to remove the reaction solvent, and washed with brine. The collected organic layers were combined, dried over Na_2SO_4, filtered, and concentrated. The crude product was purified on a silica gel column, eluting with a mixture of ethyl acetate and hexane (5−20% ethyl acetate) to afford the product as a colorless to pale yellow oil in a yield of 30−80%.

General Procedure B for Carbene Insertion of Anilines. To a solution of the aniline (1.0 equiv) and $Rh_2(OAc)_4$ (2 mol %) in anhydrous dichloromethane (1 mL/mmol) was added ethyl diazoacetate dropwise. Caution: Much N_2 is released! The reaction mixture was stirred at room temperature for 1 h. After evaporation of the volatiles, the reaction residue was purified on a silica gel column, eluting with a mixture of ethyl acetate and hexane (5−20% ethyl acetate) to afford the product as a colorless to pale yellow oil in a yield of 50−95%.

General Procedure C for the Synthesis of β-Ketoesters from Aminoacetates. Ethyl acetate (110 mol %) was added to a THF (5 mL/mmol) solution of LiHMDS (1 N in THF, 120 mol %) at −78 °C and stirred for 60 min. A THF (1 mL/mmol) solution of β-aminoacetate (1.0 equiv) was added dropwise to the reaction mixture at −78 °C. After the resulting solution was stirred at −78 °C for another 2 h, the reaction mixture was quenched with saturated NH_4Cl. The aqueous layer was extracted with ethyl acetate and washed twice with water and brine. The collected organic layers were combined, dried over Na_2SO_4, filtered, and concentrated. The crude product was purified on a silica gel column, eluting with a mixture of ethyl acetate and hexane (10−30% ethyl acetate) to afford the product as a colorless to pale yellow oil in a yield of 40−80%.

General Procedure D for Direct Amination of γ-Halo-β-ketoesters with Anilines. To a solution of $NaHCO_3$ (200 mol %), NaI (200 mol %), and the aniline (1 equiv) in acetonitrile (1 mL/mol) was added ethyl α-chloracetoacetate (200 mol %). The resulting reaction mixture was stirred at room temperature or at 80 °C for 1−16 h. After the mixture was cooled to room temperature, saturated $Na_2S_2O_3$ solution (1 mL/mol) was added. The resulting solution was extracted with ethyl acetate, and the organic layer was collected, which was then washed with water and brine. The collected organic layers were combined, dried over Na_2SO_4, filtered, and concentrated. The residue was subjected to column chromatography, eluting with a mixture of hexane and ethyl acetate (10−30% ethyl acetate) to afford the product as a pale yellow oil in a yield specified in the our published method of amination.[19]

General Procedure E for the Synthesis of Pyrazolones from β-Ketoesters. To a solution of β-ketoesters (1 equiv) in EtOH (5 mL/mmol) was added anhydrous hydrazine (200 mol %). The resulting solution was stirred at room temperature overnight. After evaporation of the volatiles, the reaction residue was purified on a silica gel column, eluting with a mixture of MeOH and dichloromethane (2−10% MeOH) to afford the product as a colorless to pale pink solid. The solid was then recrystallized in dichloromethane/hexane to give the pure product as a white solid in a yield of 60−75%.

5-((3,5-Dichlorophenylamino)methyl)-1*H*-pyrazol-3(2*H*)-one (2). Following general procedures A, C, and E provided the phenylsulfonyl protected *N*-(3,5-dichlorophenyl)-*N*-((5-oxo-2,5-dihydro-1*H*-pyrazol-3-yl)methyl)benzenesulfonamide. ^{1}H NMR (DMSO-d_6, 500 MHz): δ = 11.56 (br s, 1H), 9.45 (br s, 1H), 7.78−7.74 (m, 1H), 7.64−7.63 (m, 4H), 7.56 (s, 1H), 7.14 (d, J = 1.5 Hz, 2H), 5.21

dx.doi.org/10.1021/jm400079a | J. Med. Chem. 2013, 56, 2665−2675

(s, 1H), 4.67 (s, 2H). ^{13}C NMR (DMSO-d_6, 125 MHz): δ = 140.8, 136.6, 133.8 × 2, 133.7 × 2, 129.6 × 2, 127.6 × 2, 127.5, 127.0 ppm. MS (ESI): m/z 398.0 $[M + H]^+$.

N-(3,5-Dichlorophenyl)-*N*-((5-oxo-2,5-dihydro-1*H*-pyrazol-3-yl)-methyl)benzenesulfonamide (398 mg, 1 mmol) and 4-hydroxybenzoic acid (800 mg, 5.8 mmol, 200% weight) were added to a solution of HBr (48% in H_2O, 4 mL) and AcOH (4 mL). After the resulting suspension was stirred at 100 °C for 2 h, the reaction mixture was partitioned between 1 N HCl (10 mL) and ethyl acetate (30 mL × 2). The collected organic layers were combined, dried over Na_2SO_4, filtered, and concentrated. The residue was subjected to column chromatography, eluting with a mixture of MeOH and dichloromethane (5% MeOH) to afford **2** (142 mg, 55% yield) as a white solid. ^{1}H NMR (DMSO-d_6, 500 MHz): δ = 6.65 (t, J = 5.5 Hz, 1H), 6.61 (s, 1H), 6.59, (s, 2H), 5.35 (s, 1H), 4.10 (d, J = 5.0 Hz, 2H). ^{13}C NMR (DMSO-d_6, 125 MHz): δ = 150.7, 134.3 × 2, 114.6, 110.4 × 2 ppm. MS (ESI): m/z 280.0 $[M + Na]^+$. CHN calculated for $C_{10}H_9Cl_2N_3O$: C, 46.53; H, 3.51; N, 16.28. Found: C, 46.44; H, 3.61; N, 16.36.

5-(((3,5-Dichlorophenyl)(methyl)amino)methyl)-1*H*-pyrazol-3(2*H*)-one (3). The title compound was prepared according to general procedures D and E. ^{1}H NMR (DMSO-d_6, 500 MHz): δ = 9.93 (br s, 1H), 6.72 (m, 3H), 5.24 (s, 1H), 4.40 (s, 2H), 2.96 (s, 3H). ^{13}C NMR (DMSO-d_6, 125 MHz): δ = 150.8, 134.6 × 2, 114.8, 110.7 × 2, 88.1, 47.9, 38.6 ppm. MS (ESI): m/z 272.0 $[M + H]^+$. CHN calculated for $C_{11}H_{11}Cl_2N_3O$: C, 48.55; H, 4.07; N, 15.44. Found: C, 48.80; H, 4.13; N, 15.35.

5-((Methyl(phenyl)amino)methyl)-1*H*-pyrazol-3(2*H*)-one (4). The title compound was prepared according to general procedures D and E. ^{1}H NMR (DMSO-d_6, 500 MHz): δ = 7.15 (dt, J = 2.0, 7.5 Hz, 2H), 6.76 (d, J = 8.0 Hz, 2H), 6.63 (t, J = 7.5 Hz, 1H), 5.21 (s, 1H), 4.36 (s, 2H), 2.90 (s, 3H). ^{13}C NMR (DMSO-d_6, 125 MHz): δ = 149.0, 128.9 × 2, 116.3, 112.7, 88.4, 47.7, 38.3 ppm. MS (ESI): m/z 204.0 $[M + H]^+$. CHN calculated for $C_{11}H_{13}N_3O$: C, 65.01; H, 6.45; N, 20.68. Found: C, 64.98; H, 6.34; N, 20.68.

5-(((3-Methoxyphenyl)(methyl)amino)methyl)-1*H*-pyrazol-3(2*H*)-one (5). The title compound was prepared according to general procedures D and E. ^{1}H NMR (DMSO-d_6, 500 MHz): δ = 11.47 (br s, 1H), 9.36 (br s, 1H), 7.04 (t, J = 8.0 Hz, 1H), 6.35 (dd, J = 2.0, 7.5 Hz, 1H), 6.26–6.21 (m, 2H), 5.21 (s, 1H), 4.33 (s, 2H), 3.68 (s, 3H), 2.89 (s, 3H). ^{13}C NMR (DMSO-d_6, 125 MHz): δ = 160.2, 150.3, 129.6, 105.7, 101.6, 99.0, 88.8, 54.8, 38.4 ppm. MS (ESI): m/z 234.1 $[M + H]^+$. CHN calculated for $C_{12}H_{15}N_3O_2$: C, 61.79; H, 6.48; N, 18.01. Found: C, 61.77; H, 6.47; N, 18.09.

4-(Methyl((5-oxo-2,5-dihydro-1*H*-pyrazol-3-yl)methyl)-amino)benzonitrile (6). The title compound was prepared according to general procedures D and E. ^{1}H NMR (DMSO-d_6, 500 MHz): δ = 7.53 (d, J = 8.0 Hz, 2H), 6.82 (d, J = 8.0 Hz, 2H), 5.25 (s, 1H), 4.47 (s, 2H), 3.04 (s, 3H). ^{13}C NMR (DMSO-d_6, 125 MHz): δ = 151.6, 133.2 × 2, 120.4, 112.2 × 2, 38.4 ppm. MS (ESI): m/z 251.1 $[M + Na]^+$. CHN calculated for $C_{12}H_{12}N_4O$: C, 63.15; H, 5.30; N, 24.55. Found: C, 62.87; H, 5.35; N, 24.34.

5-(((4-Fluorophenyl)(methyl)amino)methyl)-1*H*-pyrazol-3(2*H*)-one (7). The title compound was prepared according to general procedures D and E. ^{1}H NMR (DMSO-d_6, 500 MHz): δ = 11.47 (br s, 1H), 9.34 (br s, 1H), 7.00 (t, J = 4.0 Hz, 2H), 6.75 (ddd, J = 2.5, 4.5, 11.0 Hz, 2H), 5.21 (s, 1H), 4.32 (s, 2H), 2.86 (s, 3H). ^{13}C NMR (DMSO-d_6, 125 MHz): δ = 160.3, 155.6, 153.8, 145.9, 141.5, 115.3, 115.1, 114.1, 114.0, 88.2, 48.5, 38.7 ppm. MS (ESI): m/z 222.1 $[M + H]^+$. CHN calculated for $C_{11}H_{12}FN_3O$: C, 59.72; H, 5.47; N, 18.99. Found: C, 59.53; H, 5.56; N, 18.96.

5-(((4-Chlorophenyl)(methyl)amino)methyl)-1*H*-pyrazol-3(2*H*)-one (8). The title compound was prepared according to general procedures D and E. ^{1}H NMR (DMSO-d_6, 500 MHz): δ = 7.16 (t, J = 8.5 Hz, 2H), 6.75 (d, J = 8.5 Hz, 2H), 5.20 (s, 1H), 4.36 (s, 2H), 2.90 (s, 3H). ^{13}C NMR (DMSO-d_6, 125 MHz): δ = 147.8, 128.5 × 2, 119.9, 114.1 × 2, 88.3, 47.9, 38.5 ppm. MS (ESI): m/z 238.1 $[M + H]^+$. CHN calculated for $C_{11}H_{12}ClN_3O$: C, 55.59; H, 5.09; N, 17.68. Found: C, 55.55; H, 5.17; N, 17.58.

5-(((4-Bromophenyl)(methyl)amino)methyl)-1*H*-pyrazol-3(2*H*)-one (9). The title compound was prepared according to general procedures D and E. ^{1}H NMR (DMSO-d_6, 500 MHz): δ = 7.27 (d, J = 7.5 Hz, 2H), 6.70 (d, J = 7.5 Hz, 2H), 5.21 (s, 1H), 4.36 (s, 2H), 2.90 (s, 3H). ^{13}C NMR (DMSO-d_6, 125 MHz): δ = 148.1, 131.3 × 2, 114.7 × 2, 107.4, 88.1, 47.9, 38.4 ppm. MS (ESI): m/z 282.0 $[M + H]^+$. CHN calculated for $C_{11}H_{12}BrN_3O$: C, 46.83; H, 4.29; N, 14.89. Found: C, 46.93; H, 4.30; N, 14.87.

5-(((3-Bromophenyl)(methyl)amino)methyl)-1*H*-pyrazol-3(2*H*)-one (10). The title compound was prepared according to general procedures D and E. ^{1}H NMR (DMSO-d_6, 500 MHz): δ = 11.50 (br s, 1H), 9.45 (br s, 1H), 7.08 (t, J = 8.0 Hz, 1H), 6.86 (s, 1H), 6.75 (dt, J = 2.5, 8.0 Hz, 2H), 5.22 (s, 1H), 4.37 (s, 2H), 2.92 (s, 3H). ^{13}C NMR (DMSO-d_6, 125 MHz): δ = 150.3, 130.6, 122.6, 118.5, 114.6, 111.5, 38.4 ppm. MS (ESI): m/z 282.0 $[M + H]^+$. CHN calculated for $C_{11}H_{12}BrN_3O$: C, 46.83; H, 4.29; N, 14.89. Found: C, 46.92; H, 4.36; N, 14.87.

5-(((3-Bromophenyl)(methyl)amino)methyl)-1*H*-pyrazol-3(2*H*)-one (11). The title compound was prepared according to general procedures D and E. ^{1}H NMR (DMSO-d_6, 500 MHz): δ = 7.58 (dd, J = 1.0, 8.0 Hz, 1H), 7.30 (dt, J = 1.0, 8.0 Hz, 1H), 7.13 (dd, J = 1.0, 8.0 Hz, 1H), 6.97 (dt, J = 1.0, 8.0 Hz, 1H), 5.24 (s, 1H), 4.02 (s, 2H), 2.62 (s, 3H). ^{13}C NMR (DMSO-d_6, 125 MHz): δ = 150.0, 133.5, 128.4, 124.6, 122.6, 119.2, 39.0 ppm. MS (ESI): m/z 282.0 $[M + H]^+$. CHN calculated for $C_{11}H_{12}BrN_3O$: C, 46.83; H, 4.29; N, 14.89. Found: C, 46.86; H, 4.31; N, 14.88.

5-((Methyl(naphthalen-2-yl)amino)methyl)-1*H*-pyrazol-3(2*H*)-one (12). The title compound was prepared according to general procedures D and E. ^{1}H NMR (DMSO-d_6, 500 MHz): δ = 7.70 (t, J = 9.0 Hz, 2H), 7.64 (d, J = 8.5 Hz, 1H), 7.34–7.28 (m, 2H), 7.16 (dt, J = 1.0, 8.0 Hz, 1H), 6.97 (d, J = 2.0 Hz, 1H), 5.21 (s, 1H), 4.49 (s, 2H), 3.00 (s, 3H). ^{13}C NMR (DMSO-d_6, 125 MHz): δ = 147.0, 134.6, 128.4, 127.2, 126.4, 126.1, 126.0, 121.9, 116.7, 38.5 ppm. MS (ESI): m/z 254.1 $[M + H]^+$. CHN calculated for $C_{15}H_{15}N_3O$: C, 71.13; H, 5.97; N, 16.59. Found: C, 70.94; H, 6.02; N, 16.54.

5-((Methyl(naphthalen-1-yl)amino)methyl)-1*H*-pyrazol-3(2*H*)-one (13). The title compound was prepared according to general procedures D and E. ^{1}H NMR (DMSO-d_6, 500 MHz): δ = 8.27 (d, J = 8.0 Hz, 1H), 7.90 (dt, J = 1.5, 7.5 Hz, 1H), 7.59 (d, J = 8.0 Hz, 1H), 7.53–7.49 (m, 2H), 7.41 (t, J = 8.0 Hz, 1H), 7.14 (d, J = 7.0 Hz, 1H), 5.31 (s, 1H), 4.08 (s, 2H), 2.73 (s, 3H). ^{13}C NMR (DMSO-d_6, 125 MHz): δ = 149.0, 134.4, 128.5, 128.3, 125.9, 125.8, 125.4, 123.6, 123.1, 115.7, 39.0 ppm. MS (ESI): m/z 254.1 $[M + H]^+$. CHN calculated for $C_{15}H_{15}N_3O$: C, 71.13; H, 5.97; N, 16.59. Found: C, 71.29; H, 6.01; N, 16.51.

5-(((3,4-Dichlorophenyl)(methyl)amino)methyl)-1*H*-pyrazol-3(2*H*)-one (14). The title compound was prepared according to general procedures D and E. ^{1}H NMR (DMSO-d_6, 500 MHz): δ = 7.32 (d, J = 9.0 Hz, 1H), 6.91 (d, J = 3.0 Hz, 1H), 6.74 (dd, J = 3.0, 9.0 Hz, 1H), 5.22 (s, 1H), 4.39 (s, 2H), 2.94 (s, 3H). ^{13}C NMR (DMSO-d_6, 125 MHz): δ = 148.8, 131.3, 130.3, 117.3, 113.5, 112.9, 38.5 ppm. MS (ESI): m/z 272.0 $[M + H]^+$. CHN calculated for $C_{11}H_{11}Cl_2N_3O$: C, 48.55; H, 4.07; N, 15.44. Found: C, 48.55; H, 4.04; N, 15.46.

5-(((2,4-Dichlorophenyl)(methyl)amino)methyl)-1*H*-pyrazol-3(2*H*)-one (15). The title compound was prepared according to general procedures D and E. ^{1}H NMR (DMSO-d_6, 500 MHz): δ = 7.53 (d, J = 2.0 Hz, 1H), 7.31 (dd, J = 2.0, 8.5 Hz, 1H), 7.09 (d, J = 8.5 Hz, 1H), 5.20 (s, 1H), 4.05 (s, 2H), 2.64 (s, 3H). ^{13}C NMR (DMSO-d_6, 125 MHz): δ = 147.6, 129.7, 128.5, 127.6, 126.7, 123.3, 39.0 ppm. MS (ESI): m/z 272.0 $[M + H]^+$. CHN calculated for $C_{11}H_{11}Cl_2N_3O$: C, 48.55; H, 4.07; N, 15.44. Found: C, 48.33; H, 4.18; N, 15.21.

5-(((3,5-Dichlorophenyl)(ethyl)amino)methyl)-1*H*-pyrazol-3(2*H*)-one (16). The title compound was prepared according to general procedures D and E. ^{1}H NMR (DMSO-d_6, 500 MHz): δ = 6.67 (m, 3H), 5.26 (s, 1H), 4.34 (s, 2H), 3.42 (d, J = 7.0 Hz, 2H), 1.06 (t, J = 7.0 Hz, 3H). ^{13}C NMR (DMSO-d_6, 125 MHz): δ = 149.6, 134.6 × 2, 114.3, 110.2 × 2, 44.8, 11.8 ppm. MS (ESI): m/z 286.0 $[M + H]^+$. CHN calculated for $C_{12}H_{13}Cl_2N_3O$: C, 50.37; H, 4.58; N, 14.68. Found: C, 50.54; H, 4.58; N, 14.68.

5-(((3,5-Dichlorophenyl)(isopropyl)amino)methyl)-1*H*-pyrazol-3(2*H*)-one (17). The title compound was prepared according to general procedures B, C, and E. ^{1}H NMR (DMSO-d_6, 500 MHz): δ = 7.25–7.21 (m, 3H), 5.11 (s, 1H), 4.17 (s, 2H), 1.12 (m, 9H). ^{13}C

NMR (DMSO-d_6, 125 MHz): δ = 150.5, 134.5 × 2, 114.6, 110.9 × 2, 48.1, 19.5 × 2 ppm. MS (ESI): m/z 300.1 $[M + H]^+$. CHN calculated for $C_{13}H_{15}Cl_2N_3O$: C, 52.01; H, 5.04; N, 14.00. Found: C, 52.10; H, 5.19; N, 13.87.

5-((*tert*-Butyl(3,5-dichlorophenyl)amino)methyl)-1*H*-pyrazol-3(2*H*)-one (18). The title compound was prepared according to general procedures B, C, and E. ^{1}H NMR (DMSO-d_6, 500 MHz): δ = 6.68−6.67 (m, 3H), 5.22 (s, 1H), 4.25 (s, 2H), 4.17−4.15 (m, 1H), 1.13 (d, J = 7.0 Hz, 6H). ^{13}C NMR (DMSO-d_6, 125 MHz): δ = 151.4, 133.0 × 2, 127.4, 123.9, 55.7, 17.8 × 3 ppm. MS (ESI): m/z 314.1 $[M + H]^+$. CHN calculated for $C_{14}H_{17}Cl_2N_3O$: C, 53.52; H, 5.45; N, 13.37. Found: C, 53.45; H, 5.45; N, 13.40.

5-((Cyclopropyl(3,5-dichlorophenyl)amino)methyl)-1*H*-pyrazol-3(2*H*)-one (19). The title compound was prepared according to general procedures B, C, and E. ^{1}H NMR (DMSO-d_6, 500 MHz): δ = 9.42 (br s, 1H), 6.86 (s, 2H), 6.74 (s, 1H), 5.10 (s, 1H), 4.37 (s, 2H), 2.43 (s, 1H), 0.83−0.82 (m, 2H), 0.55 (s, 2H). ^{13}C NMR (DMSO-d_6, 125 MHz): δ = 151.3, 134.2 × 2, 116.1, 112.3 × 2, 88.4, 46.7, 32.2, 9.1 × 2 ppm. MS (ESI): m/z 298.0 $[M + H]^+$. CHN calculated for $C_{13}H_{13}Cl_2N_3O$: C, 52.37; H, 4.39; N, 14.09. Found: C, 52.33; H, 4.37; N, 14.89.

5-((Benzyl(3,5-dichlorophenyl)amino)methyl)-1*H*-pyrazol-3(2*H*)-one (20). The title compound was prepared according to general procedures B, C, and E. ^{1}H NMR (DMSO-d_6, 500 MHz): δ = 7.34 (t, J = 7.5 Hz, 2H), 7.25 (t, J = 7.5 Hz, 1H), 7.21 (d, J = 7.5 Hz, 2H), 6.70 (s, 1H), 6.68 (s, 2H), 5.32 (s, 1H), 4.66 (s, 2H), 4.52 (s, 2H). ^{13}C NMR (DMSO-d_6, 125 MHz): δ = 150.0, 137.8, 134.4 × 2, 128.6 × 2, 127.0, 126.4 × 2, 115.0, 110.8 × 2, 53.8 ppm. MS (ESI): m/z 298.0 $[M + H]^+$. CHN calculated for $C_{17}H_{15}Cl_2N_3O$: C, 58.63; H, 4.34; N, 12.07. Found: C, 59.01; H, 4.63; N, 11.83.

5-(((3,5-Dichlorophenyl)(phenyl)amino)methyl)-1*H*-pyrazol-3(2*H*)-one (21). The title compound was prepared according to general procedures B, C,[33] and E. ^{1}H NMR (DMSO-d_6, 500 MHz): δ = 11.59 (br s, 1H), 9.65 (br s, 1H), 7.43 (t, J = 7.0 Hz, 2H), 7.28−7.22 (m, 3H), 6.88 (s, 1H), 6.72 (s, 2H), 5.24 (s, 1H), 4.77 (s, 2H). ^{13}C NMR (DMSO-d_6, 125 MHz): δ = 150.0, 145.6, 134.4 × 2, 130.0 × 2, 125.8 × 2, 125.6, 117.2, 113.8 × 2 ppm. MS (ESI): m/z 334.0 $[M + H]^+$. CHN calculated for $C_{16}H_{13}Cl_2N_3O$: C, 57.50; H, 3.92; N, 12.57. Found: C, 57.70; H, 4.27; N, 12.94.

5-(((3,5-Dichlorophenyl)(prop-2-ynyl)amino)methyl)-1*H*-pyrazol-3(2*H*)-one (22). The title compound was prepared according to general procedures B, C, and E. ^{1}H NMR (DMSO-d_6, 500 MHz): δ = 6.82 (s, 3H), 5.35 (s, 1H), 4.41 (s, 2H), 4.21 (d, J = 2.0 Hz, 2H), 3.26 (d, J = 2.0 Hz, 1H). ^{13}C NMR (DMSO-d_6, 125 MHz): δ = 149.4, 134.4 × 2, 116.1, 111.8 × 2, 89.1, 79.6, 75.2 ppm. MS (ESI): m/z 296.1 $[M + H]^+$. CHN calculated for $C_{13}H_{11}Cl_2N_3O$: C, 52.72; H, 3.74; N, 14.19. Found: C, 52.63; H, 3.91; N, 13.92.

5-(2-((3,5-Dichlorophenyl)(methyl)amino)ethyl)-1*H*-pyrazol-3(2*H*)-one (23). The title compound was prepared according to general procedures A, C, and E. ^{1}H NMR (DMSO-d_6, 500 MHz): δ = 11.35 (br s, 1H), 9.41 (br s, 1H), 6.69 (d, J = 1.5 Hz, 1H), 6.66 (d, J = 2.0 Hz, 2H), 5.33 (s, 1H), 3.54 (t, J = 7.5 Hz, 2H), 2.85 (s, 3H), 2.64 (t, J = 7.5 Hz, 2H). ^{13}C NMR (DMSO-d_6, 125 MHz): δ = 150.4, 134.7 × 2, 114.3, 110.0 × 2, 88.7, 51.1, 37.9 ppm. MS (ESI): m/z 286.0 $[M + H]^+$. CHN calculated for $C_{12}H_{13}Cl_2N_3O$: C, 50.37; H, 4.58; N, 14.68. Found: C, 50.66; H, 4.80; N, 14.58.

5-(3-((3,5-Dichlorophenyl)(methyl)amino)propyl)-1*H*-pyrazol-3(2*H*)-one (24). The title compound was prepared according to general procedures B, C, and E. ^{1}H NMR (DMSO-d_6, 500 MHz): δ = 11.27 (br s, 1H), 9.30 (br s, 1H), 6.66 (d, J = 1.5 Hz, 1H), 6.61 (d, J = 1.5 Hz, 2H), 5.26 (s, 1H), 3.32 (t, J = 7.5 Hz, 2H), 2.88 (s, 3H), 2.45 (t, J = 7.5 Hz, 2H), 1.76−1.73 (m, 2H). ^{13}C NMR (DMSO-d_6, 125 MHz): δ = 150.7, 134.7 × 2, 114.0, 109.8 × 2, 50.9, 38.0, 25.4 ppm. MS (ESI): m/z 300.1 $[M + H]^+$. CHN calculated for $C_{13}H_{15}Cl_2N_3O$: C, 52.01; H, 5.04; N, 14.00. Found: C, 52.23; H, 5.14; N, 14.94.

5-(Indolin-1-ylmethyl)-1*H*-pyrazol-3(2*H*)-one (25). The title compound was prepared according to general procedures D and E. ^{1}H NMR (DMSO-d_6, 500 MHz): δ = 7.02 (d, J = 7.0 Hz, 1H), 6.98 (t, J = 7.5 Hz, 1H), 6.62 (d, J = 7.5 Hz, 1H), 6.58 (t, J = 7.5 Hz, 1H), 5.31 (s, 1H), 4.12 (s, 2H), 3.24 (t, J = 8.0 Hz, 2H), 2.85 (t, J = 8.0 Hz, 2H). ^{13}C NMR (DMSO-d_6, 125 MHz): δ = 151.7, 129.8, 127.0, 124.3, 117.5, 107.5, 89.0, 52.6, 44.0, 27.9 ppm. MS (ESI): m/z 216.1 $[M + H]^+$. CHN calculated for $C_{12}H_{13}N_3O$: C, 66.96; H, 6.09; N, 19.52. Found: C, 66.85; H, 6.11; N, 19.44.

5-((3,4-Dihydroquinolin-1(2*H*)-yl)methyl)-1*H*-pyrazol-3(2*H*)-one (26). The title compound was prepared according to general procedures D and E. ^{1}H NMR (DMSO-d_6, 500 MHz): δ = 6.91 (t, J = 7.0 Hz, 1H), 6.86 (d, J = 7.0 Hz, 1H), 6.64 (d, J = 8.5 Hz, 1H), 6.47 (t, J = 7.5 Hz, 1H), 5.26 (s, 1H), 4.28 (s, 2H), 3.28 (t, J = 5.5 Hz, 2H), 2.66 (t, J = 5.5 Hz, 2H), 1.87 (p, J = 6.0 Hz, 2H). ^{13}C NMR (DMSO-d_6, 125 MHz): δ = 144.9, 128.8, 126.7, 122.2, 115.8, 111.2, 88.4, 49.1, 46.5, 39.0, 27.5, 21.8 ppm. MS (ESI): m/z 216.1 $[M + H]^+$. CHN calculated for $C_{13}H_{15}N_3O$: C, 68.10; H, 6.59; N, 18.33. Found: C, 68.02; H, 6.60; N, 18.29.

5-(3,5-Dichlorophenyl)-4,5,6,7-tetrahydro-1*H*-pyrazolo[4,3-*c*]pyridin-3(2*H*)-one (27). The title compound was prepared according to the literature procedure[34] and general procedure E. ^{1}H NMR (DMSO-d_6, 500 MHz): δ = 6.95 (s, 2H), 6.82 (d, J = 1.5 Hz, 1H), 4.06 (s, 2H), 3.59 (t, J = 6.0 Hz, 1H), 2.63−2.62 (m, 2H). ^{13}C NMR (DMSO-d_6, 125 MHz): δ = 152.1, 134.7 × 2, 116.4, 112.9 × 2, 45.0, 43.0 ppm. MS (ESI): m/z 284.0 $[M + H]^+$. CHN calculated for $C_{12}H_{11}Cl_2N_3O$: C, 50.72; H, 3.90; N, 14.79. Found: C, 50.53; H, 4.03; N, 14.83.

6-(3,5-Dichlorophenyl)-4,5,6,7-tetrahydro-1*H*-pyrazolo[3,4-*c*]pyridin-3(2*H*)-one (28). The title compound was prepared according to the literature procedure[34] and general procedure E. ^{1}H NMR (DMSO-d_6, 500 MHz): δ = 6.96 (d, J = 1.5 Hz, 2H), 6.83 (d, J = 1.5 Hz, 1H), 4.26 (s, 2H), 3.55 (t, J = 6.0 Hz, 2H), 3.16 (d, J = 5.0 Hz, 1H), 2.41−2.39 (m, 2H). ^{13}C NMR (DMSO-d_6, 125 MHz): δ = 152.0, 134.7 × 2, 116.6, 113.1 × 2, 46.2, 29.5, 18.6 ppm. MS (ESI): m/z 284.0 $[M + H]^+$. CHN calculated for $C_{12}H_{11}Cl_2N_3O$: C, 50.72; H, 3.90; N, 14.79. Found: C, 50.51; H, 3.78; N, 14.57.

2-Benzyl-5-(((3,5-dichlorophenyl)(methyl)amino)methyl)-1*H*-pyrazol-3(2*H*)-one (29). To a solution of ethyl 4-((3,5-dichlorophenyl)(methyl)amino)-3-oxobutanoate (304 mg, 1.0 mmol) and benzylhydrazine dihydrochloride (388 mg, 2.0 mmol) in EtOH (5 mL) was added anhydrous triethylamine (570 uL, 4.0 mmol). The resulting solution was stirred at room temperature overnight. After evaporation of the volatiles, the residue was purified on a silica gel column, eluting with a mixture of MeOH and dichloromethane (1−2% MeOH) to afford the product as a pale yellow solid (320 mg, 88%). The solid was then recrystallized in dichloromethane/hexane to give the product as a white solid. ^{1}H NMR (DMSO-d_6, 500 MHz): δ = 11.00 (br s, 1H), 7.28 (t, J = 7.0 Hz, 2H), 7.23 (d, J = 7.0 Hz, 1H), 7.11 (d, J = 7.0 Hz, 2H), 6.74 (d, J = 1.5 Hz, 2H), 6.69 (s, 1H), 5.12 (s, 1H), 5.01 (s, 2H), 4.33 (s, 2H), 2.98 (s, 2H). ^{13}C NMR (DMSO-d_6, 125 MHz): δ = 152.7, 151.0, 146.8, 138.0, 134.4 × 2, 128.4 × 2, 127.1, 127.0 × 2, 114.4, 110.6 × 2, 84.6, 50.3, 49.2, 38.9 ppm. MS (ESI): m/z 284.0 $[M + H]^+$. CHN calculated for $C_{18}H_{17}Cl_2N_3O$: C, 59.68; H, 4.73; N, 11.60. Found: C, 59.79; H, 4.68; N, 11.48.

5-(((3,5-Dichlorophenyl)(methyl)amino)methyl)-2-methyl-1*H*-pyrazol-3(2*H*)-one (30). To a solution of ethyl 4-((3,5-dichlorophenyl)(methyl)amino)-3-oxobutanoate (304 mg, 1.0 mmol) in EtOH (5 mL) was added anhydrous methylhydrazine (105 μL, 2.0 mmol). The resulting solution was stirred at room temperature overnight. After evaporation of the volatiles, the residue was purified on a silica gel column, eluting with a mixture of MeOH and dichloromethane (2−10% MeOH) to afford the product as a pale yellow solid (231 mg, 81%). The solid was then recrystallized in dichloromethane/hexane to give the product as a white solid. ^{1}H NMR (DMSO-d_6, 500 MHz): δ = 6.72 (d, J = 1.5 Hz, 2H), 6.68 (t, J = 1.5 Hz, 1H), 5.13 (s, 1H), 4.29 (s, 2H), 3.43 (s, 3H), 2.95 (s, 3H). ^{13}C NMR (DMSO-d_6, 125 MHz): δ = 152.5, 151.0, 146.0, 134.4 × 2, 114.3, 110.4 × 2, 84.5, 49.9, 38.5, 33.0 ppm. MS (ESI): m/z 286.1 $[M + H]^+$. CHN calculated for $C_{12}H_{13}Cl_2N_3O$: C, 50.37; H, 4.58; N, 14.68. Found: C, 50.60; H, 4.65; N, 14.62. FTIR (solid), ν 1591, 1552, 1495, 1445, 1309, 1272, 1094, 1012, 980, 950, 813, 756, 662 cm^{-1}; (DMSO), ν 1591, 1552, 1436, 1309, 1042 (bw), 950, 806, 756, 697, 663 cm^{-1}.

dx.doi.org/10.1021/jm400079a | *J. Med. Chem.* 2013, 56, 2665−2675

5-(((3,5-Dichlorophenyl)(methyl)amino)methyl)-1-methyl-1*H*-pyrazol-3(2*H*)-one (31). Compound **37** (115 mg, 0.37 mmol) was suspended in 2 N HCl (7 mL) and stirred at 60 °C overnight. Ethyl acetate was added to the mixture, and the organic layer was separated, washed with water and brine, dried over Na_2SO_4, and concentrated. The residue was purified on a silica gel column, eluting with a mixture of MeOH and dichloromethane (4% MeOH) to afford the product as a white solid (55 mg, 52%). ^{1}H NMR (DMSO-d_6, 500 MHz): δ = 9.42 (s, 1H), 6.75 (m, 3H), 5.08 (s, 1H), 4.54 (s, 2H), 3.52 (s, 3H), 2.94 (s, 3H). ^{13}C NMR (DMSO-d_6, 125 MHz): δ = 159.5, 150.8, 139.4, 134.6 × 2, 115.0, 110.7 × 2, 89.7, 46.9, 38.2, 35.7 ppm. MS (ESI): m/z 286.1 $[M + H]^+$. CHN calculated for $C_{12}H_{13}Cl_2N_3O$: C, 50.37; H, 4.58; N, 14.68. Found: C, 50.57; H, 4.73; N, 14.74. FTIR (solid), ν 1587, 1552, 1493, 1447, 1345, 1125, 1098, 1018, 959, 813, 801, 774, 663 cm^{-1}; (DMSO), ν 1587, 1552, 1493, 1435, 1282, 1043 (bw), 952, 800, 697, 664 cm^{-1}.

5-(((3,5-Dichlorophenyl)(methyl)amino)methyl)-1,2,4-trimethyl-1*H*-pyrazol-3(2*H*)-one (32). A solution of compound **30** (200 mg, 0.7 mmol), MeI (132 μL, 2.1 mmol), and K_2CO_3 (290 mg, 2.1 mmol) in acetonitrile (3.5 mL) was stirred at 50 °C for 24 h. After evaporation of the volatiles, the residue was purified on a silica gel column, eluting with a mixture of MeOH and dichloromethane (1−5% MeOH) to afford the product (compounds **32**−**34**) as a pale yellow solid or liquid. ^{1}H NMR ($CDCl_3$, 500 MHz): δ = 6.78 (t, J = 1.5 Hz, 1H), 6.65 (d, J = 1.5 Hz, 2H), 4.23 (s, 2H), 3.32 (s, 3H), 3.08 (s, 3H), 2.82 (s, 3H), 1.86 (s, 3H). ^{13}C NMR ($CDCl_3$, 125 MHz): δ = 166.5, 151.1, 147.3, 136.0 × 2, 118.2, 111.9 × 2, 108.7, 46.7, 37.6, 35.0, 29.1, 7.27 ppm. MS (ESI): m/z 314.1 $[M + H]^+$.

5-(((3,5-Dichlorophenyl)(methyl)amino)methyl)-1,2-dimethyl-1*H*-pyrazol-3(2*H*)-one (33). ^{1}H NMR ($CDCl_3$, 500 MHz): δ = 6.76 (t, J = 1.5 Hz, 1H), 6.57 (d, J = 2.0 Hz, 2H), 5.28 (s, 1H), 4.27 (s, 2H), 3.38 (s, 3H), 3.25 (s, 3H), 2.96 (s, 3H). ^{13}C NMR ($CDCl_3$, 125 MHz): δ = 166.0, 151.4, 150.4, 135.9 × 2, 118.0, 111.4 × 2, 98.1, 49.0, 38.7, 34.2, 28.8 ppm. MS (ESI): m/z 300.1 $[M + H]^+$.

3-(((3,5-Dichlorophenyl)(methyl)amino)methyl)-1,4,4-trimethyl-1*H*-pyrazol-5(4*H*)-one (34). ^{1}H NMR ($CDCl_3$, 500 MHz): δ = 6.72 (t, J = 1.5 Hz, 1H), 6.58 (d, J = 1.5 Hz, 2H), 4.17 (s, 2H), 3.30 (s, 3H), 3.00 (s, 3H), 1.23 (s, 6H). ^{13}C NMR ($CDCl_3$, 125 MHz): δ = 178.4, 162.6, 150.6, 135.8 × 2, 117.2, 110.9 × 2, 50.6, 48.0, 39.3, 31.5, 21.3 ppm. MS (ESI): m/z 314.1 $[M + H]^+$.

3,5-Dichloro-*N*-((2,3-dihydropyrazolo[5,1-*b*]oxazol-6-yl)methyl)-*N*-methylaniline (36). To a solution of ethyl 4-((3,5-dichlorophenyl)(methyl)amino)-3-oxobutanoate (304 mg, 1.0 mmol) in EtOH (5 mL) was added 2-hydroxyethylhydrazine (85 uL, 1.1 mmol), and the mixture was stirred for 3 h. After evaporation of the volatiles, the residues were dissolved with dry acetonitrile (10 mL) and triethylamine (156 uL, 1.1 mmol) followed by the addition of tosyl chloride (190 mg, 1.0 mmol). The solution was stirred for 20 min, diluted in ethyl acetate (20 mL), washed with water (10 mL), dried over Na_2SO_4, and concentrated. The residue was purified on a silica gel column, eluting with a mixture of MeOH and dichloromethane (2% MeOH) to afford the product as a pale yellow liquid **35** (400 mg, 85%).

Under an inert atmosphere, **35** was dissolved in anhydride acetonitrile (8.5 mL) followed by the addition of sodium hydride (40 mg, 1.0 mmol). The mixture was stirred overnight at room temperature and evaporated to give the residue, which was purified on a silica gel column, eluting with a mixture of MeOH and dichloromethane (1% MeOH) to afford the product as a pale yellow solid **36** (200 mg, 79%). ^{1}H NMR ($CDCl_3$, 500 MHz): δ = 6.66 (d, J = 1.5 Hz, 1H), 6.63 (d, J = 1.5 Hz, 2H), 5.19 (s, 1H), 5.00 (dd, J = 7.5, 9.0 Hz, 2H), 4.36 (s, 2H), 4.25 (t, J = 7.5 Hz, 2H), 2.99 (s, 3H). ^{13}C NMR ($CDCl_3$, 125 MHz): δ = 159.7, 155.0, 151.0, 135.6 × 2, 116.4, 111.0 × 2, 79.5, 75.3, 51.6, 45.4, 38.8 ppm. MS (ESI): m/z 298.0 $[M + H]^+$.

5-(((3,5-Dichlorophenyl)(methyl)amino)methyl)-1-methyl-2-vinyl-1*H*-pyrazol-3(2*H*)-one (37). To a solution of compound **36** (200 mg, 0.67 mmol) in anhydrous acetonitrile (6 mL) was added methyl trifluoromethanesulfonate (85 μL, 0.75 mmol), and the solution was stirred for 2 h before the addition of sodium iodide (195 mg, 1.3 mmol) and TsOH (127 mg, 0.67 mmol). After conversion to the iodinated intermediate by overnight stirring, KO-*t*-Bu (188 mg, 1.7 mmol) was added to the mixture, which was further stirred for 1 h. After evaporation of the volatiles, the residue was purified on a silica gel column, eluting with a mixture of MeOH and dichloromethane (4% MeOH) to afford the product as a yellow liquid (115 mg, 55%). ^{1}H NMR ($CDCl_3$, 500 MHz): δ = 6.85 (dd, J = 9.0, 16.0 Hz, 1H), 6.77 (t, J = 1.5 Hz, 2H), 6.56 (d, J = 1.5 Hz, 2H), 5.37 (s, 1H), 4.88−4.80 (m, 2H), 4.31 (s, 2H), 3.17 (s, 3H), 2.99 (s, 3H). ^{13}C NMR ($CDCl_3$, 125 MHz): δ = 165.4, 159.2, 150.3, 136.0 × 2, 126.3, 118.0, 111.3 × 2, 101.1, 99.5, 49.6, 39.0, 37.3 ppm.

Mutant SOD1-Induced Cytotoxicity Protection Assay. Viability and EC_{50} values were determined for **1a**, **1b**, **2a**, and **2b** according to the previously reported assay procedure.[15] PC12 cells were seeded at 15 000 cells/well in 96-well plates and incubated 24 h prior to compound addition. Compounds were assayed in 12-point dose−response experiments to determine potency and efficacy. The highest compound concentration tested was 32 μM, which was decreased by one-half with each subsequent dose. After a 24 h incubation with the compounds, MG132 was added at a final concentration of 100 nM. MG132 is a well-characterized proteasome inhibitor, which would be expected to enhance the appearance of protein aggregation by blocking the proteosomal clearance of aggregated proteins. Cell viability was measured 48 h later using the fluorescent viability probe Calcein-AM (Molecular Probes). Briefly, cells were washed twice with PBS. Calcein-AM was added at a final concentration of 1 μM for 20 min at room temperature, and fluorescence intensity was read in a POLARstar fluorescence plate reader (BMG). Fluorescence data were coupled with compound structural data, then stored and analyzed using the CambridgeSoft Chemoffice Enterprise Ultra software package.

In Vitro ADME Assays. In vitro microsomal stability, aqueous solubility, and Caco-2 permeability were determined for **1b** and **2b** at Apredica Inc. (Watertown, MA).

Computational Methods. Possible initial tautomer structures were constructed with molecular modeling software Sybyl-X 1.2 (Tripos International, St. Louis, MO). After primary optimization by use of MM2 molecular mechanical module encoded in the program CS Chem3D, these two structures were subjected to full optimization within the density-functional theory (DFT). The Lee−Yang−Parr correlation functional approximation (B3LYP) method was used in a 6-31+G(d,p) basis set.[35,36] On the basis of the optimized geometries, energy or frequency calculations were carried out at the same levels of B3LYP to verify the reasonability of the optimized structures. A frequency scaling factor of 0.964 was used in the comparison of the calculated results with the experimental spectra.[37] All of the Quantum Chemical calculations were carried out with the Gamess (2012R1) program.[38]

■ ASSOCIATED CONTENT

Ⓢ Supporting Information

NMR spectra for compounds **2**−**38**, IR spectra for compounds **30**, **31**, and **38**, and primary cortical neuron protection assay for compounds **1**, **3**, **19**−**21**, **23**, **24**, and **27**. This material is available free of charge via the Internet at http://pubs.acs.org.

■ AUTHOR INFORMATION

Corresponding Author

*Phone: 847-491-5663. Fax: 847-491-7713. E-mail: Agman@chem.northwestern.edu.

Present Address

‖For C.V.: Department of Biology, Northeastern Illinois University, Chicago, IL 60625, U.S.

Notes

The authors declare no competing financial interest.

■ ACKNOWLEDGMENTS

We thank the National Institutes of Health (Grant 1R43NS057849), the ALS Association (TREAT program), and the Department of Defense (Grant AL093052) for their generous support of this research.

■ ABBREVIATIONS USED

AAP, arylazanylpyrazolone; ADME, absorption, distribution, metabolism, excretion; ALS, amyotrophic lateral sclerosis; ASP, arylsulfanylpyrazolone; AXP, aryl heteroatom pyrazolone; CNS, central nervous system; DFT, density functional theory; FALS, familial amyotrophic lateral sclerosis; IR, infrared spectroscopy; NOE, nuclear Overhauser effect; PBS, phosphate buffered saline; PK, pharmacokinetics; SALS, sporadic amyotrophic lateral sclerosis; SOD1, Cu/Zn superoxide dismutase

■ REFERENCES

(1) Rowland, L. P.; Shneider, N. A. Amyotrophic lateral sclerosis. *N. Engl. J. Med.* **2001**, *344*, 1688−1700.
(2) Rothstein, J. D. Currenthypothese for the underlying biology of amyotrophic lateral sclerosis. *Ann. Neurol.* **2009**, *65* (Suppl. 1), S3−S9.
(3) Worms, P. M. The epidemiology of motor neuron diseases: a review of recent studies. *J. Neurol.Sci.* **2001**, *191*, 3−9.
(4) Weisskopf, M. G.; O'Reilly, E. J.; McCullough, M. L.; Calle, E. E.; Thun, M. J.; Cudkowicz, M.; Ascherio, A. Prospective study of military service and mortality from ALS. *Neurology* **2005**, *64*, 32−37.
(5) Mitsumoto, H.; Rabkin, J. G. Palliative care for patients with amyotrophic lateral sclerosis: "Prepare for the worst and hope for the best". *JAMA, J. Am. Med. Assoc.* **2007**, *298*, 207−216.
(6) Waldmeier, P. C.; Tatton, W. G. Interrupting apoptosis in neurodegenerative disease: potential for effective therapy? *Drug Discovery Today* **2004**, *9*, 210−218.
(7) Bensimon, G.; Lacomblez, L.; Meininger, V. A controlled trial of riluzole in amyotrophic lateral sclerosis. ALS/Riluzole Study Group. *N. Engl. J. Med.* **1994**, *330*, 585−591.
(8) ALS Online Genetics Database: http://alsod.iop.kcl.ac.uk/.
(9) Rosen, D. R.; Siddique, T.; Patterson, D.; Figlewicz, D. A.; Sapp, P.; et al. Mutations in Cu/Zn superoxide dismutase gene are associated with familial amyotrophic lateral sclerosis. *Nature* **1993**, *362*, 59−62.
(10) Turner, B. J.; Talbot, K. Transgenics, toxicity and therapeutics in rodent models of mutant SOD1-mediated familial ALS. *Prog. Neurobiol.* **2008**, *85*, 94−134.
(11) Nagai, M.; Re, D. B.; Nagata, T.; Chalazonitis, A.; Jessell, T. M.; Wichterle, H.; Przedborski, S. Astrocytes expressing ALS-linked mutated SOD1 release factors selectively toxic to motor neurons. *Nat. Neurosci* **2007**, *10*, 615−622.
(12) Haidet-Phillips, A. M.; Hester, M. E.; Miranda, C. J.; Meyer, K.; Braun, L.; Frakes, A.; Song, S. W.; Likhite, S.; Murtha, M. J.; Foust, K. D.; Rao, M.; Eagle, A.; Kammesheidt, A.; Christensen, A.; Mendell, J. R.; Burghes, A. H. M.; Kaspar, B. K. Astrocytes from familial and sporadic ALS patients are toxic to motor neurons. *Nat. Biotechnol.* **2011**, *29*, 824−830.
(13) Gruzman, A.; Wood, W. L.; Alpert, E.; Prasad, M. D.; Miller, R. G.; Rothstein, J. D.; Bowser, R.; Hamilton, R.; Wood, T. D.; Cleveland, D. W.; Lingappa, V. R.; Liu, J. Common molecular signature in SOD1 for both sporadic and familial amyotrophic lateral sclerosis. *Proc. Natl. Acad. Sci. U.S.A.* **2007**, *104*, 12524−12529.
(14) Matsumoto, G.; Stojanovic, A.; Holmber, C. I.; Kim, S.; Morimoto, R. I. Structure properties and neuronal toxicity of amyotrophic lateral sclerosis-associated Cu/Zn superoxide dismutase 1 aggregates. *J. Cell Biol.* **2005**, *171*, 75−85.
(15) Benmohamed, R.; Arvanites, A. C.; Silverman, R. B.; Morimoto, R. I.; Ferrante, R. J.; Kirsch, D. R. Identification of compounds protective against G93A SOD1 toxicity for the treatment of amyotrophic lateral sclerosis. *Amyotrophic Lateral Scler.* **2011**, *12*, 87−96.
(16) Chen, T.; Benmohamed, R.; Arvanites, A. C.; Ranaivo, H. R.; Morimoto, R. I.; Ferrante, R. J.; Watterson, D. M.; Kirsch, D. R.; Silverman, R. B. Arylsulfanyl pyrazolones block mutant SOD1-G93A aggregation. Potential application for the treatment of amyotrophic lateral sclerosis. *Bioorg. Med. Chem.* **2011**, *19*, 613−622.
(17) Chen, T.; Benmohamed, R.; Kim, J.; Smith, K.; Amante, D.; Morimoto, R. I.; Ferrante, R. J.; Kirsch, D.; Silverman, R. B. ADME-guided design and synthesis of aryloxanylpyrazonlone derivatives to block mutant superoxide dismutase 1 (SOD1) cytotoxicity and protective aggregation: potential application for the treatment of amyotrophic lateral sclerosis. *J. Med. Chem.* **2012**, *55*, 515−527.
(18) Trippier, P. C.; Benmohammed, R.; Kirsch, D. R.; Silverman, R. B. Substituted pyrazolones require N^2 hydrogen bond donating ability to protect against cytotoxicity from protein aggregation of mutant superoxide dismutase 1. *Bioorg. Med. Chem. Lett.* **2012**, *22*, 6647−6650.
(19) Zhang, Y.; Silverman, R. Direct amination of γ-halo-β-ketoesters with anilines. *J. Org. Chem.* **2012**, *77*, 3462−3467.
(20) Yang, M.; Wang, X.; Li, H.; Livant, P. A new route to hindered tertiary amines. *J. Org. Chem.* **2001**, *66*, 6729−6733.
(21) Hamper, B. C.; Kurtzweil, M. L.; Beck, J. P. Cyclocodensation of alkyl hydrazines and β-substituted acetylenic esters: synthesis of 3-hydroxypyrazoles. *J. Org. Chem.* **1992**, *57*, 5680−5686.
(22) Zimmermann, D.; Krogsgaard-Larsen, P.; Ehrhard, J. -D.; Madsen, U.; Janin, Y. L. Unambiguous synthesis of 1-methyl-3-hydroxypyrazoles. *Tetrahedron* **1998**, *54*, 9393−9400.
(23) Kerns, E. H.; Di, L. *Drug-like Properties: Concepts, Structure, Design, and Methods*; Academic Press: Amsterdam, 2008; p 65.
(24) Van de Waterbeemd, H.; Gifford, E. ADMET in silico modeling: towards prediction paradise? *Nat. Rev. Drug Dicovery* **2003**, *2*, 192−204.
(25) Compound **1**, which had an EC_{50} of 0.067 μM in the protection assay in our earlier report of aryloxanyl pyrazolones, showed an average activity of 0.4 μM for several parallel repeats in this study.
(26) Park, K. D.; Kim, D.; Reamtong, O.; Eyers, C.; Gaskell, S. J.; Liu, R.; Kohn, H. Identification of a lacosamide binding protein using an affinity bait and chemical reporter strategy: 14-3-3ζ. *J. Am. Chem. Soc.* **2011**, *133*, 11320−11330.
(27) Silverman, R. B. *The Organic Chemistry of Drug Design and Drug Action*, 2nd ed.; Elsevier Academic Press: Amsterdam, 2004; p 28.
(28) Zhang, Y.; Benmohamed, R.; Zhang, W.; Kim, J.; Edgerly, C. K.; Zhu, Y.; Morimoto, R. I.; Ferrante, R. J.; Kirsch, D. R.; Silverman, R. B. Chiral cyclohexane 1,3-diones as inhibitors of mutant SOD1-dependent protein aggregation for the treatment of amyotrophic lateral sclerosis. *ACS Med. Chem. Lett.* **2012**, *3*, 584−587.
(29) Knorr, L. Ueber abkommlinge der phenol form des 1-phenyl-3-methyl-5-pyrazolons. *Ber. Dtsch. Chem. Ges.* **1895**, *28*, 706−714.
(30) (a) Parchment, O. G.; Green, D. V. S.; Taylor, P. J.; Hillier, I. H. The prediction of tautomer equilibria in hydrated 3-hydroxypyrazole: a challenge to theory. *J. Am. Chem. Soc.* **1993**, *115*, 2352−2356. (b) Enchev, V.; Neykov, G. D. A semiempirical and ab initio MO study of the tautomers of N-unsubstituted pyrazolones (hyroxy pyrazoles). *Struct. Chem.* **1992**, *3*, 231−238. (c) Nagy, P. I.; Tejada, F. R.; Messer, W. S., Jr. Theoretical studies of the tautomeric equilibria for five-member N-heterocycles in the gas phase and in solution. *J. Phys. Chem. B* **2005**, *109*, 22588−22602.
(31) Hamper, B. Regioselective synthesis of 1-methyl-3-hydroxy-5-perfluoroalkyl pyrazoles by the addition of methylhydrazine to perfluoroalkylacetylenic ester. *J. Fluorine Chem.* **1990**, *48*, 123−131.
(32) Compound **5b** in ref 17.
(33) In procedure C for preparing compound **21**, the reaction time needs to be extended to 16 h while allowing the reaction temperature to rise to room temperature.
(34) Zhang, Y.; Silverman, R. B. An efficient synthesis of 1-aryl-3-piperidione derivative through MBH and RCM reactions. *Tetrahedron Lett.* **2013**, *54*, 573−575.
(35) Becke, A. D. Density-functional thermochemistry. III. The role of exact exchange. *J. Chem. Phys.* **1993**, *98*, 5648−5652.

(36) Lee, C.; Yang, W.; Parr, R. G. Development of the Colle–Salvetti correlation energy formula into a functional of the electron density. *Phys. Rev. B* **1988**, *37*, 785–789.
(37) Merrick, J. P.; Moran, D.; Radom, L. An evaluation of harmonic vibrational frequency scale factors. *J. Phys. Chem. A* **2007**, *111*, 11683–11700.
(38) Schmidt, M. S.; Baldridge, K. K.; Boatz, J. A.; Elbert, S. T.; Gordon, M. S.; Jensen, J. H.; Koseki, S.; Matsunaga, N.; Nguyen, K. A.; Su, S.; Windus, T. L.; Dupuis, M.; Montgomery, J. A. General atomic and molecular electronic structure system. *J. Comput. Chem.* **1993**, *14*, 1347–1363.